

A vibration-based bridge scour monitoring technique

Kasun Danushka Kariyawasam Katukoliha Gamage

Churchill College

May 2020

This thesis is submitted for the degree of Doctor of Philosophy

Supervisor: Professor Campbell Middleton



This page is intentionally left blank

Declaration

This thesis is the result of my own work and includes nothing which is the outcome of work done in collaboration except as declared in the preface and specified in the text. It is not substantially the same as any work that has already been submitted before for any degree or other qualification except as declared in the preface and specified in the text. It does not exceed the prescribed word limit for the Engineering Degree Committee.

Kasun Danushka Kariyawasam Katukoliha Gamage

May 2020

A vibration-based bridge scour monitoring technique

Kasun Danushka Kariyawasam Katukoliha Gamage

Abstract

Historically, the most common cause of bridge failure has been “scour” – the gradual erosion of soil around bridge foundations due to rapid water flow. A reliable technique to monitor scour could potentially guide timely repair and, in turn, mitigate the risk of future scour-induced bridge failure. Currently, there are various, mostly underwater, techniques employed by bridge managers to monitor scour, ranging from diving inspections to autonomous underwater vehicles; however, none have gained wide acceptance. A particular disadvantage of underwater monitoring techniques is that the equipment underwater is relatively difficult to install and prone to damage from fast-flowing water and debris.

One possible solution might be to use a vibration-based method to monitor scour indirectly, using changes in dynamic modal parameters (e.g. the natural frequency of vibration) captured by sensors mounted on the bridge deck or piers above the water level. There has been extensive research into the use of vibration-based monitoring methods to identify other causes of failure, such as cracking and deterioration in bridge superstructures; however, this has proven to be ineffective in practice, as the expected sensitivities in modal parameters were only single-digit percentages and therefore insufficient to overcome environmental/operational sensitivity. In contrast to superstructure damage, scour is a special damage case, which changes a boundary condition of the bridge in the form of an increase in effective pier height as a result of the lowering of the ground level and therefore, significant changes in modal parameters can be expected. Recently, this concept has been studied primarily using numerical modelling simulations of a hypothetical integral bridge with piled foundations. Only one modal parameter – natural frequency – was investigated in most of these studies and it was predicted to change by up to double-digit percentages due to scour. Although such a high change could potentially overcome environmental and operational sensitivities, a critical problem is that this has been difficult to observe in practice with experiments on either real field bridges or small-scale soil-structure models. Another problem is that there is little knowledge of the applicability of this technique to different types of bridges and forms of scour.

This research proposes a vibration-based technique based on a combination of three vibration parameters (spectral density, mode shape and natural frequency), which were studied using first-of-a-kind experiments and numerical modelling simulations on various types of bridges and forms of scour. A field trial was carried out on a bridge with pre-existing scour, which was monitored for ambient vibrations throughout a repair process involving controlled scour

backfilling, i.e., “scour in reverse”. The effect of this scour backfilling was captured by measuring changes in two of these parameters, mode shape and spectral density, derived from the ambient vibrations. The mode shapes, in particular, showed the potential to localise the presence of scour to a specific pier. The most commonly measured vibration parameter of natural frequency was also observed from ambient vibrations, but this did not capture the effects of backfilling due to high measurement uncertainties.

In order to study all three of these vibration parameters in a controlled environment, a centrifuge model testing programme was developed. These tests considered small-scale models representing three full-scale bridges with different bridge deck and foundation configurations (i.e. integral/ simply supported decks and shallow/deep foundations) and two forms of scour (i.e. local/global). The observed results of these small-scale centrifuge models were used to calibrate numerical models of full-scale bridges representative of these centrifuge models. Numerical simulation techniques were also developed to simulate the experimentally observed effects of local and global scour.

These centrifuge experiments and the associated numerical modelling found that vibration-based methods have broad applicability for bridges, although only some parameters showed sufficient sensitivity to be viable as a monitoring technique in certain types of bridges. For example, the centrifuge bridge models with a shallow foundation did not show a significant change in natural frequency or mode shapes, but they did show a significant change in modal spectral density. This research therefore concludes that a vibration-based scour monitoring technique, examining the combined effect of natural frequency, mode shape and spectral density parameters, has significant potential to measure and even localise the change of scour depths at bridge foundations.

Acknowledgements

I would like to express my deepest appreciation to my PhD supervisor, Professor Campbell Middleton, for his invaluable support and guidance throughout this research project. Every time I met him for supervision, he made it an enjoyable exploration of the deep-rooted physics and engineering behind the findings of our research, which inspired me to think deeply and carry out high-quality research. His comments regarding improving the quality and clarity of the thesis were invaluable; I am touched by how much time he spent reading this thesis within a short period of time, even during flights and at weekends. His vast experience and expertise in the area of research, his caring attitude and his instrumental nature of finding people and funding to support the research provided me with the ideal working environment to carry out this research with a great deal of enthusiasm.

Profound gratitude goes to my advisor, Dr James Talbot, for the time offered in the last three years to help me understand aspects of modal analysis; his advice has also been very helpful in conducting the experiments. I would also like to thank my first-year advisor, Dr Mohammed Elshafie, for his valuable input at a key stage at the start of my research project. I am extremely grateful to Dr Stuart Haigh and Professor Gopal Madabhushi for their guidance with the centrifuge experiments, which was much appreciated. And I am very grateful to Paul Fidler for his valuable help and advice with the field trial, for designing a data acquisition system in record time and for helping me by proofreading a chapter of this thesis.

I am most thankful and honoured to have received generous financial support from the Gates Cambridge Trust, and I am hopeful that I can support the main aim of the scholarship, to improve the lives of others, with this research. I am also very grateful to the Laing O'Rourke Centre for Construction Engineering & Technology and the Cambridge Centre for Smart Infrastructure and Construction (Innovate UK grant reference number 920035 and EPSRC grant no EP/N021614/1) for the funding provided for the experimental programme. Furthermore, I wish to express my sincere thanks to Churchill College for providing me with not only pleasant residential facilities but also a conducive environment for my academic work.

I would like to extend my profound gratitude to Professor Thishan Jayasinghe and Professor Chintha Jayasinghe for giving me an invaluable foundation in research and knowledge of structural analysis during the time I worked under their supervision in Sri Lanka. I would like to gratefully thank Dr Chinthaka Mallikarachchi, Dr Lalith Rajapakse and all the lecturers at the Department of Civil Engineering, the University of Moratuwa for the valuable research and civil engineering foundation provided during my undergraduate studies. I would also like to thank Engineer Samitha Jayakody and my Advanced Level physics teacher and Engineer Sudarshana P Jayawardana for inspiring me to choose Civil Engineering discipline.

I am grateful for the kind help provided by researchers, administrative and technical staff at the Laing O'Rourke Centre, Centre for Smart Infrastructure & Construction, Churchill College, Gates Cambridge Trust and Scofield Centre. Special thanks to Jan Wojtecki, Alessandra Cirani, Anne Debenham, Jennifer Schooling, Cedric Kechavarzi, Nicky Battista, Haris Alexakis, Tianlei Wu, Philip Keenan, Peter Knott, Jason Shardelow, Rebecca Sawalmeh, Luisa Clarke, Deryck Chan, Jad Boksmati, Geoffrey Eichhorn, Ahmed Alagha, Thejesh Garala, Kristian Pether, Chris McGinnie, Mark Smith, John Chandler and David Layfield for their valuable help at different stages of this project.

I also thank the partners of the Baildon Bridge project, Bradford Metropolitan Council and TMS Maritime Ltd, for their assistance and cooperation. Special thanks to Naveed Anwar, Senior Engineer, Bradford Council, and the TMS scour repair team, Mikael Nickson, Olly Westaway, Rob Martin, Jonathan Peers, Mark and Dave Bridger; and also to Jenny Roberts of Gaist solutions, and Cumbria Council for the sonar scanning carried out with the BridgeCat vehicle. I also wish to gratefully acknowledge Cambridgeshire County Council for permitting inspection of Nine Wells Bridge.

I greatly appreciate Amanda George, Sakthy Selvakumaran, Sumudu Herath, Mahendrini Fernando, Gemunu Kulasekara, Nathan Barnes, Tisal Edirisinghe and Geethanaga Wijeshighe for their kind help with proofreading sections of this thesis. Some special words of gratitude go to all my friends for the memorable and enjoyable times and for being there whenever I needed.

The valuable advice provided by Tom Williams and Ranjan Fernando during the planning stage of this project is also acknowledged. I am thankful to John Smith, Graham Webb, Luke Prendergast and Tina Schwamb for sharing drawings, research papers and other relevant documents. This research was possible because of the incredible help and support of many kind individuals and institutions. Indeed, I am thankful to everyone who helped me in some way to make this project a success.

Last but not least, I would like to thank my parents for their unwavering love, encouragement and support throughout my life.

Contents

- DECLARATION I**
- ABSTRACT II**
- ACKNOWLEDGEMENTS IV**
- CONTENTS VI**
- LIST OF TABLES X**
- LIST OF FIGURES XI**
- NOMENCLATUREXVI**
- CHAPTER 1 INTRODUCTION 1**
 - 1.1 BACKGROUND..... 1
 - 1.2 PROBLEM STATEMENT 3
 - 1.3 OBJECTIVES OF THE RESEARCH 5
 - 1.4 METHODOLOGY 6
 - 1.5 SCOPE OF THE RESEARCH 9
 - 1.6 INNOVATIVE ASPECTS OF THE RESEARCH 10
 - 1.7 ARRANGEMENT OF THE THESIS 12
- CHAPTER 2 LITERATURE REVIEW..... 13**
 - 2.1 SCOUR MECHANISMS 13
 - 2.1.1 *Local scour* 13
 - 2.1.2 *Contraction scour*..... 14
 - 2.1.3 *Natural scour* 14
 - 2.1.4 *Global scour*..... 15
 - 2.2 THE DANGER OF SCOUR IN BRIDGES..... 15
 - 2.3 SCOUR MONITORING TECHNIQUES 17
 - 2.3.1 *Visual inspection*..... 18
 - 2.3.2 *Single-use devices* 18
 - 2.3.3 *Physical probing* 19
 - 2.3.4 *Sounding rods*..... 20
 - 2.3.5 *Time-domain reflectometry*..... 21
 - 2.3.6 *Ground-penetrating radar* 22
 - 2.3.7 *Driven or buried rod devices*..... 23
 - 2.3.8 *Electrical conductivity devices* 25
 - 2.3.9 *Sonar* 25
 - 2.3.10 *Vibration- and tilt-based methods*..... 27
 - 2.3.11 *Smart rocks*..... 28

2.3.12	<i>Underwater surface-water vehicles</i>	29
2.3.13	<i>Common challenges and the way forward</i>	31
2.4	STATE OF KNOWLEDGE OF VIBRATION-BASED SCOUR DETECTION METHODS	35
2.4.1	<i>Natural frequency as an indicator of scour</i>	35
2.4.2	<i>Acceleration-time-history-based parameters as indicators of scour</i>	52
2.4.3	<i>Mode-shape-based parameters as indicators of scour</i>	54
2.4.4	<i>Research gaps</i>	55
CHAPTER 3 FIELD STUDIES		57
3.1	FEASIBILITY STUDY ON NINE WELLS BRIDGE	57
3.1.1	<i>Numerical Modelling</i>	58
3.1.2	<i>Natural frequency variation due to scour</i>	63
3.1.3	<i>Natural frequency variation due to deck damage</i>	64
3.2	FIELD TRIAL AT BAILDON BRIDGE	66
3.2.1	<i>Baildon Bridge</i>	66
3.2.2	<i>Riverbed scanning with sonar</i>	68
3.2.3	<i>Initial numerical scour simulation</i>	70
3.2.4	<i>Instrumentation</i>	73
3.2.5	<i>Modal analysis</i>	75
3.2.6	<i>Numerical model updating based on initial experimental results</i>	78
3.2.7	<i>Natural frequency change due to scour repair</i>	82
3.2.8	<i>Mode shape variation due to scour repair</i>	85
3.2.9	<i>Spectral density variation due to scour repair</i>	87
3.3	SUMMARY.....	89
CHAPTER 4 GEOTECHNICAL-CENTRIFUGE MODEL EXPERIMENTAL PROGRAMME		90
4.1	BACKGROUND.....	91
4.2	CENTRIFUGE MODELLING.....	91
4.3	INTRODUCTION TO THE EXPERIMENTAL METHOD AND NOMENCLATURE	93
4.4	FULL-SCALE AND SMALL-SCALE BRIDGE ELEMENT SELECTION	95
4.4.1	<i>Full-scale bridge selection</i>	95
4.4.2	<i>The method of scaling down to a simplified model</i>	97
4.4.3	<i>Properties of the small-scale simplified bridge models</i>	99
4.5	CENTRIFUGE EXPERIMENTAL PROGRAMME	101
4.5.1	<i>Model structure preparation</i>	103
4.5.2	<i>Soil model preparation</i>	105
4.5.3	<i>Excitation sources</i>	108
4.5.4	<i>Data-acquisition system</i>	110
4.5.5	<i>Centrifuge flight programme</i>	110
4.6	FIXED-BASE TESTS.....	113
4.7	MODAL ANALYSIS	114
4.7.1	<i>Models excited by the automatic modal hammer</i>	114
4.7.2	<i>Models excited by the piezoelectric actuator</i>	115

4.7.3	<i>Abnormal behaviours observed</i>	116
4.8	NATURAL FREQUENCY SENSITIVITY TO SCOUR	118
4.8.1	<i>Model 1: Integral bridge</i>	119
4.8.2	<i>Model 2: Pile bent foundation</i>	120
4.8.3	<i>Model 3: Shallow foundation</i>	121
4.8.4	<i>Model 4: single pile foundation</i>	123
4.9	SPECTRAL DENSITY SENSITIVITY TO SCOUR	124
4.9.1	<i>Model 1: Integral bridge</i>	124
4.9.2	<i>Model 2: Pile bent foundation</i>	125
4.9.3	<i>Model 3: Shallow foundation</i>	128
4.9.4	<i>Model 4: Single pile foundation</i>	130
4.10	MODE SHAPE SENSITIVITY TO SCOUR	132
4.10.1	<i>Model 1: integral bridge</i>	132
4.10.2	<i>Model 2: pile bent foundation</i>	135
4.10.3	<i>Model 3: shallow foundation</i>	136
4.10.4	<i>Model 4: Single pile foundation</i>	137
4.11	OVERALL SCOUR MONITORING POTENTIAL OF NATURAL FREQUENCIES, MODAL SPECTRAL DENSITIES AND MODE SHAPES.....	138
4.12	SMALL-STRAIN SHEAR MODULUS OF SOIL.....	141
4.12.1	<i>Derivation of small-strain shear modulus from the observed shear waves</i>	141
4.12.2	<i>Estimated small-strain shear modulus profiles</i>	143
4.13	SUMMARY.....	145

CHAPTER 5 NUMERICAL SIMULATION OF SENSITIVITIES IN BRIDGE NATURAL FREQUENCIES AND MODE SHAPES TO SCOUR..... 146

5.1	INTRODUCTION	147
5.2	WINKLER SPRING MODEL FOR PILES OF BRIDGES 1 AND 2	149
5.2.1	<i>Lateral spring stiffness from the American Petroleum Institute (API) method</i>	150
5.2.2	<i>Lateral spring stiffness from small strain shear modulus</i>	150
5.2.3	<i>Soil-pile adhesion spring stiffness from API method</i>	151
5.2.4	<i>Tip resistance spring stiffness from API method</i>	152
5.3	NUMERICAL MODELLING OF A SINGLE PILE OF FULL-SCALE BRIDGE 2 USING EXPERIMENTAL RESULTS FOR SMALL-SCALE MODEL 4: SINGLE PILE.....	153
5.3.1	<i>Numerical modelling of the single pile foundation with a fixed base</i>	153
5.4	NUMERICAL MODELLING OF FULL-SCALE BRIDGE 2 (SIMPLY SUPPORTED BRIDGE WITH A PILE BENT FOUNDATION) USING THE EXPERIMENTAL RESULTS FOR SMALL-SCALE MODEL 2 (PILE BENT FOUNDATION)....	155
5.4.1	<i>Numerical modelling of the pile bent foundation with a fixed base in small- and full-scales.</i>	156
5.4.2	<i>Inclusion of soil-structure interaction to the full-scale pile bent numerical model</i>	160
5.4.3	<i>Extension of the calibrated pile bent FE model to represent Bridge 2</i>	169

5.5	NUMERICAL MODELLING OF FULL-SCALE BRIDGE 1 (INTEGRAL BRIDGE WITH PILE BENT FOUNDATIONS) USING THE EXPERIMENTAL RESULTS FOR SMALL-SCALE MODEL 1 (INTEGRAL BRIDGE WITH PILE BENT FOUNDATIONS).....	173
5.5.1	<i>Numerical modelling of the Integral bridge with a fixed base in small- and full-scales ...</i>	173
5.5.2	<i>Inclusion of soil-structure interaction to the full-scale Bridge 1 numerical model.....</i>	176
5.6	MACRO AND WINKLER SPRING ELEMENT SOIL-STRUCTURE INTERACTION REPRESENTATION FOR SHALLOW PAD FOUNDATION OF BRIDGE 3.....	182
5.6.1	<i>Gazetas Method for determining the stiffnesses of the macro element model for modelling soil-pad footing interaction.....</i>	183
5.6.2	<i>API method for determining the stiffnesses of the macro element model for modelling soil-pad footing interaction</i>	184
5.7	NUMERICAL MODELLING OF FULL-SCALE BRIDGE 3 (SIMPLY SUPPORTED BRIDGE WITH A SHALLOW PAD FOUNDATION) USING THE EXPERIMENTAL RESULTS FOR SMALL-SCALE MODEL 3 (SHALLOW PAD FOUNDATION)	184
5.7.1	<i>Numerical modelling of the shallow pad foundation with a fixed base in small- and full-scales</i>	185
5.7.2	<i>Inclusion of soil-structure interaction to the full-scale shallow pad foundation.....</i>	186
5.7.3	<i>Extension of the calibrated shallow foundation FE model to represent Bridge 3.....</i>	191
5.8	SUMMARY.....	196
CHAPTER 6	DISCUSSION	198
6.1	COMPARATIVE FEASIBILITY OF VIBRATION-BASED SCOUR MONITORING	198
6.2	SCOUR SENSITIVITY OF THE THREE SCOUR INDICATORS	199
6.3	ASSUMPTIONS	202
6.4	NONLINEARITIES	204
6.5	POTENTIAL BEHAVIOUR IN COHESIVE SOILS.....	207
6.6	SCOUR MONITORING POTENTIAL IN DIFFERENT TYPES OF BRIDGES AND FORMS OF SCOUR	209
CHAPTER 7	LIMITATIONS OF THIS RESEARCH AND SUGGESTIONS FOR FUTURE RESEARCH AND PRACTICE	211
7.1	RECOMMENDED FURTHER RESEARCH AREAS.....	211
7.2	A RECOMMENDED APPROACH FOR USING THIS VIBRATION-BASED SCOUR MONITORING METHOD IN PRACTICE	212
CHAPTER 8	CONCLUSIONS AND RECOMMENDATIONS	214
REFERENCES	216

List of tables

Table 2.1 Advantages and limitations of single-use devices	19
Table 2.2 Advantages and limitations of physical probing	20
Table 2.3 Advantages and limitations of sounding rods	21
Table 2.4 Advantages and limitations of time-domain reflectometry	22
Table 2.5 Advantages and limitations of ground-penetrating radar	23
Table 2.6 Advantages and limitations of magnetic sliding collar device	24
Table 2.7 Advantages and limitations of vibration-based driven rods	24
Table 2.8 Advantages and limitations of electrical conductivity devices	25
Table 2.9 Advantages and limitations of different sonar monitoring techniques	26
Table 2.10 Advantages and limitations of vibration and tilt-based scour monitoring	28
Table 2.11 Advantages and limitations of smart rocks	29
Table 2.12 Advantages and limitations of underwater/surface-water vehicles	30
Table 2.13 A study on the best location for bridge scour monitoring	33
Table 3.1 Details of the structural elements used for the numerical model of Nine Wells Bridge	59
Table 3.2 Natural frequencies estimated by the FE model (before correcting the in-plane deck stiffness)	61
Table 3.3 Natural frequencies estimated by the FE model (after correcting the in-plane deck stiffness)	62
Table 3.4 The natural frequency change of the bridge due to the introduced damage case in the deck	65
Table 3.5 Mode shapes captured with the initial FE model and the expected frequency shifts due to scour hole at the south pier	72
Table 3.6 Experimentally observed mode shapes versus mode shapes estimated by the FE model .	81
Table 3.7 Natural frequency change due to scour backfilling: comparison between experiment and FE simulation with the updated model	83
Table 4.1 The three types of full-scale bridges considered	96
Table 4.2 Scaling laws applicable to small-scale centrifuge models (Madabhushi, 2014)	99
Table 4.3 Model element selection (shaded properties adhere to the scaling laws)	100
Table 4.4 Geotechnical properties of Hostun sand (Futai et al., 2018)	105
Table 4.5 The scour steps around the bridge models	112
Table 4.6 Analysis of the hypothesis: a foundation undergoing local scour can be located using changes of mode shape (Model 1)	133
Table 5.1 The relationship between tip resistance and axial tip deflection of a pile (API, 2002).....	152
Table 5.2 Eight numerical analysis cases with different modelling assumptions	163

List of figures

Figure 1.1 An example set-up of the vibration-based bridge scour monitoring technique	2
Figure 1.2 Soil-structure interaction change from no scour to global and local scour	5
Figure 1.3 Methodology flow chart	9
Figure 2.1 Contraction scour (CIRIA, 2015)	14
Figure 2.2 Shape of a local and global scour	15
Figure 2.3 Top 10 causes of bridge failures in the US during 1989 and 2000: based on the data from Wardhana and Hadipriono(2003)	16
Figure 2.4 Shi-Ting-Jiang Bridge failed because of scour in 2010 (CNTV, 2010)	17
Figure 2.5 Bridge sites based on the type of fixed scour monitoring instruments present (Hunt, 2009)	18
Figure 2.6 Simple float-out device	18
Figure 2.7 A diver carrying out an underwater bridge inspection (Diving Services Inc., 2017).....	20
Figure 2.8 The arrangement of a typical TDR (Yu, Zhang and Tao, 2013).....	22
Figure 2.9 Magnetic sliding collar (Fondriest Environmental Inc., 2017)	23
Figure 2.10 The prototype robotic system (a) 3D rendering of the device (b) device in operation	29
Figure 2.11 (a) Unmanned surface vehicle (USV) (b) Remotely operated vehicle (ROV) (c) Unmanned underwater vehicles (UUV).....	31
Figure 2.12 Different locations studied for placing sensors to measure scour at a bridge foundation.	32
Figure 2.13 Natural frequency and scour depth relationship of a pier modelled as a fixed cantilever	36
Figure 2.14 Experimental setup in Elsaid and Seracino (2014)	38
Figure 2.15 (a) Natural frequency variation of the single pile with scour and (b) experimental setup in Prendergast et al. (2013).....	39
Figure 2.16 Experimental setup of the deep foundation (a) during the experiment (b) schematic diagram (Briaund et al., 2010).....	40
Figure 2.17 Change of fundamental natural frequency for (a) shallow foundation, which failed after 7 hours and (b) deep foundation, which failed after 4 hours in the flume (Briaund et al., 2010)	41
Figure 2.18 Frequency change with scour in the field experiment (Prendergast et al., 2013).....	41
Figure 2.19 Arrangement of an impact test by Shinoda, Haya and Murata (2008) (a) illustration (b) in practice	43
Figure 2.20 Foundation exposure of Hsichou Bridge, Taiwan (Ko et al., 2010).....	44
Figure 2.21 Natural frequency variation with scour depth observed by Briaund et al. (2010)	45
Figure 2.22 Laboratory experiment (a) test setup and (b) the representative numerical model (Prendergast et al., 2013).....	46
Figure 2.23 vehicle-bridge-soil interaction model in Prendergast, Hester and Gavin (2016a).....	47
Figure 2.24 Variation of the natural frequency with scour depth for three types of soil	48
Figure 2.25 Changes in natural frequencies of the first five modes due to 5 m of scour (Prendergast et al., 2017).....	49
Figure 2.26 Determining the point corresponding to the critical frequency ratio of the bridge.....	50

Figure 2.27 Effect of inclusion of water-structure interaction on scour and natural frequency relationship of the FE model.....	52
Figure 2.28 Distance versus the scour indicator, different scour levels were simulated at 60 m from the bridge start (Fitzgerald et al., 2019)	53
Figure 2.29 Variation of RMS acceleration values in the small-scale experiment, as shown in Masui and Suzuki (2009)	54
Figure 2.30 Simulation results of local scour at the bridge pier of Malekjafarian et al. (2019).....	55
Figure 3.1 Nine Wells Bridge used for the scour simulation (courtesy of Tina Schwamb)	58
Figure 3.2 FE model of Nine Wells Bridge	59
Figure 3.3 Natural frequency change with hypothetical scour depths.....	64
Figure 3.4 Baildon bridge crossing the river Aire © 2020 Bing maps / Blom	67
Figure 3.5 Elevation of Baildon Bridge. All dimensions in m (courtesy of Bradford Metropolitan Council).....	67
Figure 3.6 BridgeCat mobile bridge inspection system scanning the riverbed using sonar.....	68
Figure 3.7 Sonar scans showing the change of the bed profile (Image courtesy of Jenny Roberts, Gaist Solutions)	69
Figure 3.8 Scour backfill at the south bridge pier	69
Figure 3.9 Initial Finite-Element model developed to represent Baildon Bridge	70
Figure 3.10 Data-acquisition system at Baildon Bridge.....	74
Figure 3.11 (a) cables run on a pre-tensioned wire (b) an accelerometer mounted on the bridge.....	74
Figure 3.12 Arrangement of accelerometers at Baildon Bridge	75
Figure 3.13 (a) An example acceleration time history trace of a dataset, (b) the PSD plot corresponding to the full dataset and (c) the corresponding dynamic displacement trace	77
Figure 3.14 First SVPSD of adjacent datasets showing consistent peaks at 4.5 Hz and 18.75 Hz.....	79
Figure 3.15 Modal assurance criteria for the dataset combinations at modal peaks near 4.5 Hz and 18.75 Hz	79
Figure 3.16 Lateral spring stiffness profiles used for the numerical model	82
Figure 3.17 SVPSD spectra of six adjacent 10-minute datasets before and after	83
Figure 3.18 Natural frequency variation estimated by numerical simulations compared with the experimentally observed natural frequency uncertainty	84
Figure 3.19 Change of the shapes due to scour	86
Figure 3.20 The variation of mean modal PSD of horizontal vibration at the middle of the south bridge pier (accelerometer 2)	88
Figure 4.1 Properties of full-scale and 1/N scale soil models (both at 1g)	92
Figure 4.2 Turner beam centrifuge, where all tests were conducted. Photograph from SERIES (2011)	93
Figure 4.3 Scaling down of three full-scale bridge types to four small-scale centrifuge models.....	98
Figure 4.4 Experimental setups, sensor arrangement and scour levels corresponding to all the models in the centrifuge container – all dimensions are in mm.	102
Figure 4.5 The cylindrical centrifuge container with all four structural models and the excitation setup	103
Figure 4.6 Automatic sand pourer during calibration.....	106

Figure 4.7 Automatic sand pouring around Model 3 – the shallow pad foundation	107
Figure 4.8 Instrument placement at different sand fill heights	108
Figure 4.9 Amplified piezoelectric actuator setup (a) in the experiment (b) diagram	109
Figure 4.10 Setup of the automatic modal hammer controlled by air-pressure (a) in the experiment (b) diagram.	110
Figure 4.11 A 20-mm deep local scour hole created at the pier foundation of Model 1 (M1S1 scour step)	111
Figure 4.12 Fixed base test being carried out for Model 1	113
Figure 4.13 Time histories of Model 3 – scour step M3S5 (a) input force, (b) part of a segmented input force and (c) corresponding output acceleration of M3P1	114
Figure 4.14 Accelerance FRF and coherence spectra of Model 3 during the scour step of M3S5....	115
Figure 4.15 Measured input excitation and the response acceleration of one sensor in Model 1 (scour step M1S7b)	116
Figure 4.16 First SVPSD of Model 1 response for the same scour depth but with two excitation sources: no actuator (step M1S7a) and with the actuator (step M1S7b)	116
Figure 4.17 Variation of first SVPSD spectrum for tests performed at different centrifuge acceleration levels for the same scour step (M1S6)	117
Figure 4.18 The jammed automatic modal hammer during no scour case	118
Figure 4.19 Estimated full-scale natural frequency variation of the integral bridge (Model 1) for different cases of scour	119
Figure 4.20 Estimated full-scale natural frequency variation of the pile bent foundation (Model 2) for different cases of scour	121
Figure 4.21 Estimated full-scale natural frequency variation of the shallow pad foundation (Model 3) for different cases of scour	122
Figure 4.22 Estimated full-scale natural frequency variation of the single pile foundation (Model 4) for different cases of scour	123
Figure 4.23 First singular values (SVPSD) at the modal peak vs different scour cases of Model 1 (integral bridge) in equivalent full-scale	125
Figure 4.24 The variation of normalised accelerance FRF of Model 2 with scour at its foundation... ..	126
Figure 4.25 Model 2 first singular value (SVPSD) spectra for different scour cases.	128
Figure 4.26 Model 3: Variation of FRF accelerance magnitude with scour depth (FRF normalised on maximum resulting from local scour at 1.3 m depth)	129
Figure 4.27 Model 3: the first SVPSD of representative full-scale shallow foundation	130
Figure 4.28 Model 4: Relationship between normalised spectral density at first modal peak and full-scale scour	132
Figure 4.29 Model 1: integral bridge normalised mode shapes.	134
Figure 4.30 Model 1: integral bridge: Power Spectral Density (PSD) of three different sensor types with three different scour cases	135
Figure 4.31 Model 2: pile bent mode shape variation with different scour cases	136
Figure 4.32 Model 3: shallow foundation, the variation of mode shape with local and global scour cases	137

Figure 4.33 Model 4: single pile foundation, the normalised mode shapes under different scour cases	137
Figure 4.34 Summary of frequency sensitivities at the full-scale	138
Figure 4.35 Sensitivity of SVPSD at the modal peak to scour	140
Figure 4.36 A shear wave captured by a column of accelerometers, C11 – C15	141
Figure 4.37 Variation of G_0 profiles with scour near the Model 1 integral bridge in equivalent full-scale	144
Figure 5.1 Change in stiffness profile around a bridge due to local and global scour cases	147
Figure 5.2 Methodology followed to create a numerical model for the full-scale bridge using experiment results	149
Figure 5.3 Winkler spring representation of soil-pile interaction.....	149
Figure 5.4 Model 4 fixed base (a) experimental setup and (b) FE model	154
Figure 5.5 Sensitivity of natural frequency of the FE model to its input properties	154
Figure 5.6 The fixed base small-scale Model 2 for the case of no scour	157
Figure 5.7 Variation of the fundamental natural frequency with scour depth of Model 2 with fixed base	158
Figure 5.8 The fixed base small-scale Model 2 for the case of no scour	159
Figure 5.9 Comparison of natural frequency vs scour depth at full-scale and small-scale (converted to full-scale) for fixed base pile bent foundation	160
Figure 5.10 Pile bent (with soil) for the case of no scour numerical modelling and experiment setup	161
Figure 5.11 Deflection bowl of a foundation element on springs.....	162
Figure 5.12 Lateral spring stiffness (K_H) profiles used in different FE numerical analysis cases.....	164
Figure 5.13 Natural frequency variation with scour depth: Experimental observations and FE estimation for local scour simulated by using spring deleting method	165
Figure 5.14 Comparison of natural frequency variation estimated by two simulation techniques and experimentally observed for local and global scour	167
Figure 5.15 Change of mode shape with scour – FE simulation and experimental observations	168
Figure 5.16 FE model developed to simulate simply supported bridge with deep pile bent in full-scale (Bridge 2)	170
Figure 5.17 Change in frequency with scour depth for the simply supported bridge with deep pile bent foundation (Bridge 2) estimated by the FE model.....	171
Figure 5.18 Change in mode shape with scour depth for Bridge 2 (two-span simply supported bridge with piled foundation).....	172
Figure 5.19 FE model developed to represent small-scale Model 1 (two-span integral bridge with piled foundations) with a fixed base	175
Figure 5.20 FE model developed to represent full-scale Bridge 1 (two-span integral bridge with piled foundations) with either fixed base or soil-structure interaction	175
Figure 5.21 FE models with fixed base simulating scour at all different scales	176
Figure 5.22 Scour simulation with the FE model and the centrifuge experiment	177
Figure 5.23 Comparison of the mode shapes estimated by the FE and the experiment for the case where there was no scour present	179

Figure 5.24 Mode shape variation with pier scour (FE estimates vs experiment observations)	180
Figure 5.25 Mode shape variation for abutment scour cases (FE estimates vs experiment observations)	181
Figure 5.26 Types of soil-structure interaction models used to represent a pad foundation	182
Figure 5.27 Micro-element model representation of a soil-pad footing interaction	183
Figure 5.28 The fixed based experiment and the FE models simulating it at small-scale and full-scale	186
Figure 5.29 Natural frequency variation simulated by the fixed based experiment and the FE models at small-scale and full-scale	186
Figure 5.30 FE model for the structure of the shallow foundation combined with a Winkler model and a macro element model representing soil.	187
Figure 5.31 Natural frequency estimated by the FE model and the experiment	189
Figure 5.32 Experiment and FE estimate of the fundamental mode shape (shallow foundation)	190
Figure 5.33 FE model of the Bridge 3 (a two-span simply supported bridge with the shallow foundation: view from the bottom of the bridge)	192
Figure 5.34 Natural frequency sensitivity to scour of the Bridge 3 (a two-span simply supported bridge with the shallow pad foundation)	193
Figure 5.35 Sensitivity study on the effect of change in bearing stiffness on the natural frequency change resulting from scour.	194
Figure 5.36 Variation of mode shapes for local and global scour, as simulated by the FE model of the simply supported bridge with shallow foundation (Bridge 3).	195
Figure 6.1 Reduction in stiffness properties due to increased strain caused by scour	205

Nomenclature

<i>A</i>	<i>Cross-sectional area</i>
<i>APA</i>	<i>Amplified piezoelectric actuator</i>
<i>API</i>	<i>American Petroleum Institute</i>
<i>B</i>	<i>Width</i>
<i>C04</i>	<i>Accelerometer number 04 that measured shear waves during the centrifuge test</i>
<i>D</i>	<i>depth from the ground level</i>
<i>D</i>	<i>The diameter or the depth of the smallest dimension of a structural element</i>
<i>D₁₀</i>	<i>particle diameter at 10% finer</i>
<i>D₅₀</i>	<i>particle diameter at 50% finer</i>
<i>d_f</i>	<i>Full-scale depth</i>
<i>D_r</i>	<i>Relative density</i>
<i>d_s</i>	<i>Small-scale depth</i>
<i>E</i>	<i>Young's modulus of elasticity</i>
<i>E₀</i>	<i>Small strain elastic modulus of soil</i>
<i>E_f</i>	<i>Full-scale Young's modulus of elasticity</i>
<i>e_{max}</i>	<i>Maximum void ratio</i>
<i>e_{min}</i>	<i>Minimum void ratio</i>
<i>E_s</i>	<i>Small-scale Young's modulus of elasticity</i>
<i>f</i>	<i>Natural frequency</i>
<i>FDD</i>	<i>Frequency domain decomposition</i>
<i>FE</i>	<i>Finite element</i>
<i>FEM</i>	<i>Finite element modelling</i>
<i>FRF</i>	<i>Frequency response function</i>
<i>g</i>	<i>normal gravity on the earth surface (9.81 ms⁻²)</i>
<i>G</i>	<i>Shear Modulus</i>
<i>G₀</i>	<i>Small-strain shear modulus</i>
<i>G_s</i>	<i>The specific gravity of solids</i>
<i>G_{yy}(f)</i>	<i>Matrix of PSD at discrete frequencies, f</i>
<i>H</i>	<i>Horizontal direction</i>
<i>I</i>	<i>The second moment of area</i>
<i>k</i>	<i>Stiffness</i>
<i>K</i>	<i>initial modulus of subgrade reaction</i>
<i>K₀</i>	<i>Lateral earth pressure at rest</i>
<i>K_H</i>	<i>The stiffness of a Winkler spring representing lateral horizontal soil-pile interaction</i>
<i>k_i</i>	<i>Initial modulus of subgrade reaction</i>
<i>K_{rx}</i>	<i>Macro element spring representing rotational stiffness about the x-axis</i>
<i>K_{rz}</i>	<i>Macro element spring representing rotational stiffness about the z-axis</i>
<i>k_s</i>	<i>coefficient of subgrade reaction</i>
<i>K_T</i>	<i>Stiffness of a Winkler spring representing soil-pile interaction at the toe of a pile</i>
<i>K_v</i>	<i>Stiffness of a Winkler spring representing vertical shear skin friction at the soil-pile interface</i>
<i>K_y</i>	<i>Macro element spring representing horizontal (y-direction) translational stiffness</i>

K_z	Macro element spring representing vertical (z-direction) translational stiffness
L	Length
L_0	Initial height (before scour)
M	Mass
MAC	Modal assurance criterion
MEMS	Microelectromechanical systems
M1M3	Centrifuge <u>Model number 1</u> <u>MEMS ADXL1002 accelerometer number 3</u>
M2m2	Centrifuge <u>Model number 2</u> <u>MEMS ADXL78 accelerometer number 2</u>
M3P1	Centrifuge <u>Model number 3</u> <u>Piezoelectric accelerometer number 1</u>
M4S3	Centrifuge <u>Model number 4</u> <u>Scour step 3</u>
N	Scale factor
P	Lateral soil resistance per unit length
PSD	Power spectral density
P_u	Ultimate bearing capacity of soil
Q	Mobilised end bearing
R	Radius
R_c	Critical frequency ratio
RMS	Root mean square
RTRI	Railway Technical Research Institute (Japan)
s	Spacing between two adjacent Winkler springs
$S(f)$	Matrix of singular values at discrete frequencies, f
SNR	Signal to noise ratio
SPT	Standard penetration test
SVPSD	Singular values of the power spectral density matrix
t	Soil-pile adhesion
$U(f)$	Matrix of singular vectors at discrete frequencies, f
V	Vertical direction
ν_p	Poisson's ratio
ν_s	Shear wave velocity
x, \ddot{x}	Displacement, acceleration
y	Lateral deflection of a section of pile surrounded by soil
z	soil-pile deflection in the vertical direction
3D	Three-dimensional
Δd	Spacing between two accelerometers
ΔL	Deflection
Δt	time lag
δ	Friction angle between the soil and the pile wall
ρ	bulk density
σ'_0	Mean principle effective stress
σ_f	Full-scale self-weight stress
σ_s	Small-scale self-weight stress
σ'_v	Vertical effective stress
Φ_{crit}	Critical state friction angle
ω	Angular velocity

Chapter 1

Introduction

This chapter provides the background to this research on vibration-based bridge scour monitoring. The research project is introduced with the problem statement, the list of objectives, the research methodology adopted, and an overview of the innovative aspects of the research. Finally, the content of the various chapters is summarised.

1.1 Background

Bridges are the lynchpins of any rail or road network, allowing safe and efficient passage for people and goods traffic across various physical obstacles. Bridges overcome these obstacles while providing seamless connectivity for rail or road traffic. Such connectivity, however, cannot be taken for granted, as bridges can, and sometimes do, fail. There are many potential causes of bridge failure, such as overloading, earthquakes, fire and corrosion. Nevertheless, one cause of failure stands out – scour. Recent surveys have indicated that scour and related hydraulic causes account for more than 50% of bridge failures around the world (Wardhana and Hadipriono, 2003; Hunt, 2009)

Scour is the result of the erosion of soil around bridge foundations due to the action of fast-flowing water. Extensive scour around the foundations results in deep pits, which are commonly referred to as scour holes. The creation of such scour holes removes soil, which was previously supporting the bridge foundations. Such loss of soil support, especially during flooding, can lead to a rapid reduction in bridge support stiffness, and even catastrophic collapse (Arneson et al., 2012). A large number of such bridge collapses in the past have resulted in the loss of human lives, severe transport disruption and economic loss (Construction Industry Research and Information Association (CIRIA), 2015). These collapses could have been avoided if scour had been detected early and remedial action taken to mitigate the scour-induced damage.

Vibration-based scour monitoring is an indirect monitoring technique to detect scour at bridge foundations. It aims to identify changes in bridge vibration properties to detect scour. Vibrations are typically present in bridges as a result of ambient excitations caused by vehicle and wind excitation. Bridge vibrations can also be generated artificially. Any bridge will have its own inherent vibration properties, such as natural frequency. Such vibration-based properties remain constant under normal circumstances when bridge stiffness, mass and damping are unchanged. However, scour is an exceptional circumstance, which can result in a reduction in stiffness due to the loss of soil support around the bridge foundations. Therefore, scour results in changes in modal properties, for example, natural frequency (Prendergast and Gavin, 2014).

Hence, simply by monitoring bridge vibrations, any changes in scour depth around the piers could potentially be captured, in theory at least, as a change in vibration property.

An example set-up of vibration-based scour monitoring is shown in Figure 1.1. Here, vehicles passing over the bridge generate small ambient structural vibrations, which are continuously captured by an accelerometer mounted near the top of the pier. The accelerometer measurements can then be analysed to estimate vibration properties such as natural frequency, which do not change under normal circumstances, thus indicating the “structural health” of the bridge. When scour occurs, the vibration properties change as a result of the change in bridge stiffness, allowing detection of the presence of scour. This method is particularly appealing for bridges that usually experience a degree of continuous ambient excitation, which can be measured using continuous real-time remote monitoring techniques. Additionally, unlike most other monitoring techniques, there is no requirement for instrumentation to be installed underwater, making vibration-based techniques reliable and durable even during heavy flooding.

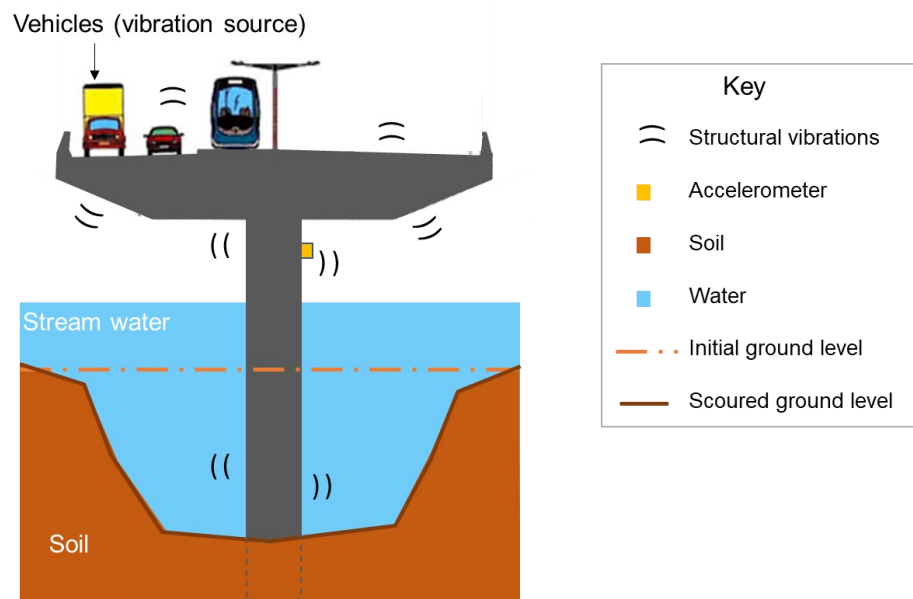


Figure 1.1 An example set-up of the vibration-based bridge scour monitoring technique

Vibration-based techniques have been studied extensively, although the primary focus has been on the detection of local structural damage (e.g. crack detection of superstructure beams). However, these studies found insufficient sensitivity of vibration parameters such as the natural frequency to reliably identify the location or extent of the damage. For example, even when there was extensive damage, in the form of cracks up to half the depth of a bridge beam or pier, the resulting changes in fundamental frequency were found to be of the same order as the expected effects of environmental changes (such as temperature) and operational load effects (Farrar et al., 1994; Peeters and Roeck, 2001; Kim, Yun and Yi, 2003; Caetano and Magalha, 2009; Koo, Brownjohn and Cole, 2010; Döhler et al., 2014). Such localised

structural damage results in only local changes in stiffness and/or damping and therefore relatively small changes in the frequencies of global vibration modes. Scour, however, is a special damage case – effectively it causes a change of boundary condition at the bridge foundations. Such a change of boundary condition would result in a global stiffness reduction and therefore significantly greater changes in natural frequency of lower-order global modes of vibration. A simple model of a cantilever column idealising a bridge pier illustrates this (Figure 2.13); the natural frequencies of the column are inversely proportional to the square of the exposed length, if it is assumed to be fully fixed at ground level. In practice, the support at the base of a pier is dependent on the soil stiffness, and this would need to be taken into account for any vibration analysis.

Vibration-based studies targeting scour have emerged relatively recently and have indicated much higher frequency sensitivities than those measured as a result of local structural damage. Several numerical studies have estimated a 30 – 40% change in natural frequency for a 50% loss of pile embedment (Klinga and Alipour, 2015; Prendergast, Hester and Gavin, 2016a). Such high sensitivity in natural frequency due to scour indicates its potential for use in early scour indication. Therefore, vibration-based scour monitoring techniques, such as those using natural frequency, have significant potential to safeguard bridges from scour-induced failure and make rail and road networks more resilient.

1.2 Problem statement

Bridge scour is a dynamic and complex process that depends on the properties of water flow, sediments in the bed of the water body and properties of bridge substructure (Deng and Cai, 2010). Hence, the scour depth estimated using empirical formulae could often have a significant degree of error in the real scenario. Therefore, *in situ* scour monitoring is vital to detecting bridge scour and hence indicating when countermeasures or repairs are necessary. Even during repairs to bridge foundations, the measurement of scour depth can be important. There are examples where the repairs themselves have led to additional scour (Department for Transport UK, 2016). These problems could potentially be addressed by a reliable, real-time remote scour monitoring technique.

Various techniques have been used to monitor bridge scour, ranging from scuba divers using crude depth-measuring instrumentation underwater to high-tech autonomous underwater vehicles using sonar-based systems. Many of these current techniques only measure scour depths at a single location and/or are susceptible to damage from debris in the fast-flowing water, whilst others are labour-intensive and expensive (Prendergast and Gavin, 2014). Only some provide real-time data or information on the extent and depth of scour. These challenges hinder the ability of bridge engineers to assess the risk associated with scour-related damage to the same degree of confidence as is possible with other types of damage. This could

perhaps be one of the reasons behind a significant number of scour-induced bridge failures around the world (Melville and Coleman, 2000; Hunt, 2009; Ko et al., 2010; Dikanski et al., 2016). Hence, there is an immense need for a reliable scour monitoring technique that could reliably ensure the safety of bridge assets.

A vibration-based scour monitoring technique has significant potential since no equipment has to be underwater, and it has real-time remote monitoring capabilities. However, there are only a few field trials on real bridges, and almost all of them have found it difficult to prove the viability of this technique (Section 2.4.1.2). Testing scour monitoring techniques in practice is difficult – a monitoring system would need to be installed on a candidate bridge with no guarantee of measuring any scour within the timespan of the project. On the other hand, full-scale testing of controlled scouring of a bridge is not viable because of the costs involved, and tests on scaled-down soil-structure models at normal gravity are unable to simulate the real natural frequencies of a full-scale structure because of the incorrect scaling of the soil properties (explained in detail in Section 4.2). Centrifuge modelling can be used to eliminate this problem by allowing full-scale (also referred to as prototype-scale in centrifuge modelling) stress levels to exist within a small-scale model (Madabhushi, 2014). However, to the author's knowledge, centrifuge modelling has not yet been used for vibration-based testing of bridges.

Another important consideration is whether or not vibration parameters of a bridge is less sensitive to “local scour” than to “global scour” and how to simulate these different effects numerically, which has not yet been examined (see Chapter 2). As shown in Figure 1.2, local scour involves only a local lowering of the bed level immediately around the foundation; and global scour involves lowering of the bed soil level uniformly everywhere (Sumer, Bundgaard and Fredsøe, 2005; Mohamed, 2012). In global scour, Case (1), the scoured ground level has no overburden pressure and thus no stiffness provided by the soil at that level; thus, the full-scour profile looks as if it has shifted down by the depth of scour. In contrast, with local scour, Case (2), the scoured ground level has some retention of overburden stress, and thus some stiffness, due to the remaining soil surrounding the scour hole. This reduced influence on stiffness may result in the natural frequencies and other modal parameters being less sensitive to local scour than to global scour; thus, this aspect requires detailed examination for the development of this monitoring technique.

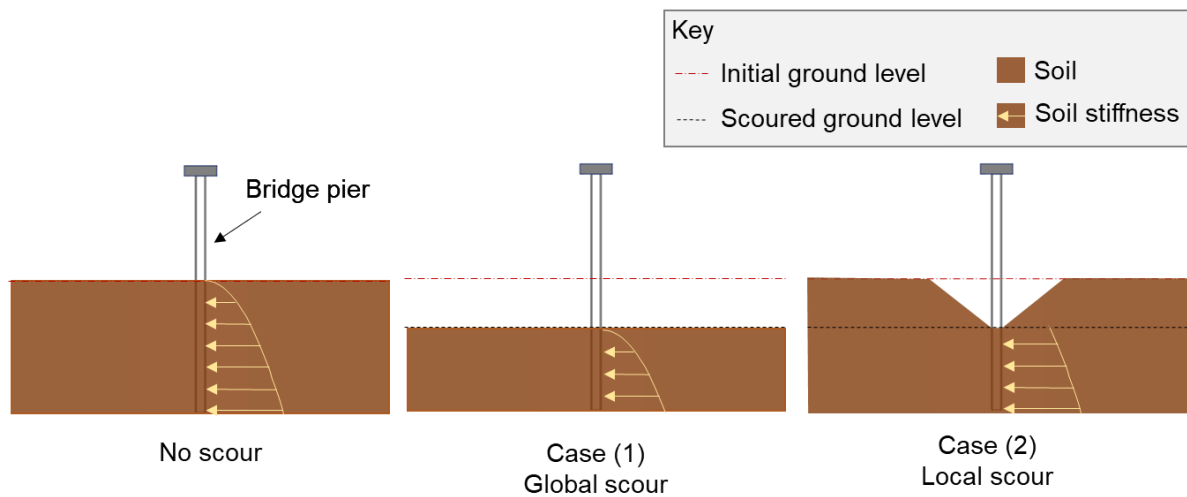


Figure 1.2 Soil-structure interaction change from no scour to global and local scour

According to Bao and Liu (2016), there are significant gaps in research related to the performance of this monitoring technique for different shapes of scour, different types of bridges and locations of sensors. Additional research gaps also exist in relation to vibration-based scour monitoring parameters other than natural frequency, as discussed in Chapter 2. The research objectives of this project were chosen to answer these research problems.

1.3 Objectives of the research

The main objective of this research was to examine the potential of vibration-based techniques for monitoring bridge scour. The following sub-objectives have been considered in the research:

1. To understand the comparative feasibility of vibration-based and other scour monitoring techniques available in the literature.
2. To evaluate the field viability of vibration-based scour monitoring.
3. To discover vibration-based parameters other than the natural frequencies for detecting scour.
4. To develop a small-scale centrifuge experimental regime for testing the broad applicability of the identified parameters for different types of:
 - a. foundation (piled/shallow pad);
 - b. bridge deck (integral/simply supported);
 - c. scour (global/local).
5. To develop numerical techniques for simulating local and global scour in different bridge configurations.

1.4 Methodology

The research objectives were achieved by following the methodology shown in Figure 1.3. This methodology is explained below.

1. Compare scour monitoring techniques

A detailed literature review first compared twelve different scour monitoring techniques, including sonar, single-use devices and vibration-based methods. The comparative limitations and advantages of these monitoring techniques indicated that a vibration-based technique has significant potential for reliable, real-time remote monitoring. Therefore, a vibration-based technique was chosen for further research.

2. Find research gaps

The state of knowledge of the vibration-based scour monitoring technique was studied to identify research gaps. A number of research gaps were identified related to the lack of field studies and small-scale-model experiments, lack of understanding on the potential of this monitoring technique in different bridge types and forms of scour, the lack of numerical scour simulation techniques, and relying primarily on only one modal parameter. The research programme was then planned to address these research gaps.

3. Examine the feasibility of vibration-based scour monitoring (Nine Wells Bridge)

The feasibility of natural frequency-based scour monitoring was examined next. The natural frequencies were estimated by creating a numerical model for Nine Wells Bridge, a three-span semi-integral bridge recently built in Cambridge. This bridge was studied because its field measurements of natural frequency were already available from a previous study of Whelan et al. (2010). These field measurements could be used to validate the numerical model created. This validated numerical model simulated two hypothetical damage cases: (i) scour damage to two bridge pier foundations; and (ii) crack damage to the deck. The aim of this feasibility study was to assess whether natural frequencies based scour damage detection has greater potential than natural frequency based deck damage detection, which has proven to be ineffective in practice due to insufficient sensitivity (Section 2.4.1). This feasibility study was an important step of verification before proceeding to the next experimental steps.

4. Trial in the field (Baildon Bridge)

A field trial was conducted at Baildon Bridge in Bradford, in the UK, to study the potential of the vibration-based scour monitoring technique in practice. Baildon Bridge was found to have been scoured under part of one pier, and the scoured region was

due to be backfilled as part of a repair programme. It thus provided a rare opportunity to monitor a bridge in both a scoured and a repaired state (“scour in reverse”). The ambient vibration characteristics of this bridge were measured throughout the repair period using a set of accelerometers. The foundation-bed profiles were measured before and after repair using sonar scanning to aid numerical modelling. Three vibration-based parameters were studied: the common parameter of natural frequencies, and two parameters that had not been studied in previous research, namely, mode shape and spectral density. The changes in bridge natural frequencies and mode shapes due to scour were predicted numerically and compared with measured experimental findings.

5. Study with small-scale bridge models

The three potentially scour-sensitive parameters, namely, natural frequency, mode shape and spectral density, needed to be tested in a controlled environment to assess their potential for different bridge configurations and scour types. As such an experiment is not feasible in the field or at full-scale, small-scale testing was crucial. A small-scale testing programme was therefore developed using geotechnical centrifuge modelling. Centrifuge modelling is an experimental method used to test small-scale models at the correct stress levels, thus providing a platform to study full-scale dynamic behaviour changes of the bridge using only a small-scale model (Madabhushi, 2014). Four small-scale bridge models were constructed in the sand to represent three different full-scale hypothetical bridges representing shallow/deep foundations and integral/simple supported decks. Although the possibility of replicating Baildon Bridge properties in a small-scale laboratory model was initially attempted, uncertainties in the definition of boundary conditions led to the selection of alternative, hypothetical integral bridge models, of which boundary conditions were known and could be modelled more reliably.

Simplified versions of the bridges had to be considered in small-scale as a result of the space limitation in the standard container used in centrifuge testing, and in order to limit the number of joints required to fabricate. Only one small-scale model represented the entire hypothetical bridge (deck and foundations), while all of the others represented the different standalone foundations (“simplified” versions) of the full-scale bridges. Corresponding “small-scale simplified” bridge models (i.e. small-scale standalone foundations) do not represent the “full-scale” bridges but a “full-scale simplified” version of the bridge (i.e. full-scale standalone foundation). These simplified models were sufficient to capture changes in dynamic behaviour due to the effects of the scour cases being modelled, and, in turn, to calibrate numerical models of the simplified bridges. Two controlled types of scour were considered, namely, local scour and global scour

(Figure 1.2); and these were simulated in the experiment by vacuum suction of the soil. Automatic impact hammers were developed to excite the models; however, ambient vibration was also present during testing. The effect of water in the soil was not explicitly modelled based on the assumption that natural frequency sensitivities would not change as a result of soil saturation (see Section 2.4.1.4).

In order to confirm the results of the centrifuge tests and to support numerical modelling, fixed base tests were conducted for all bridge models providing fixed bases at the soil surface level of all scour depths considered. At any given scour depth, the fixed base test provides an upper bound natural frequency estimate to the corresponding centrifuge test, with soil, since soil provides a lower stiffness than a fixed base. The sensitivities of the considered modal parameters of small-scale simplified models were brought to their full-scale (“full-scale simplified”) by applying appropriate scaling factors.

6. Numerical modelling study

The estimated results for the simplified bridges in the centrifuge test do not directly represent bridges with bridge decks. Therefore, numerical models were developed to extrapolate the experimentally observed results from small-scale simplified models to full-scale simplified models, and then to full-scale bridges with bridge decks. Initially, numerical models were created for the simplified bridges, both in small- and full-scale, but with fixed bases (without soil). The accuracy of the scaling of structures could be confirmed by comparison of the natural frequencies estimated by these two models with the fixed-based experimental results. Confirming the accuracy of scaling was important since there were material property changes from full-scale (reinforced concrete) to small-scale (aluminium), and a number of assumptions were made during the selection of sections (see Section 4.4.2). Once the scaling from small-scale simplified bridges to full-scale simplified bridges had been confirmed, the full-scale simplified bridges were included with numerical soil-structure interaction, as explained in Sections 5.2 and 5.6. These numerical models of full-scale simplified bridges were calibrated for the estimated full-scale behaviour of centrifuge tests. Once calibrated, techniques were developed to simulate the effects of local and global scour observed for different levels of scour depth modelled in the centrifuge tests. These calibrated numerical models for full-scale simplified bridges were then extended to the corresponding full-scale bridges by adding the bridge deck elements, and later simulated for scour using the identified scour simulation techniques. The natural frequency and mode shape sensitivities of the centrifuge models were estimated using numerical eigenvalue analysis. All numerical modelling was carried out using CSiBridge structural analysis software.

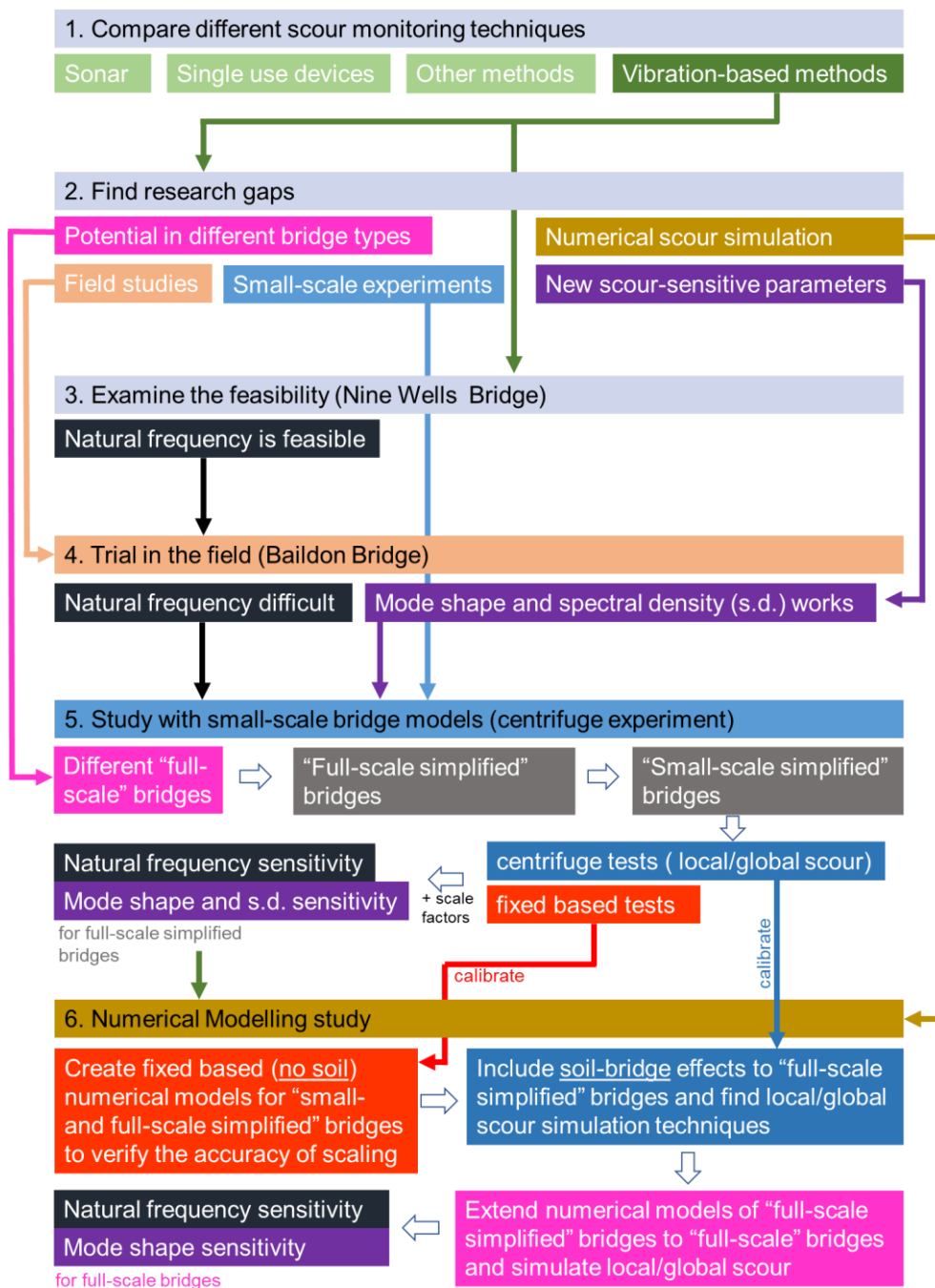


Figure 1.3 Methodology flow chart

1.5 Scope of the research

The research in this thesis focuses on monitoring one cause of bridge failure, namely, scour, using structural vibrations. Different types of bridge decks and foundations were considered in this research; however, all the bridges considered were reinforced concrete beam-slab type bridges. Other bridge types such as masonry arch bridges and suspension bridges are out of the scope of this research project, although the numerical and experimental methods developed can be extrapolated to these bridges in future studies. Only granular soils (sand/gravel) were considered in this research, and therefore, the findings of this research may not directly reflect the behaviour expected in a bridge with foundations in cohesive soils (clay).

Experimental studies examined three vibration-based parameters, namely, natural frequencies, mode shapes and spectral density. The numerical modelling aimed to study sensitivities in natural frequencies and mode shapes and to develop techniques to simulate the observed effects of scour. Therefore, numerical eigenvalue analysis was considered, which only considers undamped free vibration. Damped vibration and more complex soil-bridge-vehicle interaction models that consider the input excitation of the vehicles can estimate the spectral densities; however, such modelling is difficult to validate in practice and thus beyond the scope of this research. All numerical modelling in this research is validated by the corresponding experimental observations. The structural models were idealised by different types of finite elements, and soil-structure interaction was idealised by linear springs based on a “Winkler spring model” or a “macro element spring model” representation (Section 5.6). Other forms of modelling soil-structure interaction, such as continuous elastic half-space, are beyond the scope of this research.

1.6 Innovative aspects of the research

The research in this thesis made innovative contributions to the area of research, in identifying novel vibration-based scour-sensitive approaches to monitoring bridge scour and in conducting first-of-a-kind field experiments, laboratory experiments and numerical simulations.

A key innovation in this research is the identification of two modal parameters, separate to the natural frequency, for detecting scour in bridge foundations. The first is using the spectral density estimate at the modal peaks, which showed significantly higher sensitivity than the commonly studied vibration-based parameter of natural frequency according to both field and laboratory experiments. Another scour-sensitive parameter is mode shape, which was found to help with both the identification of a change in scour depth and the localisation of which foundation was undergoing local scour (Kariyawasam *et al.*, 2019b). Other mode-shape-based parameters, such as mode-shape ratio and mode-shape curvature, were recently proposed by Malekjafarian *et al.* (2019) and Elsaid and Seracino (2014) to detect scour (Section 2.4.3). However, the research in this thesis found that mode shapes alone can detect and even locate the foundations undergoing local scour.

This research carried out one of the first successful field experiments to showcase the potential of ambient vibration-based scour monitoring. Such field studies are essential, since the numerical modelling estimates, on which much of the potential of this monitoring technique has been based, may not always hold true in the field where there are complex environmental and operational conditions to consider. Due to the difficulty of validating this technique in the field, different approaches have been attempted in the limited number of previous studies. Some studies monitored for scour but unfortunately were not successful in detecting any scour within the monitoring period (Masui and Suzuki, 2009; Yao *et al.*, 2010b). Two studies had

some success when indirect techniques were used to study different scour depths in medium span bridges, one compared the scour levels of different piers using impact vibration (Shinoda, Haya and Murata, 2008) and another artificially scoured a bridge and studied ambient vibration (Ko et al., 2010). The research presented in this thesis adopts a new approach of monitoring ambient vibrations during backfilling of a scour hole, i.e. “scour in reverse” of a short-span bridge (Kariyawasam *et al.*, 2019c, 2021). This approach was successful in identifying the potential of using mode shapes and spectral density for monitoring scour.

To the author’s knowledge, this research also developed the first-ever centrifuge experiment for testing vibration-based methods for measurement of bridge scour (Kariyawasam *et al.*, 2020a). The limited number of previous small-scale experiments undertaken outside a centrifuge would have experienced some inevitable inaccuracies of soil stiffness scaling (Section 4.2). Centrifuge modelling corrects such scaling of soil properties, including stiffness properties, making the small-scale centrifuge models more representative of the full-scale structures. This research developed a centrifuge modelling technique involving its own automatic modal hammer excitation system, which could aid future experimental research on vibration-based monitoring techniques. This experimental programme also allowed, for the first time, comparison of multiple bridge foundation and superstructure types, and also different types of scour in a controlled experimental environment, which helped to identify which configurations of bridges have the most potential with this scour monitoring technique.

Finally, this research provided further development to existing numerical modelling techniques used to simulate vibration-based scour monitoring. Previous researchers have mainly adopted Winkler spring models of deep piled foundations, where scour was simulated by deleting the springs without distinguishing between the effects of local and global scour (Prendergast, Hester and Gavin, 2016a). The research in this thesis found that such a “spring deleting” method is appropriate to local scour simulation, but global scour simulation instead requires an alternative “spring lowering” approach (see Section 5.1). A research gap was found, in that previous work on numerical modelling only looked at the scour of deep foundation models; thus, this research has developed a shallow foundation modelling technique using macro-element models and a Winkler spring model of soil stiffness.

These new contributions support bridge engineers in leveraging the potential of vibration-based scour monitoring of bridges and encourage further development and practical implementation of this monitoring technique in the future.

1.7 Arrangement of the thesis

Chapter 1 introduces this research and the thesis. It provides a background to the vibration-based scour monitoring technique and highlights other aspects of the research, such as the objectives and the methodology followed.

Chapter 2 is a detailed literature review of the fundamentals behind scour, the current scour monitoring techniques, and the vibration-based scour monitoring method, in particular.

Chapter 3 presents two field studies on Nine Wells Bridge and Baildon Bridge. Nine Wells Bridge was studied for its feasibility in capturing scour and deck damage. This feasibility study was the deciding step before carrying out the experimental research on Baildon Bridge, where a field trial was carried out to test the potential of the vibration-based scour monitoring technique.

Chapter 4 presents the development of a centrifuge experiment to test three hypothetical full-scale bridges with small-scale models. This chapter also discusses the results of the experiment in terms of the scour monitoring potential of natural frequency, mode shape and spectral density parameters in all the models.

Chapter 5 presents a numerical modelling study that extrapolates the centrifuge experiment results to full-scale bridges. It also assesses the scour simulation techniques for local and global scour.

Chapter 6 – 8 present a discussion based on all the experimental and numerical research carried out, provide suggestions for future research, and finally, summarise the conclusions that can be drawn from the findings of this research.

Unless otherwise noted, *natural frequency* and *frequency*, in the following sections of this thesis, refer to the fundamental natural frequency of vibration of a bridge or any other structure, *mode* indicates the mode of vibration of a bridge, and *scour* refers to a certain depth of scour at a bridge foundation. *Fundamental mode* refers to the first mode of vibration or the lowest-order mode in a mentioned direction. *Longitudinal* refers to the direction along the length of an element, for a horizontal bridge deck, *longitudinal* is the horizontal direction along the centreline. *Transverse* refers to the horizontal direction normal to the longitudinal direction. *Lateral* refers to any direction in the plane normal to the length of an element, for a vertical pile, *lateral* refers to any horizontal direction. *Output-only method* refers to a system identification method that utilises only the output vibration measurements (i.e. without the input excitation measurements). *Spectral density* or *modal spectral density* refers to the spectral density estimate at a modal peak of a spectral density (e.g. power spectral density) spectrum. *Centrifuge modelling* and *centrifuge testing* refer to the geotechnical centrifuge modelling technique.

Chapter 2

Literature review

Highlights

- Scour has been reported as the most common cause of bridge failure.
- Based on a detailed review of current scour monitoring techniques, vibration-based scour monitoring was selected.
- A comprehensive review of the vibration-based scour monitoring literature identified the existing research gaps.

Scour is the engineering term that refers to the erosion of soil from around structural foundations as a result of the action of water (CIRIA, 2015). Higher scour levels around a bridge foundation can lead to its instability and even, eventual collapse. Scour is a complex process, and its monitoring and evaluation require inter-disciplinary inputs from hydraulic, geotechnical and structural engineers.

This chapter initially introduces the different scour mechanisms and the danger of bridge scour. It follows with a review of the existing scour monitoring techniques, with the intention of identifying a feasible monitoring technique for further study. The state of knowledge of this feasible monitoring technique, the vibration-based scour monitoring technique, was studied in detail at the end of this chapter with the aim of finding key research gaps.

2.1 Scour mechanisms

Scour occurs as a result of the interaction between water and bed materials. A bridge foundation embedded in any waterbed, a seabed or a riverbed, is therefore prone to scour, although only some bridges experience extensive amounts of scour. Seabed scour mechanisms have primarily been categorised as local and global scour, based on the resulting shape of scour (Sumer, Bundgaard and Fredsøe, 2005; Mohamed, 2012). Riverbed scour mechanisms have been categorised as local scour, contraction and natural scour (CIRIA, 2015), based on the resulting shape and the relative sizes of the bridge opening and the river channel.

2.1.1 Local scour

Local scour in both the seabed and riverbed results from the direct impact of water on individual structural elements. These individual structural elements cause the flow velocity to increase,

and hence create vortices that exert erosive forces on the adjacent bed. As this flow velocity increase occurs primarily near the structural element, scour occurs only in the immediate *locality* of the structure, as the name implies. Local scour has been researched extensively, since it can be tested in laboratories with physical models, and scour estimation formulae for a variety of situations have been developed. Based on these formulae, the maximum local scour depth near a bridge pier depends on factors such as the width of the pier, flow depth and erodibility of the bed materials (CIRIA, 2015; Zampieri et al., 2017).

Each of the factors that contribute to scour, such as flow rate, sediment characteristics and type of structure, has a significant degree of uncertainty or difficulty in making long-term predictions. For example, flow condition may change as a result of the changes in the catchment use or climate. Hence, the scour depth reaching a particular depth, and causing damage to an adjacent bridge, cannot be estimated with the same accuracy as is possible with structural design (CIRIA, 2015).

2.1.2 Contraction scour

The second type of scour mechanism of riverbeds, namely, contraction scour, occurs because of increased flow velocity resulting from narrowing of a channel. A significant part of the contraction is often due to the approach embankments to a bridge, which cause the flow along the floodplain to join the main channel and pass through the bridge opening, as shown in Figure 2.1.

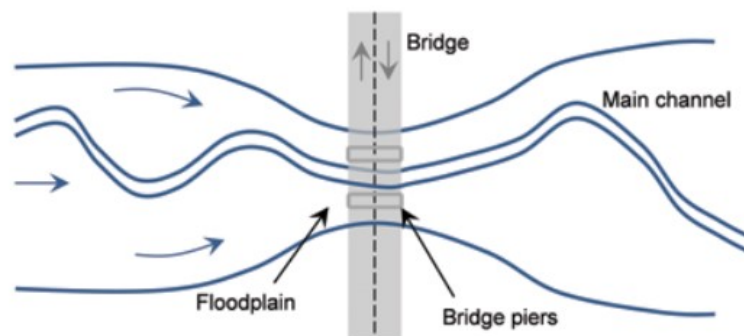


Figure 2.1 Contraction scour (CIRIA, 2015)

2.1.3 Natural scour

Natural scour (some researchers call this general scour), in contrast to both of the above mechanisms, occurs naturally, even without the presence of a structure. This process includes long-term bed degradation, channel migration through bank erosion and bend scour. Degradation is the long-term erosion of bed material in a river, perhaps over a decade or a century, and this affects its longitudinal profile. Bend scour is the additional scour occurring as

a result of the curvature of a river. Channel migration involves lateral migration of a river channel across its floodplain (Prendergast and Gavin, 2014; CIRIA, 2015).

2.1.4 Global scour

Global scour, as the name implies, refers to the lowering of the bed level everywhere (Sumer, Bundgaard and Fredsøe, 2005; Mohamed, 2012), as opposed to bed lowering in the locality of the foundation (Figure 2.2). In both local and global scour, the scour depth refers to the maximum depth measured at the foundation surface relative to the initial position of the bed level (Mory et al., 1999). Although global scour has primarily been used with reference to structures on a seabed, the shape of global scour is similar to the shape resulting from mechanisms of natural and contraction scour in riverbeds. Global scour in the seabed occurs as a result of either the diffraction of sea waves by a large structural foundation or the morphodynamical changes in the sea bed that are independent of the presence of the structural foundation (Mory et al., 1999).

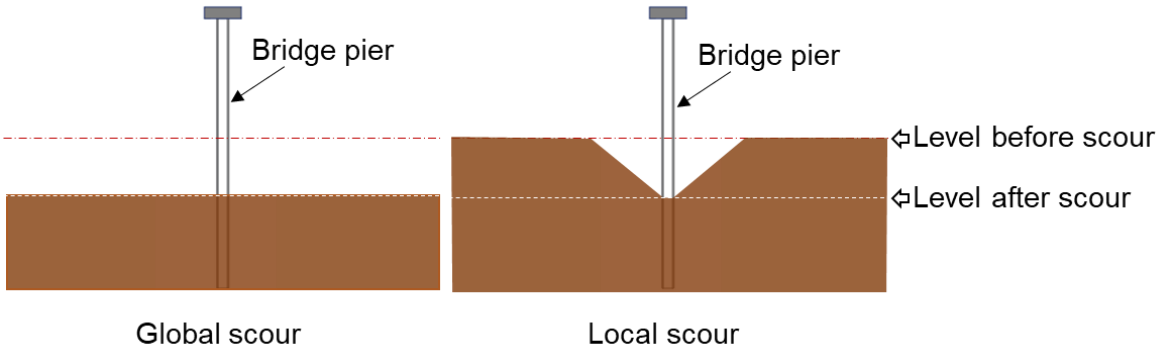


Figure 2.2 Shape of a local and global scour

2.2 The danger of scour in bridges

Bed scour at bridge foundations has been identified as the leading cause of bridge failure in New Zealand (Melville and Coleman, 2000), Taiwan (Ko et al., 2010), the USA (Hunt, 2009), the UK and around the rest of the world (Dikanski et al., 2016). A study conducted on 500 bridge failures, which occurred in the period between 1989 and 2000 in the United States, has shown that hydraulic causes contribute to 53% of bridge failures (Wardhana and Hadipriono, 2003). Another two studies in the USA on 823 bridge failures since 1950 (Shirole and Holt, 1991), and 1502 documented bridge failures from between 1966 and 2005 (Hunt, 2009), identified the same finding, i.e. hydraulic causes are the main reason for bridge failure, accounting for approximately 60% of the total failures. One survey of 347 bridge failures around the world over the period from 1444 A.D. to 2004 found that natural hazard is the primary cause of bridge failures (29.3%), of which flooding/scour accounted for 66% and earthquakes

contributed to 14% (Imhof, 2004). One more study of 104 bridge collapses in China from 2007 to 2015 found flooding to be the leading cause, which had contributed to 43% of the collapses, and, unfortunately, killed 101 people (Liu, Liu and Yu, 2017).

The top 10 causes of bridge failures found in Wardhana and Hadipriono (2003) are illustrated in Figure 2.3. In comparison to the significant number of failures with hydraulic causes, there remains a small number of failures resulting from other causes, such as steel fatigue, earthquakes and fire. The hydraulic causes have been further subdivided as flooding (33%) and scour (15.5%). These authors presume that the causes identified as flooding could also mostly be the result of scour, although given separately to comply with the original sources where both terms may have been used interchangeably.

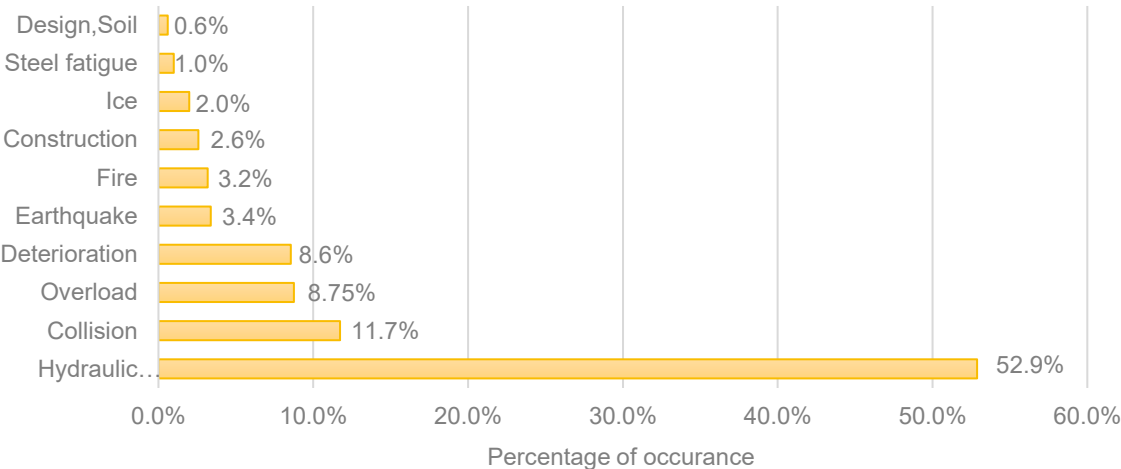


Figure 2.3 Top 10 causes of bridge failures in the US during 1989 and 2000: based on the data from Wardhana and Hadipriono(2003)

Lin et al. (2013) studied 36 bridge failures that occurred as a result of scour in New Zealand, the USA and Canada. The main scour mechanism for these bridge failures was identified as local scour (64% of the bridge failures), in contrast to global, contraction or natural scour. The main component failure was with the bridge piers, as noticed in 61% of the events.

The scour depths measured at most failure sites of Lin et al. (2013) were between 0.5 and 5 m, although maximum scour depths as high as 15 m had been recorded. Another study on shallow coastal waters has measured scour depths of up to 6.3 m (Rudolph, Bos and Luijendijk, 2004).

Scour induced bridge failure could occur without any prior warning, putting the lives of those crossing the bridge in danger. Figure 2.4 shows one of many such bridge failures in the past, which occurred because of scour. This collapse caused two train coaches to fall into the river, and they were washed away (Bao and Liu, 2016).



Figure 2.4 *Shi-Ting-Jiang Bridge failed because of scour in 2010 (CNTV, 2010)*

2.3 Scour monitoring techniques

Scour monitoring can direct bridge engineers to implement timely countermeasures, thus reducing the risk of bridge failure. Scour depth was historically measured using sounding rods in shallow waters and lead-weight sounding lines in deeper waters. Today, modern devices use non-contact sensing techniques and remote technology, with data transmitted to a logger and then to a central office or an online cloud platform. Scour monitoring methods can be divided into two main categories based on use, as mentioned below:

1. Portable equipment

These techniques are suitable for occasional readings. They are cheaper but do not provide a continuous record.

2. Fixed equipment

These are mounted on the bridge or in the riverbed and give a continuous record of measurements.

Hunt (2009) surveyed fixed scour monitoring equipment in the USA. As shown in Figure 2.5, sonar was found to be the most common type of fixed equipment, with magnetic sliding collar coming second. Other equipment, such as tiltmeters, float-out devices, time-domain reflectometry and piezometric film sensors had a lower presence. In addition to these, a number of new scour monitoring techniques are currently available.

The following sub-sections explain these scour monitoring techniques, highlighting their advantages and limitations.

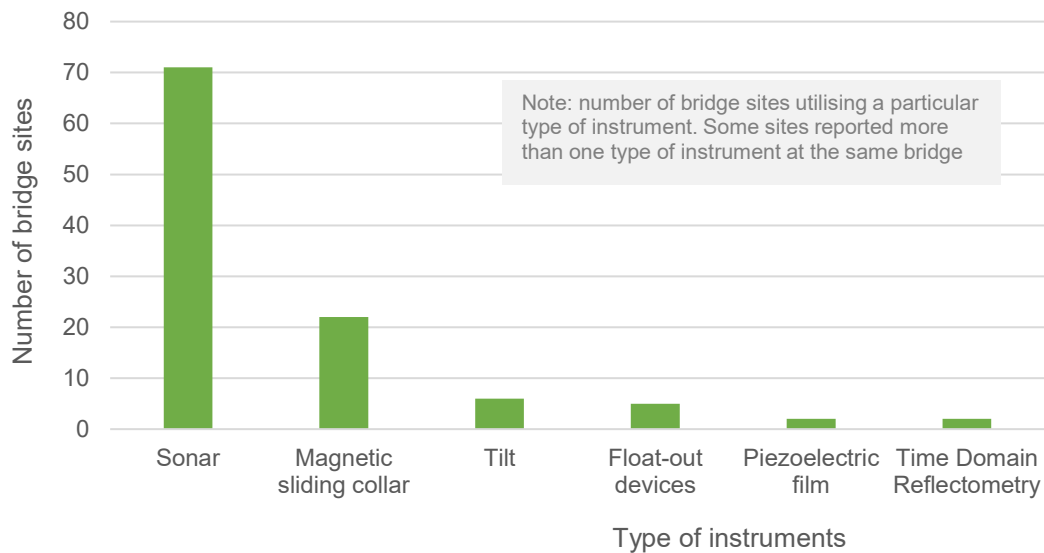


Figure 2.5 Bridge sites based on the type of fixed scour monitoring instruments present (Hunt, 2009)

2.3.1 Visual inspection

For site inspections, access can be difficult in flood conditions. A simple method is to place indicator stones wrapped in brightly coloured tape and bury these at specific known depths. Their appearance or absence can indicate the mobility of the bed material. Alternatively, cameras (infrared, if night vision is also needed) can be used to monitor water level, the presence of debris and large bridge movement. These are simple methods to implement, but they give limited valuable information on scour (CIRIA, 2015).

2.3.2 Single-use devices

There are two common single-use devices, namely, float-out devices and tethered buried switches. The float-out devices are embedded in a vertical orientation at a desired level. As shown in Figure 2.6, when the original ground level (Stage 1) reaches the installed depth of the device (Stage 2), the device simply floats out up to the water surface (Stage 3). When the device changes from vertical to horizontal orientation after floating on water (Stage 3), an electrical switch triggers and a wireless signal is sent to a data-acquisition system nearby (CIRIA, 2015).

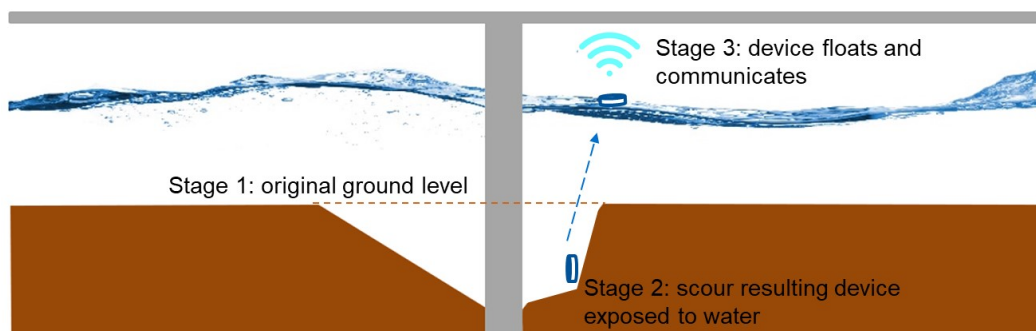


Figure 2.6 Simple float-out device

Table 2.1 Advantages and limitations of single-use devices

Advantages	Limitations
<ul style="list-style-type: none"> • Simple • Low-cost devices • Buried parts do not require maintenance, and are not affected by ice, debris and vandalism 	<ul style="list-style-type: none"> • Single-use – need to reinstall for further readings • Limited value – only indicates that the depth of embedment has reached but gives no data on further scouring or deposition • Expensive installation, especially in deep water; requires drilling or coring • Scour depth only at one location • Power-related issues: <ul style="list-style-type: none"> TBS wires are susceptible to damage due to debris Float-out devices have battery life limitations

(Briaud et al., 2011; Prendergast and Gavin, 2014; CIRIA, 2015)

Tethered buried switches work similarly but are permanently connected to a power source. Thus, they have three states: “in position”, “device rotated” and “not operational” (Briaud et al., 2011; Prendergast and Gavin, 2014). In contrast to float-out devices, tethered buried switches remove the doubt of not knowing whether the device is in position or not operational when a signal is not sent. When the scour level reaches its embedded depth, this device rotates as a result of the hydraulic force but not buoyancy. The estimated design life of these switches is approximately twenty years (CIRIA, 2015). The advantages and limitations of single-use devices are presented in Table 2.1. While these have the advantages of being simple and low-cost, they also come with the limitations of being single-use and difficult to install. They are best suited to new bridges or bridges crossing ephemeral watercourses, having only seasonal water flow, where it is easier to install the devices.

2.3.3 Physical probing

In this method, either a ranging pole or sounding weight on a cable is used to locate the bed level or depth to the undisturbed soil. Sounding rods or sounding weights can be used from the bridge, a boat or by a diver (CIRIA, 2015). In the same way the visual inspection is commonly used for bridge superstructures, underwater inspection is commonly being carried out by divers (Figure 2.7) rather than by instrumentation. Maintenance engineers often feel that the most reliable way to measure scour is to use divers (Elsaid and Seracino, 2012). The advantages and limitations of physical probing are presented in Table 2.2. While there are advantages related to simplicity and physical sense, there are major limitations related to the safety of the divers. Furthermore, it does not provide an accurate estimate of the criticality of scour, since divers cannot be deployed during flooding when the scour is at its peak, and the resulting scour holes are often refilled when the flood recedes (Prendergast, Hester and Gavin, 2016).



Figure 2.7 A diver carrying out an underwater bridge inspection (Diving Services Inc., 2017)

Table 2.2 Advantages and limitations of physical probing

Advantages	Limitations
<ul style="list-style-type: none"> • Simple • Not affected by air entrainment or high sediment loads • Low-cost for small areas • Provides a physical sense (compared to Sonar) 	<ul style="list-style-type: none"> • Not suitable for deep water • High velocities of water and debris can disturb the probing method used • Does not provide real-time information • Expensive and time-consuming for large areas (for each inspection, it is necessary to send divers in with all their equipment and/or using a dedicated boat) • The accuracy of the measurements is subjective • Using divers or boats during flooding is dangerous and hence not feasible

(Hunt, 2009; CIRIA, 2015)

2.3.4 Sounding rods

Sounding rods are vertical rods with a base plate at the bottom, which can only be used to locate the bed level. These are rested on the bed of a river with a sleeve at the top to keep them vertical. The rod moves downwards as scour occurs and stays at the most scoured level in its history since the deployed time. The displacement at the top of the sounding rod shows the maximum scour depth experienced since it was installed. To monitor the next scour event, the rod has to be forcibly raised out. Table 2.3 presents the advantages and limitations of sounding rods.

These rods are difficult to mount on structures that have inclined piers. Furthermore, if scour occurs below the foundation level, substantial mountings are needed. Sounding rods are best suited for coarse bed materials and rip rap. With sand or other fine bed materials, the sounding rods can settle into the because of their own weight and the vibration caused by the flowing water. Hence, suitably sized base plates are required (CIRIA, 2015).

Table 2.3 Advantages and limitations of sounding rods

Advantages	Limitations
<ul style="list-style-type: none"> • Simple • Reliable • Not affected by air entrainment or high sediment loads • Lower operational cost compared to using divers and boats 	<ul style="list-style-type: none"> • Not suitable for deep water because of the long, unsupported length of rod, which can suffer vibration • If an aggressive groundwater or surface water condition is prevalent, the sounding rod will be prone to corrosion • Hydrodynamic forces, ice and debris can damage the sounding rod • Does not provide real-time information • Not suitable for inclined piers or abutments and fine bed materials

(CIRIA, 2015)

2.3.5 Time-domain reflectometry

Time-domain reflectometry (TDR) is a guided electromagnetic wave technology that measures reflections along a conductor to derive the electrical characteristics of the surrounding material (Yu, 2009). The arrangement of a typical TDR system is shown in Figure 2.8. The system includes a set of measurement probes, the TDR device and a connection cable. The TDR device sends a fast-rising step impulse to the measurement probe, and when dielectric permittivity¹ changes in the surrounding medium of the probe, part of the energy is returned to the source via another parallel vertical rod (Hunt, 2009; CIRIA, 2015). There is a significant difference between dielectric permittivity of water (81) and soil (3 – 7). Hence, the water-soil interface can be identified with the use of this technique and scour depth can be measured in real-time (Yu and Yu, 2010; Yu, Zhang and Tao, 2013; Prendergast and Gavin, 2014).

TDR has been extensively researched in the laboratory environment to understand the effect of different environmental conditions. Also, there are many example applications (Fisher et al., 2013). However, CIRIA (2015) has indicated that there were no suppliers at the time of the report. The advantages and challenges of TDR are explained in Table 2.4. While the TDR technique has the advantage of being robust and real-time, there are limitations related to the difficulty of installation underwater and the limit of maximum depth.

¹ Dielectric permittivity relates to the ability of a dielectric material to resist an electric field. Dielectric is a material that does not conduct electricity, but an applied electric field displaces its charge rather than causing the electricity to flow.

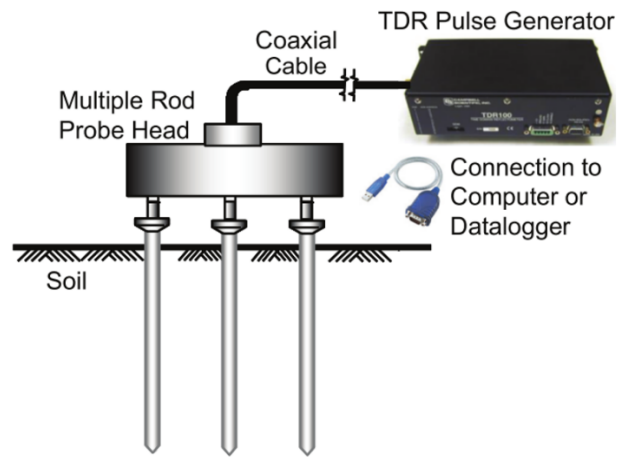


Figure 2.8 The arrangement of a typical TDR (Yu, Zhang and Tao, 2013)

Table 2.4 Advantages and limitations of time-domain reflectometry

Advantages	Limitations
<ul style="list-style-type: none"> • Real-time • Robust – resistant to ice, rapid flow and debris 	<ul style="list-style-type: none"> • Limit on maximum length of signal reliability • Suspended sediment, salinity and temperature can affect the measurement accuracy • Underwater installation and cable handling

(Hunt, 2009; Lagasse et al., 2009; Fisher et al., 2013)

2.3.6 Ground-penetrating radar

Ground-penetrating radar (GPR) is a geophysical technique that can determine the bed profile of a stream. The GPR device, which is placed on, or immediately above, the water surface, uses a transmitter antenna to emit electromagnetic waves (frequency in the range of MHz) to the ground (Anderson, Ismael and Thitimakorn, 2007). When these waves encounter a boundary with different dielectric permittivity, some of the waves are refracted or reflected back. A receiver antenna in the GPR device records the return signal in order to determine the depth to the boundary. It can be towed across, or over, the water surface to establish a continuous profile of the riverbed. The advantages and limitations of this technique are presented in Table 2.5. This device differs from sonic fathometers and echo sounders in that it can also create a geophysical map of the subsurface information (Anderson, Ismael and Thitimakorn, 2007; Prendergast and Gavin, 2014; CIRIA, 2015). However, it involves manual, time-consuming operations and it does not provide real-time scour monitoring.

Table 2.5 Advantages and limitations of ground-penetrating radar

Advantages	Limitations
<ul style="list-style-type: none"> • Gives the geophysical profiles of the riverbed and subsurface information • The antennas can be moved rapidly across (or above) the surface of a stream, being free of an operator • A continuous record of the riverbed • The device does not need to be submerged in water and can be operated remotely 	<ul style="list-style-type: none"> • Requires manual, time-consuming operation and specialised training • Not practical for water depths of more than 10 m • Not a real-time monitoring solution • The measurement accuracy is affected by air entrainment and high sediment loads • The reflections and echoes from pier foundations can add noise to the data • Not suitable for saline water or dense, moist clays since the signal will not penetrate conductive material

(Anderson, Ismael and Thitimakorn, 2007; Hunt, 2009; Deng and Cai, 2010; CIRIA, 2015)

2.3.7 Driven or buried rod devices

Driven or buried rod devices used for scour monitoring can be broadly categorised as below:

- 1 Collar-based and other non-vibration-based rod devices
- 2 Vibration-based rod devices

With *collar-based devices*, a driven rod, along which a collar, rests on the stream bed and moves downwards as scour occurs. One of the most common collar-based devices is the magnetic sliding collar, shown in Figure 2.9. It involves a set of magnetic switches along the rod, and these switches close with the downward movement of the collar as scour occurs. This device can measure scour depth up to a maximum of around 3 m (Nassif, Ertekin and Davis, 2002). The advantages and limitations of the magnetic sliding collar are presented in Table 2.6. While these have the advantage of cost-effectiveness and easy installation, there are limitations related to providing only a localised (point measure) scour depth measurement and potential jamming of the collar.

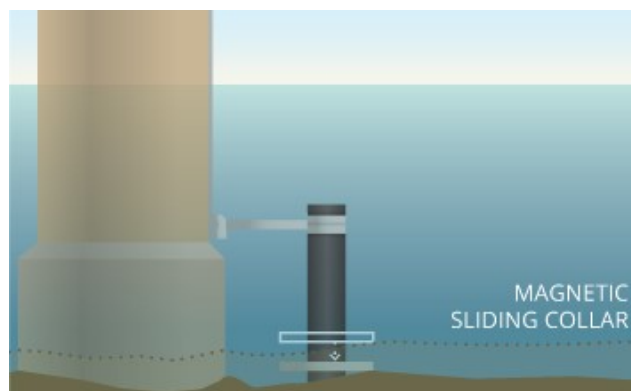


Figure 2.9 Magnetic sliding collar (Fondriest Environmental Inc., 2017)

Table 2.6 Advantages and limitations of magnetic sliding collar device

Advantages	Limitations
<ul style="list-style-type: none"> • Widely used, inexpensive and simple • Easy to install and operate • High scour depth resolution, 0.15 m 	<ul style="list-style-type: none"> • Scour hole refilling is not indicated • Provides only a local scour depth measurement • Jamming of the collar when the rod is tilted; the intrusion of stones between the collar and the support; corrosion • Excavation required for driving support tube, and hence high maintenance and repair cost • Vulnerable to ice and debris damage, unsupported length

(Nassif, Ertekin and Davis, 2002; Lagasse et al., 2009; Briaud et al., 2011; CIRIA, 2015)

The *vibration-based rod devices* correlate the scour depth to the dynamic properties of a partially buried rod. Zarafshan, Iranmanesh and Ansari (2012) developed a vibration-based device that measures dynamic strain measurements along a rod. The exposed length of the rod due to scour results in reduced lateral stiffness of the rod and a lower natural frequency. The measured dynamic strain history is converted to the frequency domain using modal analysis. The change in frequency is correlated to the exposed depth by developing a Winkler spring system for the soil rod system. The advantages and limitations of these techniques are presented in Table 2.7. This system allows self-calibration: the natural frequency measured at the installed location and the known depth of embedment can be used to choose an appropriate modulus of subgrade reaction.

Fisher et al. (2013) also developed a similar device, which has vibration-based turbulent pressure sensors (VTP) along the length of a driven rod. Each of these sensors has an accelerometer to measure vibration, and a flexible disc that vibrates as a result of the dynamic pressure of turbulent water. The energy content of each sensor is calculated as the mean squared value of acceleration. The sensors subjected to turbulence from water flow have two to three orders of magnitude higher energy content than those embedded in the soil layer and at rest. This difference in energy content is used to estimate the water-soil interface, thereby determining the scour depth.

Table 2.7 Advantages and limitations of vibration-based driven rods

Advantages	Limitations
<ul style="list-style-type: none"> • Real-time monitoring • Not affected by turbid water conditions • Simple and robust in harsh hydraulic conditions 	<ul style="list-style-type: none"> • Labour intensive and costly installation • Provides only a local scour measurement • The connection cables to the sensors are prone to flood/debris-induced damage

(Fisher et al., 2013; Prendergast and Gavin, 2014)

2.3.8 Electrical conductivity devices

Electrical conductivity-based scour monitoring devices include multiple electrical conductivity sensors spaced equally along a rod. The rod is driven vertically into a riverbed, with part of it exposed to surface water. The bed level is located by the difference in electrical conductivities measured below the riverbed (saturated soil) and above the riverbed (surface water). When scour occurs, one or a few previously buried sensors will be exposed to surface water and measure a different conductivity. This principle can be used to track the scour depth (Hayes and Drummond, 1995). Table 2.8 shows the advantages and limitations of this technique. Although this technique has the advantage of real-time, long-term monitoring capability, the metal rod is prone to corrosion.

Table 2.8 *Advantages and limitations of electrical conductivity devices*

Advantages	Limitations
<ul style="list-style-type: none">• Allows long-term monitoring• Real-time measurements	<ul style="list-style-type: none">• Works only where surface water and saturated sediment conductivities have a measurable difference• The device may pose a hazard to navigation• Electrodes are prone to corrosion, and the rod is prone to damage due to debris

(Hayes and Drummond, 1995; Anderson, Ismael and Thitimakorn, 2007)

2.3.9 Sonar

Sonar refers to sound navigation ranging. Sonar devices work on the principle that a sound wave reflects part of its energy when propagating through an interface that changes density such as the soil-water interface. Therefore, the depth of the soil-water interface can be estimated by recording the time interval between emission and return of a sound wave. Sonar devices are best suited to bridges in coastal regions (Hunt, 2009). Some proprietary sonar sensors have shown centimetre-scale depth-measurement accuracies and measurement ranges of between 0.4 – 200 m water depth (AIRMAR, 2017). Three different types of sound-wave-based scour monitoring devices are explained below, and their advantages and limitations are highlighted in Table 2.9.

2.3.9.1 Sonic fathometers

These sensors are placed below the surface level of the water and emit sound waves through the water medium to the ground, from where the waves are reflected back. Sonic fathometers are commonly used in fishing boats to locate fish (Hayes and Drummond, 1995). They can be mounted on bridge piers to monitor scour depth (Prendergast and Gavin, 2014).

Sonic fathometers are one of the most widely used methods for scour monitoring. The performance of this device has been assessed by many researchers for scour monitoring, and

some of the findings are highlighted in Table 2.9 (Falco and Mele, 2002; Nassif, Ertekin and Davis, 2002; Hunt, 2005; Holnbeck and McCarthy, 2010; Fisher et al., 2013).

Table 2.9 Advantages and limitations of different sonar monitoring techniques

	Advantages	Limitations
Sonic fathometers	<ul style="list-style-type: none"> Records infilling; can be built with off-the-shelf components Extensively researched: scour holes of 0.23 – 1.2 m in depth have been accurately measured; successfully operated during hurricanes 	<ul style="list-style-type: none"> A limited depth tolerance Interference from debris, high sediment loading and entrained air present in turbulent flow When the sound-wave beam encounters a variable depth profile at the bed level, only the lowest depth is given Often the device is mounted on a bridge pier, which can settle during scour, leading to an inaccurate measure of the real scour depth
Reflection seismic profilers	<ul style="list-style-type: none"> Gives an accurate depth structure model of the bed surface and the subsurface, with depths in the order of tens of metres Records infilling 	<ul style="list-style-type: none"> Noise with variable streambeds leads to the crossing-over of signals; much manual input is needed to obtain measurements Both the source and the receiver need to be submerged, and hence measurements cannot be taken continuously over sand bars Multiple reflections and echoes from the pier foundation, shoreline and channel bed can add noise to the data Interference from debris, high sediment loading and entrained air present in turbulent flow
Echo sounders	<ul style="list-style-type: none"> Gives an accurate depth structure model of the riverbed Records infilling 	<ul style="list-style-type: none"> Compared to reflection seismic profilers, only the depth of the sediment-water interface profile can be measured because of the high attenuation of high-frequency waves Both the source and receiver need to be submerged, and hence measurements cannot be taken continuously over sand bars Multiple reflections and echoes from the pier foundation, shoreline and channel bed can add noise to the data Interference from debris, high sediment loading and entrained air present in turbulent flow

(Falco and Mele, 2002; Nassif, Ertekin and Davis, 2002; Hunt, 2005; Anderson, Ismael and Thitimakorn, 2007; Holnbeck and McCarthy, 2010; Yao et al., 2010a; Fisher et al., 2013)

2.3.9.2 Reflection seismic profilers

This method uses a coupled source transducer and receiver transducer positioned just below the water surface. The sound-wave source transducer produces pulsed waves at regular time or distance intervals, with frequencies in the range of kilohertz. The signal propagates through water and soil, with part of it being reflected at the riverbed and other acoustic impedance interfaces. The reflected waves are captured by the receiver transducer. This device is towed across the water surface to capture the distributed scour depth profile. Then, the profile of the streambed can be built by converting time-depth profile measurements to a depth profile using the estimated seismic interval velocities (Anderson, Ismael and Thitimakorn, 2007; Prendergast and Gavin, 2014).

2.3.9.3 Echo sounders

Echo sounders work similarly to reflection seismic profilers, but the waves used are of high frequency (dominant frequency in 100s of kHz). The waves are highly attenuated while travelling through soil layers, and hence they are only effective in identifying the depth to the bed level. The depth profile can be obtained by converting time-depth plots to depth plots, similar to the method used with reflection seismic profilers (Anderson, Ismael and Thitimakorn, 2007; Prendergast and Gavin, 2014).

2.3.10 Vibration- and tilt-based methods

Scour causes erosion of the soil that supports bridge foundations from the side and underneath. Such loss of support results in a change in the overall stiffness of the bridge. When this stiffness change is significant enough to cause a measurable shift in natural frequency or tilt, the parameters themselves can aid in identifying (Prendergast and Gavin, 2014; Bao and Liu, 2016).

Tiltmeters measure rotation, and they can be used to monitor differential settlements of a bridge that occur because of scour (Lagasse et al., 2009). Experimental research by Briaund et al. (2010) and Yao et al. (2010a) has found that vibration-based parameters show earlier scour detection than tilt. Therefore, vibration-based monitoring may have more potential than tilt.

Table 2.10 highlights the advantages and limitations of vibration- and tilt-based techniques. These techniques have limitations such as the requirement of an associated FE model and being an indirect measure of scour. They also have a number of advantages such as cost-effectiveness, capability for real-time monitoring and durability of the instrumentation.

Table 2.10 Advantages and limitations of vibration and tilt-based scour monitoring

Advantages	Limitations
<ul style="list-style-type: none"> • Real-time monitoring • Durable: the sensor can be installed above the waterline, which avoids most of the challenges associated with water and soil • Indicates a distributed rather than a single point measure of scour depth • Cost-effective and easy to install; low maintenance required • The scour depth measurements by other methods do not indicate the effect of scour on the bridge behaviour. Hence, bridge owners find it difficult to assess the risk of scour-related failure. In contrast, with this method, a shift in structural response shows a direct effect on the structure by scour 	<ul style="list-style-type: none"> • Does not provide a direct indication of scour depth • Vibration: forced vibration by the impact is not suitable for old bridges as no set-up is pre-made for impact equipment installation. On the other hand, ambient vibration has a low signal to noise ratio • A finite element model is often used to estimate scour depth; hence, the estimated depth involves some inaccuracies inherited from the errors and variabilities of the input parameters of the finite element model • Accelerometers: a high volume of acceleration data needed; high-power requirement

(Lagasse et al., 2009; Briaud et al., 2011; Prendergast and Gavin, 2014; Bao and Liu, 2016)

2.3.11 Smart rocks

Smart rocks are essentially powerful magnets encased in concrete. Once dropped on to the bed underwater, smart rocks change the magnetic field nearby, even above water. Measuring this magnetic field, it has been possible to locate the position of these smart rocks. The idea is that when scour occurs, the position of the smart rocks changes, as they roll down to the bottom of the scour hole. The resulting change in the magnetic field above water indicates the location and depth of the scour hole. The magnetic field can be measured by a magnetometer placed on either an unmanned flying vehicle (UFV) or a moving platform. Table 2.11 lists some of the advantages and limitations of smart rocks. A limitation of this technique is that the measurement accuracy depends on many factors, such as the power of the magnet, the accuracy of the magnetometer, the direction of the smart rock and the presence of steel bridge girders (Chen et al., 2018; Tang et al., 2019). A key advantage is that these smart rocks can also be used as part of rip-rap countermeasures to check its effectiveness (Tang, 2017). The effective monitoring range of smart rocks has been as high as 12 m, while the depth resolution has been as high as 0.1 m, although these measurements were taken outside water and the underwater performance may be different (Tang et al., 2019).

Table 2.11 Advantages and limitations of smart rocks

Advantages	Limitations
<ul style="list-style-type: none"> • Ability to locate the position of the rocks • Effective monitoring range up to 12 m • Error of scour depth measurement as low as 0.1 m • Riprap countermeasure effectiveness indication ability 	<ul style="list-style-type: none"> • Measurement reliability dependence on the direction of the rock and the steel content of the bridge • Requirement for a magnetometer: only intermittent measurements • Provides only a local scour measurement at the rock location • Washing away during heavy flooding

(Tang, 2017; Chen et al., 2018; Tang et al., 2019)

2.3.12 Underwater surface-water vehicles

Robotic underwater and surface-water vehicles have recently been developed as a replacement for the use of scuba divers for scour monitoring. These devices often use sonar to produce 3D images of the bed profile.

Fadool et al. (2012) developed a prototype robotic system that can be operated autonomously. It is temporarily affixed to the bridge pier or exposed pile underwater with a vertical drive mount, as shown in Figure 2.10. This device can move to different places along the pile/pier, either vertically on the vertical drive mount or around it on a circular guide rail. The sonar scanner can also be directed downwards to various vertical angles, to obtain a 3D image of the whole bed profile near the foundation. This autonomously operated device was validated in the laboratory environment and has shown a maximum depth measurement error of 2-2.5 cm.

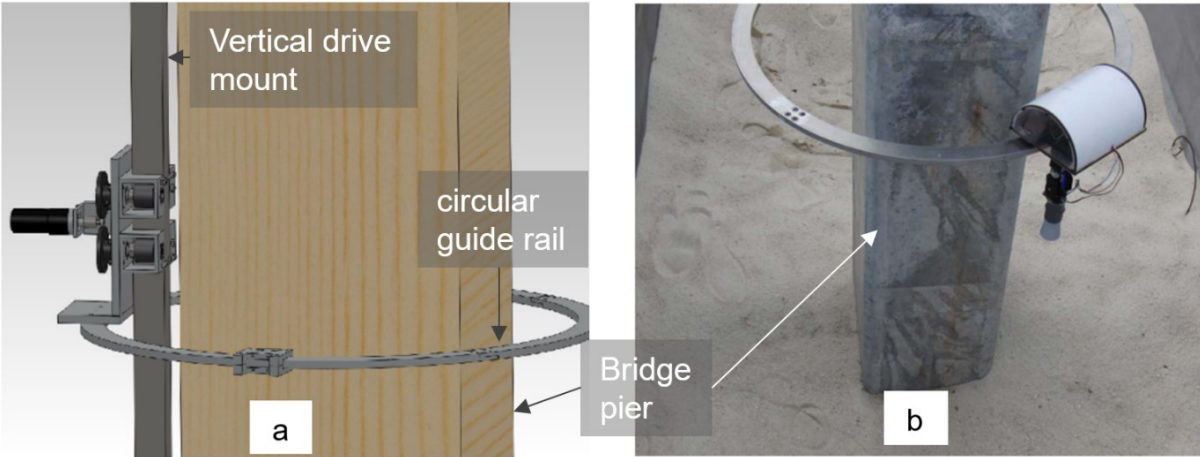


Figure 2.10 The prototype robotic system (a) 3D rendering of the device (b) device in operation

Hill (2016) used unmanned surface vessels (USVs) to carry out bridge inspections. These USVs can autonomously navigate and operate while collecting underwater acoustic images and transmitting them to a remote station. The acoustic images can be used to detect

underwater structural damage, scour and undermining. The USV has also been used to capture photos of the underside of the bridge above water, which are difficult to capture.

Unmanned vehicles are particularly crucial for bridges crossing marine environments, where high currents and wind make it difficult to deploy scuba divers (Hill, 2016). According to a review of autonomous underwater vehicles used in marine geoscience (Wynn et al., 2014), autonomous underwater vehicles (AUVs) are usually used in conjunction with other types of surface and underwater vehicle. Initially, vessel-mounted multibeam echo sounders (MBES) or 3D seismic provides a bed profile with a spatial resolution of 10 – 100s of metres. Then, AUV mounted MBES provides a more accurate bed profile measurement with a spatial resolution of 0.5 – 5 m. Finally, remotely operated vehicles (ROVs) are used to get a bed profile at specific locations of interest, with a spatial resolution of cm scale.

Murphy et al. (2011) present a case study of using underwater and surface-water vehicles (Figure 2.11) for a successful post-disaster bridge inspection. Table 2.12 highlights the advantages and limitations of these systems. These have the advantages of being capable of autonomous and rapid monitoring and are especially suitable to inspect bridges crossing marine environments. However, they have a number of limitations related to cost, technological challenges and the environmental sensitivities of the scanning device.

Table 2.12 *Advantages and limitations of underwater/surface-water vehicles*

Advantages	Limitations
<ul style="list-style-type: none"> • Autonomous operation – no operators are required on-site – and possible to use in harsh weather conditions • Faster monitoring • Can do things that are difficult for divers, if technology permits 	<ul style="list-style-type: none"> • AUVs employed in marine environments have limited speeds (up to 1.5–2 ms⁻¹), and hence they are vulnerable to being moved away by tidal currents • High military, shipping or fishing activity present can cause acoustic interference, collision risk and entanglement • Areas of significant water turbidity can obstruct camera-based bed mapping • Some technological challenges need to be addressed: human-robot interaction, 3D obstacle avoidance, station-keeping, handling large data sets, GPS drop-out rates and uncertain sensor readings

(Bovio, 2005; Murphy *et al.*, 2011; Hill, 2016)

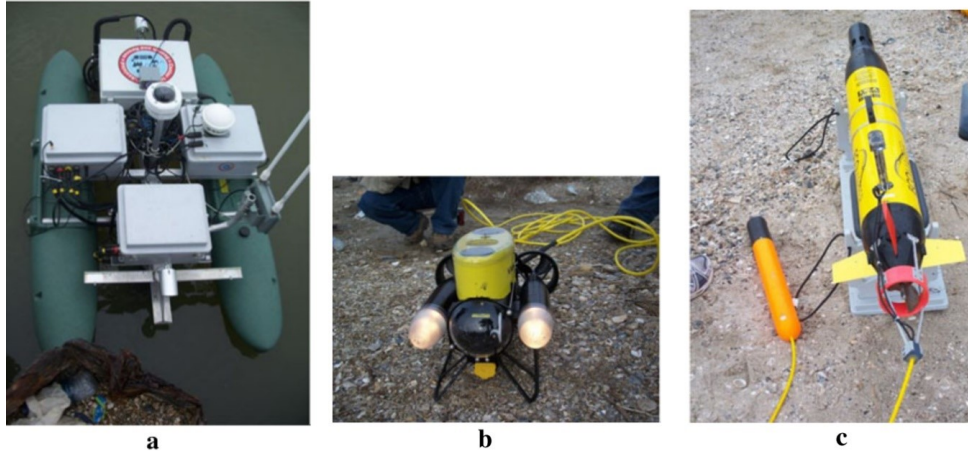


Figure 2.11 (a) *Unmanned surface vehicle (USV)* (b) *Remotely operated vehicle (ROV)* (c) *Unmanned underwater vehicles (UUV)*

2.3.13 Common challenges and the way forward

The monitoring techniques explained above possess inherent advantages and limitations when compared against one another. The most common limitations are as follows:

1. Durability issues, i.e. monitoring device being susceptible to damage by moving debris;
2. Provides only a local (point) measurement of scour depth;
3. Limited amount of details provided to assess the scour-related risk (do not provide enough data on the scour depth, scour hole refilling and soil properties);
4. Not feasible during flooding because of inaccessibility, air bubbles and/or rapid flow;
5. No real-time data (this is important, as scour-related damage could occur and develop rapidly during flooding);
6. Environmental parameters such as salinity, suspended sediment and temperature can affect the measurement accuracy;
7. High-cost, labour-intensive installation and/or operations required.

Most of these challenges seem to arise as a result of the barriers of water and/or soil and due to the fact that scour depth is monitored directly. Hence, a comparison study was carried out, considering four possible locations where scour sensors could be placed to monitor scour depth directly or indirectly (Figure 2.12). The sensor-location-related constraints and benefits are highlighted in Table 2.13, with current examples and suggestions for the future.

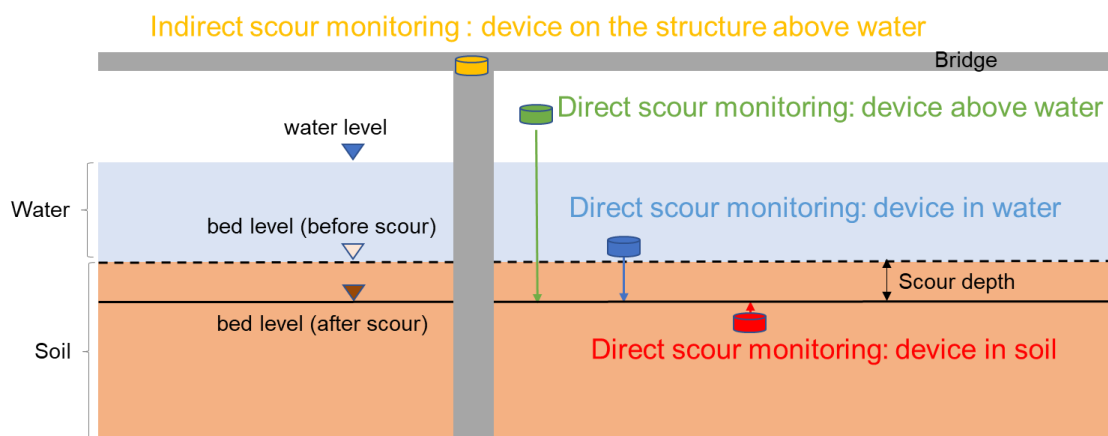


Figure 2.12 Different locations studied for placing sensors to measure scour at a bridge foundation

As shown in Table 2.13, if the scour depth is monitored directly using a device in water, there will be many challenges related to corrosion, durability and debris accumulation, while there is an opportunity to use the soil-water interface as part of the monitoring technique (e.g. magnetic sliding collar). If the scour depth is directly monitored using a device in soil, some of the challenges are installation of the device, its power management and the fact that it is oftentimes a single-use device, while a key advantage is that the device would be safe from damage by debris or water flow. If the scour depth is measured directly using a device located anywhere above water, the method of monitoring has to be through some wave-based remote monitoring technique. Therefore, wave-transmission-related issues such as sensitivity to salinity and air bubbles arise. If the scour depth is monitored indirectly by using a structural behaviour monitoring device located on the structure, but above the water level, most of the challenges associated with water and soil barriers can be mitigated, although this provides an indirect measurement of scour. Vibration-based scour monitoring is this type of a monitoring technique, and it has already indicated some potential based on numerical modelling predictions, although there has been limited research, according to Prendergast and Gavin (2014) and Bao and Liu (2016). Therefore, the state of knowledge on vibration-based scour monitoring was studied as is presented in detail in the next section.

Table 2.13 A study on the best location for bridge scour monitoring

	Device above water (direct scour monitoring)	Device in water (direct scour monitoring)	Device in soil (direct scour monitoring)	Device on the structure (indirect scour monitoring)
Challenges and constraints	<p>Should be electromagnetic wave, sonar or magnetic based</p> <p>Air bubbles and suspended sediments can interfere, and hence it is not suitable during flood conditions</p> <p>Wave refraction at the air-water interface can result in inaccuracies, and hence either the device should be on the waterline or waves should be sent vertically from above, in which case the device needs to be moved to obtain distributed scour depth profile</p> <p>Susceptible to vandalism</p>	<p>Can corrode if it is metal, especially the parts that are at the air-water interface, because of the constant wetting and drying</p> <p>Rapid flow speed can affect the performance of the device</p> <p>Flowing debris can damage the device</p> <p>Environmental parameters such as salinity, turbidity and temperature can affect accuracy, and hence they also have to be measured and compensated</p>	<p>Installation is costly and labour-intensive</p> <p>Power and connectivity-related issues can arise</p> <p>Hard to use wave-based devices, and hence, unless the device is halfway in the water, it is likely unable to monitor the real-time riverbed level</p>	<p>If the structural response is measured, it is an indirect measurement of scour</p> <p>A good structural response will need time, and when a measurable difference is noticed it can be too late</p> <p>The response as a result of scour can be too small and can interfere with other responses</p> <p>Susceptible to vandalism</p>
Competitive advantages	<p>Device is safe from potential damage by debris and rapid flow speed</p> <p>Installation and maintenance are low cost and easy</p>	<p>Can use the movement of water as a way to distinguish water from the soil bed</p> <p>There is no interference by water-air interface when wave-based devices locate water-soil interface</p>	<p>No interference by flowing water or debris</p>	<p>Scour depth measured does not give a direct indication of how much damage is caused by scour, but structural response does</p> <p>Device is safe from potential damage by debris and rapid flow speed</p> <p>provide a global scour measure</p> <p>Real-time, remote monitoring is feasible</p>

(continued on next page)

Table 2.13 A study on the best location for bridge scour monitoring (continued)

	Device above water (direct scour monitoring)	Device in water (direct scour monitoring)	Device in soil (direct scour monitoring)	Device on the structure (indirect scour monitoring)
Currently available examples	Ground-penetrating radar	<p>Devices that use the reflection of waves at soil-water interface (sonar-based devices)</p> <p>Devices that use the physical barrier of the water-soil interface (magnetic sliding collar, sounding rods)</p>	Float-out device, tethered buried switches	Structural vibration and tilt-based methods
		<p>Devices that use the movement of water and static state of soil to measure scour (vibration-based driven rods)</p> <p>Devices that use the pressure difference between water and soil layers (piezoelectric film sensors)</p> <p>Devices that use the electrical properties of water and soil layers (electrical conductivity probes, time-domain reflectometry)</p>		
Suggestions for the future	<p>Drone with GPR or sonar that sends signal vertically while flying above the water</p> <p>A GPR device that moves on railings along the deck and around the pier on railings</p>	<p>A wind turbine type underwater driven rod – the turbine generates electricity to power the sensors (self-powered); shaft has a mems strain sensor to measure the strain caused by water flow; flow speed measured by the turbine and the strain value can be correlated to estimate the scour depth</p>		<p>A combination of acceleration, tilt and displacement sensors can give the full response due to scour, and the pier will not generally be moved as a result of causes other than scour or ship impact</p> <p>Distributed strain sensors in the piles</p>
		<p>An underwater robot with sonar and an inspection arm: such a device can use sound waves with different frequencies to identify the locations of the soil layers and bridge foundation. Furthermore, the arms can be used to carry out <i>in situ</i> soil tests.</p>		<p>A combination of different vibration parameters measured by accelerometers</p>

2.4 State of knowledge of vibration-based scour detection methods

Several researchers in the past have researched vibration-based methods for scour monitoring. The primary vibration-based parameter they studied was the natural frequency of vibration, in addition to several other parameters derived from the mode shapes and acceleration time histories. The following sections review the existing state of knowledge on the potential of such vibration-based parameters to detect scour. The identified gaps in knowledge in the literature will be discussed at the end of this chapter.

2.4.1 Natural frequency as an indicator of scour

Natural frequency-based damage detection has already been studied by multiple researchers, many with little success in practice as a result of the main focus being on structural damage such as crack detection rather than scour. Even considerable damage, in the form of cracks as deep as half a bridge beam or pier, indicated relatively small fundamental frequency sensitivities of 7% (Döhler et al., 2014), 5.6% (Kim, Yun and Yi, 2003) and 0.4% (Farrar et al., 1994). These sensitivities are difficult to capture in practice, as they are of the same order of magnitude as the expected environmental/operational frequency sensitivity of a bridge (Peeters and Roeck, 2001; Kim, Yun and Yi, 2003; Caetano and Magalha, 2009; Koo, Brownjohn and Cole, 2010). Such relatively low sensitivity of natural frequency can be expected since cracks result in only local changes in stiffness and damping, which may not have much effect on the global modes. Scour, in contrast, is a special damage case – effectively a change of boundary condition – that results in a global stiffness reduction and therefore significantly greater changes in natural frequency. A simple cantilever model with lumped mass illustrates this, as discussed below.

Consider a bridge with its pier and the pile foundations having the same flexural rigidity of EI . Assume the mass of the bridge (m) is primarily contributed by the bridge deck rather than by the bridge pier and foundation. If the bridge deck to abutment connections can be assumed as roller support like condition and the ground level can be assumed as full fixed, the full bridge can be idealised as a lumped mass cantilever column, as shown in Figure 2.13(a). This idealised model can be further simplified to a single degree of freedom system with a mass and a spring, where the spring stiffness represents the overall stiffness of the cantilever column (Figure 2.13(b)). Any horizontal displacement of x from the stationary position of the lumped mass leads to a reverse acceleration of \ddot{x} . Thus, any displacement of x generates an inertial force of $m\ddot{x}$ (according to Newton's 2nd law) and a spring force of kx (Hooke's law), as shown in Figure 2.13(c).

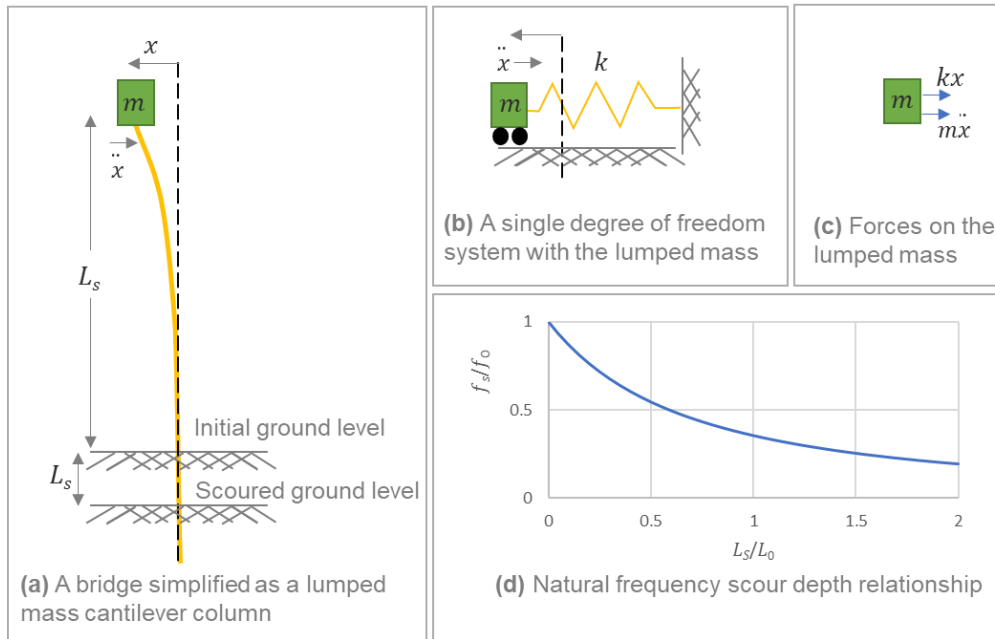


Figure 2.13 Natural frequency and scour depth relationship of a pier modelled as a fixed cantilever

The equation of motion for undamped free vibration applicable to the above system is:

$$m\ddot{x} + kx = 0$$

$$\ddot{x} = -\frac{k}{m} x \quad \text{Equation 2.1}$$

Undamped free vibration involves simple harmonic motion and hence the displacement is given as:

$$x = A \sin(\omega t + \varphi) \quad \text{Equation 2.2}$$

, where A is the amplitude of vibration, ω is the angular velocity and φ is the phase shift.

Double derivative of displacement in Equation 2.2 and combining with Equation 2.2 give:

$$\ddot{x} = -A\omega^2 \sin(\omega t + \varphi)$$

$$\ddot{x} = -\omega^2 x \quad \text{Equation 2.3}$$

Thus, Equations 2.1 and 2.3 give:

$$\omega^2 = \frac{k}{m}$$

$$\omega = \sqrt{\frac{k}{m}}$$

Thus, natural frequency (f) is given by:

$$f = \frac{1}{2\pi} \sqrt{\frac{k}{m}} \quad \text{Equation 2.4}$$

The fundamental mode involves lateral sway, where the column bends due to the inertial force at the top of the column. Livermore (2007) gives the stiffness for a similar fixed cantilever column tip deflection as:

$$k = \frac{3EI}{L^3} \quad \text{Equation 2.5}$$

Equation 2.4 and 2.5 give the natural frequency for the fundamental mode of this idealised bridge as:

$$f = \frac{1}{2\pi} \sqrt{\frac{3EI}{mL^3}}$$

$$f = \frac{0.276}{L^{1.5}} \sqrt{\frac{EI}{m}} \quad \text{Equation 2.6}$$

For the case of scour, where the ground level at the foundation exposes, the exposed height (L) increases but all other properties remain the same. Therefore, for initial height above the ground level of L_0 , initial natural frequency of f_0 , scour depth of L_S , and scoured natural frequency of f_S the following equations apply based on Equation 2.6.

$$f_0 = \frac{0.276}{L_0^{1.5}} \sqrt{\frac{EI}{m}} \quad \text{Equation 2.7}$$

$$f_S = \frac{0.276}{(L_S+L_0)^{1.5}} \sqrt{\frac{EI}{m}} \quad \text{Equation 2.8}$$

Equations 2.7 and 2.8 give:

$$\frac{f_S}{f_0} = \frac{L_0^{1.5}}{(L_S+L_0)^{1.5}}$$

$$\frac{f_S}{f_0} = \frac{1}{\left(\frac{L_S}{L_0}+1\right)^{1.5}} \quad \text{Equation 2.9}$$

This simple relationship between $\frac{f_S}{f_0}$ and $\frac{L_S}{L_0}$ in Equation 2.9 is plotted in Figure 2.13(d). It shows that there is a significant relationship between natural frequency and the scour depth. For example, a scour depth equal to the initial pier height ($\frac{L_S}{L_0} = 1$) leads to a significant natural frequency reduction of 65% ($\frac{f_S}{f_0} = 0.35$). While this model predicts significant natural frequency sensitivity to scour, the soil fixity, free end at the top and lumped mass idealisation are significant simplifications in this model and need to be considered carefully.

Studies examining bridge natural frequencies as a potential indicator of scour have emerged only relatively recently and have indicated much higher frequency sensitivities than the reported natural frequency sensitivities to structural damage. Several numerical studies have estimated a 30 – 40% change in natural frequency for a 50% loss of pile embedment (Klinga and Alipour, 2015; Prendergast, Hester and Gavin, 2016). A field study on a bridge, globally

scoured by 3 m for repair purposes, indicated a 20% change in natural frequency (Ko et al., 2010). These studies will be discussed in detail in the following sections, mainly under categories: (1) laboratory tests (2) field deployments, and (3) numerical modelling.

2.4.1.1 Small-scale or full-scale laboratory tests

The laboratory tests that studied natural frequency and scour relationship used small-scale and full-scale bridge models. Some of these models ignored soil-structure and water-structure interaction. These laboratory studies are explained in the following sections.

2.4.1.1.1 Small-scale models without soil or water

Elsaid and Seracino (2014) studied vibration-based techniques using a fixed base small-scale bridge in a laboratory, as shown in Figure 2.14. In this bridge model, scour was simulated by simply increasing the effective height of piers. The results revealed that natural frequencies of predominantly horizontal modes are more sensitive to scour than their vertical counterparts. The first horizontal natural frequency reduced from 18.71 Hz to 14.47 Hz, that is, by 23%, as a result of 0.6 m of small-scale scour depth. However, soil-structure interaction was neglected in this study, which could have a significant effect on the dynamic response of the bridge. In addition, the negligence of the bridge deck removes the stiff horizontal diaphragm effect typically present in a bridge. This bridge, hence, represents a space frame behaviour, which may not represent an actual bridge.

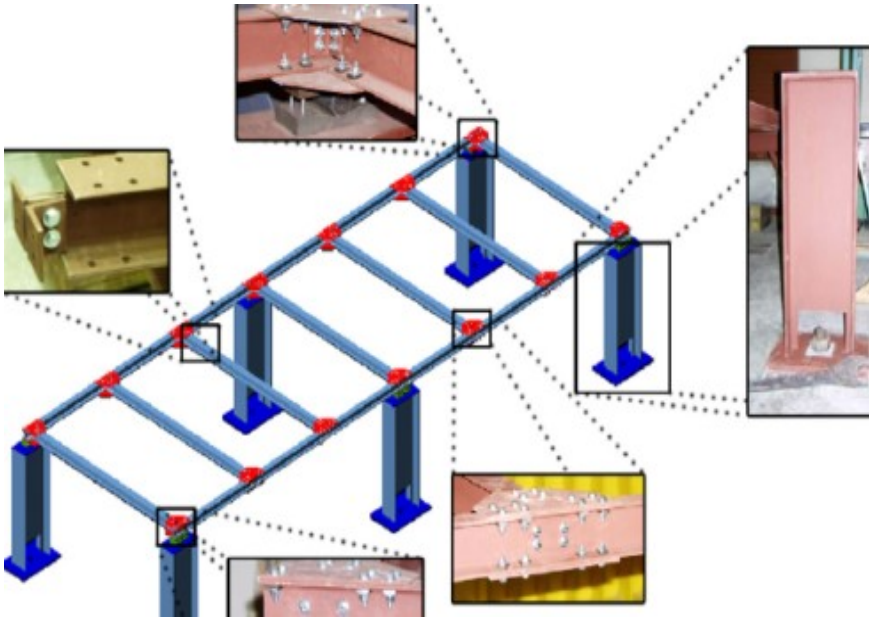


Figure 2.14 Experimental setup in Elsaid and Seracino (2014)

2.4.1.1.2 Small-scale models with soil

Several researchers have looked at the natural frequency and scour-depth variation using small-scale models at normal gravity. When a soil scales down by a length scale factor of N at normal gravity, the self-weight stress of soil also lowers by a factor of N (Madabhushi, 2014).

However, the stiffness properties of soil are dependent on stress, and hence the stiffness properties also scale down as stress level scales down. Therefore, these small-scale soil models would not have represented the behaviour of the corresponding full-scale structure. This scaling issue is discussed further in Chapter 4.

Prendergast et al. (2013) tested a small-scale soil-pile model at normal gravity, as an additional test to a full-scale pile tested in the field. The small-scale pile was a steel rectangular hollow section buried in the sand. Scour was simulated by removing layers of sand incrementally up to 200 mm depth, as shown in Figure 2.15(b). The natural frequency values found for different depths are plotted against scour depth in Figure 2.15(a). The natural frequency showed a 50% reduction as a result of scour depth of 200 mm, which is equivalent to 40% of the initial depth of pile embedment.

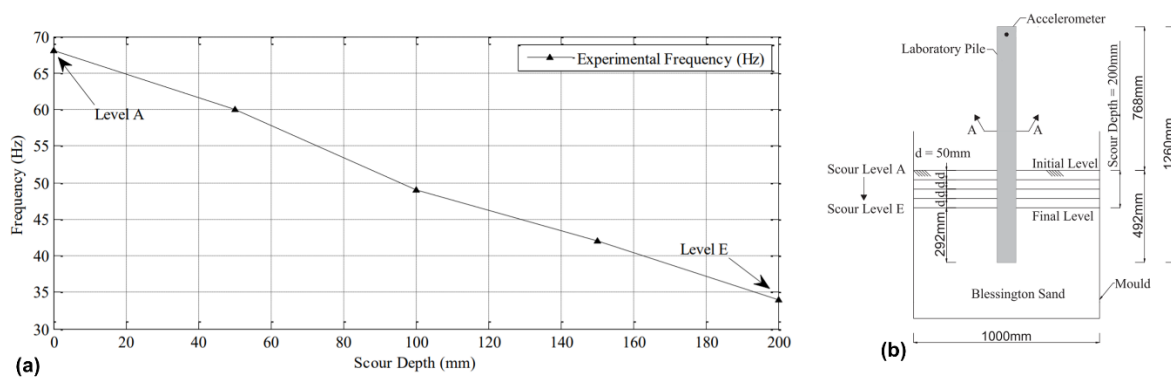


Figure 2.15 (a) Natural frequency variation of the single pile with scour and **(b)** experimental setup in Prendergast et al. (2013)

Similarly, Boujia et al. (2017) studied the relationship between natural frequency and scour of rods embedded in the soil. Two rods of different lengths (60 cm and 80 cm) showed a similar relationship between the exposed length and natural frequency, suggesting that the frequency is independent of the embedded depth. The average frequency change resulting from 5 cm of scour was 15%.

While the natural frequency variations shown in both of the above studies were significant, the soil-pile interaction provided for a rod does not directly represent a bridge behaviour. A bridge with a complex superstructure arrangement with added stiffness and mass may have a vastly different variation with scour. Additionally, this soil-structure model does not represent a full-scale pile because stiffness properties do not scale correctly in small-scale soil models tested at normal gravity, as explained before.

2.4.1.1.3 Full-scale models

Researchers at Texas A&M University conducted a full-scale bridge model experiment in a flume to artificially create scour and study the feasibility of different scour monitoring techniques, including the vibration-based method (Briaund et al., 2010; Yao et al., 2010a). Two

bridge models were considered, one representing a single-pile deep foundation (Briaund et al., 2010), and the other representing a single-pile shallow foundation (Yao et al., 2010a); and the same bridge models were simulated using FEM in this research, as explained in Section 2.4.1.3.2. A precast slab was rested at the top of the pile foundation to model a bridge, as shown in Figure 2.16. The foundations were embedded in fine, clean silica sand. The speed of water in the flume was gradually increased until the sand eroded, creating a scour hole large enough to cause significant foundation tilt when it was declared as failed.

As shown in Figure 2.17, the horizontal natural frequencies of both the deep and shallow foundation bridge models did not provide early warning of scour. A vertical mode of shallow foundation did provide an early warning; however, this is an unreliable result, since horizontal direction modes are typically more sensitive to scour than vertical direction modes (Elsaid and Seracino, 2014).

This research in Texas A&M University was one of the first laboratory experiments in a flume to study the natural frequency variation of a bridge due to scour (Briaund et al., 2010; Yao et al., 2010a). However, the foundation depth considered was a minimal value of around 0.3 m for a shallow foundation and 0.45 m for a deep foundation, both of which are lower than the foundation depths of a typical bridge. Additionally, this bridge does not represent a typical full-scale simply supported bridge, since there were only 1.8 m spans with no bearings.

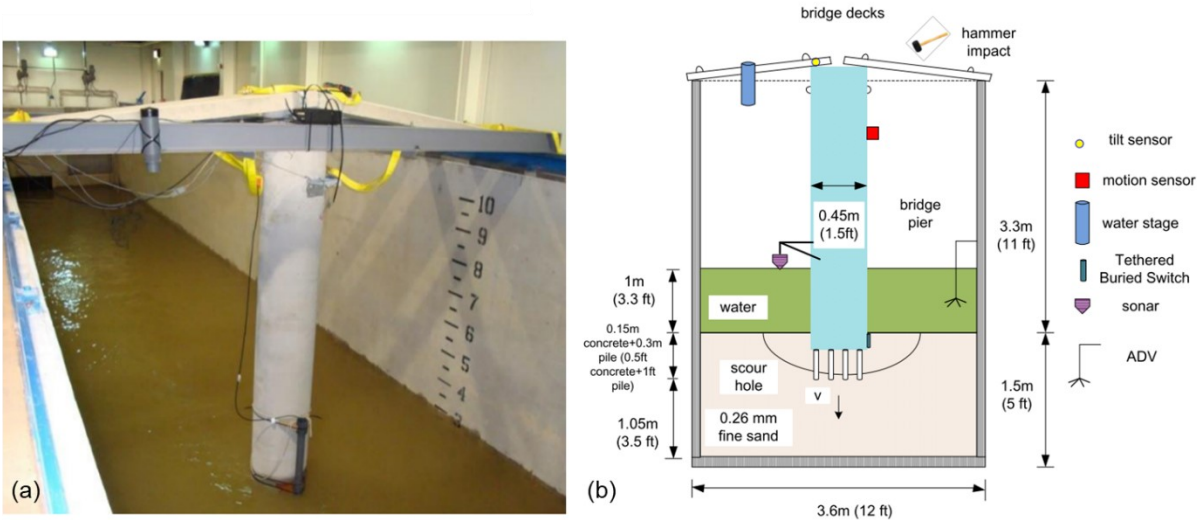


Figure 2.16 Experimental setup of the deep foundation (a) during the experiment (b) schematic diagram (Briaund et al., 2010)

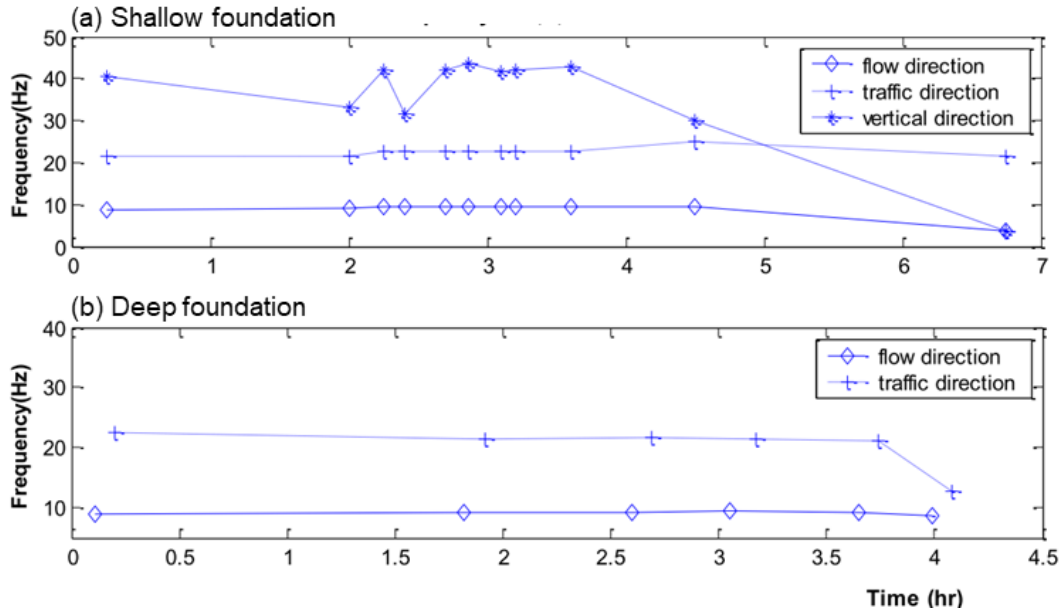


Figure 2.17 Change of fundamental natural frequency for (a) shallow foundation, which failed after 7 hours and (b) deep foundation, which failed after 4 hours in the flume (Briaund et al., 2010)

Prendergast et al. (2013) conducted a field experiment with a full-scale single circular hollow steel pile embedded in a dense sand bed. Layers of sand were removed around the pile in 0.5 m steps using an excavator to simulate scour. At each scour step, impact testing was carried out to find the natural frequency of the pile. The measured variation of fundamental natural frequency with the scour depth is shown in Figure 2.18. The experimental natural frequency lowered from 33 Hz to 2 Hz (94%) as a result of scour of 6 m of the piles initially embedded by 6.5 m. The numerical natural frequency variation estimated is also shown in Figure 2.18, and it has also estimated a significant reduction in natural frequency (90 – 95% drop for 6 m of scour depth). This study indicates that a full-scale pile in soil has significant sensitivity in natural frequency to the depth of scour.

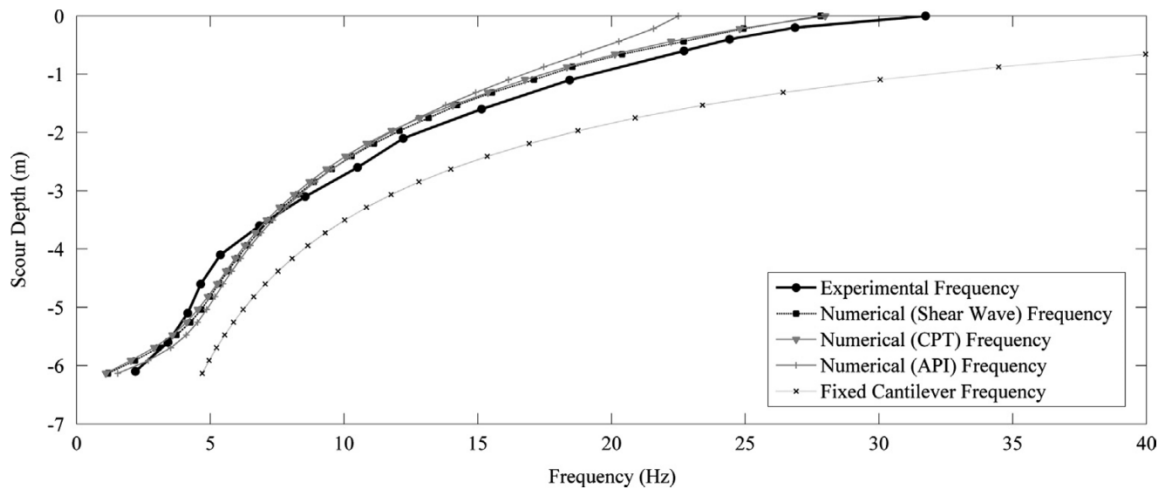


Figure 2.18 Frequency change with scour in the field experiment (Prendergast et al., 2013)

2.4.1.2 Field sensor deployments in real bridges

Field sensor deployments that have attempted to study natural frequency and scour relationship can be mainly categorised based on the source of vibration. In one study, impact vibration was the source of vibration, while all other studies looked at a more practical method of using ambient vibration as the source of vibration. These studies are discussed in detail in the following sections.

2.4.1.2.1 Impact vibration tests

One of the earliest mentions of vibration-based scour monitoring of bridges was found in Japanese Railway Technical Research Institute (Shinoda, Haya and Murata, 2008). These researchers used impact vibration rather than ambient vibration for exciting the bridge in order to capture a vibration signal. The impact was generated by an iron ball released to hit a bridge pier, as shown in Figure 2.19. The bridge considered for this impact test had four piers with a simply supported steel truss deck. Some of these piers had higher scour levels than others. Each of these piers was subjected to impact testing. The results revealed that bridge piers with higher scour depths have lower natural frequencies. The most-scoured bridge pier had a natural frequency of 7.69 Hz, while the least-scoured pier had a natural frequency of 12.70 Hz, meaning that there was a significant difference (40%) between the two. The scour depths of these piers were not explicitly mentioned, but a diagram of the bridge shown in Shinoda, Haya and Murata (2008) indicates that the difference in scour depths between the least and most-scoured piers was in the order of 3 – 5 m, assuming that it was to scale. Although this study did not demonstrate the relationship between scour depth and natural frequency of one pier over time, the correlation between scour depth and natural frequency between similar bridge piers shows the potential of natural frequency-based scour detection.

Shinoda, Haya and Murata (2008) claim that the impact vibration test has been a standard method to evaluate the performance of Japanese railway bridges for over twenty years. However, impact testing of a bridge with an iron ball has practical implementation difficulties, since it involves dangerous handling of weights, and potential damage to the bridge, and it can provide only intermittent rather than continuous measurements.

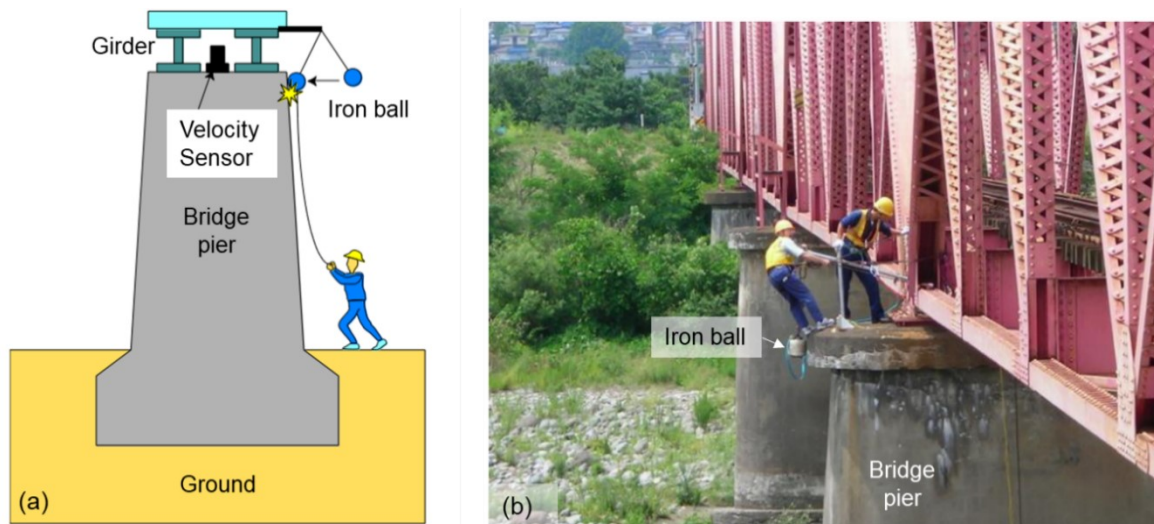


Figure 2.19 Arrangement of an impact test by Shinoda, Haya and Murata (2008) (a) illustration (b) in practice

2.4.1.2.2 Ambient vibration monitoring

Masui and Suzuki (2009) attempted to use the ambient vibration of a railway bridge to measure the scour depth of a bridge pier. Over half a month, a wireless sensor system was captured ambient vibration of the bridge caused by the impact of turbulent water on the bridge piers. The natural frequency was successfully captured using the monitored data. An impact vibration test was also used to verify the natural frequencies of the bridge. However, any change in natural frequency was not captured as the monitoring lasted less than one month, when there may not have been sufficient scour to result in a measurable change in natural frequency.

Yao et al. (2010b) presented two case studies on the installation of different scour monitoring sensors, including vibration monitoring, in real bridges in Texas, USA. Both bridges were monitored with the expectation of capturing any scour. However, neither of the ambient vibration-based sensor installations were successful in showing the potential of the monitoring technique. The main issue was with the modes of the bridge not being sufficiently excited by the ambient vibration from the traffic, and therefore the frequency domain data were not clear enough to resolve the modal frequencies. Additionally, in both bridges, practical implementation difficulties arose, as a result of a large amount of power being drawn by the accelerometers and also network errors. During that time, some other sensors, including tethered buried switches (Section 2.3.2), functioned but were not able to show scour monitoring potential since there was not enough scour to trigger a change in these sensors.

Ko et al. (2010) conducted a field study on Hsinchu Bridge in Taiwan, which suffered from scour. Retrofitting work involved a further increase of riverbed level due to excavations near the foundations, as shown in Figure 2.20. The natural frequency was assessed in the pier before and after retrofitting using ambient vibration measured in both longitudinal and transverse directions. In the longitudinal direction of the bridge, the frequency of the first mode

reduced from 3.6 Hz to 3.4 Hz as a result of the excavation. This difference is not significant (5%), and the reason for this small difference could be the effect of the longitudinal constraint by the superstructure. The lateral fundamental natural frequency, however, reduced from 2.0 Hz to 1.5 Hz, a 25% reduction for the 3 m of excavation. The excavation is representative of the removal of soil due to scour, and hence this case study has shown the potential of frequency-based techniques to measure the change in bed level in a real bridge. However, the water was not present during the study and the retrofitting is representative of an extensive global scour case.



April 2009 (piles exposed around 4.5m)



July 2009 (piles exposed around 7.5m)

Figure 2.20 Foundation exposure of Hsichou Bridge, Taiwan (Ko et al., 2010)

2.4.1.3 Numerical modelling

A number of researchers have carried out numerical studies to identify the natural frequency variation in bridges due to scour and to validate laboratory experiments. One study used the natural frequency measurements for risk analysis of scour induced bridge failure. These numerical studies are explained in the following sections.

2.4.1.3.1 Numerical modelling without considering soil-structure interaction

Elsaid and Seracino (2014) analysed the laboratory experiment of a small-scale bridge model with a fixed base (Section 2.4.1.1.1) using an FE model developed with SAP2000 structural analysis software. The FE model analysis verified the experimental finding that the scour (increased pile height) causes greater natural frequency changes in horizontal than vertical modes. Hence, Elsaid and Seracino (2014) suggested that the frequency of vertical mode shapes could help in assessing the damage resulted from other causes, such as fatigue. The frequency change was found not to be high in the several higher-order modes, in which there was no pier excitation in the mode shape. The difference in the natural frequencies of the numerical model and the experimental model was less than 8%. However, the soil-structure interaction was ignored in this FE model.

2.4.1.3.2 Numerical modelling of soil-structure interaction with elastic half-space

The full-scale flume bridge tests conducted by Briaund et al. (2010) (Section 2.4.1.1.3) were also numerically simulated. These experiments had two bridge models, one with a deep foundation and the other with a shallow one, tested in a hydraulic flume to study the effect of scour on the natural frequency of vibration. The numerical 3D FE models were generated by HyperMesh software and then analysed in the LS-Dyna software program. The soil-structure modelling was performed as an elastic half-space. The soil modulus of elasticity was taken as a constant value: this is likely to be a significant error of the FE model, as soil stiffness is depth-dependent, as explained in Section 4.12. Scour was simulated by removing a section of the soil model around the foundation. The eigenvalue analysis was conducted to obtain the mode shapes and natural frequencies at each of those scour levels. The results of the experiment and the simulation, shown in Figure 2.21, matched only in some cases. For example, the experimental and numerical results showed a difference of 10% in the traffic (longitudinal) direction and about 60% in the flow (transverse) direction. However, both the experiment and the simulations showed a trend of natural frequency reduction with scour.

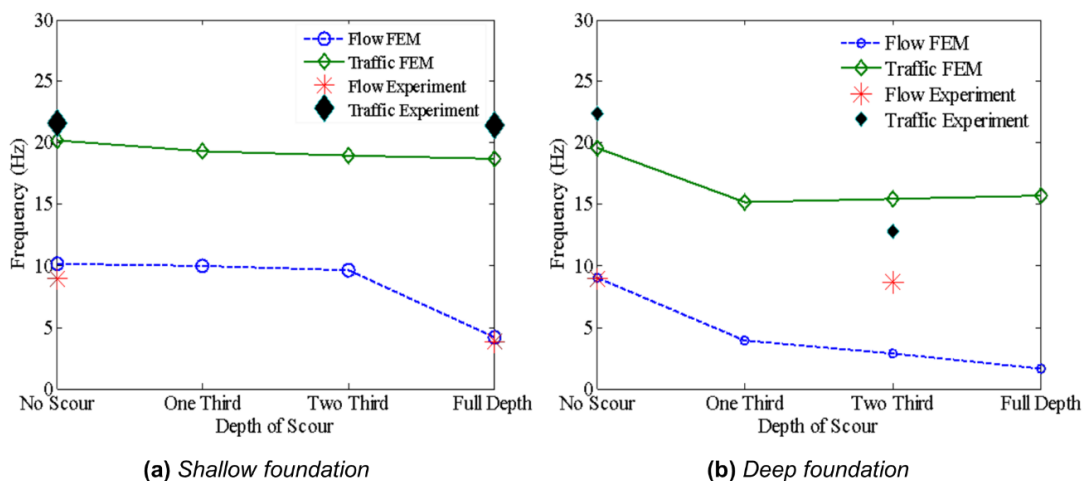


Figure 2.21 Natural frequency variation with scour depth observed by Briaund et al. (2010)

2.4.1.3.3 Numerical modelling with soil-structure interaction of a pile by Winkler model

Prendergast et al. (2013) numerically simulated the laboratory-scale pile test (Section 2.4.1.1.2) and the full-scale driven pile test (Section 2.4.1.1.3). The numerical models were created in MATLAB as shown in Figure 2.22; the structural elements were modelled using beam FE elements and the soil-pile interaction was modelled by using a Winkler spring model, which represents the soil as a series of discrete, mutually independent, closely spaced springs (Winkler, 1867; Dutta and Roy, 2002; Prendergast, Hester and Gavin, 2016a). These springs were assumed to behave under the small-strain condition, and the stiffnesses were estimated by two *in situ* measurements (shear wave and cone penetration tests) and one empirical estimate, the American Petroleum Institute (API) Code. The scour process was simulated by

progressively deleting these springs down to the depth of scour below the initial soil surface level.

The numerical model for the laboratory experiment showed a good match with the experiment only when a constant stiffness distribution was modelled, but not when a varying stiffness distribution was modelled as in the API method. As the author states, the compaction mechanism may have resulted in such a constant stiffness distribution, and hence the laboratory experiment results may not have replicated a realistic field condition.

Subsequently, the field experiment was also simulated numerically for the effect of scour. Figure 2.18 shows the natural frequencies obtained in the simulation for different scour levels. The cone penetration and shear wave-based spring set-ups gave the closest relationship to the experimental observations. In contrast, the API method estimated a slightly lower frequency estimate than was observed. All estimates were below the upper bound for the frequency of a cantilever assumed to be fully fixed at the ground surface. These findings show that the experimental natural frequency of a full-scale pile with scour can be simulated with a Winkler spring model.

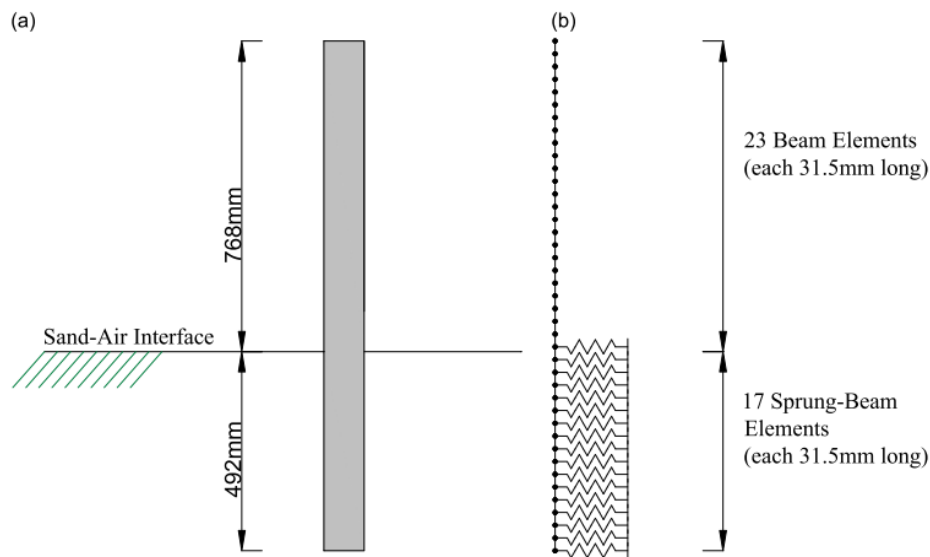


Figure 2.22 Laboratory experiment (a) test setup and (b) the representative numerical model (Prendergast et al., 2013)

2.4.1.3.4 Winkler spring model-based vehicle-bridge-soil interaction model

Prendergast, Hester and Gavin (2016a) and Prendergast, Hester and Gavin (2016b) extended the numerical soil-pile model in Prendergast et al. (2013) to a vehicle-bridge-soil interaction model shown in Figure 2.23. The bridge was modelled to represent a hypothetical integral bridge with two spans and piled foundation. The fluid-structure interaction was neglected, since the reduction of natural frequency due to the presence of water was found to be insignificant (Section 2.4.1.4). The bridge model was developed using MATLAB. The elements used were

six degrees of freedom Euler-Bernoulli frame elements, with equivalent properties of the full deck, pier and pile foundation. Damping ratio of 2% was assumed. Soil spring stiffnesses were estimated from hypothetical cone-penetration resistance profiles. The vehicle model considered suspension, body weight and the effect of tyres. However, the effect of braking and acceleration of the vehicle was neglected. An iterative approach was used to solve this vehicle-bridge-soil interaction model.

The bridge model was assumed to be excited by the sudden arrival of the vehicle, which acts as an impulse load. The vehicle was excited by the presence of a road profile, which causes it to pitch and bounce. Hence, the forces on the bridge are not constant. Ambient vibration of the hypothetical bridge was simulated by obtaining the frequency response at the top of the pier due to the moving vehicle. Then, Fast Fourier Transformation (FFT) was used to identify the natural frequency of the bridge.

The pile groups in this bridge were combined and represented by a single pile, however one pile in practice may not adequately account for the behaviour of the pile group. Similarly, the deck and piers were all represented by single-beam elements in the vertical and longitudinal directions. This would not therefore estimate the mode shapes in the transverse direction of the bridge. However, this vehicle-bridge-soil interaction model has the significant benefit of being able to simulate the vibration-based scour monitoring technique numerically.

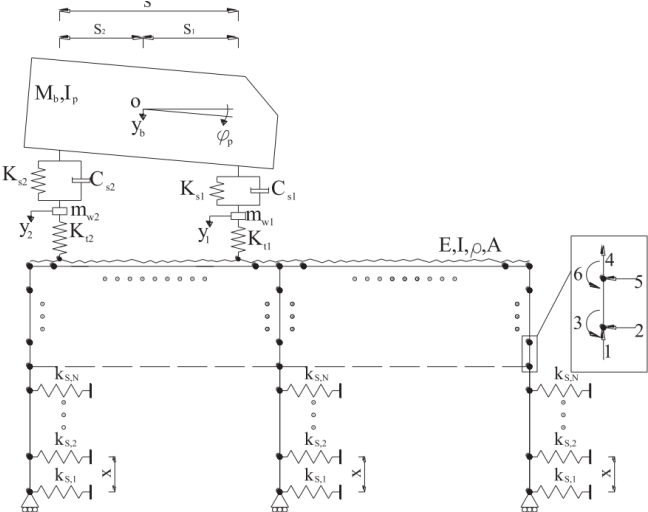


Figure 2.23 vehicle-bridge-soil interaction model in Prendergast, Hester and Gavin (2016a)

Prendergast, Hester and Gavin (2016a) carried out a sensitivity study on natural frequency using the FE model explained above. The following parameters were considered for the study:

1. Signal to Noise Ratio (SNR) in the acceleration signal measured (5 to 20)
2. Vehicle speed (50 kmh⁻¹ to 100 kmh⁻¹)
3. Vehicle properties (front-axle stiffness 400 – 600 kNm⁻¹, gross body mass 9000 – 13000 kg, and body bounce frequency 1.42 – 1.84)

4. Road surface profile (class A to C)
5. Relative density of sand (loose sand, medium dense sand and dense sand)
6. Scour depth (0 – 10 m)

This study found that there was no significant sensitivity of the bridge natural frequency to the first four causes listed above. However, the last two causes, relative density of sand and scour depth, were found to have an effect on the natural frequency. Figure 2.24 shows the high sensitivity of natural frequency to scour depth for three differently dense types of sand. The natural frequency versus scour depth graphs were almost parallel to each other for all three sand types considered. This finding implies that, even if there was an error of the relative density of sand used in the numerical model, the estimated change in natural frequency due to a change in scour depth would not differ.

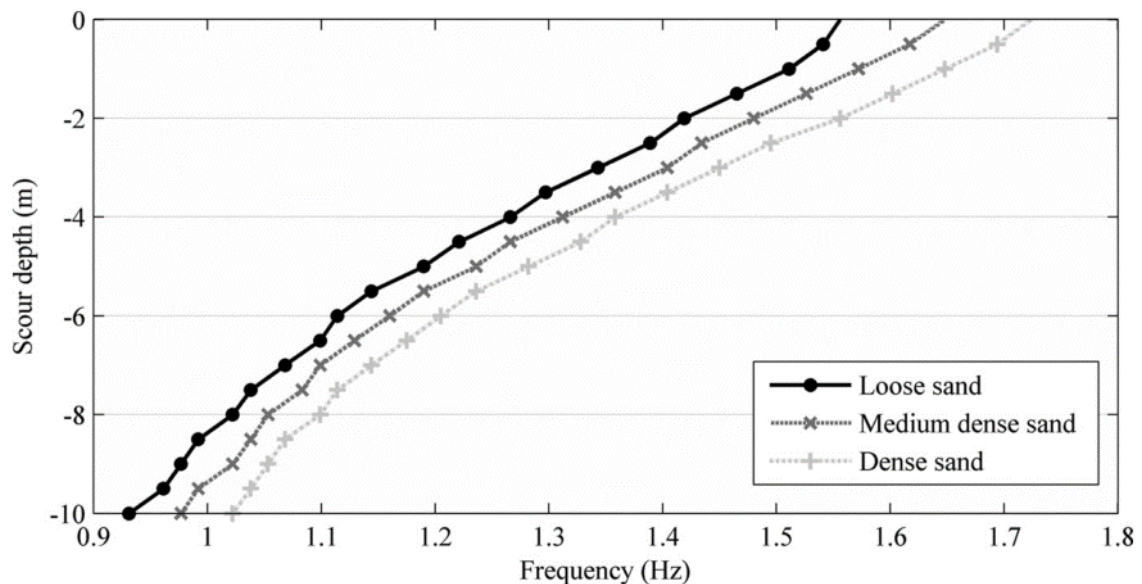


Figure 2.24 Variation of the natural frequency with scour depth for three types of soil

Prendergast et al. (2017) carried out a numerical study to try to identify the location of a scour hole by monitoring the changes in natural frequencies. The numerical model in this study was extended from the vehicle-bridge-soil interaction model developed in Prendergast, Hester and Gavin (2016), as explained above. The soil-pile interaction was provided by a series of lateral and vertical springs, of which the stiffness was based on the API method. The vertical stiffness provided here, however, must not have been contributing to the dynamic properties of the model since the pile bases were assumed fully restrained. The changes in the first five natural frequencies due to four different scour cases were compared, as shown in Figure 2.25. Local scour at a pier, or an abutment, was found to result in significant changes in natural frequency only in the local mode of that pier or abutment, i.e. the mode shape oscillations are local to the pier or abutment. For example, local scour at the left-hand side abutment (“Location A LHS scour” in Figure 2.25) results in significant changes in natural frequency of only the local

vibration mode of the left-hand side abutment, Mode 4 (M4). In contrast, scour across all foundations, i.e. global scour, was found to cause natural frequency reduction in multiple modes. Therefore, there is some potential for scour localisation, by comparing the natural frequency changes of the first five modes, given that these higher-order local modes of vibration can be captured with sufficient signal to noise ratio in the field.

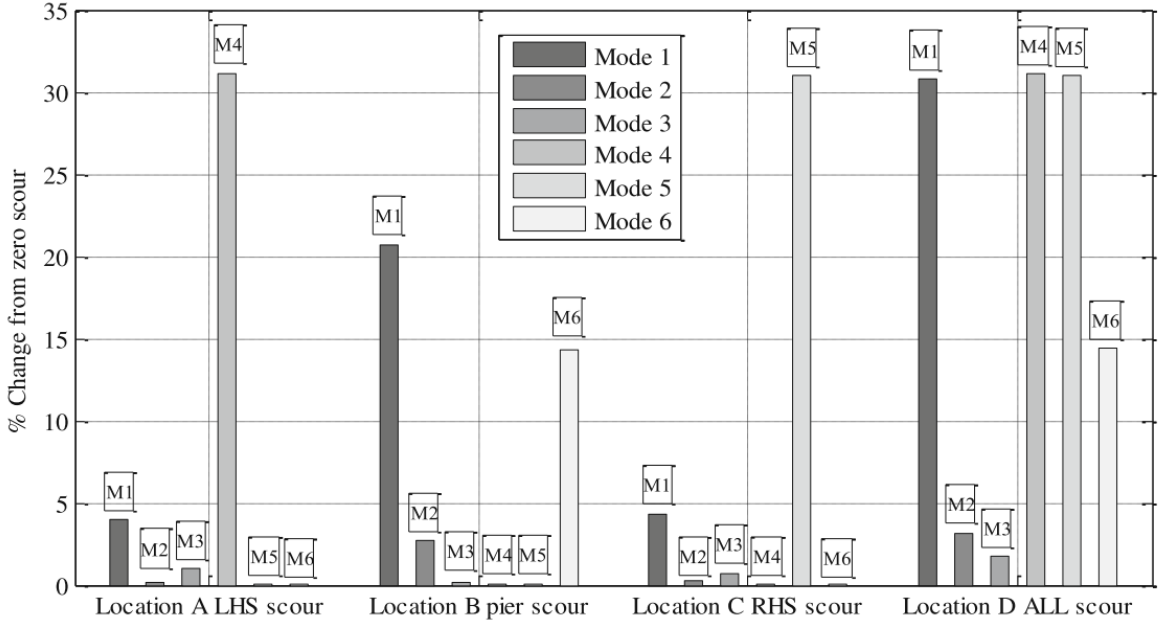


Figure 2.25 Changes in natural frequencies of the first five modes due to 5 m of scour (Prendergast et al., 2017)

2.4.1.3.5 Frequency ratio and maintenance requirements

To help identify maintenance priorities, Shinoda, Haya and Murata (2008) and Liao et al. (2016) discussed the potential to use the frequency ratio between the current natural frequency and initial natural frequency when no scour was present. One challenge in using this ratio was finding the initial natural frequency of the bridge when it was first built. For this, Shinoda, Haya and Murata (2008) referred to a group of equations developed by the Japanese Railway Technical Research Institute (RTRI), which were based on regression analysis of many field data. Only highly sensitive parameters to the natural frequencies, such as the weight of the superstructure, the SPT-N value of soil and the height of the pier, were considered for these equations, making them easy to use. According to Shinoda, Haya and Murata (2008), the RTRI design code further provides frequency ratios, at which different maintenance levels are applicable. The maintenance requirement for different frequency ratios is as follows: (1) less than 0.7: urgent repair is needed; (2) within 0.7–0.85: careful observation needed; and within 0.85–1.0: only a minor problem is present. If there is a frequency ratio of more than 1.0, no maintenance measures are required. All of the piers in a case study bridge studied by Shinoda, Haya and Murata (2008) fall into this category of frequency ratio above 1.0; this is, however,

questionable since the experiment was conducted in a scoured bridge, and hence the frequency ratio should realistically be lower than one.

Liao et al. (2016) studied critical frequency ratio (R_c), which is the frequency ratio of a bridge reaching failure. The critical frequency is reached when the capacity (lateral resistance) of a bridge equals its demand (hydraulic force by flood). If the measured frequency ratio of a bridge is less than R_c , the bridge can be categorised as vulnerable to flood-induced damage. Both the capacity and demand of R_c depend on the scour depth. For calculating the capacity of the bridge due to flooding, a similar approach to that used for earthquake analysis was adopted. The base shear and top displacement of the bridge were plotted for different scour depths by analysing the bridge with push-over analysis using SAP2000 structural analysis software. After that, the yield points of the pier were connected to form the capacity envelope. The demand envelope of the bridge was obtained from the hydraulic pressure equations provided in Taiwan's national code of practice. An example capacity envelope and demand envelope are shown in Figure 2.26. The critical point was taken as the point where demand and capacity envelopes cross each other. The natural frequency representative of this point was found from the SAP2000 model. A parametric study was carried out for five different types of bridge. The parametric study indicated that R_c was in the range of 0.7–0.92 for all of the bridges evaluated. This implies that the natural frequency reductions of finer than 8 – 30% should be measurable in these bridges, in order to provide an early warning of scour damage.

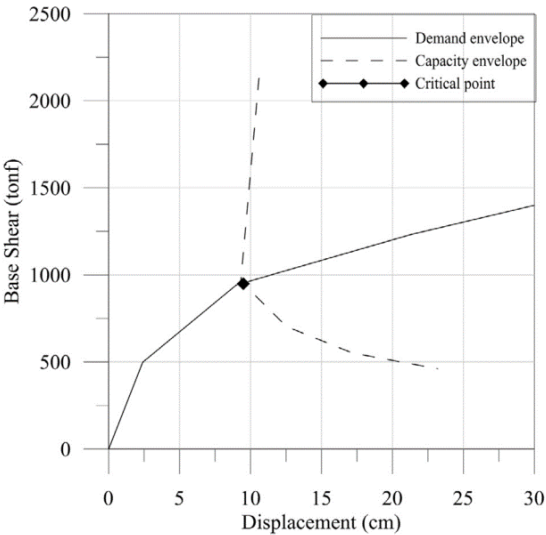


Figure 2.26 Determining the point corresponding to the critical frequency ratio of the bridge

This study was limited to simply supported bridges with multiple spans located in the Gaoping River Basin in Taiwan. Further research and analysis would be required to develop maintenance guidelines based on frequency ratio. This method of comparison of frequency ratio with the critical frequency ratio can aid as an initial health-investigating tool against

hydraulic failure. If the ratio is close to the R_c value, further analysis such as push-over analysis could be carried out to identify the risk of bridge failure.

2.4.1.4 Natural frequency sensitivity to environmental and operational conditions

For reliable scour detection, the measured natural frequency change due to scour should be sufficiently above the expected variability that results from environmental and operational changes. Understanding this variability helps in assessing the feasibility of the monitoring technique.

The natural frequency may vary as a result of environmental and operational causes such as changes in temperature, water level and the effect of vehicles passing over the bridge. Several weeks of monitoring two bridges found natural frequency variations of only 0.3% (Caetano and Magalha, 2009) and 3.5% (Koo, Brownjohn and Cole, 2010). Numerical modelling by Prendergast et al. (2016) found that natural frequencies have little effect (less than 1%) from a passing vehicle. However, a field experiment on a rail bridge found the natural frequencies measured were lower by 8% when the train traversed the bridge (Cantero, Ülker-Kaustell and Karoumi, 2016).

Monitoring of the Z24-Bridge over a one year period by Peeters and Roeck (2001) found only around a 5% difference in natural frequencies for a large temperature range between 0 °C and 30 °C. However, when temperatures went below 0 °C, there was a drastic change in natural frequency (nearly 10%), which was assumed by Peeters and Roeck (2001) to be the result of freezing of supports or asphalt. Kim et al. (2003) studied a simply supported single-span, stainless-steel, plate-girder bridge model in a laboratory environment. When the temperature of the model was changed from -3 °C to 23 °C, the natural frequency of the first mode lowered by 16%, while the second to fourth modes lowered by 6 – 11%, although there was no drastic change near the freezing point.

There is evidence to suggest that the effect of water level can be negligible on the natural frequency of a stiff bridge pier. Prendergast et al. (2013) conducted a small-scale laboratory experiment with three steel cantilever piles with different flexural rigidities. When these piles were tested in air and water mediums, the natural frequency difference between the two mediums was as low as 0.3% for the stiffest pile, which was most representative of a realistic bridge pier. Ju (2013) created an FE model of a bridge considering both soil-structure and water-structure interaction, which was validated using a field measurement. The natural frequency estimated by this FE model reduced slightly as a result of the inclusion of water-structure interaction; however, the natural frequency *change* for a certain depth of scour had almost no effect as a result of the inclusion of water-structure interaction (Figure 2.27).

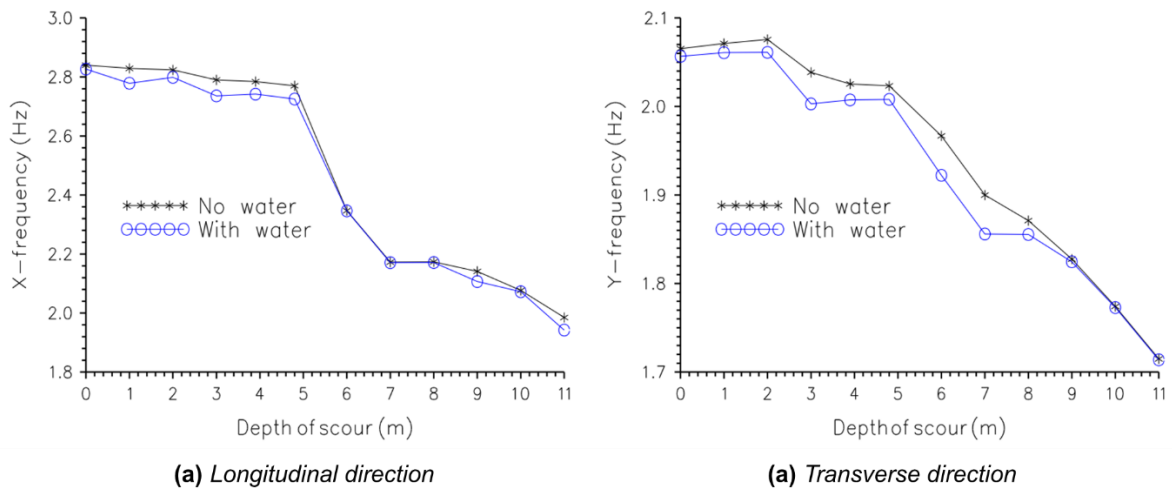


Figure 2.27 Effect of inclusion of water-structure interaction on scour and natural frequency relationship of the FE model

2.4.2 Acceleration-time-history-based parameters as indicators of scour

There are several other research that looked into scour-sensitive vibration parameters other than natural frequency. Fitzgerald et al. (2019) studied the potential of one such parameter; an indicator derived from drive-by acceleration measurements. This research created a train-bridge-soil interaction model, similar to the model developed by Prendergast et al. (2016), but a multi-span, simply supported bridge with shallow foundations at bridge piers. The modelling of the bridge-soil system, however, made several major simplifying assumptions, which may affect the accuracy of the model. These assumptions ignored the lateral resistance of soil and the bearing stiffness effects, and simulated scour as a 30% reduction in vertical stiffness. Simulation of scour in this train-bridge-soil interaction model found that it is possible to identify the presence of scour and the location of scour based on drive-by acceleration measurements alone. Drive-by monitoring of a railway bridge involves placing accelerometers on the wheel boogie of a passing train, without having to place accelerometers on the bridge. The scour indicator was based on the difference of continuous wavelet transform (CWT) coefficients between the healthy and the scoured batches of acceleration measurements. Figure 2.28 shows this scour indicator measured by a train passing over a bridge with a scoured pier located 60 m from the start of the bridge. The scour indicator here peaked when the vehicle passed over the scoured location, showing the potential for scour localisation. As this peak intensity increased with a higher percentage of scour, it also showed the potential to capture the progression of scour. The accuracy of this indicator can be improved by taking averages over a large set of drive-by acceleration measurements; however, such a large set of measurements can delay scour identification after a severe event, since more trains have to pass to provide more averages.

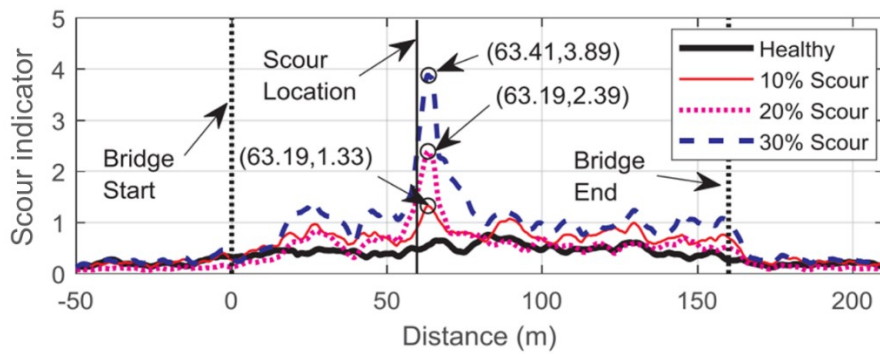


Figure 2.28 Distance versus the scour indicator, different scour levels were simulated at 60 m from the bridge start (Fitzgerald et al., 2019)

Several researchers have proposed a vibration-based parameter called the beta factor, which is the ratio of horizontal and vertical Root Mean Square (RMS) acceleration measurements. This is a parameter that can easily be derived using acceleration traces without having to carry out modal analysis. Beta factor parameter considers a ratio between two direction accelerations, both of which are dependent on the properties of the vehicles passing the bridge. Hence, Masui and Suzuki (2009) presumed that the beta factor (i.e. the ratio of RMS accelerations) is independent of the vehicle properties, and it is dependent only on changes in bridges stiffness, which can be expected during scour.

In order to assess the potential of the beta factor to measure scour, Masui and Suzuki (2009) ran a scaled-down train over a scaled-down bridge, with one pier modelled with scour and another pier without scour. The regression lines of the plot of vertical and horizontal RMS acceleration values of these two piers are shown in Figure 2.29. The plot indicates that the beta factor (gradient) is higher for the scoured pier, which is to be expected, as scour reduces horizontal flexural stiffness of a pier more than its vertical axial stiffness.

Masui and Suzuki (2009) attempted to study the use of the beta factor using ambient vibration monitoring of a real railway bridge. Although the laboratory study found the beta factor to be sensitive to scour, it was unable to verify this in the bridge as a result of no scour being present over the monitoring period. Despite the absence of any scour, the beta value increased from 5.18 to 5.57. Hence, consideration of a margin of error was proposed for the beta factor method; the risk of scour being present should thus be only considered when a limit above the margin of error is exceeded. Yao et al. (2010b) presented two case studies of installation of different scour monitoring sensors, including vibration monitoring, in real bridges in Texas, USA. Both bridges were monitored with the expectation of capturing any potential scour. The beta factors were studied, but a change was not identified, possibly as a result of no scour being present during the time of monitoring.

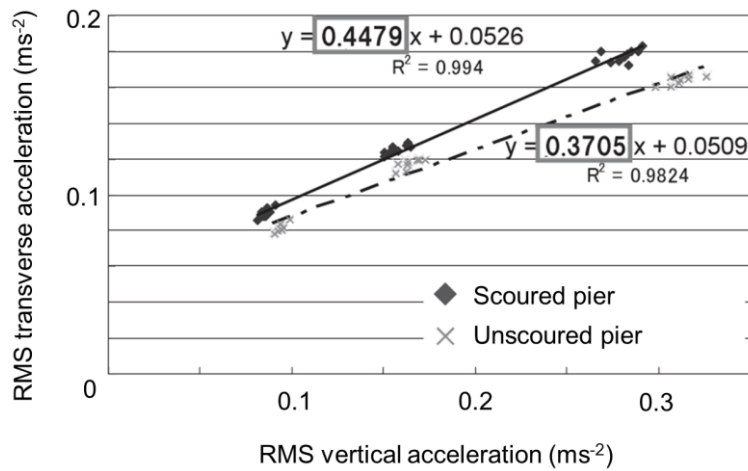


Figure 2.29 Variation of RMS acceleration values in the small-scale experiment, as shown in Masui and Suzuki (2009)

2.4.3 Mode-shape-based parameters as indicators of scour

Elsaid and Seracino (2014) studied a fixed base small-scale bridge in a laboratory, as shown in Figure 2.14 and previously explained in Section 2.4.1.1.1. The modal analysis of the bridge found three damage indicators, namely, (i) mode shape curvature (ii) flexibility-based deflections and (iii) flexibility-based curvatures, which were able to determine the location of scour. The change in flexibility-based curvature was found to be less effective than the other two indicators. These findings were however based on a fixed base experiment setup which did not consider the effects of soil-structure interaction; thus, a bridge with its foundations embedded in soil may behave differently.

Malekjafarian et al. (2019) extended the vehicle-bridge-soil interaction model developed by Prendergast et al. (2016) to study changes in mode shapes due to scour. The Mode-Shape Ratio (MSR) between two sensors on the bridge pier was found to be able to indicate scour, based on numerical modelling predictions. Furthermore, the MSR was found to be more sensitive to scour than natural frequency. As shown in Figure 2.30, a simulated scour case of 5 m local scour resulted in a natural frequency reduction of 20% of the fundamental sway mode, but the MSR reduced by almost 50%. However, MSR was not as reliable as natural frequency under 20% Signal to Noise Ratio (SNR). The authors studied the effect of temperature on these two parameters by assuming different temperature changes in bridge elements cause reductions in material elastic modulus. This simulation found that higher temperatures resulted in an increase in MSR but a decrease in natural frequency, although both parameters reduced as a result of scour. Therefore, both MSR and natural frequency reduction could be directly attributed to scour.

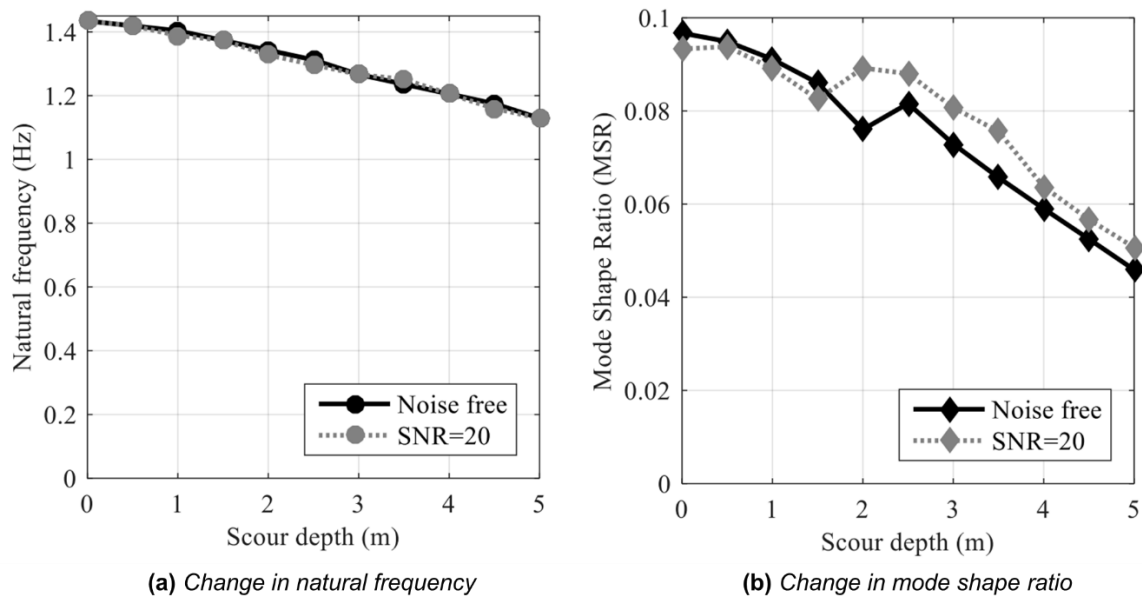


Figure 2.30 Simulation results of local scour at the bridge pier of Malekjafarian et al. (2019)

2.4.4 Research gaps

On the basis of this detailed literature review on the state of knowledge of vibration-based bridge scour monitoring techniques, the following research gaps have been identified:

1. The main scour monitoring parameter in most studies was the natural frequency of vibration, while a handful of studies looked at alternative parameters such as drive-by acceleration, beta factor (RMS value of the acceleration) and mode shape derived indicators. As these alternative parameters may provide more sensitivity than natural frequency, identifying and studying these parameters is vital for the development of the vibration-based scour monitoring technique.
2. It is crucial to establish the types of bridges that show the feasibility of vibration-based scour monitoring via experiments with realistic bridge arrangements. This feasibility study would require considering multiple types of foundations, bridge superstructure arrangements and soil types. The existing experimental studies are either highly simplified or fail to represent realistic foundation conditions; for example, Elsaid and Seracino (2014) neglected soil-structure interaction. Also, Briaund et al. (2010) considered the soil-structure interaction but represented a shallow foundation by part of a column rather than a more realistic pad foundation, while its deep foundation was not deep enough to represent realistic conditions.
3. Centrifuge modelling can represent the field condition of the soil in a laboratory environment, where it is easier to control the foundation exposure level. However, this testing method has not previously been used to assess the feasibility of a natural frequency-based scour monitoring technique of bridges.

4. There is insufficient proof of ambient-vibration-based scour monitoring in real bridges. This is especially applicable in short-span bridges, which may not get sufficiently excited by ambient vibration due to high stiffness, although these bridges are more common than long-span bridges (Kaundinya and Heimbecher, 2011). Ambient vibration monitoring is more practical than the impact vibration method study conducted by Shinoda, Haya and Murata (2008) since it provides real-time, continuous measurements without having to deal with dangerous handling of impacting weights. However, ambient, vibration-based scour monitoring has proved to be difficult to validate in practice. Two bridges studied by Yao et al. (2010b) found that the ambient vibration was not high enough to excite the bridge to find natural frequencies. Masui and Suzuki (2009) saw enough ambient vibration, but no scour occurred underwater during the monitoring period to validate the technique. Ko et al. (2010) did capture a significant change in natural frequency in a long-span bridge; however, the scour was artificially created around the bridge foundation without water present. Therefore, further proof in practice is essential if this monitoring technique is to be practically implemented by bridge engineers. Such proof would require measuring scour depth with another scour monitoring technique as well.
5. The resolution of scour depth measurable by natural frequencies needs more consideration, rather than the expected change in natural frequency. Bridge engineers ideally need to know the exact resolution of scour that the natural frequency-based scour monitoring technique can monitor after compensating for environmental and operational variabilities.
6. Numerical scour simulation techniques discussed in Section 2.4.1.3 require further development to consider different shape of scour (e.g. local and global scour); modes of vibrations in all longitudinal, transverse and vertical directions; and bridges with shallow foundations.

With the aim of addressing these research gaps, the research programme described in the next chapters of this thesis performed a series of centrifuge experiments, field studies and numerical modelling simulations.

Chapter 3

Field studies

Highlights

- The potential for vibration-based scour detection was studied on two bridges: Nine Wells Bridge and Baildon Bridge.
- Nine Wells Bridge was a feasibility study where a field validated numerical model simulated a hypothetical scour case.
- Baildon Bridge was a field trial where ambient vibration was monitored for six months during scour backfilling, i.e. “scour in reverse”, and compared with numerical predictions.
- Natural frequencies showed scour monitoring potential numerically but not in practice.
- First field demonstration of the use of mode shape and spectral density for indicating scour.

This chapter presents a study on the potential to monitor scour using vibration parameters of two bridges, Nine Wells Bridge and Baildon Bridge. A feasibility study was conducted on Nine Wells Bridge, for which a field validated numerical model simulated two damage cases, namely, scour at the foundation and structural damage to the deck. Baildon Bridge, on the other hand, provided a unique opportunity to monitor a bridge while it was being repaired for scour. As this scour repair involved controlled raising of the bed level, i.e. “scour in reverse”, it was an opportunity to study vibration-based scour monitoring in practice. Both these studies fill significant research gaps for the development of a vibration-based scour monitoring technique.

3.1 Feasibility study on Nine Wells Bridge

Recent literature has predicted the natural frequencies of bridges to be highly sensitive to scour depths (Chapter 2); thus, it seems feasible to detect scour by monitoring natural frequencies. However, a plethora of literature, primarily focused on structural damage detection in practice, has found natural frequencies of a bridge to be insufficiently sensitive to damage (Section 2.4.1). Therefore, a numerical modelling feasibility study was conducted with the aim of examining whether natural frequencies of a bridge shows higher sensitivity to scour damage

than to deck damage. This feasibility study was, therefore, an initial step before deciding on starting the experimental programme at Baildon Bridge.

Most recent literature has used simplified 2D numerical models to model bridges and study the effect of scour (Section 2.4.1.3). This section describes the use of a more advanced full 3D FE model of a real bridge to simulate scour and study changes in natural frequencies in both longitudinal and transverse directions. The bridge considered here was Nine Wells Bridge in Cambridgeshire, the UK, shown in Figure 3.1. This is a three-span prestressed-concrete semi-integral bridge with 91.8 m in total length with two piers and two abutments supported on piled foundations. Figure 3.1 also shows the nomenclature used for each abutment, pier and span.

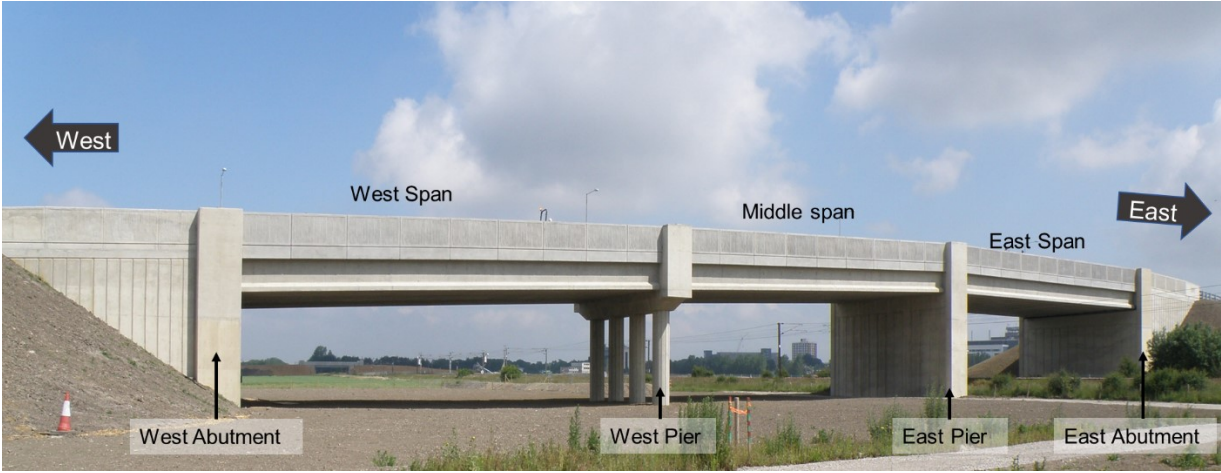


Figure 3.1 *Nine Wells Bridge used for the scour simulation (courtesy of Tina Schwamb)*

3.1.1 Numerical Modelling

The bridge was numerically modelled using CSiBridge2017 structural analysis software. A grillage model was adopted to represent the bridge superstructure. The slight longitudinal inclination of the superstructure present in the real bridge was neglected in the numerical model, and the levels of the foundations were changed such that the piers have their correct heights.

The types of structural elements used in the model are highlighted in Table 3.1, and the FE model is shown in Figure 3.2. Both bridge bearings and soil-pile interactions were modelled using elements that provide stiffness at discrete points. The east pier was modelled using shell elements while all other bridge components were modelled using beam elements. All bridge elements were made of either reinforced concrete or prestressed concrete and were assumed to have uniform elastic Young’s modulus of 35 GPa and density of 2450 kgm⁻³.

The superstructure of Nine Wells Bridge has a skew of about 10%; however, an orthogonal grillage, with longitudinal and transverse grillage members, was still used since it can represent the behaviour of the deck better than a skew grillage (Clark and Cope, 1984). The superstructure of the bridge has prestressed concrete super Y beams with an in-situ composite

reinforced concrete top slab. The longitudinal members of the grillage were placed at the prestressed beam locations, and the transverse grillage members were placed at 0.2 m spacings to allow the piers to be positioned with the skew. The overall section properties of both the prestress beam and the section of the slab spanning over that beam were used for the longitudinal members whilst weightless elements were used for the transverse members to avoid double counting of the mass but represent the transverse stiffness provided by the bridge deck.

Table 3.1 Details of the structural elements used for the numerical model of Nine Wells Bridge

Component of the real bridge	Finite elements used in the model	Details of the elements
Bearings	One-joint links	Define translational and rotational stiffnesses provided from a fully restrained ground support (Computers & Structures Inc., 2016b)
Foundation piles, West pier and parapets	Frame elements	Uses a three-dimensional, beam-column formulation (Computers & Structures Inc., 2016b)
Deck	Frame elements (Grillage model)	Orthogonal grillage with members in the longitudinal and transverse directions
Soil-structure interaction	Springs	Winkler spring model
Pile caps and East pier	Shell elements	Define both membrane and plate bending behaviour (Computers & Structures Inc., 2016b)

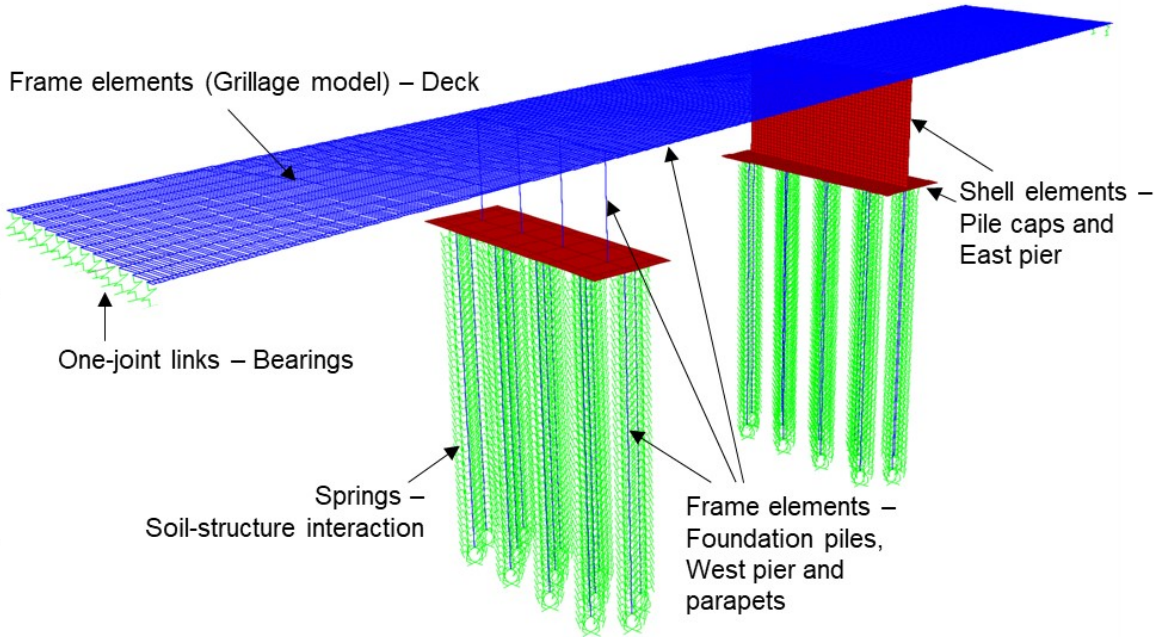


Figure 3.2 FE model of Nine Wells Bridge

The dynamic soil-pile interaction in the transverse and longitudinal directions of the bridge was represented by a Winkler spring model, which represents soil as a series of discrete mutually independent springs along the pile springs (Winkler, 1867; Dutta and Roy, 2002; Prendergast, Hester and Gavin, 2016a). The vertical skin friction of the piles was neglected, and a fully fixed restraint was provided vertically at their base levels. This restraint results in higher vertical stiffness than the real bridge. However, it would not affect the accuracy of the estimated natural frequency of the first few modes: in a typical bridge, horizontal modes account for most lower order modes of vibration that have low frequency, since the vertical axial stiffness of a bridge pier is significantly higher than its horizontal bending stiffness. The spring constant was obtained from soil stiffness properties using Ashford and Juirnarongrit (2003) method, as explained in detail in Section 5.2.2. All the soil stiffness properties at Nine Wells Bridge were obtained from Schwamb (2010).

Although this specific bridge does not cross a water body, it was considered to be representative of a typical semi-integral bridge that crosses a water body and hence prone to scour. The water around such a bridge pier would, in theory, lower the natural frequency of the bridge, but this frequency difference is insignificant for a typical bridge that has very stiff piers, as discussed in Chapter 2, Section 2.4.1.5. Therefore, the effect of water on the dynamic behaviour of piers was neglected in this model.

The bridge deck is a semi-integral bridge; thus, it has integral connections at pier-deck joints and bearings at the abutment-deck joints. The bearing properties of this bridge were not available at the time of modelling, and hence the properties of a representative elastomeric bearing given in Akogul and Celik (2008) were used. In order to represent the actual behaviour of the bearings of a typical semi-integral bridge, one of the bearings on the west abutment was restrained against both longitudinal and transverse translations; another bearing on the middle of the east abutment was restrained against transverse translations. The two abutments are highly restrained against horizontal movement by the retained soil and the abutment foundation. Therefore, the abutments were assumed to provide rigid supports to the bearings.

The natural frequency was found by performing an eigenvalue analysis on the FE model (Figure 3.2) developed as explained above. Scour was simulated by progressively removing individual springs along the piles of both West and East pier foundations down to the level of scour, in order to represent a uniform scour condition (as discussed later in Section 4.1, this type of spring removal is representative of simulating local scour at the foundations). The bridge was assessed for the effect of scour around both pier foundations in 1 m thick layers of soil up to a maximum of 5 m.

Table 3.2 Natural frequencies estimated by the FE model (before correcting the in-plane deck stiffness)

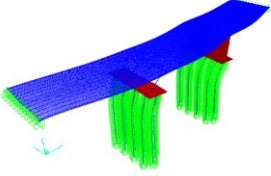
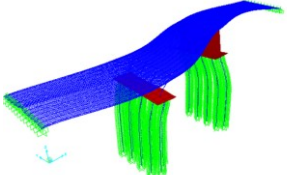
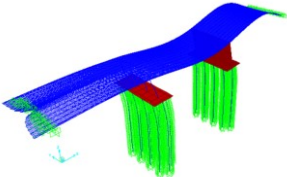
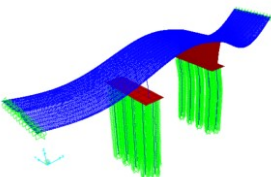
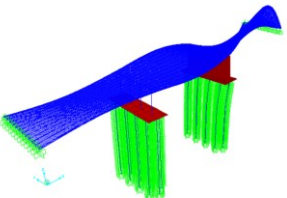
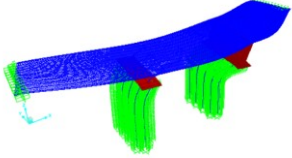
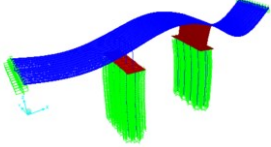
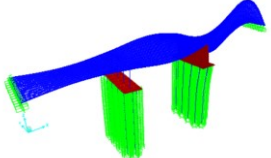
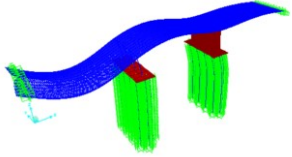
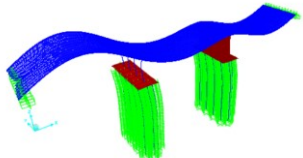
Mode shape	Natural frequency and mode order		Natural frequency change
	No scour (before scour)	5 m scour (after scour)	
Transverse sway (in phase) 	3.08 Hz (Mode 1)	2.13 Hz (Mode 1)	30.8%
Transverse sway (out of phase) 	3.97 Hz (Mode 2)	3.17 Hz (Mode 2)	20.2%
East span bending+ Longitudinal sway 	4.12 Hz (Mode 3)	3.68 Hz (Mode 3)	10.6%
All spans bending 	4.65 Hz (Mode 4)	4.37 Hz (Mode 4)	6.0%
East span twisting 	5.01 Hz (Mode 5)	4.98 Hz (Mode 5)	0.6%

Table 3.3 Natural frequencies estimated by the FE model (after correcting the in-plane deck stiffness)

Mode shape	Natural frequency and mode order		Natural frequency change
	No scour (before scour)	5 m scour (after scour)	
Transverse sway (in phase) 	3.49 Hz (Mode 1)	2.57 Hz (Mode 1)	26.4%
East span bending 	4.46 Hz (Mode 2)	4.25 Hz (Mode 2)	4.7%
East span twisting 	4.91 Hz (Mode 3)	4.88 Hz (Mode 4)	0.6%
Longitudinal sway + west span bending 	5.09 Hz (Mode 4)	4.62 Hz (Mode 3)	9.2%
All spans bending 	5.23 Hz (Mode 5)	5.10 Hz (Mode 6)	2.5%

3.1.2 Natural frequency variation due to scour

The natural frequencies of the first five modes, obtained from the analysis of the maximum scour depth of 5 m, are presented in Table 3.2. A large (over 10%) change in natural frequency was observed in the first three modes. The order of the natural frequencies of the modes did not change after scour.

Generally, out of plane bending of the deck becomes the first mode of vibration in a bridge (Briaund et al., 2010); whereas here both the first and second modes involve in-plane bending of the deck. This behaviour was later found to be due to the grillage model not providing sufficient in-plane bending stiffness. O'Brien and Keogh(1998) state that grillage models adopt inaccurate in-plane stiffness due to the likelihood that the grillage beams tend to bend individually in a similar manner to a Vierendeel girder. In order to correct this issue, massless, plane-stress, membrane elements were used to connect the nodes of the grillage. Table 3.3 and Figure 3.3 shows the natural frequency variation estimated by this corrected FE model with its in-plane bending stiffness of the deck provided by membrane elements. The corrected FE model has also shown a significant (more than 10%) change of the fundamental natural frequency due to an assumed scour depth of 5 m, whereas the other modes showed smaller (less than 10%) change in natural frequencies.

The order of the last three modes have changed, i.e. the order of the third, fourth and fifth modes, respectively, before scour have changed to fourth, fifth and sixth modes after scour. Such a change of the order of modes has occurred due to differential natural frequency sensitivity for scour, i.e. a higher-order mode had reduced its natural frequency significantly such that it has passed below the natural frequency of the lower-order mode. For example, the Mode 3 before scour ("East span twisting") has reduced its natural frequency from 4.91 Hz to only 4.88 Hz, whereas the Mode 4 before scour ("Longitudinal sway + west span bending") had reduced from 5.09 Hz (higher than east span twisting mode before scour - 4.91 Hz) to 4.62 Hz (lower than east span twisting mode after scour - 4.88 Hz), such that the Mode 4 before scour has become the Mode 3 after scour. This mode order change after scour was the cause for the inconsistent frequency reduction of third and fourth modes at different depths of scour (Figure 3.3). For the first mode that did not have a change of its order shows a consistent frequency reduction for each increase of scour depth. Thus, when comparing different scour depths, it is important to focus on the same mode shape, rather than the same mode number. Therefore, the next parts of the thesis will use the mode shape to compare natural frequencies of two scour cases, and the mode number will always refer to the mode shape corresponding to the mode number before scour. For example, "East span twisting" mode in Table 3.3 was the third mode before scour and hence when "Mode 3" will always refer to the "East span twisting" mode.

The fundamental mode of vibration of this bridge was experimentally established as bending of the deck in the east span with a frequency of 4.53 Hz (Whelan et al., 2010). This mode shape corresponds to any of the bending modes from second to the fourth mode of the corrected numerical model, which have close natural frequencies in the range of 4.46 to 5.09 Hz. The first mode shape identified with the simulation may not have been captured by the experiment since the accelerometers were placed on the deck during this experiment only in the vertical direction and the forced vibration was applied vertically.

There was a limitation on estimating the required thickness of the membrane layer used. Since the grillage was already providing some resistance against in-plane bending, a membrane of only 50 mm was used, with the assumption that the natural frequency will be insensitive to the membrane thickness. However, when the thickness of this membrane was doubled, the fundamental natural frequency of the bridge (without scour) slightly changed from 3.49 Hz to 3.60 Hz. However, this limitation is unlikely to have a significant effect on the expected natural frequency change as the magnitude of the natural frequency change due to even doubling the membrane depth was not significant. This FE model could be further refined using shell elements for the bridge deck slab and frame elements for the bridge deck beams, as was attempted for the Baildon Bridge FE model in Section 3.2.3.

Both the uncorrected and corrected models estimated the natural frequency of the fundamental sway mode to be highly sensitive to scour (26 – 30% change for 5 m of scour).

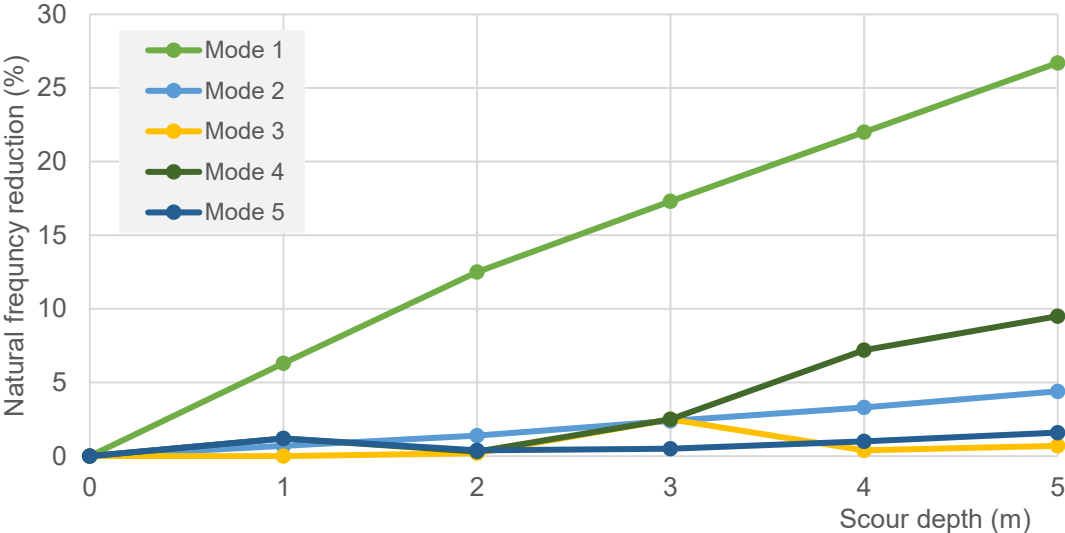


Figure 3.3 Natural frequency change with hypothetical scour depths

3.1.3 Natural frequency variation due to deck damage

The significant natural frequency change estimated for scour damage was compared with a deck damage case. The damage scenario considered in the bridge superstructure was removing of a 200 mm long, longitudinal grillage element that represents both a section of the prestressed beam and the composite top slab section spanning over the beam. This damage

scenario was assumed to represent a full depth flexural crack and hence a significant capacity reduction of the bridge deck. Table 3.4 shows the change in natural frequencies of the first five modes noted in both grillage models explained above. The maximum change in natural frequency was 1.1%, with the overall average being only 0.3%. Hence, the scour induced frequency changes estimated in the scour simulation can be considered as significant, especially the near-30% change of the fundamental natural frequency. These results suggest that natural frequency-based methods show potential for monitoring scour despite the fact that they have not proved effective for detecting deck damage.

Table 3.4 *The natural frequency change of the bridge due to the introduced damage case in the deck*

Mode	Grillage model			Corrected grillage model (membrane providing in-plane deck stiffness)		
	Natural frequency (Hz)		Natural frequency change	Natural frequency (Hz)		Natural frequency change
	Without damage	With damage		Without damage	With damage	
1	3.08	3.08	0%	3.49	3.49	0%
2	3.97	3.97	0%	4.46	4.41	1.1%
3	4.12	4.11	0.2%	4.91	4.90	0.2%
4	4.65	4.61	0.9%	5.09	5.09	0%
5	5.01	5.00	0.2%	5.23	5.22	0.2%
Average			0.3%	Average		0.3%

This feasibility study at Nine Wells Bridge, therefore, concluded that natural frequencies, especially of the lower order modes, have the potential to indicate scour at bridge foundations and it would be worth trialling this method in practice on a full-scale bridge at risk of scour damage.

3.2 Field trial at Baildon Bridge

The feasibility study on Nine Wells Bridge and most numerical modelling studies in the literature (Section 2.4.1.3) indicated that there is significant potential for a scour monitoring technique that uses the changes in natural frequency as an indicator of scour. However, as discussed in Section 2.4.1.1.3, there have been very few field trials assessing this technique on real bridges, none on small-span bridges. Most of these trials have not been able to prove the scour monitoring potential of this technique; thus, this represents a significant gap in the existing studies.

Although field trials are essential to identify the real feasibility of this monitoring technique, they are difficult in practice. This difficulty arises due to the unpredictable nature of scour; a monitoring system would have to be installed on a candidate bridge with no guarantee that natural scouring would occur within the typical timespan of a research project. On the other hand, it is not practical to create scour artificially in a real bridge or construct a full-scale model, and such trials would also pose significant safety issues. Therefore, a different approach was taken for a field trial at Baildon Bridge, which had been subjected to extensive scour at one pier and was due to be repaired by backfilling the scour hole.

As a result of this repair programme, Baildon Bridge provided a rare opportunity to monitor the bridge in both a scoured state, a repaired state, and at various intermediate states as the repairs progressed. The repair works allowed for monitoring of the bridge as the riverbed was raised – in effect, “scour in reverse”. As the repairs involved a controlled variation of the level of the riverbed, this provided an opportunity to undertake a field trial of the ambient vibration-based scour monitoring for a real bridge. The lessons learned from this trial, together with the potential for scour monitoring, are presented in the following sections. The development of the sensor system, riverbed level scanning and initial and final numerical modelling are also discussed in detail. Some of the data collected at this bridge is available from the University of Cambridge Open Data repository (Kariyawasam *et al.*, 2019a).

3.2.1 Baildon Bridge

Baildon Bridge is a three-span reinforced concrete road bridge in Bradford, UK carrying the four-lane Otley Road (A6038) over the River Aire. An aerial image and a diagram of the bridge are shown in Figure 3.4 and Figure 3.5. It has an overall length of 23 m, a width of 20 m and skew angle of 23°. It has two bridge piers, each 4.55 m tall, 0.75 m thick and 21.5 m wide. Each pier is supported on a row of 11 piles. These piles are 6 m deep with square cross-section dimensions 0.4 m x 0.4 m. This bridge was constructed in 1931 replacing a masonry arch bridge. The masonry abutments from the original bridge and reinforced concrete extensions have formed the abutments at the north and the south ends of the bridge (Waterman, 2016). There was no specific information on the abutment foundations; however,

the drawings provided by Bradford Metropolitan Council (Figure 3.5) indicate that they are gravity abutments partially embedded in the banks.



Figure 3.4 Baildon bridge crossing the river Aire © 2020 Bing maps / Blom

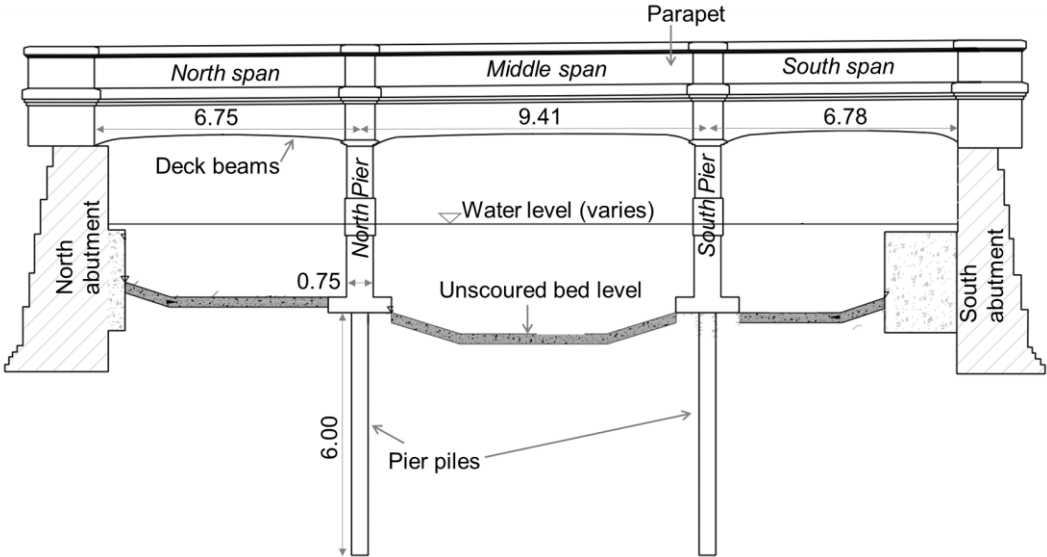


Figure 3.5 Elevation of Baildon Bridge. All dimensions in m (courtesy of Bradford Metropolitan Council)

After a flooding event in 2015, underwater inspection using divers found scouring on one side of the south pier foundation. Bradford Metropolitan Council planned a repair programme to backfill this scour hole.

3.2.2 Riverbed scanning with sonar

Sonar scans were obtained before and after the scour repair works, with the aim of capturing the riverbed profile change due to scour backfilling. These bed profiles were essential to correlate any measured change of vibration parameters to the changes in scour depth.

Sonar scanning of the riverbed was carried out by BridgeCat mobile bridge inspection system shown in Figure 3.6. The BridgeCat system consists of a Unimog all-terrain vehicle fitted with a crane capable of extending 14.8 m below the level of the crane base (Roberts, 2017). With the vehicle parked on the pedestrian pavement and one lane of the bridge near the parapets, the crane was able to reach all locations of interest under the bridge. Once the crane was extended to the desired location underwater, a sonar scanning head at the end of the crane captured 2D sonar images. BridgeCat scanning of the whole bridge was carried out over 6 hours during off-peak daytime traffic after 09:00. The traffic management was provided by Bradford Council to deviate two lanes of traffic in one direction into the middle lane of the bridge while the BridgeCat was in operation.

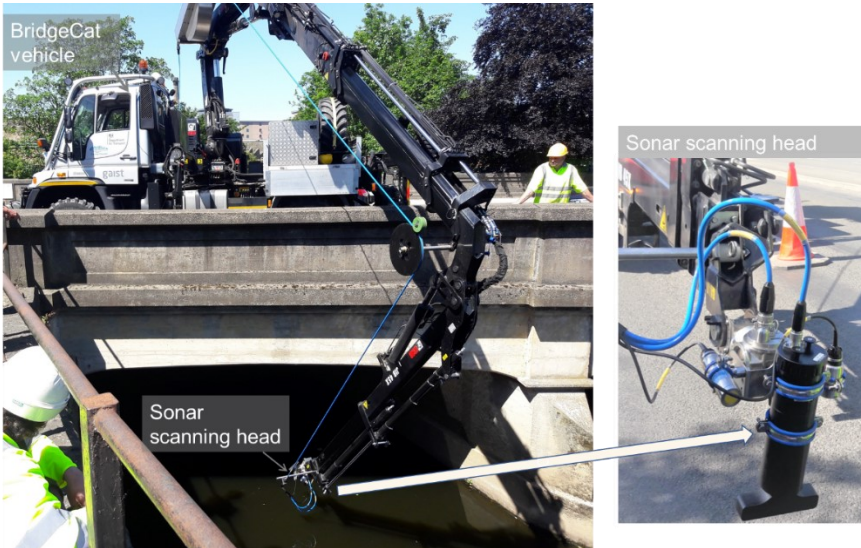


Figure 3.6 BridgeCat mobile bridge inspection system scanning the riverbed using sonar

The sonar images captured before and after the repair are shown in Figure 3.7(a) and Figure 3.7(b), which were obtained by overlaying sonar images taken at each of the three bays. These images have been superimposed in Figure 3.7(c), which shows the scour backfilling at the most heavily scoured location near longitudinal centreline of the bridge (i.e. mid-width of the piers). The backfilling predominantly occurred in the mid-span region between the piers and towards the south pier, while there was little change of bed level below the north pier. The bed level profile below the south pier was estimated by interpolating the depths found from these bed scans taken at different widths along the pier. The bed level change below the south bridge pier and approximate heights of material backfilled are shown in Figure 3.8. The maximum

scour depth of about 1.8 m under the south pier was backfilled with 1.2 m depth of soil topped by a layer of concrete-filled bags and a concrete mat.

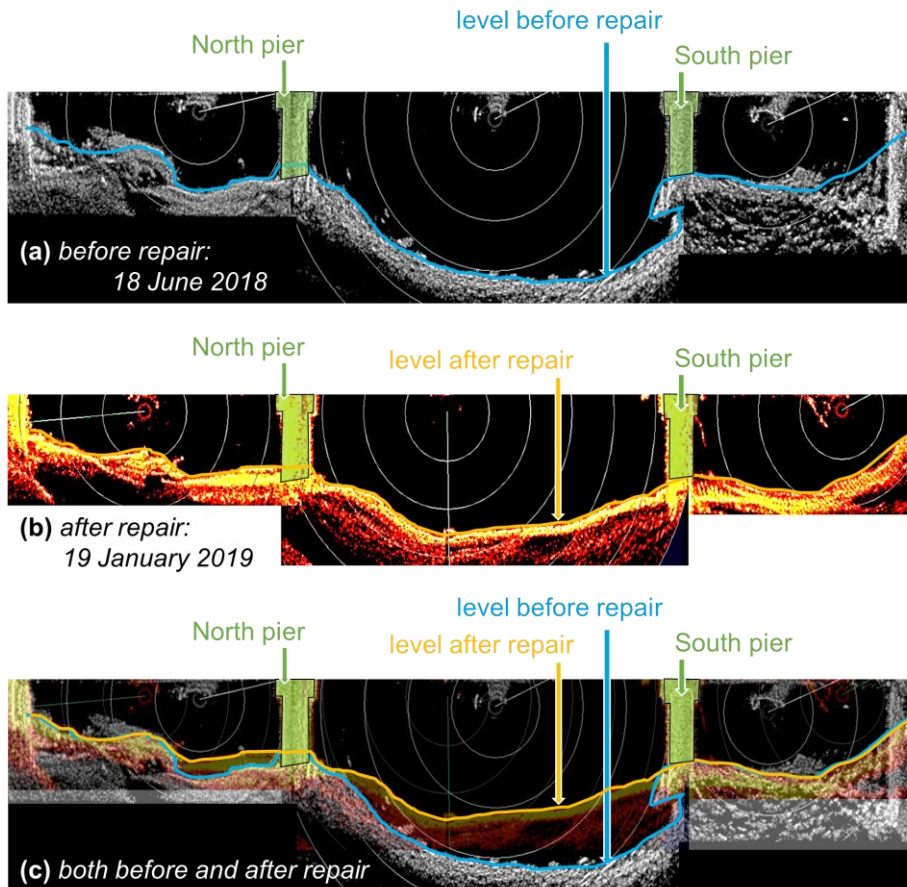


Figure 3.7 Sonar scans showing the change of the bed profile (Image courtesy of Jenny Roberts, Gaist Solutions)

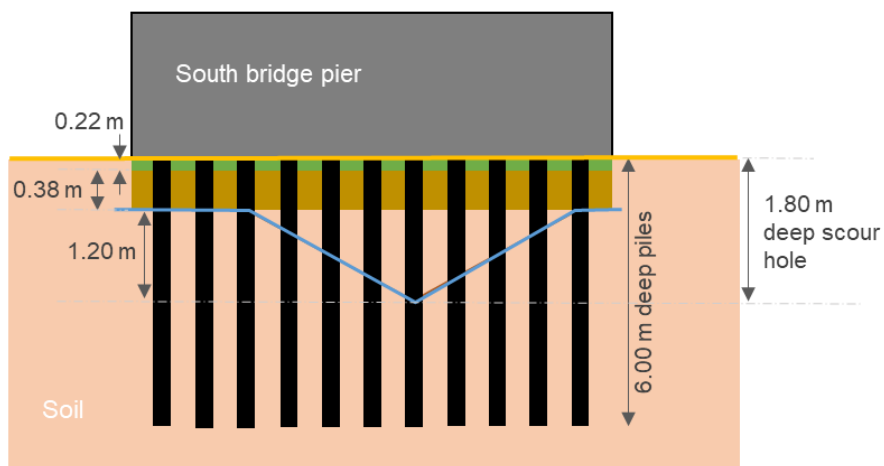


Figure 3.8 Scour backfill at the south bridge pier

3.2.3 Initial numerical scour simulation

Based on the riverbed profile captured before the repairs started, an initial numerical Finite-Element (FE) model was developed. This initial FE model was created to simulate the change in the dynamic behaviour of the bridge due to the planned scour repair. These initial predictions helped to identify an appropriate field instrumentation system.

Figure 3.9 shows the finite elements used to represent the bridge. The bridge deck slab was represented by shell elements that model both membrane and plate bending behaviour. Bridge deck beams and piles were represented by frame elements, which use a three-dimensional beam/column formulation. The soil-pile interaction was represented by a Winkler spring model. The spring stiffnesses were estimated by the American Petroleum Institute (API) method, as explained in Section 5.2.1.

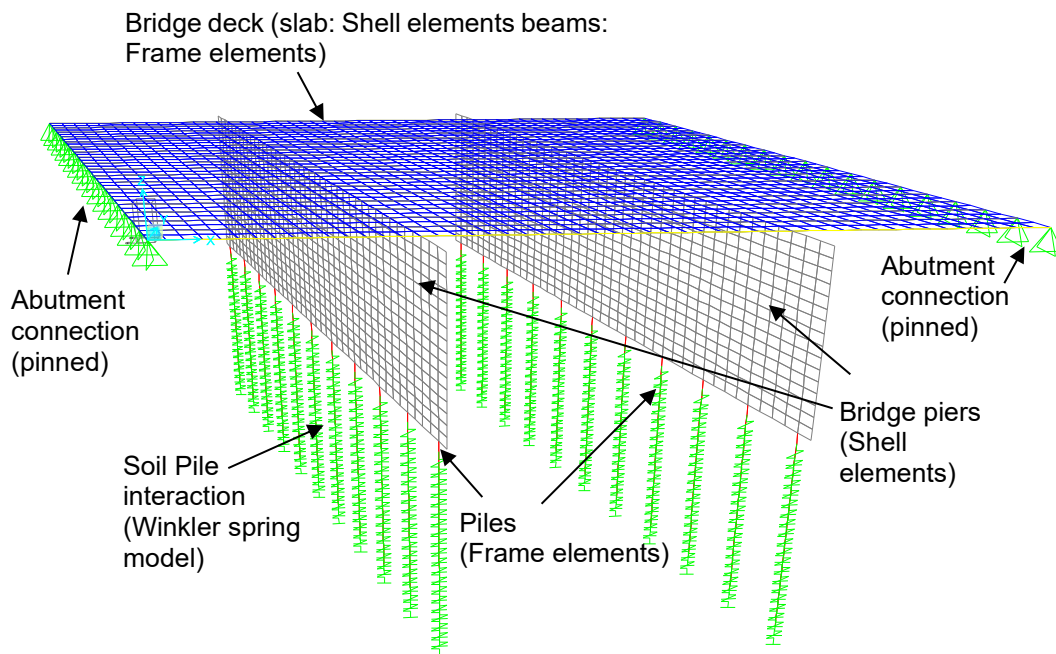


Figure 3.9 Initial Finite-Element model developed to represent Baildon Bridge

The bridge deck slab has two sections: an original 150 mm thick slab; and a 65 mm top layer that was added in 1995 to strengthen the bridge deck. This top layer was dowelled into the existing slab using threaded studs, and hence a “no-slip” connection could be assumed. The deck was therefore considered as a 215 mm composite concrete slab. The beams were offset from the slab to provide the composite beam slab behaviour. The piers are skewed relative to the deck, and hence the size of the deck elements in the longitudinal direction was chosen such that the pier could be connected to the deck while keeping the accurate skew.

The reinforcement arrangement indicated a continuous connection of bridge deck beams over the piers. These beams are coupled with diaphragm beams which rest on the bridge piers and abutments. The interface between these diaphragm beams and the top of each pier or

abutment may have significant friction; hence the connection was assumed to provide full translational restraint. Although the bridge drawings indicated no reinforcement connecting the piers to the deck, some bending stiffness would be present at this interface due to friction. Therefore, an integral (fully fixed) connection was assumed at the beam-pier interface under low-intensity ambient vibration caused by traffic. The connection at the abutment was assumed to provide only translational restraint (pinned) since flexural resistance may not develop as only the end of the deck is resting on the abutments.

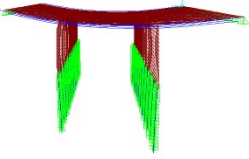
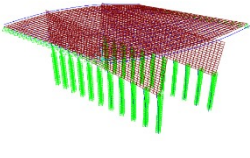
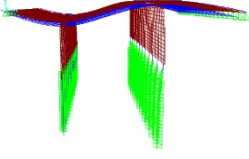
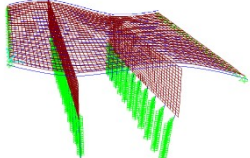
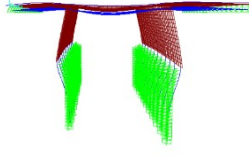
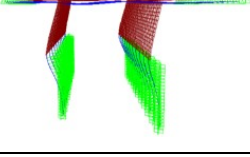
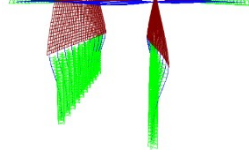
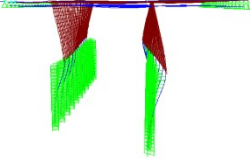
Some other properties of the bridge were not available at the time of modelling and assumptions were therefore made based on engineering judgement. The concrete grade of the piles, pier and deck beams was assumed to be the same as that indicated for the deck slab (C40). Underwater inspection and two borehole records from 1930 identified the soil type up to the pile-driven depth as sandy gravel. The soil was therefore assumed as medium dense sand with 50% relative density.

The springs representing the soil were estimated based on the API method, assuming small-strain behaviour. To allow for 3D behaviour, spring stiffnesses were provided for the piles in both the transverse and longitudinal directions. In the vertical direction, the spring stiffness was taken as the tangent stiffness based on the large-strain value of soil under the dead load of the bridge.

A standard, linear eigenvalue modal analysis was conducted to determine the undamped vibration modes of the system. The repaired bridge after backfilling of the scour hole (“no scour” condition) was first modelled with soil springs along the full depth of piles. The effect of the scour (“with scour” condition) was then simulated by removing the springs at the locations where the scour hole was present in each pile. The effect of the concrete bag wall and the concrete mat was assumed to be similar to the effect of soil.

Table 3.5 shows the initial analysis results for all vibration modes up to 20 Hz. The first four modes were predominantly vertical. The first longitudinal mode, Mode 5, was the most scour-sensitive, showing a 0.73 Hz (4.3%) reduction in natural frequency due to scour. It was therefore expected that scour backfilling would show the reverse (0.73 Hz increase in natural frequency). Instrumentation used in the field test was therefore focused on capturing this mode of vibration.

Table 3.5 Mode shapes captured with the initial FE model and the expected frequency shifts due to scour hole at the south pier

Mode number	Mode shape	Natural frequency (Hz)		
		no scour	with scour	change (%)
1		3.78	3.76	0.5
2		5.42	5.30	2.2
3		8.97	8.96	0.1
4		11.05	10.98	0.6
5		17.10	16.37	4.3
6		18.00	17.72	1.6
7		19.27	18.87	2.0
8		19.70	19.55	0.8

3.2.4 Instrumentation

The initial numerical modelling suggested that the most sensitive mode of vibration to scour depth would have a relatively high frequency (17.10 – 16.37 Hz) and that the expected natural frequency variation would not be significant (only 4.3%). These high-frequency modes may not get significantly excited by the ambient traffic (Wenzel and Pichler, 2005); thus obtaining the expected level of measurement accuracy (less than 4.3%) may be challenging without high accuracy accelerometers. Therefore, high-sensitivity and low-noise accelerometers were needed. The accelerometers used for the deployment were Epson M-A550 QMEMS devices, which claim low output noise of $0.5 \mu\text{g}/\sqrt{\text{Hz}}$ over 0.5 – 6 Hz frequency band and $60 \mu\text{g}/\sqrt{\text{Hz}}$ noise over 6 – 100 Hz band (EPSON, 2018). An internal filter that uses a Kaiser window with 512 taps and a cut-off frequency of 20 Hz was chosen to avoid aliasing when sampled at 200 Hz. With this setting, there was about 6 dB reduction of power spectral density at 40 Hz, and 140 dB reduction of power spectral density at 100 Hz (EPSON, 2018).

The data-acquisition system, developed by Paul Fidler, comprised a data logger, Raspberry Pi and power supplies, as shown in Figure 3.10. The data was logged at 200 Hz by National Instruments NI CompactRIO-9063 system running a custom LabVIEW programme. This data logger connects to accelerometers through three National Instruments NI 9871 RS-485/RS-422 plug-in modules. Each of these modules provided four individually controllable sockets, allowing up to 12 accelerometers to be connected in total in the RS-422 one-to-one configuration (National Instruments (NI), 2016). The Raspberry Pi transferred the logged data to a server located in the University of Cambridge. This data acquisition system was located at the Contractor's yard (Figure 3.4), rather than at the bridge, to protect it from vandalism and sensor cables were run from the data acquisition system to the bridge.

The site conditions required careful consideration in respect of mounting sensors and securing cables in order to minimise drilling while over water. It is challenging to drill a hole into a bridge pier while on a boat as the boat tends to move away from the pier. Therefore, drilling was minimised by running a steel wire between anchor bolts in holes drilled into the two abutments. The sensor cables were run along this steel wire and secured with cable ties and connected to the accelerometers, as shown in Figure 3.11 (a and b). The steel wire was tensioned to avoid it sagging below the soffit level of the bridge beams due to the weight of the sensor cables. Additional steel wires were fixed across the width of the two piers. The accelerometer mountings also avoided drilling by using an adhesive baseplate. This baseplate was pre-fitted with bolts to receive an accelerometer after gluing on to the bridge using high-strength, marine-safe adhesive. These base plates were first glued in place and the following day, once the adhesive was set, the sensors were simply connected to the base plate with nuts and bolts, as shown in Figure 3.11(b). This process allowed mounting the accelerometers without drilling and decommissioning accelerometers by simply unscrewing the nuts.

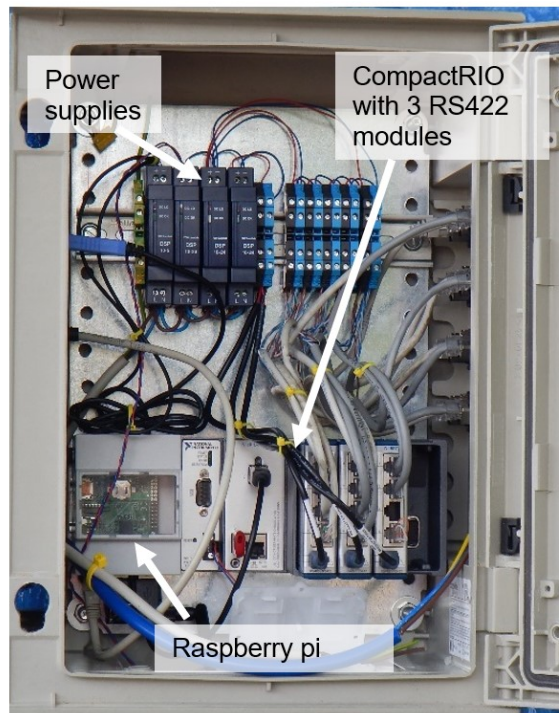


Figure 3.10 Data-acquisition system at Baildon Bridge

The sensor arrangement was chosen in order to capture scour-sensitive longitudinal modes of vibration, as shown in Figure 3.12. Seven M-A550 accelerometers (Nos. 1, 2, 3, 6, 7, 8 and 9) were placed in one vertical plane at the upstream edge of the bridge. Three M-A550 accelerometers (Nos. 4, 5 and 10) were placed halfway along the transverse width of the pier for validation, redundancy and to capture additional modes of vibration. Unfortunately, sensors 3 and 4 did not function – possibly due to damage to the sensor cables caused during installation. The eight remaining sensors provided continuous results throughout the project.

A sampling rate of 200 Hz and a recording period of ten minutes was used for each dataset to obtain acceptable frequency resolution and enable sufficient averaging during modal analysis.

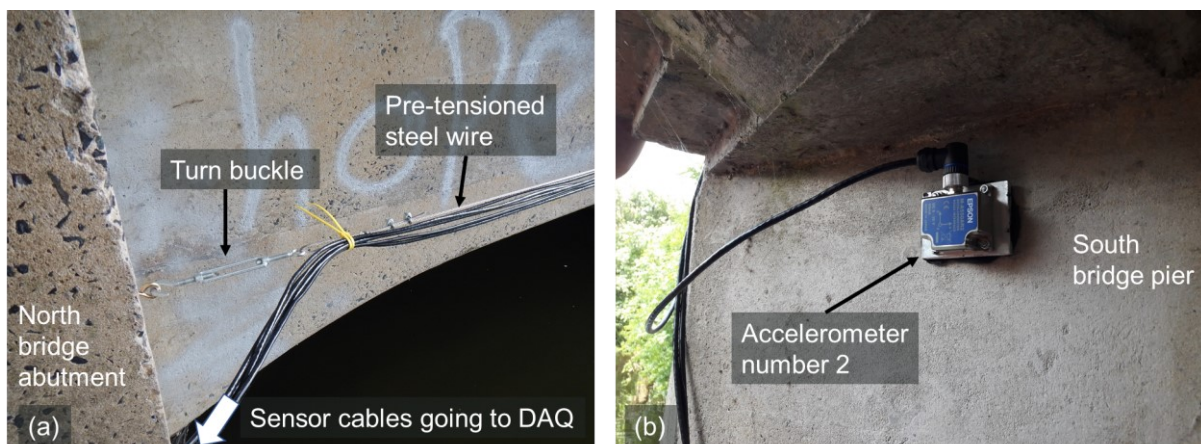


Figure 3.11 (a) cables run on a pre-tensioned wire (b) an accelerometer mounted on the bridge



Figure 3.12 Arrangement of accelerometers at Baildon Bridge

3.2.5 Modal analysis

The accelerometer datasets captured from eight different accelerometer channels were pre-processed to remove any datasets with time synchronisation errors of more than 250 μs (5% of the sampling interval). For these data files, modal analysis was carried out using power spectral density (PSD) and frequency domain decomposition (FDD) methods.

Figure 3.13 shows one example time history acceleration signal and the corresponding PSD and displacement estimates. The acceleration time history in Figure 3.13(a) is part of a 10-minute-long dataset starting from 16:02 on 25th July 2018, and it was captured by the accelerometer number 2 in the longitudinal direction. This time history acceleration has a root mean square (RMS) acceleration of 642 $\mu\text{m/s}^2$. The mean square acceleration is equal to the area under a graph of spectral density (Newland, 1993). Therefore, the PSD curve in Figure 3.13(b) could, in theory, be used to back-calculate the RMS acceleration. The area under the PSD curve is $4.03 \times 10^{-7} \text{ m}^2\text{s}^{-4}$. As this is equal to the mean square acceleration, the RMS acceleration is simply its root, 634 $\mu\text{m/s}^2$, which is almost equal to the RMS acceleration of the time history signal (642 $\mu\text{m/s}^2$), verifying the PSD estimates. The small difference between these two estimates of RMS acceleration arises due to the filtering and averaging used when estimating the PSD values from the time history signal.

Figure 3.13(c) shows the dynamic displacement derived by double integrating the acceleration time history signal in the time domain. This displacement time trace has an RMS displacement of 46 nm, which is extremely low. The displacement corresponding to each mode can also be derived from the PSD plot assuming the structural response is dominated by a single vibration mode over the PSD peaks. Over the range of 4.0Hz to 5.0Hz where a peak is present, the average PSD estimate is -92.6 dB ($5.5 \times 10^{-10} \text{ m}^2\text{s}^{-4}/\text{Hz}$), and hence this range represents a

mean square acceleration of $5.5 \times 10^{-10} \text{ m}^2\text{s}^{-4}$. This corresponds to an RMS acceleration of $23 \text{ } \mu\text{ms}^{-2}$. The RMS value of a sine wave, which represents the modal behaviour at a single point, is equal to 0.71 times the peak value (OpenLearn, 2020). Hence the corresponding peak acceleration is $32 \text{ } \mu\text{ms}^{-2}$. The peak acceleration (\ddot{x}) of a single location of a mode can be related to the displacement amplitude (x) and natural frequency (f) using $[\ddot{x} = -(2\pi f)^2 x]$ based on the double derivative of a sine wave displacement response that represents the modal displacement variation at a point. Hence the displacement amplitude that corresponds to this first peak is 40 nm $[32/(2\pi \times 4.5)^2]$. Similarly, over 18.25Hz to 19.25Hz range where there is a second peak, the PSD estimate is -74.6 dB ($3.44 \times 10^{-8} \text{ m}^2\text{s}^{-4}$), which corresponds to an RMS acceleration of $185 \text{ } \mu\text{ms}^{-2}$, peak acceleration of $270 \text{ } \mu\text{ms}^{-2}$ and a displacement amplitude of 19 nm $[270/(2\pi \times 18.75)^2]$. Therefore, nanometre-scale displacement amplitudes were found to be present at the location of accelerometer 2 based on the amplitudes derived from both the frequency domain and time domain methods discussed above. The manufacturer of these accelerometers do not claim a specific amplitude of vibration the accelerometers can measure; however, there is a claim that the noise density over the frequency band of $0.5 - 6 \text{ Hz}$ to be of $0.5 \text{ } \mu\text{g}/\sqrt{\text{Hz}}$ (EPSON, 2018), which is approximately $4.9 \text{ } \mu\text{ms}^{-2}/\sqrt{\text{Hz}}$ near the first peak discussed above, assuming the noise density is uniform. Hence capturing of $23 \text{ } \mu\text{ms}^{-2}$ ($> 4.9 \text{ } \mu\text{ms}^{-2}$) accelerations and nanometre-scale displacements seems probable. Such low displacement vibrations can be expected since this bridge is short span and stiff with its overall length of only 23 m is supported by two 20 m wide bridge piers. Moreover, the considered sensor is on the bridge pier near the ground level where there can be lower amplitudes of vibration than at the deck. The other accelerometers showed slightly higher spectral density estimates in the singular value plot, which provides an average spectral density estimate of all the sensors (Section 3.2.6). The accelerometer 2 is one of the nearest accelerometers to the ground level. The below ground level displacements and strains could be even smaller and hence this verifies the small-strain soil-structure interaction assumption made for estimating the spring stiffnesses.

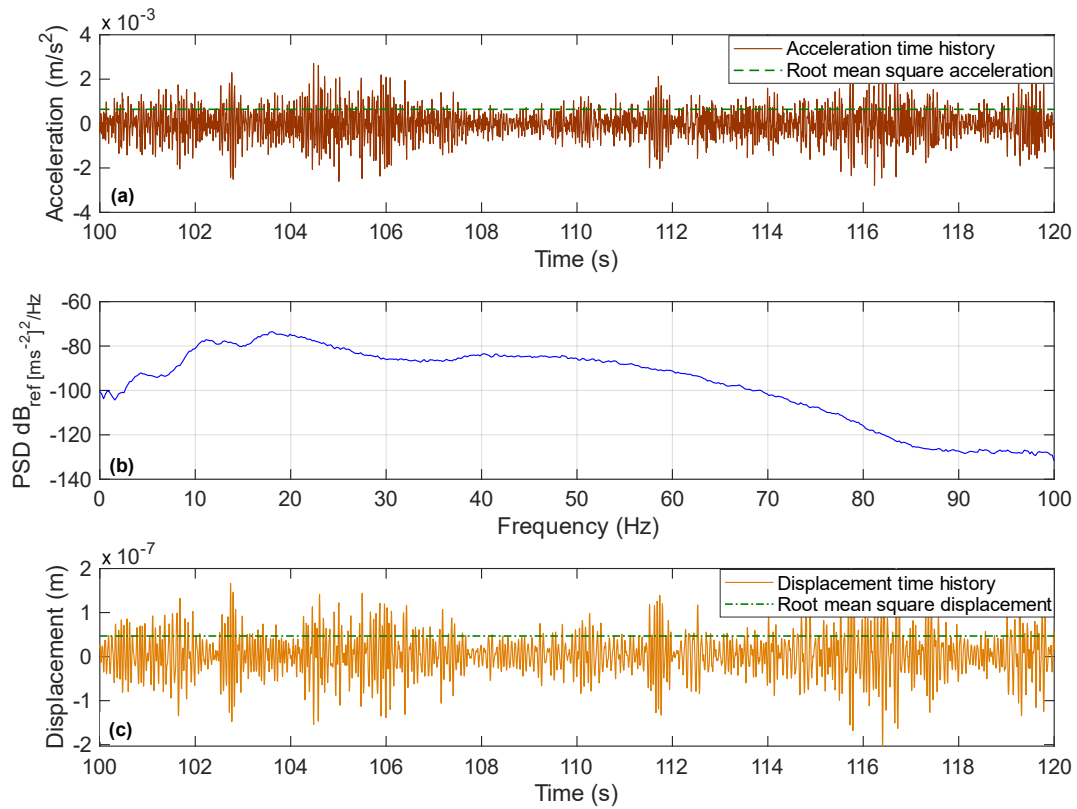


Figure 3.13 (a) An example acceleration time history trace of a dataset, (b) the PSD plot corresponding to the full dataset and (c) the corresponding dynamic displacement trace

Modal analysis was carried out for multiple acceleration measurements from all these eight channels using Frequency Domain Decomposition (FDD) method. FDD requires the Power Spectral Density (PSD) matrix of datasets from all channels at discrete frequencies; this matrix has auto-PSD values of individual channels along the diagonal and cross-PSD values of couple combinations of channels off-diagonal. The FDD method is based on the singular value decomposition of this PSD matrix $G_{yy}(f)$ at discrete frequencies f , as shown in Equation 3.1, where $U(f)$ is the matrix of singular vectors and $S(f)$ is the diagonal matrix of singular values. Over the frequency range associated with a peak in the first singular values of the PSD matrix, the structural response is dominated by a single vibration mode, with the first singular vector being an estimate of the mode shape and the corresponding first singular value being the auto-PSD of the modal contribution found from all sensor channels. The first singular value of the PSD matrix thus provides a single spectral density estimate for multiple accelerometer channels, unlike the auto-PSD estimate of individual sensor channels. Singular value of the PSD matrix is referred to in this thesis as “SVPSD” to differentiate it from auto-PSD of individual channels, which will be referred to with the commonly used terminology “PSD”. The FDD method assumes that the input excitation is broad-band (white noise) and that the structure is lightly damped (Brincker, Zhang and Andersen, 2001; Brincker, Anderson and Jacobsen, 2007).

$$G_{yy}(f) = U(f)[S(f)]U(f)^T \quad \text{Equation 3.1}$$

FDD was carried out in MATLAB. The transverse direction of the bridge showed lower vibration and a lower signal-to-noise ratio than the other directions. Therefore, only the longitudinal and vertical direction sensor channels were taken for FDD analysis. The accuracy of the identified mode shapes was assessed with the modal assurance criterion (MAC) (Pastor, Binda and Harcarik, 2012). MAC estimates the similarity between two mode shapes as a value from 0 to 1, 0 being absolutely no similarity and 1 being perfect similarity.

One main assumption made in FDD is that the source of vibration is a broad-band excitation. The main source of vibration of Baildon Bridge is traffic, which does not provide a perfect broad-band excitation. However, during peak hours, a large number of vehicles passing over the bridge was assumed to provide a reasonably broad-band excitation. Therefore, datasets at peak traffic hours of 16:00-17:00 on were chosen to identify the bridge modes. This one-hour period encompasses six 10-minute datasets thus six natural frequency observations, which should all be ideally same since no significant environmental changes would occur within a short period of one hour.

3.2.6 Numerical model updating based on initial experimental results

The initial modal analysis studied six datasets between 16:02 to 17:02 on 24 July 2018, before scour repair started, in order to update the numerical FE models based on the modal characteristics of the system. These six consecutively-timed datasets of all acceleration measurements showed the first singular values (SVPSD) shown in Figure 3.14. A peak in the first SVPSD indicates a potential mode shape when a consistent mode shape is present. Two prominent peaks with similar mode shape between the datasets were observed. The first peak near 4.5 Hz (uncertainty ± 0.6 Hz) was identified as Mode 1 (a sway mode), but this was not predicted to exist in the initial FE model. The second peak near 18.75 Hz (uncertainty ± 0.8 Hz) was identified as Mode 2, first bending mode, predicted to be the first mode at 16.37 Hz in the initial FE model (Table 3.5).

The peaks at Mode 1 and 2 were further confirmed to be real modes by the high MAC (over 98%, see Figure 3.15) observed when the mode shapes were compared for different consecutively timed datasets measured in the field. The other peaks shown in Figure 3.14, near 0.58 Hz, 10.95 Hz and 11.95 Hz, were assumed to be spurious (non-physical) modes or harmonics of vehicle traffic excitations as these peaks did not estimate consistent mode shapes and natural frequencies at these six consecutively timed datasets. These three peaks near 0.58 Hz, 10.95 Hz and 11.95 Hz showed the same peak present in higher-order SVPSDs - which is a property of harmonics (Jacobsen, Andersen and Brincker, 2007). Therefore, only the two peaks that were near 4.5 Hz and 18.75 Hz were assumed to represent real modes.

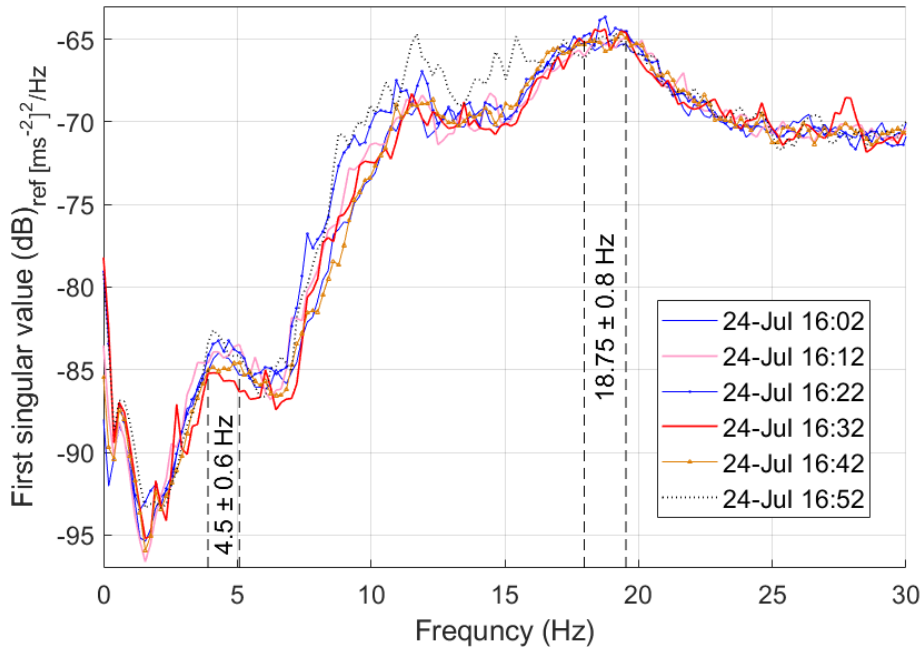


Figure 3.14 First SVPSD of adjacent datasets showing consistent peaks at 4.5 Hz and 18.75 Hz

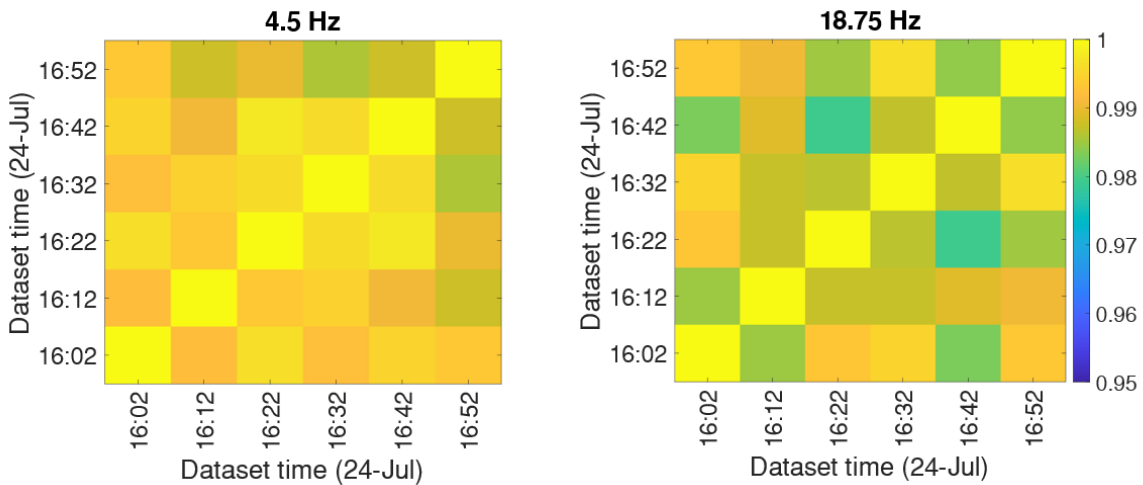


Figure 3.15 Modal assurance criteria for the dataset combinations at modal peaks near 4.5 Hz and 18.75 Hz

The low-frequency, predominantly vertical, modes of vibration predicted in the initial FE model were not detected in the real bridge. This suggests that the vertical skin friction and end bearing at the soil-pile interface was higher than what was assumed with the API design code and 50% relative density for the soil.

Therefore, the API spring representation and the boundary conditions of the initial numerical model were updated to improve the FE model, as shown in Table 3.6. The observed mode near 4.5 Hz was a sway mode which was not detected with the initial FE model. Since the bridge deck beams are joined by a solid diaphragm wall that had been cast on top of the bridge abutments, a pinned connection was assumed at this interface in the initial FE model. The presence of a sway mode in the real bridge indicates that the bridge abutment-to-beam

connections do not provide significant restraint against longitudinal translation. Thus, the FE model was changed (update 1 in Table 3.6) by allowing free longitudinal translation (i.e. assuming a roller support condition) at each of these interfaces, after which, the FE analysis showed a sway mode matching (95% MAC) to the experimentally observed sway mode.

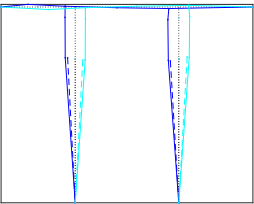
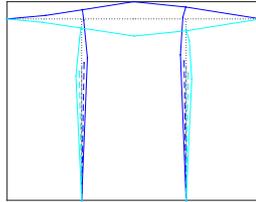
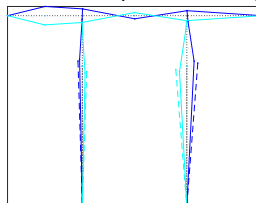
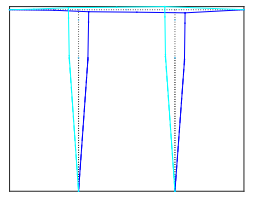
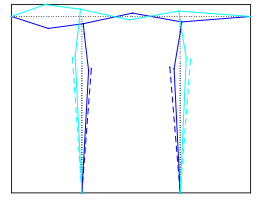
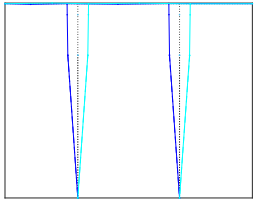
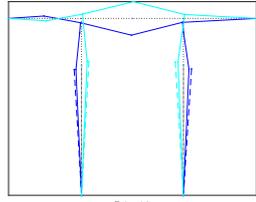
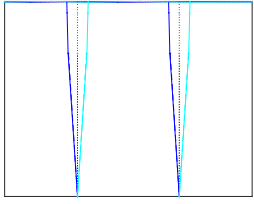
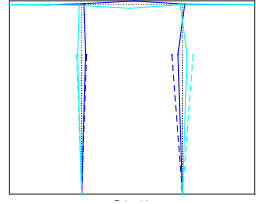
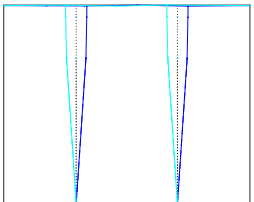
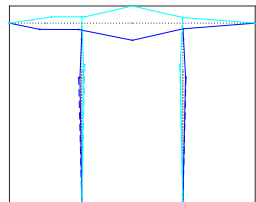
The FE model was further updated (update 2 in Table 3.6) by preventing vertical movement at the base of the piles since no predominantly vertical vibration modes were observed. This change increased the MAC of Mode 2 from 0.3% to 57.8%.

The moment capacity at the pier-deck interface was unclear at the time of initial numerical modelling. It was assumed that moment resistance was present due to the material interlocking friction. However, the drawings indicated no reinforcement connecting the bridge beams to bridge pier and hence one can also argue that there should be no moment capacity at this interface. The FE model was therefore changed to allow for this (update 3 in Table 3.6) by fully releasing the rotational restraint at the top of the bridge pier. This change, however, weakened the MAC of Mode 2 from 58% to 14%, and hence the previous model (update 2 in Table 3.6) with the integral connection at the top of the pier was reselected as the best fitting FE model. This integral connection like behaviour may be present at the top of the piers due to the small-strain levels experienced by vehicle traffic, when interlocking friction may provide moment resistance.

The FE model with update 2 was further updated (update 4 in Table 3.6) with a hyperbolic lateral spring stiffness profile, which was found to be a better representation of soil stiffness than a linear stiffness profile, as explained in Chapter 5 (Section 5.4.2). Similar to Chapter 5, the hyperbolic stiffness profile was derived from Kloeppel and Glock (Kloeppel and Glock, 1970) and Seed and Idriss (Seed and Idriss, 1970). This stiffness profile assumed a saturated bulk density of 1920 kgm^{-3} (50% relative density) and Poisson's ratio of 0.3. The lateral spring stiffness profiles of the initial model and the updated models are shown in Figure 3.16. The API stiffness profile used in the initial model and in FE model updates 1 – 3 in Table 3.6 has a linear change of stiffness with depth. The hyperbolic stiffness profile derived for FE model update 4 gives a higher spring stiffness than the initial FE models over the pile depth of 6 m considered.

The FE model update 4 in Table 3.6, with a hyperbolic soil spring profile, increased the MAC of Mode 2 between the FE model and the experiment to 68%. This update slightly reduced Mode 1 MAC, while still maintaining it at 96%. Therefore, the overall mode shape estimation has improved with the FE model update 4. The natural frequency of the FE analysis has also become closer to the observed mean natural frequency, i.e. natural frequency difference between the FE model and the experiment was 18% for Mode 1 and 0.1% for Mode 2.

Table 3.6 Experimentally observed mode shapes versus mode shapes estimated by the FE model

Stages of modal updating	Mode 1: Sway mode (two piers in phase)	Mode 2: Bending mode (two piers out of phase)
Target: Experimentally Observed	4.50 Hz 	18.75 Hz 
FE no update: Initial FE model	Not detected	16.37 Hz (MAC 0.3%) 
FE update 1: Releasing the longitudinal translation at abutments	2.73 Hz (MAC 95%) 	16.31 Hz (MAC 0.03%) 
FE update 2: Fixing pile base vertical translation + update 1	2.77 Hz (MAC 97%) 	15.87 Hz (MAC 58%) 
FE update 3: Releasing pier top moment capacity + update 2	1.94 Hz (MAC 98%) 	13.11 Hz (MAC 14%) 
Final FE update 4: Spring stiffnesses were updated to hyperbolic profile + update 2	3.69 Hz (MAC 96%) 	18.73 Hz (MAC 68%) 

(MAC compares the mode shape similarities of FE estimates with the experimental observations. Mode shapes: modal amplitudes representing the sensors at the upstream edge are marked in solid lines, and the sensors at halfway along the piers are marked in dashed lines. Two blue colours indicate two extreme sides of the mode shapes)

The FE model with update 4 incorporates a hyperbolic stiffness profile, pile base vertical translation fixity and free longitudinal restraint at the abutments. This FE model may further improve if partial fixities due to friction of the abutment interface can be assumed, though such properties are difficult to predict. Update 4 provided natural frequency and mode shapes that were considered acceptably similar to the experimentally observed results, so it was adopted as the final FE model to estimate the natural frequency and mode shape changes due to the scour repair.

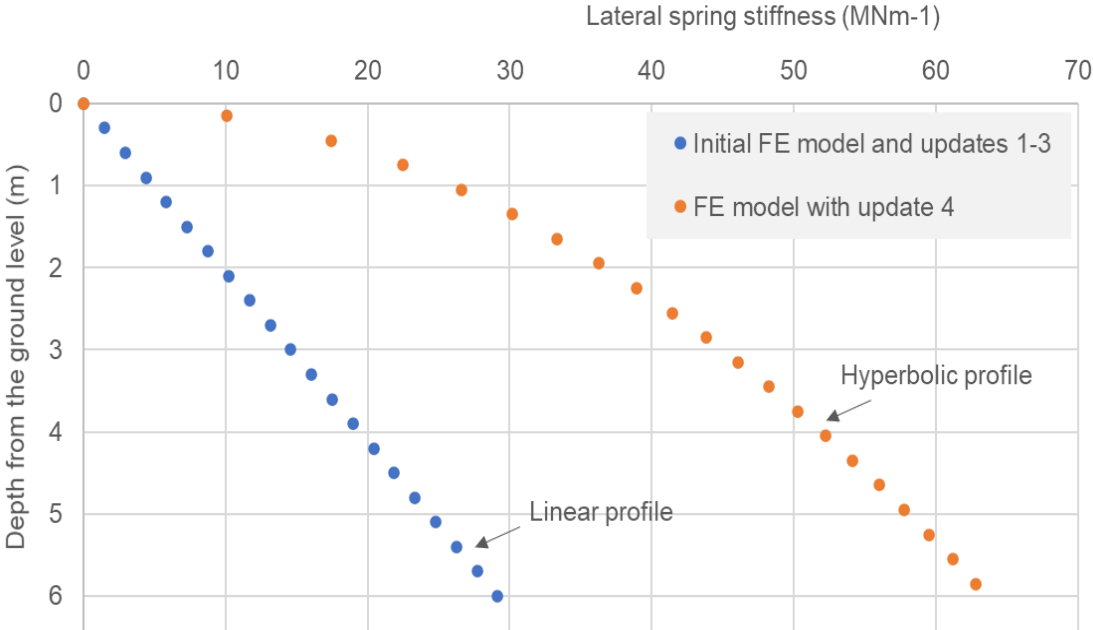


Figure 3.16 Lateral spring stiffness profiles used for the numerical model

3.2.7 Natural frequency change due to scour repair

Despite using high-sensitivity accelerometers in the field study, it proved difficult to track natural frequencies with high certainty. This was due to a combination of the low responsiveness of the bridge (as a relatively massive and stiff structure) and the level of background noise making it difficult to resolve frequency peaks. The natural uncertainty observed is shown in Figure 3.17, which shows six 10-minute datasets before the repair and six 10-minute datasets after the repair. The natural frequency of the first mode (sway) was observed near 4.5 Hz before the repair with an uncertainty of ± 0.6 Hz ($\pm 13\%$). This mode remained in the same frequency range of 4.5 ± 0.6 Hz after the repair. The second mode (pier and deck bending) natural frequency was near 18.75 Hz before the repair with an uncertainty of ± 0.8 Hz ($\pm 4\%$); however, a clear peak was not present near 18.75 Hz after the repair. Despite having natural frequency uncertainties, these two peaks near 4.5 Hz and 18.75 Hz were found to represent real modes due to the high modal assurance between adjacent timed datasets, as previously shown in Figure 3.15.

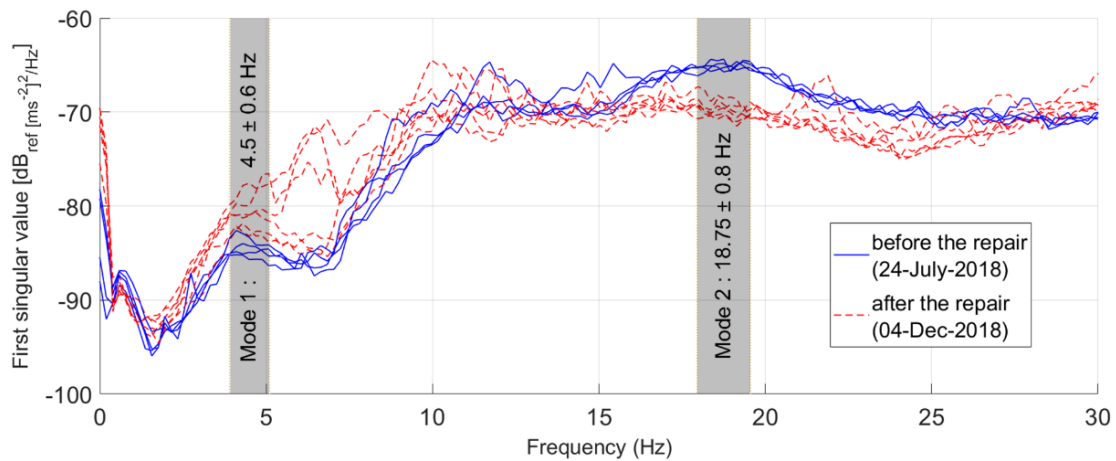


Figure 3.17 SVPSD spectra of six adjacent 10-minute datasets before and after

In comparison to the experimentally observed natural frequency uncertainties, the FE model estimated changes of 0.35 Hz (9%) for the first mode and 1.11 Hz (6%) for the second mode due to the scour (Table 3.7). These estimated frequency changes of the bridge were of the same order of magnitude as the experimentally observed natural frequency uncertainties. Therefore, scour induced natural frequency changes may have gone undetected.

Table 3.7 Natural frequency change due to scour backfilling: comparison between experiment and FE simulation with the updated model

Scour case	FE model frequency [Hz]		Experiment frequency [Hz]	
	Mode 1	Mode 2	Mode 1	Mode 2
No scour (after repair)	4.04	19.84	4.5 ± 0.6	18.75 ± 0.8
south pier local scour: 1.8 m max depth (real profile observed by sonar)	3.69	18.73		not recognised

The experimental natural frequency uncertainty indicates a limitation of this monitoring technique that any future monitoring project would have to overcome. Natural frequency would only indicate a measurable change when its change due to scour is above its measurement uncertainty. Therefore, for this method to work, a lower uncertainty or high-frequency change is desired. Frequency measurement uncertainty may potentially reduce in any future deployment by using higher sensitivity and lower noise accelerometers. On the other hand, natural frequency change would be greater than the uncertainty if the scour depth present in this bridge was far more extensive than the relatively narrow region of maximum 1.8 m depth under the central region of the south pier (Figure 3.8).

With the aim of identifying the depths of scour that would have been potentially measurable in this bridge, the updated FE model was used to simulate extensive scour cases. Two hypothetical scour cases were studied with FE models: (1) “full-width local scour under the

south pier” and (2) “full-width global scour under both north and south piers”. Both these cases consider more extensive soil loss than the real scour profile, which has only a narrow region of maximum 1.8 m depth. Numerical simulation results of these two hypothetical cases and the real scour profile case were compared with the experimentally observed measurement uncertainties as shown in Figure 3.18(a) for Mode 1 and Figure 3.18(b) for Mode 2.

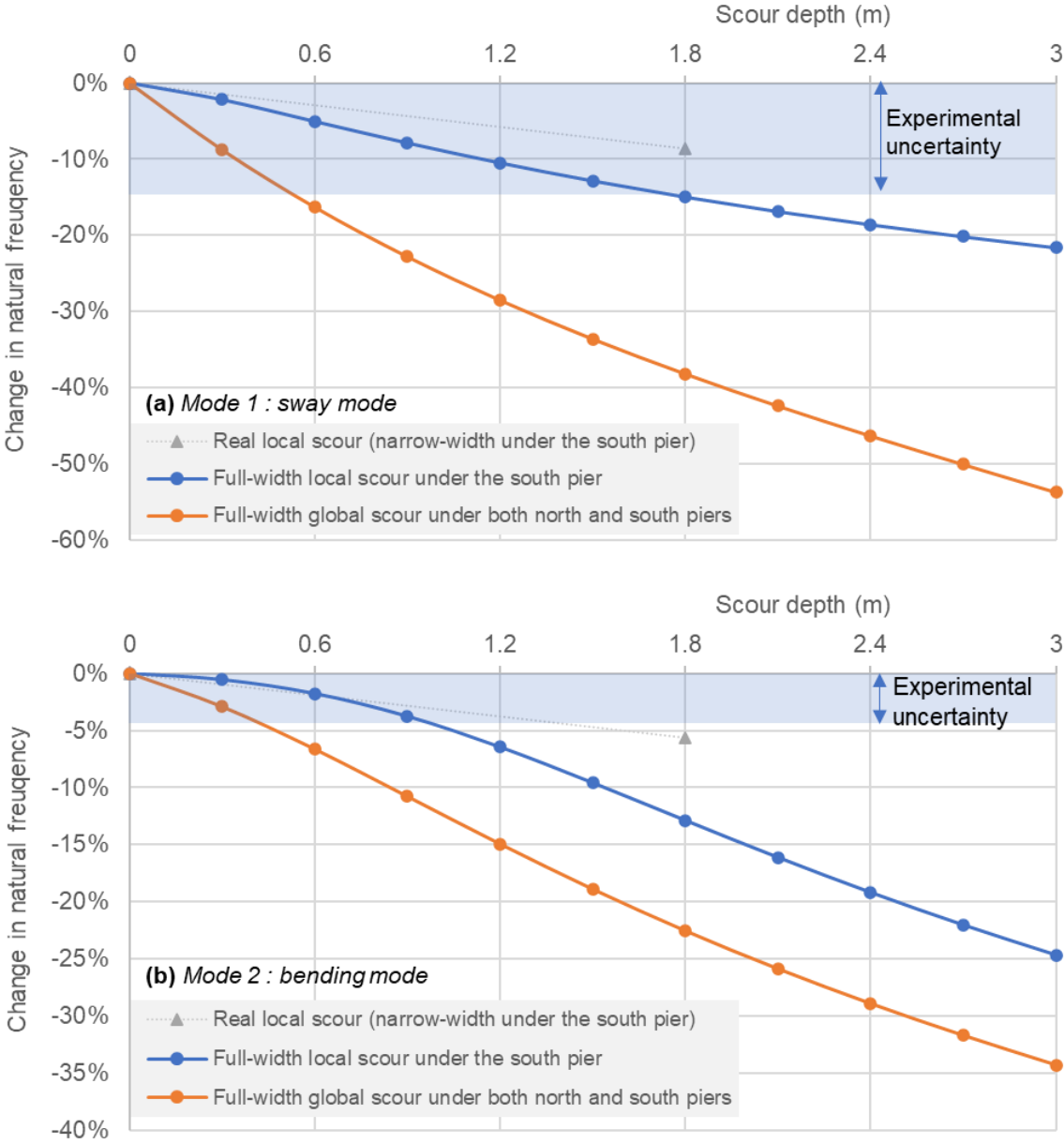


Figure 3.18 Natural frequency variation estimated by numerical simulations compared with the experimentally observed natural frequency uncertainty

As shown in Figure 3.18(a), natural frequency measurement uncertainty of Mode 1 was (13%), higher than the estimated frequency change due to the real scour profile (9%). Therefore, any change in the natural frequency of the bridge may have gone undetected, as previously explained. For other cases with more extensive scour, the frequency change becomes higher than the 13% measurement uncertainty value when the “full-width local scour under the south

pier” is more than 1.7 m or “full-width global scour under both north and south piers” is more than 0.5 m.

As shown in Figure 3.18(b), natural frequency change of Mode 2 for the real scour profile was 6% according to the numerical models. Although the experimental uncertainty of natural frequency (4%) was lower than this predicted change, a change was not experimentally observed due to the fact that the Mode 2 peak was not recognisable, as this peak was not prominent (flatter) when no scour was present (after repair in Figure 3.17). Nevertheless, when there was scour present in the experiment (before the repair in Figure 3.17), the Mode 2 peak was prominent and recognisable. As shown in Figure 3.18(b), the frequency change became higher than the 4% uncertainty value when either the south pier local scour is more than 1 m or global scour is more than 0.4 m. However, as the Mode 2 peak was difficult to resolve when there was no scour, the scour depth monitoring would only become possible after some initial scour has occurred making the Mode 2 peak prominent.

Therefore, based on the experimental uncertainties observed, measuring any type of scour depth below 0.4 m seems unrealistic for this bridge. The realistic potentially measurable scour depths are global scour depths above 0.5 m (8% of the 6 m pile embedment) or south pier local scour depths above 1.7 m (28% of the 6 m pile embedment). As these embedment losses due to scour are unlikely to cause bridge damage, the potential to measure a change in natural frequencies to indicate scour at these depths would still provide sufficient warning to plan countermeasures. The numerical scour simulation studies tested scour up to 50% of the pile embedment depth (i.e. 3 m), which is a significant scour depth and could even pose a risk of damage to the bridge. For this depth of global scour, natural frequency changes as high as 54% for Mode 1 and 34% for Mode 2 were estimated by the FE models. These high natural frequency changes indicate that natural frequencies in this bridge have the potential to indicate extensive scour depths.

3.2.8 Mode shape variation due to scour repair

In addition to the natural frequency, other modal parameters were explored for the potential indication of scour. Firstly, the change in mode shapes due to the effects of scour was explored. The mode shapes before and after scour backfilling repair are shown in Figure 3.19(a) for Mode 1 and Figure 3.19(b) for Mode 2. Note that the mode shapes show a side elevation view of the bridge.

The sway mode, Mode 1, displayed little change between before and after scour repair (MAC 99%), according to the experimental findings. Mode 1 estimated by the FE model was similar in shape to the experimental Mode 1. The FE model also displayed an insignificant change (less than 2% change in amplitudes) of mode shape, except below the lowest accelerometer level (“A” in the Figure 3.19(a)). The experimental mode shape was based on a limited number

of accelerometer sensor points, of which lowest was at the level “A”, and any changes below that level were undetected experimentally. In contrast, the FE model gives a finer resolution for the modal amplitudes based on a large number of points everywhere in the bridge. The FE model estimated unmeasurably small change at “A” level in Figure 3.19(a) and visible change near the ground level of the scoured south pier. However, near-ground-level modal amplitude changes would be difficult to measure as accelerometers would then be underwater, removing a key advantage of this monitoring technique, i.e. above water instrumentation is note susceptible to damage by moving debris, fast water flow and corrosion in comparison to underwater instrumentation.

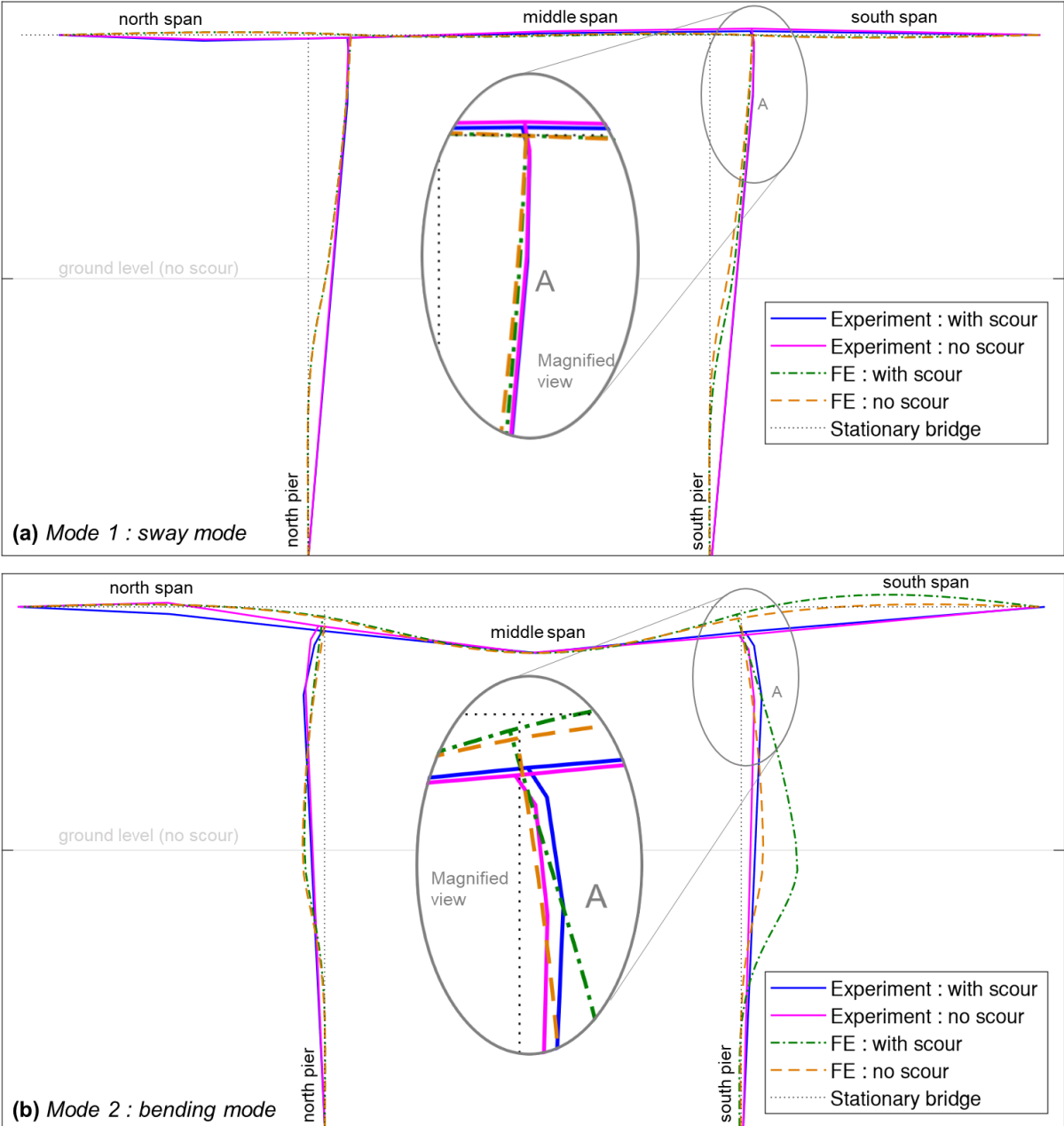


Figure 3.19 Change of the shapes due to scour

The pier and deck bending mode, Mode 2, has changed (MAC 74%) according to the experiment. The change was most noticeable at the south bridge pier (see the magnified view of Mode 2 in Figure 3.19). The south pier had the local scour hole. Therefore, the backfilling of this scour hole may have caused the bridge pier to become stiffer and increase in modal mass, resulting in a reduction of the modal amplitude. The FE model also estimated Mode 2 to have reduced modal amplitudes on the south pier as a result of scour backfilling. The FE model showed that the modal amplitude change is most noticeable near the ground level of the scoured south bridge pier. The experiment modal amplitudes do not show the correct modal amplitudes near the ground level since there are only a limited number of accelerometers of which the lowest accelerometer, at “A” in Figure 3.19, was significantly above the ground level. The FE model also shows that the vertical modal amplitude of the south span increases due to scour. However, the accelerometer at this location did not function, and therefore, this was unable to be verified. The accelerometer at the north span, however, did function and showed a significant reduction in modal amplitude experimentally. This behaviour was not shown in the FE model; it estimated the modal amplitude increase was limited to the south bridge pier and south end span. It is unknown precisely why the vertical amplitudes near the northmost span increased, but part of the repair that involved work at the expansion joints of the deck or measurement errors are potential causes.

Mode 2 changed in shape near the south pier according to both experimental and numerical results. This behaviour indicates the potential for using mode shapes of a bridge to indicate its scour. The modal amplitude increase was primarily near the scoured pier, which demonstrates the potential to also use changes in modal amplitude to locate the foundations undergoing scour.

3.2.9 Spectral density variation due to scour repair

Figure 3.17 clearly showed a distinct difference between the first SVPSDs before and after scour repair. In addition, the most noticeable change of the mode shape was in the middle of the south bridge pier (shown in Figure 3.19), where accelerometer 2 was located. Therefore, the variation of the PSD at the modal peaks derived from horizontal direction vibrations measured by the accelerometer 2 was studied over the whole period of scour repair. The mean PSD across the range of variation of the modal peaks was used to ensure that the peak was captured, and thus this parameter is referred to as “mean modal PSD”. Figure 3.20 shows the variation of the mean modal PSD on every Tuesday from 4 pm to 5 pm during the repair period. A peak hour traffic time during a weekday (Tuesday from 4 – 5 pm) was used with the assumption that the traffic level would not significantly differ and thus the effect of changes in traffic excitation on the estimated PSD would be minimum. The observed trend from 120 datapoints has been highlighted in blue colour, ignoring several outliers. One possible explanation for the outliers in Figure 3.20 is that they are the result of abnormal excitations

due to heavy vehicles with vehicle vibration properties in the same frequencies as the bridge modes.

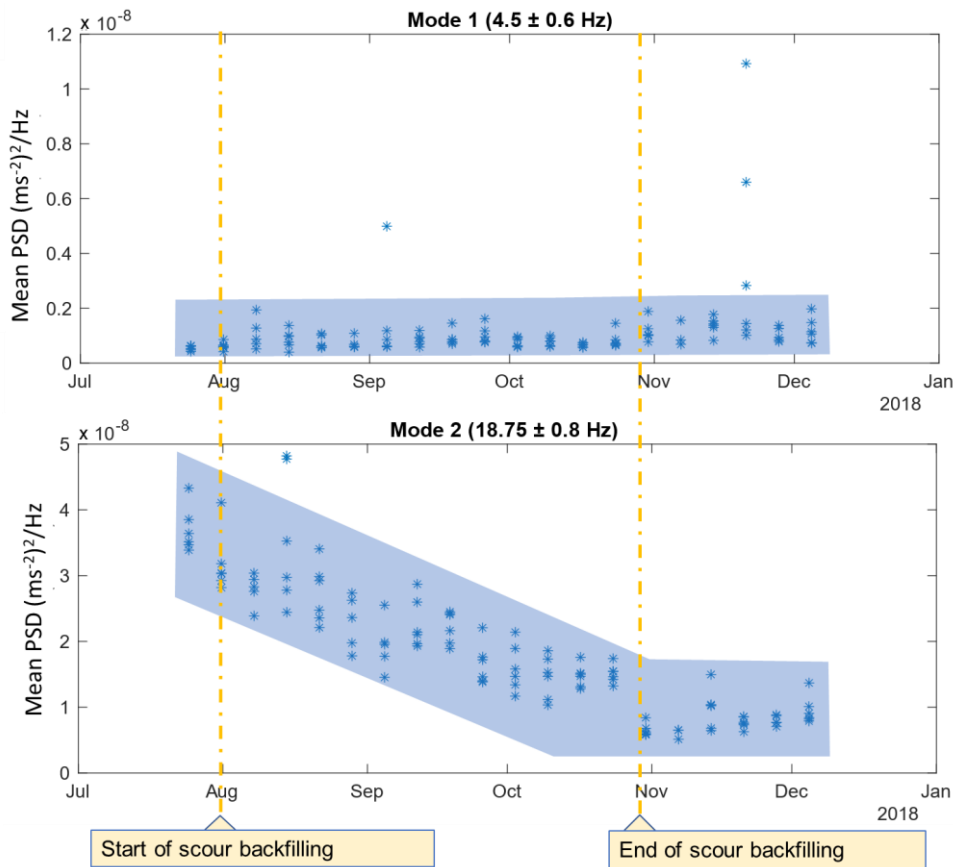


Figure 3.20 The variation of mean modal PSD of horizontal vibration at the middle of the south bridge pier (accelerometer 2)

The Mode 1 peaks showed a trend of stable mean PSD for the whole period. Mode 2 peaks, however, showed an overall trend of mean PSD reduction with the progression of scour backfilling repair. The mean PSD has reduced from around $4 \times 10^{-8} \text{ m}^2/\text{Hz}$ before repair to about $1 \times 10^{-8} \text{ m}^2/\text{Hz}$ after repair. It has an uncertainty of around $\pm 1 \times 10^{-8} \text{ m}^2/\text{Hz}$ before repair, which represents a significant, 25% uncertainty of measurement. However, this uncertainty was smaller than the overall change observed, $3 \times 10^{-8} \text{ m}^2/\text{Hz}$ (75%) for 1.8 m of scour backfilling at the south bridge pier. The scour backfilling process ended with placing concrete mats at the end of October 2018, after which the mean PSD of Mode 2 has stabilized, as expected. Therefore, mean modal spectral density measured by an accelerometer on a pier near the scour hole seems to be able to indicate the change of scour depth at that foundation, given measurements are considered under similar traffic conditions. Based on the observed measurement uncertainties (25%) and the change due to scour (75%), modal PSD could provide a scour depth resolution of approximately 0.6 m for local scour and potentially higher than that for global scour.

3.3 Summary

Vibration-based scour monitoring was studied at two bridges, first a feasibility study at Nine Wells Bridge and second a field trial at Baildon Bridge. The feasibility study at Nine Wells Bridge attempted to numerically model a bridge subjected to hypothetical cases of scour and deck damage to see whether the natural frequency sensitivity to scour is higher than the sensitivity for deck damage, which has already been proven to be insufficiently sensitive in practice. The fundamental natural frequencies were predicted to be significantly sensitive to scour damage (26 % change for 5 m scour depth) than to deck damage (less than 0.01% change for a full depth crack of a prestressed beam). Therefore, the natural frequency showed significant potential to indicate scour than to indicate deck damage, and that it would be worthwhile to trial this in practice.

The field trial at Baildon Bridge in Bradford involved monitoring this bridge during a backfilling process to repair scour damage. Sonar scanning before and after the repair recorded a change of the bed level up to a maximum of 1.8 m near the south bridge pier. Initial scour simulation predicted the fundamental longitudinal, pier-bending mode would experience a 4% change due to scour. This mode was observed in the operational modal analysis results from the experiment, but with low modal assurance and a sway mode that was not predicted by the FE model was also observed. Thus, the FE model was updated to improve its predictive capability. The updated FE models estimated that the natural frequencies of the two observed modes would change by 9% and 6% respectively due to backfilling. However, it was too difficult to capture this change with experimental data based on the frequency domain decomposition technique, as the modal peaks were uncertain with variabilities of the same order of magnitude as the expected natural frequency changes. This inability to obtain high enough frequency certainty indicates a potential limitation for monitoring scour of small-span bridges with vibration-based methods. Numerical modelling found that full-width global scour resolution for this bridge was potentially about 0.5 m, and local pier full-width scour resolution about 1.7 m, in order to overcome the experimental measurement uncertainties.

The modal amplitude of the second mode at the south pier of Baildon Bridge showed a clear reduction after the repair. This could have been anticipated due to the stiffening of the south bridge pier after repair. In addition, the mean modal power spectral density at the same location showed a clear reduction with the progression of the repair. Mean modal power spectral density of Mode 2 reduced by $3 \times 10^{-8} \text{ m}^2/\text{Hz}$, which was above its uncertainty of $1 \times 10^{-8} \text{ m}^2/\text{Hz}$. Therefore, the spectral density and the mode shape which have, to date, had little attention as scour detection parameters, may have greater potential for vibration-based scour detection than the more commonly studied parameter of natural frequency.

Chapter 4

Geotechnical-centrifuge model experimental programme

Highlights

- A centrifuge testing methodology was developed to simulate vibration-based bridge scour monitoring.
- Four small-scale models, a bridge as well as two deep and one shallow foundations, were constructed in dense sand and tested with different levels of local and global scour.
- The models represented, in full-scale, three hypothetical bridges with various configurations of bridge deck types (integral and simply supported) and foundation types (deep piled and shallow pad foundations).
- Experiments estimated the full-scale natural frequency sensitivities of 3.5 – 11% and spectral density sensitivities of 40 – 1205% per 1 m depth of scour, which suggests that this technique has potential for scour monitoring.
- Mode shape showed potential to identify and localise scour.

This chapter describes the development of a small-scale experimental methodology using centrifuge modelling to assess the full-scale potential of a vibration-based bridge scour monitoring technique, which uses the three scour monitoring parameters identified in the field trial at Baildon Bridge. These parameters were studied for different forms of scour and multiple bridge types, with the aim of assessing their wider applicability as scour monitoring parameters. The initial selection of full-scale bridges, the conversion of these to small-scale models, the construction of the small-scale models in a centrifuge container and the final centrifuge testing are described in detail. The potential for different vibration-based parameters to detect scour is evaluated at the end of this chapter. These observations also helped calibrate numerical models of small-scale and full-scale bridges in the next chapter. The data collected during this experimental programme is available from the University of Cambridge Open Data repository (Kariyawasam *et al.*, 2020b).

4.1 Background

As highlighted in Chapter 2, the literature on vibration-based scour monitoring has centred around computer simulations using numerical models. These numerical models make a number of assumptions on the complex soil-bridge interaction before and after scour. Experiments are essential to validate these assumptions and, most importantly, to assess the practical viability of this monitoring technique for various types of bridges and forms of scour in a controlled environment.

Testing small-scale models subjected to scour is one option for assessing this vibration-based scour monitoring technique. However, previous efforts on testing scaled-down soil-structure models at normal gravity did not accurately simulate the representative full-scale bridge dynamics (Section 2.4.1.1). Although material properties of the structural elements (e.g. steel/concrete beams before yielding) of such scaled models do not depend on the stress-level, and hence depth, soil strength and the lateral stiffness provided by the soil to the foundation elements are stress-dependent. A scaled-down model, therefore, provides lower stress, and hence a lower stiffness, than is realised in practice, and non-linear soil behaviour may make it impossible to scale up the dynamic properties such as the natural frequency to equivalent full-scale behaviour, as elaborated in Section 4.2.

Centrifuge modelling can be used to overcome this problem by allowing full-scale stress levels to exist within a small-scale model (Madabhushi, 2014). Centrifuge modelling thus provides an ideal platform to establish the expected variation in natural frequency and other dynamic parameters with scour depth at a real bridge.

The experimental programme was developed with the aim of studying different bridges and forms of scour in small-scale. The objectives of this experimental programme were:

- (1) To develop a scale-model testing methodology for assessing vibration-based scour monitoring techniques.
- (2) To identify the sensitivities of natural frequency, mode shapes and spectral density of different bridge types to scour.
- (3) To study the change of scour parameters and soil stiffness due to local and global scour around bridge foundations (Figure 1.2).

4.2 Centrifuge modelling

Centrifuge Modelling is a technique used to correct inaccuracies in soil property scaling that is involved when attempting to model a full-scale (also called prototype-scale) soil mass with a small-scale (also called model-scale) soil model. To understand this scaling inaccuracy in the

context of vibration behaviour applicable to this research, consider a 1/N scale model at normal gravity (1g) attempting to represent a full-scale soil mass, as shown in Figure 4.1.

Any full-scale depth d_f is represented in the 1/N small-scale model by a corresponding depth of d_f/N . The full-scale self-weight stress (σ_f) at depth d_f and the small-scale self-weight stress (σ_s) at the corresponding depth (d_f/N) are simply:

$$\text{stress} = \frac{\text{force}}{\text{area}} \quad \sigma_f = \frac{d_f L^2 \rho g}{L^2} = \frac{d_f \rho g}{L} \quad \text{Equation 4.1}$$

$$\sigma_s = \frac{\frac{d_f}{N} \left(\frac{L}{N}\right)^2 \rho g}{\left(\frac{L}{N}\right)^2} = \frac{d_f \rho g}{N} \quad \text{Equation 4.2}$$

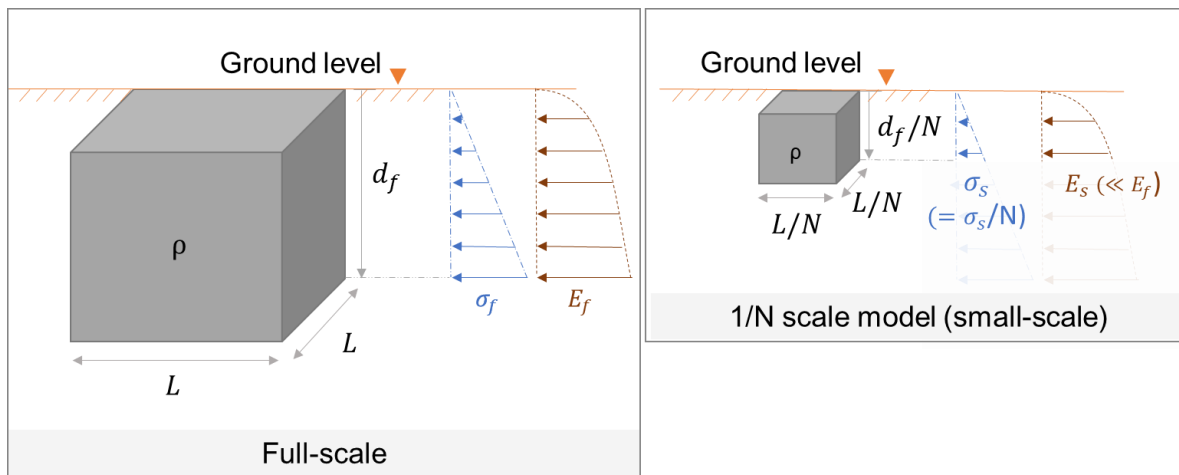


Figure 4.1 Properties of full-scale and 1/N scale soil models (both at 1g)

Equations 4.1 and 4.2 give $\sigma_s = \sigma_f/N$ which suggests that the small-scale stress levels are 1/N times the full-scale stress levels at representative depths. The level of stress determines the stiffness properties of soil. For example, the small-strain elastic modulus of soil is directly related to the effective vertical stress, as presented in Equations 4.8 and Section 5.3 and illustrated in Figure 4.1. Therefore, in the same way as the small-scale stress level is lower than the full-scale stress level at a corresponding location, the small-scale elastic modulus (E_s) at d_f/N depth is smaller than the full-scale elastic modulus (E_f) at the corresponding full-scale depth (d_f). Therefore, the stiffness profile of soil is different in the small-scale and the full-scale. This type of a small-scale model with inaccurate stiffness profile would not accurately estimate the vibration behaviour of the full-scale structures.

Accurate stiffness properties will only be observed if the stress levels in the 1/N scale model and the full-scale match. Equal stress condition, i.e. $\sigma_s = \sigma_f$, in Equation 4.2 is attainable if the gravitational acceleration in the model is Ng instead of $1g$. Centrifuge modelling does this, replicating full-scale stress-fields within a small-scale model, by increasing the effective gravitational field strength to compensate for the reduction in length, such that self-weight

stresses are identical (Madabhushi, 2014). This necessitates testing a $1/N$ scale model at an effective gravity of Ng , which is generated by centrifuge rotation such that the centripetal acceleration produces an increased vertical acceleration in the model.

It is noteworthy that an additional gravity field is not necessary to obtain the accurate dynamic behaviour of a small-scale structural model, given the material components have a constant elastic modulus everywhere, unlike soil that changes its elastic modulus with depth. A soil-structure model must be tested under centrifuge acceleration purely to correct the inaccuracies in the property scaling of the soil but not the structure.

Stress similitude between small- and full-scale at a length scale factor of N allows scaling laws to be derived for other parameters of interest, including natural frequency (Madabhushi, 2014). The natural frequencies exhibited by a $1/N$ scale model can be shown to be N times higher than the natural frequencies of the full-scale model. Other applicable scaling laws are discussed in Section 4.4.3.

All tests for this research were conducted using the Turner Beam centrifuge (Figure 4.2) at the Scofield Centre, University of Cambridge. This is a 10 m diameter centrifuge capable of subjecting models with a mass of up to 1000 kg to centripetal accelerations of 125 g (Schofield, 1980). This centrifuge testing programme modelled the soil-structure interaction with a centrifuge model of 434 – 485 kg in mass and it was tested under a 40 g and a 60 g effective gravitational field.



Figure 4.2 Turner beam centrifuge, where all tests were conducted. Photograph from SERIES (2011)

4.3 Introduction to the experimental method and nomenclature

This section briefly introduces the methodology and nomenclature used; a detailed methodology is provided in the next sections of this chapter. This experiment attempted to use small-scale testing to study the expected full-scale sensitivity of natural frequency, mode shape and modal spectral parameters of different bridges undergoing local and global scour.

Firstly, the properties of the full-scale and small-scale bridges were selected (Section 4.4). Three full-scale reinforced concrete bridges were considered to represent various foundation and deck arrangements. These three hypothetical bridges were named as “Bridge 1”, “Bridge

2” and “Bridge 3”, as shown in Figure 4.3. Bridge 1 is an integral bridge with deep piled foundations; Bridge 2 is a simply supported bridge with a deep piled foundation; and Bridge 3 is a simply supported bridge with a shallow pad foundation. The properties of Bridge 1, Bridge 2 and Bridge 3 were scaled down to create small-scale aluminium structural models “Model 1”, “Model 2” and “Model 3”, respectively. An extra small-scale aluminium structural model, “Model 4” was also created to represent one pile of the Bridge 2. Model 1 represented its complete full-scale bridge with both the bridge deck and piled foundations, while all other models represented the standalone foundations of the full-scale bridge. Models 1, 2 and 4, all of which have deep foundations, were scaled down by “60” times. However, the Model 3, which has a shallow pad foundation, was scaled down by only “40” times in order to maintain a sufficient depth to the pad footing in small-scale.

Secondly, these four small-scale structural models were constructed in a soil medium in a cylindrical centrifuge container, as explained in Section 4.5. These structural models in the centrifuge were excited by two actuators, namely, a piezoelectric actuator and an automatic modal hammer. The input excitations were measured by load cells located in the actuators. The output vibrations of the structural models were measured by a set of accelerometers. High sensitivity piezoelectric (referred to as “P”) accelerometers were mounted at the top of all structural models, and two types of smaller size and low sensitivity MEMS (referred to as “M” or “m”) accelerometers were mounted on the piles/columns of the models. The accelerometers were named with four characters, as for example “M1P2”, where the first two characters refer to the model name (Model 1) and the last two characters refer to the type of accelerometer and its number (Piezoelectric accelerometer number 2). Another set of piezoelectric accelerometers were placed in soil to measure the shear wave velocities; these were referred to as C01 – C15. Their arrangement is provided in Figure 4.4. Note that the soil in the centrifuge model was maintained dry, with the assumption that the changes, rather than the absolute values, in vibration properties of the bridges are independent of the water-soil interaction effects, as further discussed in the literature review (Section 2.4.1.4).

Thirdly, the constructed Centrifuge Models 1, 2, 3 and 4 were all tested under centrifuge acceleration. Models 1, 2 and 4 were scaled down by 60 times, and therefore they all were tested at, “60g”, 60 times the normal gravity acceleration. Model 3 was scaled down by 40 times, and thus this model was tested at the centrifuge acceleration equal to “40g”, 40 times the normal gravity. Different cases of local scour and global scour profiles were created for each model. These various steps of scour were named with four characters, as for example “M1S4”, where the first two characters refer to the model name (Model 1) and the last two characters refer to the scour step number (Step 4).

Fourthly, two other types of additional tests were performed for all four models and different levels of scour modelled at normal gravity to help confirm the accuracy of the centrifuge test

results. The first type of additional test was performed for the same centrifuge model containing soil but at normal gravity, “1g”; hence, it was referred to as “1g with soil” test. This test provided a lower bound natural frequency estimate to the 40g or 60g centrifuge tests as soil stiffnesses were lower at 1g than at 40g or 60g. The second type of additional test was also performed at normal gravity but with a fixed base representing the ground level (without any soil). The fixed base natural frequency does not depend on the level of gravitational acceleration; therefore, this test was referred to as the test “with fixed base”. These fixed base tests provided an upper bound natural frequency estimate to the centrifuge tests (with soil) at 40g or 60g as soil stiffnesses were lower than the stiffness given by the fixed base.

Finally, the measured data of the structural models and soil were separately analysed. The acceleration and input force measurements of the structural models (Models 1 – 4) were analysed using two modal identification methods, Frequency Domain Decomposition (FDD) method and the Frequency Response Function (FRF) method, as explained in Section 4.7. The natural frequencies, spectral densities and mode shapes derived using modal identification of small-scale experiments were all brought to representative full-scale by applying appropriate scaling factors given in Table 4.2. The sensitivities of these estimated full-scale natural frequencies, spectral densities and mode shapes were studied for the potential to capture scour. The accelerations measured by accelerometers in the soil during shear wave tests were analysed (Section 4.12) to estimate the change in small-strain stiffness of soil due to the effects of local and global scour.

4.4 Full-scale and small-scale bridge element selection

The following sections discuss how three different full-scale bridges were selected to represent different bridge deck and foundation configurations and how these bridges were scaled down to create small-scale centrifuge models. Note that the constraints in the centrifuge model container and typical field conditions required iterative selection of the full-scale and small-scale properties. Only the finally selected properties and applicable constraints are given here.

4.4.1 Full-scale bridge selection

Three hypothetical full-scale bridges were selected to compare the viability of the vibration-based monitoring method in different types of bridges. The key differences and similarities among these bridges are listed in Table 4.1. All three of these bridges were selected to have the same material properties and deck arrangement. However, either the type of the bridge deck or the foundation was kept different between these bridges for comparison purposes. The Bridge 1 has an integral bridge deck while the Bridges 2 and 3 both have simply supported bridge decks. The Bridges 1 and 2 both have pile bent (deep) foundations, while the Bridge 3 has a pad (shallow) foundation.

Table 4.1 *The three types of full-scale bridges considered*

Bridge	Deck type	Foundation type	Bridge deck arrangement	Spans	Material
1	Integral	Pile bent (deep)	Reinforced concrete composite deck with 0.2 m thick <i>in situ</i> slab on 8 Y1 precast beams	Two (15 m each)	Reinforced/prestressed concrete (C40)
2	Simply supported				
3		Pad (shallow)			

The full-scale Bridge 1 was considered to be an “integral” bridge. Integral bridges have low maintenance costs because they have a monolithic connection at superstructure-substructure connections, without any bearings or expansion joints. Highways England recommends integral bridges as the first option to be considered for bridges with lengths not exceeding 60 m, skews not exceeding 30°, and settlements that are not excessive (Highways Agency, 2001). There are also a large number of integral bridges in the existing bridge stock (24% of EU bridges, according to (Kaundinya and Heimbecher, 2011)). Therefore, a two-span integral bridge with piled foundations was chosen. A flexible support abutment, which is a common abutment type used by bridge designers for integral bridges, was selected (Steel Construction Institute, 2018). Flexible support abutments avoid any backfill interaction with the piles by adding piles through sleeves to create an annular void around the piles. This means that a full centrifuge model of this type of bridge does not require modelling of the abutment backfill.

The full-scale Bridge 2 and 3 considered were both “simply supported”. A significant portion of the existing concrete bridge stock around the world also have simply supported bridge decks (Kaundinya and Heimbecher, 2011). Simply supported concrete bridges were constructed in the past due to their simplicity, ease of construction and ability to accommodate differential settlement of the supports. Due to their many joints and bearings, this type of construction is no longer favoured in practice (O’Brien and Keogh, 1999). However, bridges with simply supported spans have been found to be the most susceptible to scour failure (Lin et al., 2013), perhaps due to the lack of redundancy compared to continuous and integral bridges.

The full-scale Bridges 1 and 2 were both selected to have pile bent foundations (a row of piles from deck level to the bottom of the foundation). This pile bent foundation arrangement included four piles of 18 m in length, 12 m of which was driven into the soil with the remaining 6 m above ground level. The pier piles were assumed to be 760 mm in diameter. The abutment piles in Bridge 1, an integral bridge, were selected to be 540 mm in diameter. The abutments of Bridges 2 and 3, simply supported bridges, were assumed to behave as rigid.

Bridge 3 was considered as a pier with a shallow pad foundation. According to the Wisconsin Department of Transport (2018), the minimum depth of embedment of shallow foundations for a bridge should be 1.2 m, and shallow foundations are economically viable only when the

required soil properties are present within 3 – 4.5 m from ground level. Hence, a shallow foundation depth of 3 m was assumed. The size of the shallow foundation was chosen as 4 m x 4 m in plan.

The maximum span of beam-slab type bridges is between 10 and 30 m in the majority of bridges in Europe (Kaundinya and Heimbecher, 2011). Therefore, a two-span bridge deck, with equal spans of 15 m, was chosen. The bridge deck was composed of 8 Y1 precast beams, each with a second moment of area of $1.1 \times 10^{-2} \text{ m}^4$ and a cross-sectional area of 0.31 m^2 . The spacing between Y1 beams was chosen as 1.5 m and the in-situ slab depth was chosen as 0.2 m, based on the typical details given in a precast beam catalogue by Concast Precast Ltd (2009).

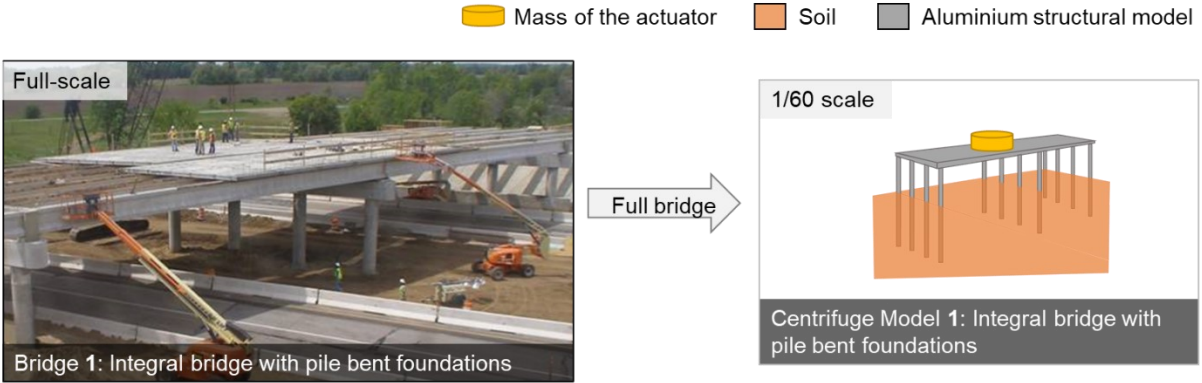
These full-scale hypothetical bridges were considered to be newly concreted bridges with a history of low stress levels, without significant cracking. Thus, all full-scale bridge elements constructed of C40 grade were assumed to have a modulus of elasticity of 35 GPa and a bulk density of 2550 kgm^{-3} (European Standard, 2002). The effect of the higher elastic modulus of reinforcing and prestressing steel was ignored, since these contribute to only a small proportion (0.13 – 4%) of a typical cross-sectional area of a concrete element (European Standard, 2004). All foundations were assumed to be in a layer of uniform dense sand with 66% relative density.

4.4.2 The method of scaling down to a simplified model

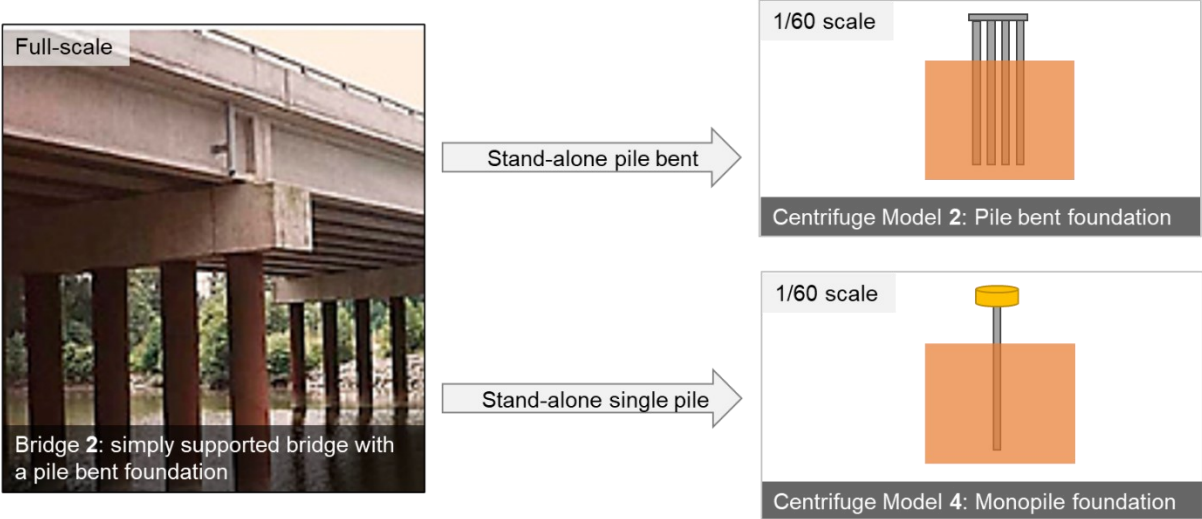
Every connection in the scaled-down model introduces some imperfections and there was only a limited space in a typical 850-mm diameter cylindrical centrifuge container. Therefore, simplified versions of the full-scale bridges were scaled down to create the structural models for the centrifuge test. Figure 4.3 shows the transition from the three hypothetical full-scale bridges to four scaled-down centrifuge models. Note that these figures are not to scale, and the photographs are not the real full-scale bridges but only examples of similar types of bridges.

Figure 4.3(a) shows the scaling down of the full-scale Bridge 1. The full-scale bridge (with 15 m spans) was scaled down to a 1/60 scale (with 250 mm spans), to create Model 1 in the centrifuge container. Dynamic excitation for Centrifuge Model 1 was generated with an actuator. The mass of this actuator and other accelerometers (0.5 kg) at small scale was $1.1 \times 10^5 \text{ kg}$ in full scale, which was assumed to represent the extra mass of the three diaphragm beams in addition to the mass of the overlapping deck. The introduction of a concentrated mass, rather than the distributed superimposed dead load that it represents, was assumed to have an insignificant effect on the natural frequencies of the fundamental sway modes. The composite beam-slab deck in the full-scale Bridge 1 was simplified a rectangular-slab bridge deck having the representative flexural rigidity and mass in small-scale Model 1. The aim of

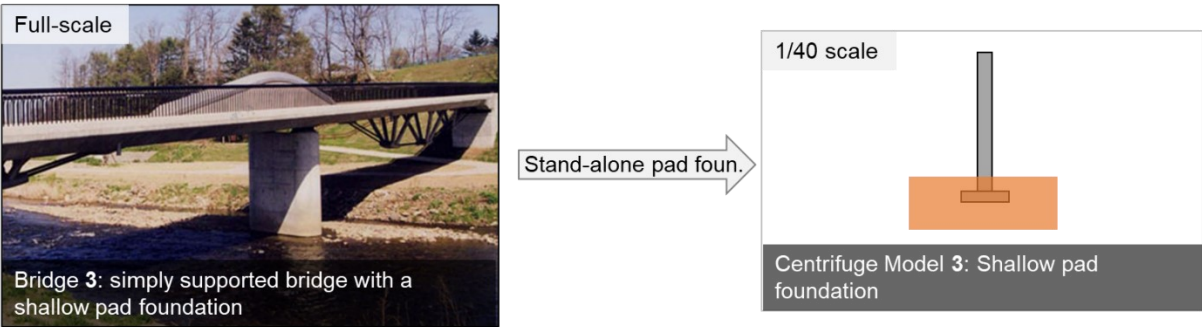
this simplification is to use simple-to-fabricate bridge deck in the small-scale bridge but to ensure that it has the same flexural and sway modes of vibration as the full-scale bridge.



(a) Full-scale Bridge 1 and small-scale Centrifuge Model 1



(b) Full-scale Bridge 2 and small-scale Centrifuge Model 2 and 4



(c) Full-scale Bridge 3 and small-scale Centrifuge Model 3

Figure 4.3 Scaling down of three full-scale bridge types to four small-scale centrifuge models

The presence of bearings in full-scale Bridges 2 and 3 complicates the testing of simply supported bridges in small-scale experiments. Therefore, only the “standalone foundations” (foundation only models) of the bridge piers of Bridges 2 and 3 were scaled down as centrifuge models, with the aim of using their results to compare general trend between different

foundations and use the experimental results to calibrate numerical models of the full-scale standalone foundation models. Then these calibrated numerical models were included with simply supported numerical bridge decks numerically, to study the potential of a vibration-based method of these Bridges 2 and 3, as further explained in Chapter 5.

As shown in Figure 4.3(b), Bridge 2 with pile bent type pier foundation was scaled down to a 1/60-scale standalone pile bent foundation model, Centrifuge Model 2. The scour induced dynamic behaviour changes of a single pile provide simpler insights into the change of soil-structure interaction. Therefore, an individual pile foundation of Bridge 2 pier foundation was scaled down to obtain an extra model, Centrifuge Model 4. Model 4 was excited with the same actuator that was used in Model 1. The small-scale Model 4, with its single pile and the mass of the actuator, top slab, and piezoelectric accelerometer at the top (0.5 kg), was assumed to represent a full-scale single pile of 740 mm diameter with a mass of 1.1×10^5 kg at the top.

As shown in Figure 4.3(c), Bridge 3 with a shallow pad foundation was scaled down to a 1/40-scale standalone foundation model, Centrifuge Model 3. This foundation was scaled down by a factor of 40, instead of the factor of 60 used in the other models. A lower scaling factor of 40 was chosen for this shallow-foundation model to avoid the shallow depth of embedment in the small scale from being too small in order to be able to accurately model for different scour depths.

4.4.3 Properties of the small-scale simplified bridge models

All model structures were made from aluminium alloy elements with Young's modulus of 70 GPa and density of 2700 kgm^{-3} . The geometric properties of the scaled-down centrifuge models were carefully selected to adhere to the required centrifuge scaling laws. The scaling factor (N) was chosen as 40 for Model 3 and 60 for all other models, as explained before.

Table 4.2 *Scaling laws applicable to small-scale centrifuge models (Madabhushi, 2014)*

Parameter	Scaling factor (small-scale/full-scale)	Units
Length	$1/N$	M
Area	$1/N^2$	m^2
Mass	$1/N^3$	Nm^{-1}s^2
Stress	1	Nm^{-2}
Strain	1	-
Force	$1/N^2$	N
Frequency	N	s^{-1}
Pseudo acceleration due to gravity	N	ms^{-2}
Flexural rigidity (EI)	$1/N^4$	Nm^2
Mass per unit length (m_0)	$1/N^2$	Nm^1s^2

Table 4.3 Model element selection (shaded properties adhere to the scaling laws)

Full-scale (reinforced concrete)					Small-scale (aluminium)				
Bridge	Element	EI (Nm ²)	m_0 (kgm ⁻¹)	Soil-structure dimension (m)	Model	Element	EI (Nm ²)	m_0 (kgm ⁻¹)	Soil-structure dimension (m)
Bridge 1	eight Y1 beams and a 0.20 m x 12.00 m top slab (composite deck)	1.6 x 10 ¹⁰	12444	NA	Model 1	one 12.7 mm x 100.0 mm rectangular solid section	1195	3.43	NA
	four 0.56 m diameter circular solid piles (abutment)	1.7 x 10 ⁸	628	0.56		four 9.0 mm outer diameter 0.9 mm thick wall circular hollow tube (abutment)	13	0.06 (0.12 below ground level)	0.009
	four 0.74 m diameter circular solid piles (pier)	5.2 x 10 ⁸	1097	0.74		four 12.7 mm outer diameter 0.9 mm thick wall circular hollow tube (pier)	40	0.09 (0.23 below ground level)	0.0127
Bridge 2 pier foundation	four 0.74 m diameter circular solid piles	5.2 x 10 ⁸	1097	0.74	Model 2	four 12.7 mm outer diameter 0.9 mm thick wall circular hollow tube piles	40	0.09 (0.23 below ground level)	0.0127
	one 1.05 m deep 1.85 m wide rectangular solid capping beam	6.2 x 10 ⁹	4953	NA		one 12.7 mm x 40.0 mm beam rectangular solid beam	478	1.37	NA
Bridge 3 pier foundation	one 1.00 m x 0.70 m rectangular solid column	1 x 10 ⁹	1785	1	Model 3	one 12.7 mm x 32.5 mm rectangular solid column	388	1.11	0.0325
	one 1.27 m deep 4.00 m wide rectangular solid pad footing	2.4 x 10 ¹⁰	12950	4		one 25.4 mm deep x100 mm wide rectangular solid pad footing	9560	6.86	0.1
Bridge 2 single pile	one 0.74 m diameter circular solid pile	5.2 x 10 ⁸	1097	0.74	Model 4	four 12.7 mm outer diameter 0.9 mm thick wall circular hollow tube	40	0.09 (0.23 below ground level)	0.0127
	one 1.05 m deep 1.85 m wide rectangular solid slab section	6.2 x 10 ⁹	4953	NA		12.7 mm x 40.0 mm rectangular solid slab section	478	1.37	NA

Table 4.2 summarises the general scaling laws applicable to centrifuge testing. All lengths of the elements were scaled down by 1/N. The flexural rigidity (EI) and mass per unit length (m_0)

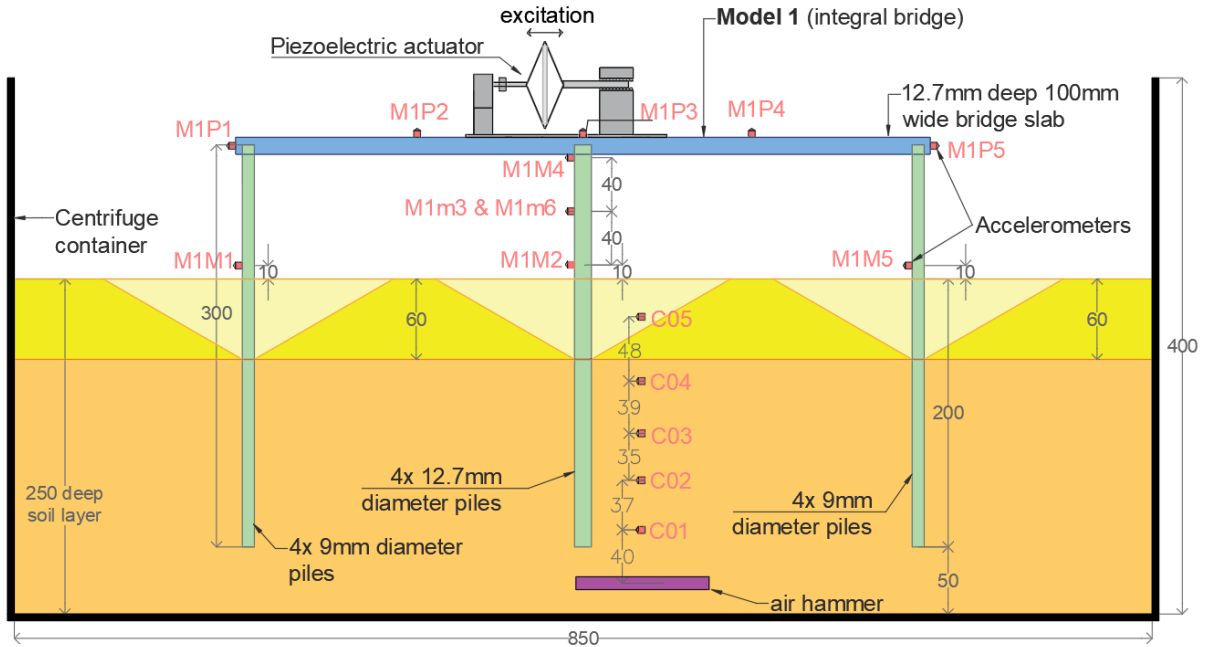
should be correctly scaled down by $1/N^4$ and $1/N^2$, respectively, to obtain the dynamic behaviour of the structural elements. Furthermore, to obtain the correct soil-structure interaction, the foundation width should also be correctly scaled down by $1/N$.

Due to the change of material properties from full-scale (concrete) to model (aluminium), not all of these centrifuge scaling laws could be met at the same time. Only the most critical parameters required were therefore selected to model the mass and stiffness properties needed to simulate the dynamic behaviour of the full-scale bridge. The correctly scaled critical properties are shaded in Table 4.3. For elements in soil (the piles and pad foundation), the most critical properties were selected as the flexural rigidity (EI) and the soil-structure dimensions. This selection required the piles to be thin hollow tubes, which leads to the mass per unit length of the model piles being lower than that required according to the scaling laws. Therefore, the hollow tubes were kept open-ended to enable the filling of soil mass into the piles as they were pushed into the soil model. For example, scaling laws require each 12.7 mm diameter pile to have a mass per unit length (m_0) of 0.31 kgm^{-1} , but the pile alone provides only 0.09 kgm^{-1} (71% error) whereas the pile filled with soil provides 0.23 kgm^{-1} (25% error). For the elements above ground level, such as the deck and columns, the flexural rigidity and mass per unit length were chosen as the main parameters for scaling, as the soil-structure dimension does not contribute to their dynamic behaviour.

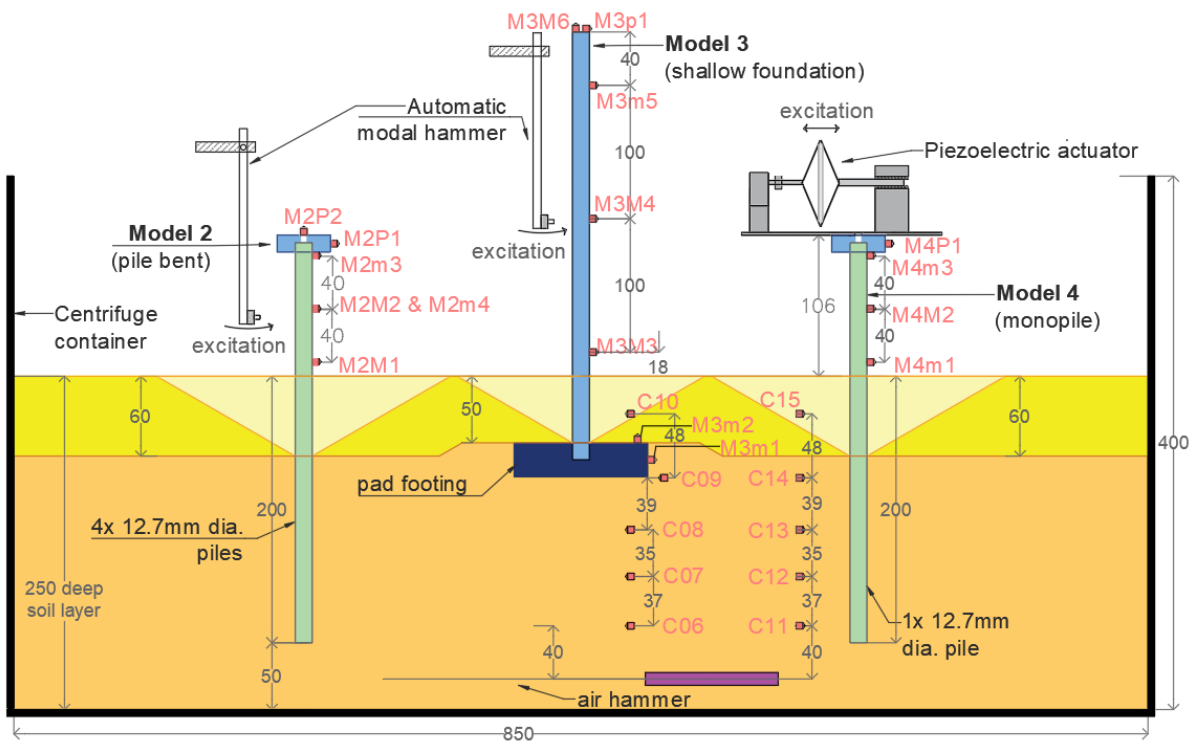
4.5 Centrifuge experimental programme

Based on the small-scale properties derived in the previous section, the bridge Models 1 – 4 were constructed in a soil medium in a cylindrical centrifuge container, as shown in Figure 4.4. Figure 4.5 shows a corresponding photograph during the experiment. All model foundations were kept at least 100 mm away from the centrifuge container wall and 50 mm away from the bottom of the container to limit boundary effects on the soil-structure interaction (Teymur and Madabhushi, 2003). All four models were placed adjacent to one another in the cylindrical centrifuge container, and only two models could be tested simultaneously during each centrifuge test flight due to the number of excitation sources available. All models were instrumented with accelerometers to measure their vibration response. Accelerometers and air hammers were also embedded in the soil near the models to measure shear wave velocities and hence estimate the soil stiffness profiles. The centrifuge rotational speed was set to test Model 3 at 40g and all other models at 60g. The preparation of the structural models, the soil and the full experimental setup is discussed in detail in the following sections.

Key		Accelerometer label nomenclature	
	removed soil for local scour	Centrifuge 'M'odel number 'x'	
	removed soil for global scour		
	soil remaining after global scour	Accelerometer type	
	Accelerometers facing + direction	'm'- MEMS type 1, 'M' - MEMS type 2 and 'P'-Piezoelectric	
		Accelerometer number 'y'	



(a) Centrifuge Model 1



(b) Centrifuge Models 2, 3 and 4

Figure 4.4 Experimental setups, sensor arrangement and scour levels corresponding to all the models in the centrifuge container – all dimensions are in mm.

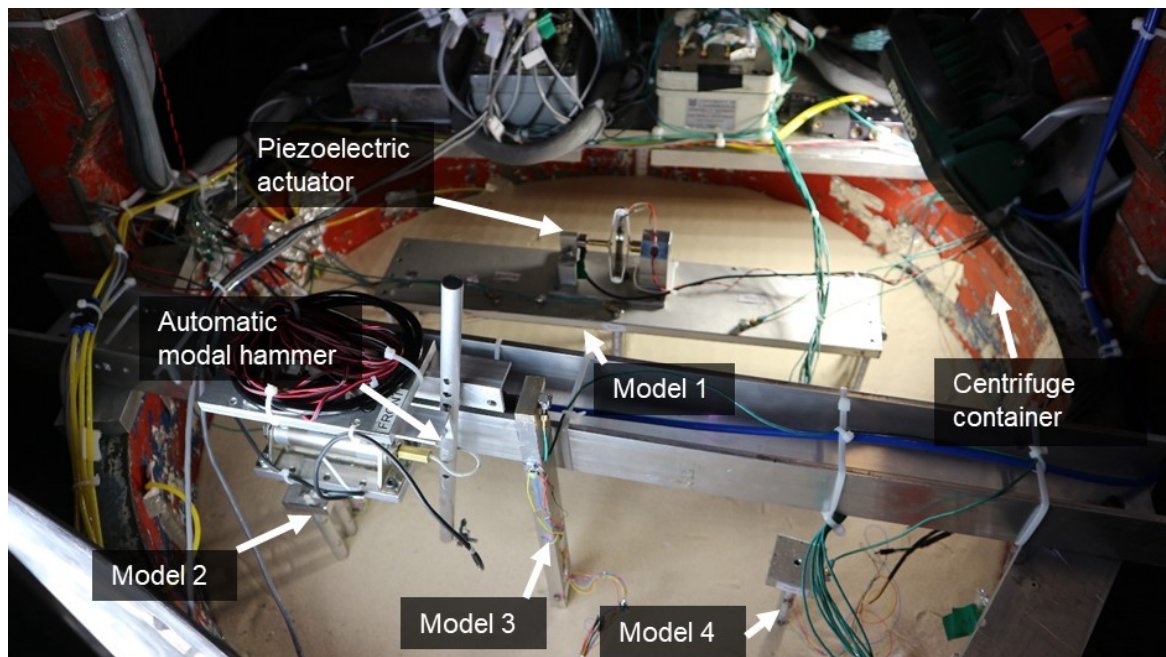


Figure 4.5 The cylindrical centrifuge container with all four structural models and the excitation setup

4.5.1 Model structure preparation

The model structures were made from aluminium sections and had the small-scale properties listed in Table 4.3. Aluminium sections were used instead of the full-scale material, reinforced/prestressed concrete, as aluminium sections can be machined and fabricated to a high degree of accuracy at small-scale than it is possible to do with concrete. All models were instrumented with accelerometers, as shown in Figure 4.4. Paper rulers were glued on to all model foundations with the aim of using them as a reference level when creating scour holes.

4.5.1.1 Material properties

The circular hollow piles in the model structures were made of aluminium alloy 6061-T6, and the rest of the solid sections were made of aluminium alloy 6082-T6. These aluminium alloys have Young's modulus of 70 GPa and density of 2700 kgm^{-3} (Aalco, 2019b, 2019a).

4.5.1.2 Integral connections

The small-scale model structures were selected to be more simplified, i.e. to have a minimum number of connections, than the full-scale bridges to reduce the effects of connection imperfections on dynamic response. However, all of the model structures had at least one integral connection either at the foundation to deck connection or at the stub column to pad foundation connection. To obtain these integral connections, sockets of the same diameter as the column/pile elements were first machined up to half the depth of the slab/pad section. The columns/piles were then inserted into these sockets and glued in place with a high-strength retainer adhesive. The connection rigidity of each pile/column was tested by finding the fundamental sway natural frequency of the piles when the slab/base was fixed. The piles

without adequate integral connection showed a varying frequency for repeated tests or a lower frequency than other similar piles. These piles were removed and reconnected to obtain the desired integral connection.

4.5.1.3 Instrumentation

The accelerometer locations on Model 1 are shown in Figure 4.4(a). The sensor arrangement was chosen to capture the fundamental sway mode of vibration. Six MEMS accelerometers were mounted on the piles, and five piezoelectric accelerometers were mounted on the bridge deck. All accelerometers except M1m6 was in one vertical plane. In order to help verify the longitudinal sway mode shape, M1m6 accelerometer was mounted on a pile, different from the pile with all the other accelerometers on the middle pier. This was placed at the level as M1m3; thus, both these on different identical piles should show similar modal amplitudes for the longitudinal sway mode.

The accelerometer locations on Models 2, 3 and 4 are shown in Figure 4.4(b). Piezoelectric accelerometers were placed at the top of the models. The piles and columns were mounted with MEMS accelerometers. The arrangement of accelerometers was chosen to capture both the fundamental sway mode and the pier bending mode of vibration. Similar to Model 1, two accelerometers (M2M2 & M2m4) were mounted on two out of the four different identical piles of Model 2 to help confirm the longitudinal mode shapes.

The labelling of the accelerometers on Models 1 – 4 in Figure 4.4(a) and Figure 4.4(b) indicates the model number by the first two characters (M1, M2, M3 or M4), sensor type by the third character (“m”= type 1/ADXL78 MEMS, “M”= type 2/ADXL1002 MEMS and “P”=Piezoelectric), and a unique accelerometer number corresponding to each model by the last character. The piezoelectric (“P”) accelerometers were DJB A/23/TS accelerometers, with a working frequency range of 10 – 10,000 Hz (DJB Instruments, 2018). The ADXL78 (“m”) accelerometers claim 1100 $\mu\text{g}/\sqrt{\text{Hz}}$ noise density for 10-400 Hz frequency range and a range of 35g (Analog Devices, 2010). The ADXL1002 (“M”) accelerometers claim far less noise density of 40 $\mu\text{g}/\sqrt{\text{Hz}}$ for 1 – 10,000 Hz frequency range and a range of 50g (Analog Devices, 2017). A high acceleration range was chosen since horizontal accelerometers, even with a slight tilt, may measure part of the effective gravity field (40 – 60g) in the centrifuge.

The MEMS accelerometers measure the static acceleration measurements, and thus they capture the component of acceleration due to gravity when they are at any inclination. Using this principle, MEMS accelerometers were calibrated at a special calibration bed with controllable inclinations. Piezoelectric accelerometers however only measure dynamic acceleration, and hence those were calibrated by using special calibration equipment, available at this testing facility, which can provide a sine wave excitation of amplitudes $\pm 1\text{g}$ for a given mass.

4.5.2 Soil model preparation

The soil model was prepared in a cylindrical steel container, as shown in Figure 4.6. Paper rulers were glued on to the inside wall of this container to act as a reference to the level of the sand fill (Figure 4.7). The cylindrical centrifuge container was 850 mm in diameter and 400 mm in depth and filled with a 250 mm deep layer of sand. The sand filling was carried out with an automatic sand pourer (Madabhushi, Houghton and Haigh, 2006).

4.5.2.1 Material properties

The soil used for the centrifuge test was Hostun sand acquired from Drôme in the southeast of France. This sand type is widely used in centrifuge model tests. It is a high silica ($\text{SiO}_2 > 98\%$) sand of grain shape varying from angular to sub-angular (Futai et al., 2018). The properties of Houston sand are given in Table 4.4.

Table 4.4 Geotechnical properties of Hostun sand (Futai et al., 2018)

Property	Value
D_{10} (particle diameter at 10% finer)	0.286 mm
D_{50} (particle diameter at 50% finer)	0.424 mm
e_{\min} (minimum void ratio)	0.555
e_{\max} (maximum void ratio)	1.010
G_s (specific gravity of solids)	2.65
Φ_{crit} (critical state friction angle)	33°

4.5.2.2 Sand pouring

The sand was poured with an automatic sand pourer (Figure 4.6) developed by Madabhushi et al. at the Scofield Centre centrifuge testing facility (Madabhushi, Houghton and Haigh, 2006). The small container used for calibration, shown here, was replaced with the 850-mm diameter centrifuge container for final sand pouring. The sand pourer machine pours sand from a user-specified height while moving in a zig-zag motion to fill a small layer of soil of about 1-2 mm. Once this layer is filled, the pourer automatically moves up by the depth of the layer recently completed (pre-specified by the user) to maintain the same drop height. This constant drop height allows the preparation of a sand sample of uniform density in the centrifuge container.

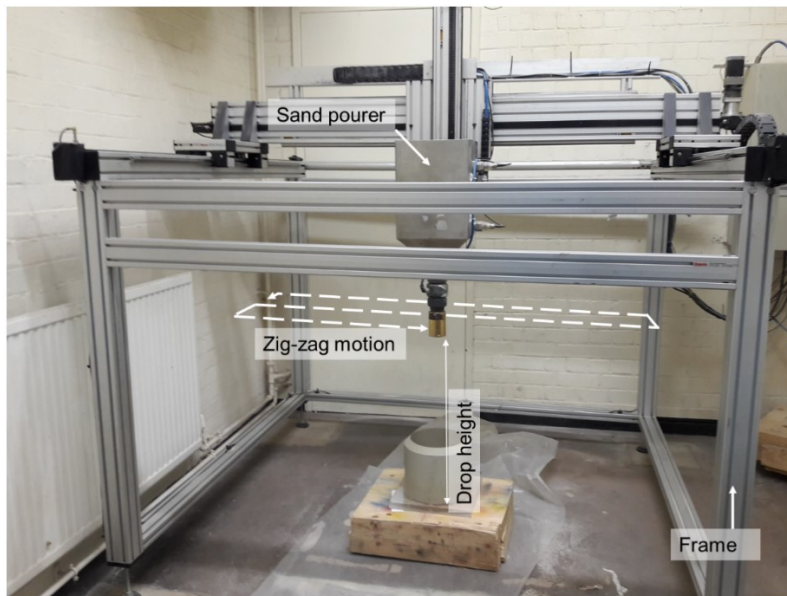


Figure 4.6 Automatic sand pourer during calibration

After a calibration sand-pouring test, shown in Figure 4.6, a drop height of 690 mm through a 5 mm diameter nozzle (no sieve), with a 20 mm spacing between consecutive motions, was selected to target a relative density of 70%. A 250 mm deep layer of sand was poured with this setup. The relative density (D_r) of the final sand layer in the centrifuge container was determined to be 66% from Equation 4.3 (Lade, Liggio and Yamamuro, 1998). The void ratio (e) was estimated from the pre-post weight difference and the properties given in Table 4.4. The bulk density of the soil was found to be 1550 kgm^{-3} based on the pre-post weight difference and the volume of the filling.

$$D_r = \frac{e_{max} - e}{e_{max} - e_{min}} \times 100\% \quad \text{Equation 4.3}$$

The sand pouring was paused to place all instruments and the pad foundation model (Model 3) at their respective heights in the soil, previously shown in Figure 4.4. The Model 3 was also placed on the soil during the sand pouring, and sand pouring continued to embed the pad foundation while the sand dropped above the pad was collected using a small container, as shown in Figure 4.7. The collected sand was vacuumed out, and the collector was removed when the soil level reached the top of the pad. This collection and removal of soil above the pad made sure a pile of sand does not form due to uniform sand pouring everywhere in the container, including over the pad. The paper rulers helped confirm the depth of embedment of the foundations, as shown in Figure 4.7.

The structural models with pile foundations (Models 1, 2 and 4) were inserted into the soil model at the end of the sand pouring. The piles were pushed down until the desired embedment depth of 200 mm had been reached. It was assumed that the piles with open ends would not cause significant disturbance to the soil when inserted at normal gravity.

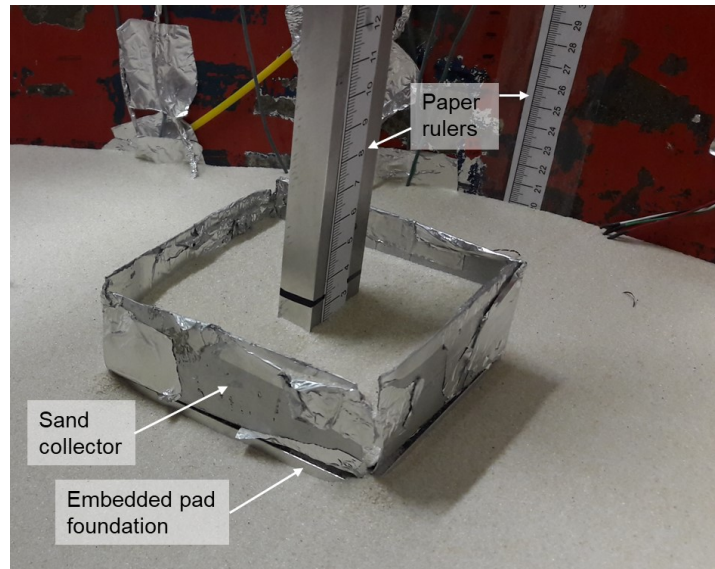


Figure 4.7 Automatic sand pouring around Model 3 – the shallow pad foundation

4.5.2.3 Instrumentation

The variation of soil stiffness due to scour was studied using shear wave velocity measurements. Shear waves were generated by two air hammers, which were placed when the sand fill was 23 mm, as shown in Figure 4.8(a). The shear waves travelled vertically and were captured by accelerometers at different heights above the air hammers (Figure 4.4). These accelerometers were placed above each other at five different fill heights with the help of a thin vertical rod driven at a known distance from them. Placing accelerometers at one of these five different fill heights is shown in Figure 4.8(b). This is a top view of the centrifuge container during sand pouring. “X” reference mark in both Figure 4.8(a) and Figure 4.8(b) shows the same location on the container wall. All the accelerometers embedded in soil were piezoelectric DJB A/23/TS (DJB Instruments, 2018).

Each air hammer has a small brass tube with a metal pellet inside. High-pressure air from one end of the tube causes the pellet to accelerate and strike the other end creating an impulse. Some sand particles had been affixed to the external wall of this metal tube to improve its coupling with the surrounding sand body (Dong, 2016). Thus, each horizontal impulse generated in the air hammer transfers a shear wave to the sand. This process was repeated by a relay switch that alternated a single air pressure input between the two ends of the air hammer tube. Both the air hammers were connected to one relay switch due to the limited availability of switches.

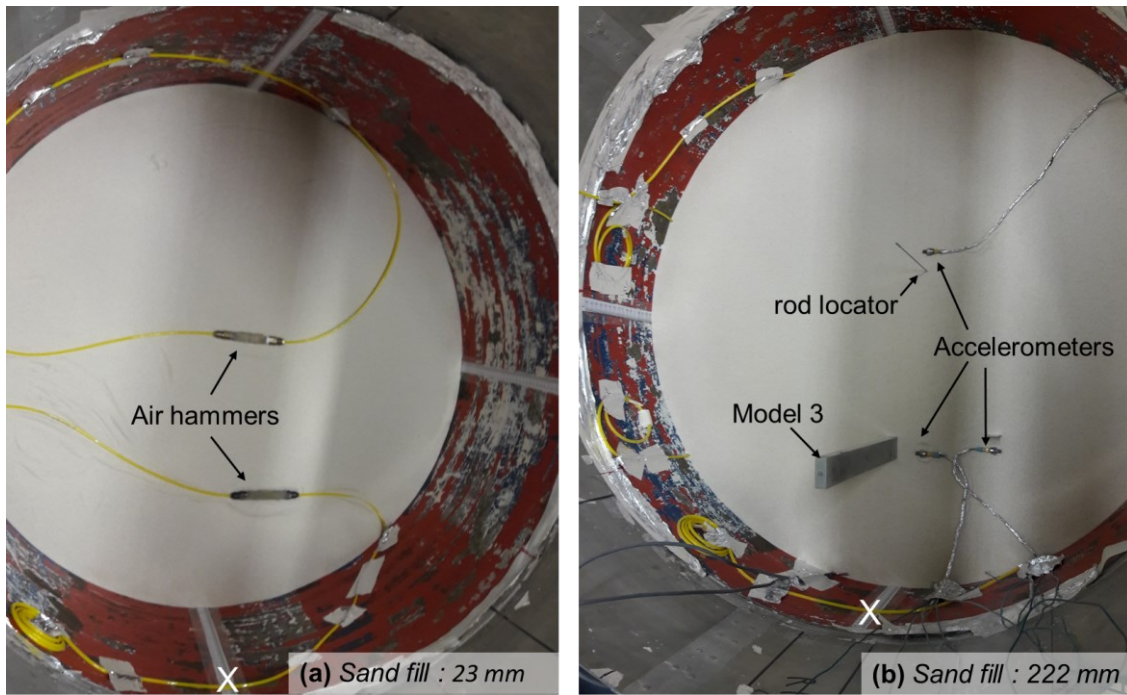


Figure 4.8 Instrument placement at different sand fill heights

Near Model 1, a column of accelerometers (C01 – C05 in Figure 4.4(a)) was placed with an air hammer directly below them.

Near Models 3 and 4, two columns of accelerometers (C06 – C10 and C11 – C15 in Figure 4.4(b)) were placed. An air hammer was positioned in between the models. The two columns of accelerometers lie close to the two ends of this air hammer. It was assumed that there was enough coupling between the air hammer wall and the soil to generate a wide shear wave that travels vertically along both these columns of accelerometers. Note the C09 accelerometer had to be shifted from the respective column of accelerometers due to the presence of the pad foundation. Nevertheless, this is unlikely to have affected the measurements, given the shear wave was vertical and sufficiently wide.

Near Model 2, it was not possible to place such a shear wave monitoring setup due to the limited availability of air hammers and the concern about the interference of air hammer signals. As all air hammers were controlled by a single relay switch, even with the two air hammers used in the experiment, interference of shear waves was observed at certain instances (see Section 4.12). The shear wave profile at the Model 2 foundation can be taken as similar to the profile at the Model 1 pier foundation as they have the same setup of piles.

4.5.3 Excitation sources

Two excitation sources were used to test two structural models together in each centrifuge flight. At any given “centrifuge flight” (i.e. a centrifuge test, where the centrifuge model is flying at the end of the rotating centrifuge beam), the piezoelectric actuator was used with either the Model 1 or 4, and an automatic modal hammer was used with either the Model 2 or 3. The

piezoelectric actuator was already available from a previous experimental programme that studied wind turbine vibrations (Futai et al., 2018). It was necessary to be able to test multiple structural models at the same time in a centrifuge flight due to the fact that each centrifuge flight cost a significant amount of time and electricity. Therefore, a second excitation setup, an automatic modal hammer, was developed from an air hammer setup available in the laboratory. Based on the frequency spectra observed during the centrifuge tests with these two excitation sources, automatic modal hammer proved to provide stronger external impact excitations to allow easier modal identification, as further discussed in Section 4.7.

4.5.3.1 Amplified piezoelectric actuator

The amplified piezoelectric actuator (APA) used was an APA400MML (Cedrat Technologies, 2014). As shown in Figure 4.9, this actuator has one end fixed to its base through a load cell and the other end connected to a brass mass on roller bearings. Excitation of the piezoelectric material transfers a horizontal inertial force excitation to the APA base, which was fixed on the top of either Model 1 or 4 during the experiment.

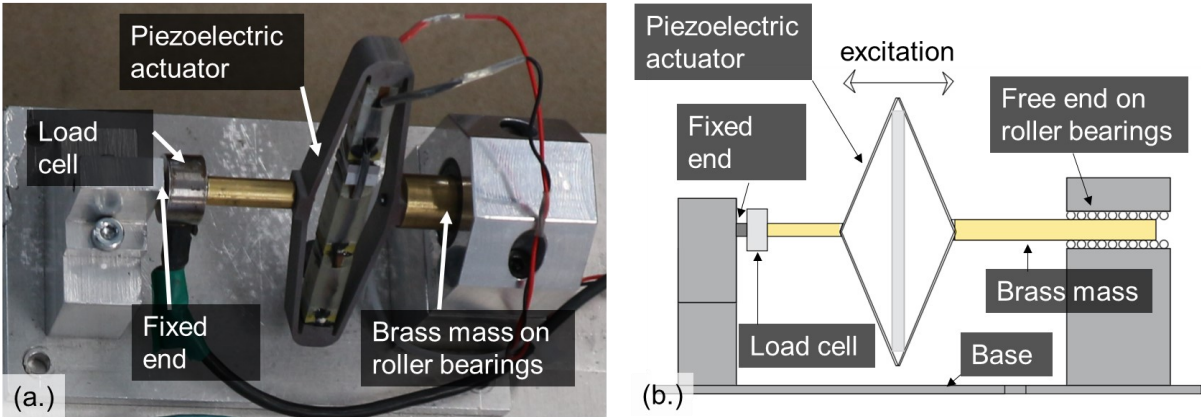


Figure 4.9 Amplified piezoelectric actuator setup (a) in the experiment (b) diagram

4.5.3.2 Automatic modal hammer

Automatic modal hammer developed is shown in Figure 4.10. It generates impulsive excitation on the structural models by impact of a load cell at the bottom end a free-hanging kicker made from an aluminium tube. An air hammer, with two high-pressure airlines controlled through a relay switch, was used to provide an impulse to the kicker. The impulse was transmitted to the model through the load cell, which measures the force input to the model. A voltage input to the relay automatically excited the modal hammer every 2 s.

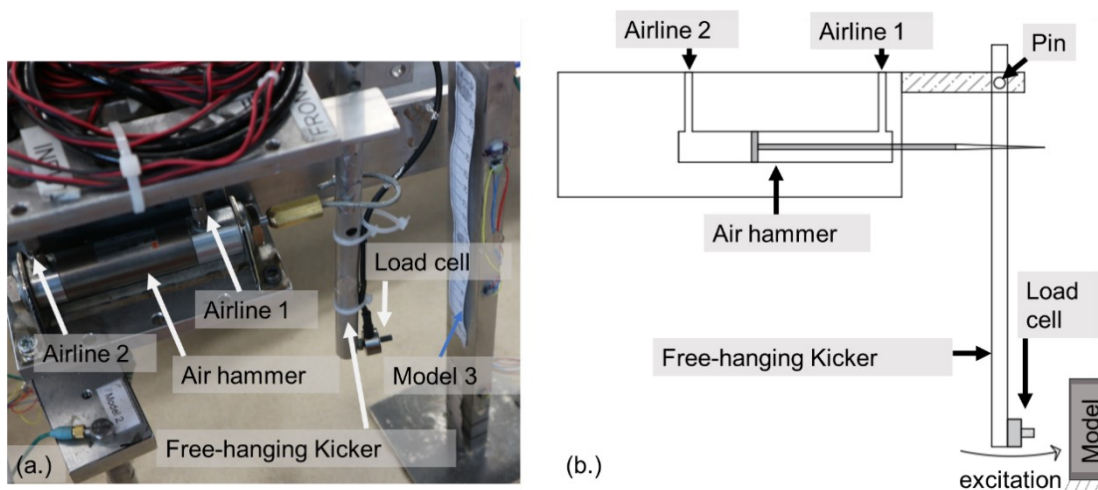


Figure 4.10 Setup of the automatic modal hammer controlled by air-pressure (a) in the experiment (b) diagram.

4.5.4 Data-acquisition system

All data acquisition during the centrifuge tests was carried out with the centrifuge data-acquisition system, which uses slip rings to transfer data from the centrifuge container to the computers in the centrifuge control room. All signals were transmitted through a set of amplifiers and then through an analogue to digital converter (Madabhushi, 2014). The digitalised signals were logged by DasyLab software.

The expected fundamental natural frequencies of the structural models were below 2kHz based on fixed based tests conducted on these structural models outside the centrifuge (See Section 4.6). Therefore, a sampling of 10 kHz was chosen for the accelerometers on these model structures to ensure the Nyquist frequency (half of the sampling frequency – 5kHz) was above the natural frequencies of the structures.

A higher sampling rate of 30kHz was chosen for the accelerometers embedded in the soil. Such a high sampling rate was required to allow the accelerometers to capture the different arrival times of a shear wave and its speed with sufficient resolution (e.g. Dong (2016) used 20KHz).

4.5.5 Centrifuge flight programme

Before each centrifuge flight started, the desired scour hole was created using vacuum suction in order to limit disturbance to the underlying soil. The depths of the scour hole were measured with reference to the paper rulers that were on all of the structural model foundations. Figure 4.4(a) and Figure 4.4(b) show the maximum local and global scour holes. With global scour, the soil surface level was maintained horizontal. With all local scour holes, an approximate inclined angle of 30° was maintained around all sides (Figure 4.11), which was slightly below the angle of the response of Hoston sand (33°). The typical slope of a local scour hole is equal

to the angle of response of the bed material for the upstream side but could be lower than that for the downstream side (Hafez, 2016).

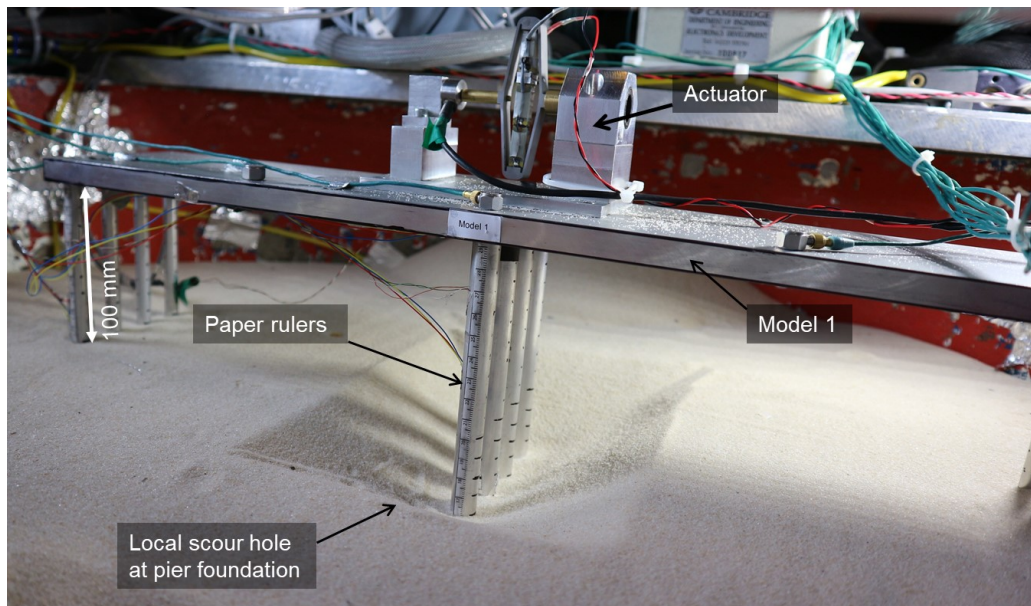


Figure 4.11 A 20-mm deep local scour hole created at the pier foundation of Model 1 (M1S1 scour step)

Following the creation of the scour holes, the natural frequencies of the models were measured at “1g”, to confirm the operation of the excitation sources and data logging before the centrifuge flights were started. Then the centrifuge beam rotation was initiated. When the rate of rotation of the beam provided the desired centripetal acceleration (40g or 60g) to the models, natural frequency test was conducted again, and data was logged while the impulses were provided by the two excitation sources. Afterwards, the air hammers in soil were activated to create shear waves while the accelerometers in soil logged the responses. Finally, the centrifuge flight was stopped, and the next scour step started.

The different steps of scour tested around each centrifuge model are summarised in Table 4.5. Each step of scour was named with four characters (e.g. M1S1), with the first two characters referring to the name of the centrifuge model and the last two characters referring to the scour step number. For example, scour step “M1S1” indicates Centrifuge Model 1 and Scour step 1.

In total, the natural frequencies of Centrifuge Model 1 were tested at seven different scour depths. Note that all these cases were cumulative. For example, at step M1S5, when 60 mm (3.6 m in the full-scale) of local scour at the left abutment was introduced, there was already 60 mm of local scour (M1S4) at the middle pier. Model 1 excitation was provided by the piezoelectric actuator for the case simulating local scour around the middle pier, and also for the final global scour case.

Table 4.5 *The scour steps around the bridge models*

Model	Step name	Centrifuge Flight number	Equivalent full-scale scour case	Location of scour for each step	Excitation source
1	M1S1	1	no scour	Middle pier only	Piezoelectric actuator
	M1S2	2	1.2 m local scour		
	M1S3	3	2.4 m local scour		
	M1S4	4	3.6 m local scour		
	M1S5	6	3.6 m local scour	+ Left abutment	Ambient vibration
	M1S6	7	3.6 m local scour	+ Right abutment	
	M1S7a	8	3.6 m global scour	Everywhere	Ambient vibration
	M1S7b	9			Piezoelectric actuator
2	M2S1	5	no scour	Pier	Automatic modal hammer
	M2S2	6	1.8 m local scour		
	M2S3	7	3.6 m local scour		
	M2S4	8	3.6 m global scour		
3	M3S1	1	no scour	Column	Automatic modal hammer
	M3S2	2	0.68 m local scour		
	M3S3	3	1.36 m local scour		
	M3S4	4	2.00 m local scour		
	M3S5	9	2.00 m global scour		
4	M4S1	5	no scour	Pile	Piezoelectric actuator
	M4S2	6	1.8 m local scour		
	M4S3	7	3.6 m local scour		
	M4S4	8	3.6 m global scour		

During the initial centrifuge flights, it was found that the Model 1 was experiencing high ambient vibration, possibly due to the wind created by the centrifuge beam rotation. Therefore, the Model 1 could be sufficiently vibrated with the ambient vibration of the centrifuge, without having to rely on the piezoelectric actuator. Hence, some additional tests were conducted with ambient vibrations in Model 1, and the Model 4 was being tested with the piezoelectric actuator. To maintain the same mass of the Model 1 in all tests, the mass of the piezoelectric actuator removed from Model 1 during these additional tests was replaced by a standard metal mass plate of 0.5 kg. There was an unintended error here since the mass of the actuator was 0.44 kg, not 0.5 kg; 0.5 kg was the mass of the combined mass of the actuator and all the accelerometers (accelerometers remained in the model, but only the actuator was replaced). This unintended error in the additional tests, however, was found to have not affected the natural frequency observations (see Section 4.7.2). These additional tests of Model 1

simulated local scour at the bridge abutments. Further, one scour case, 60 mm global scour case, was tested in two centrifuge flights one with the piezoelectric actuator and the other with ambient vibration (and the 0.5 kg mass replacing the actuator), to confirm whether these two excitation setups provide the same natural frequencies.

With Model 3, local scouring was introduced in 17 mm steps (0.68 m in the full-scale), with a final 50 mm (2 m) global scour case; requiring a total of five centrifuge flights. With Models 2 and 4, local scouring was introduced in two 30 mm steps (1.8 m) up to 60 mm (3.6 m), and a final global scour of the same depth was tested, making a total of four centrifuge flights.

The air temperature during the one-week centrifuge flight programme was measured at the end of every centrifuge flight. The temperature was stable (12.5 – 16 °C) throughout the experimental programme, as the centrifuge is located underground. Therefore, it was assumed that there were negligible temperature effects on the modal parameters of the models, and they varied entirely due to scour.

4.6 Fixed-base tests

For each scour level, the soil around the piles provides some stiffness to the models. The maximum soil stiffness, and thus the maximum natural frequency, is reached when the embedded layer of soil provides full fixity.

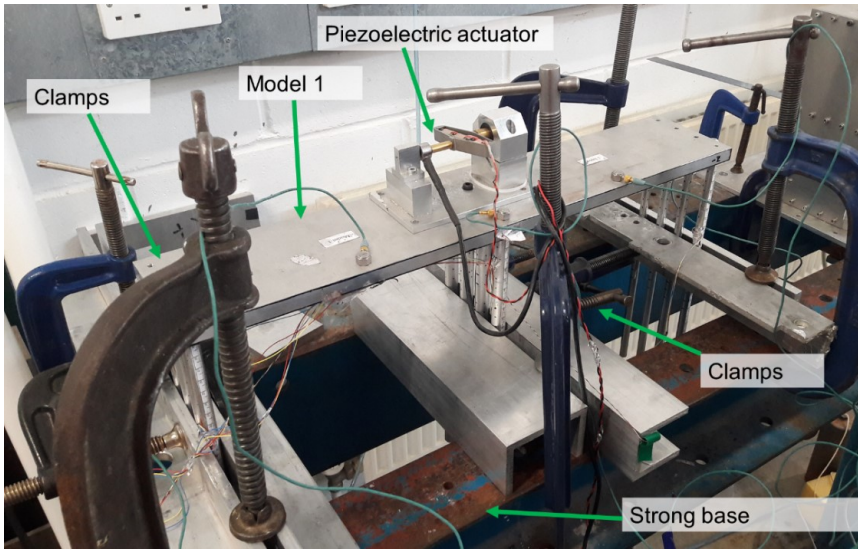


Figure 4.12 Fixed base test being carried out for Model 1

Therefore, as shown in Figure 4.12, the models were tested with fixity in order to obtain an upper-bound natural frequency to help confirm the centrifuge test results. The exposed height of the models was increased to simulate the scour depths. It is noteworthy that the fixity was provided using clamps, and therefore the fully fixed condition may not have reached.

4.7 Modal analysis

The measured vibration data was analysed to find the modal properties. The modal analysis techniques used for models excited by the piezoelectric actuator and those excited by the modal hammer are discussed in the following sections. The abnormal conditions observed that might affect the vibration properties are also discussed.

4.7.1 Models excited by the automatic modal hammer

The models excited by impacts from the automatic modal hammer (Models 2 and 3) were analysed with a simple frequency-response function (FRF) to find modal parameters. The FRF quality was improved by segmenting the signals by individual impacts and applying a force window to each segment of input and an exponential window to each segment of output, as shown in Figure 4.13 (Brandt and Brincker, 2010). The accelerance FRF estimate was computed in MATLAB. Example spectra of accelerance FRF magnitude and coherence are shown in Figure 4.14. Peaks in the FRF with high coherence correspond to vibration modes, the first of which in this case is 88.5 Hz (2.21 Hz in full-scale). The ratio of FRF magnitudes of different accelerometers at the modal peaks presents the corresponding mode shape (He and Fu, 2001).

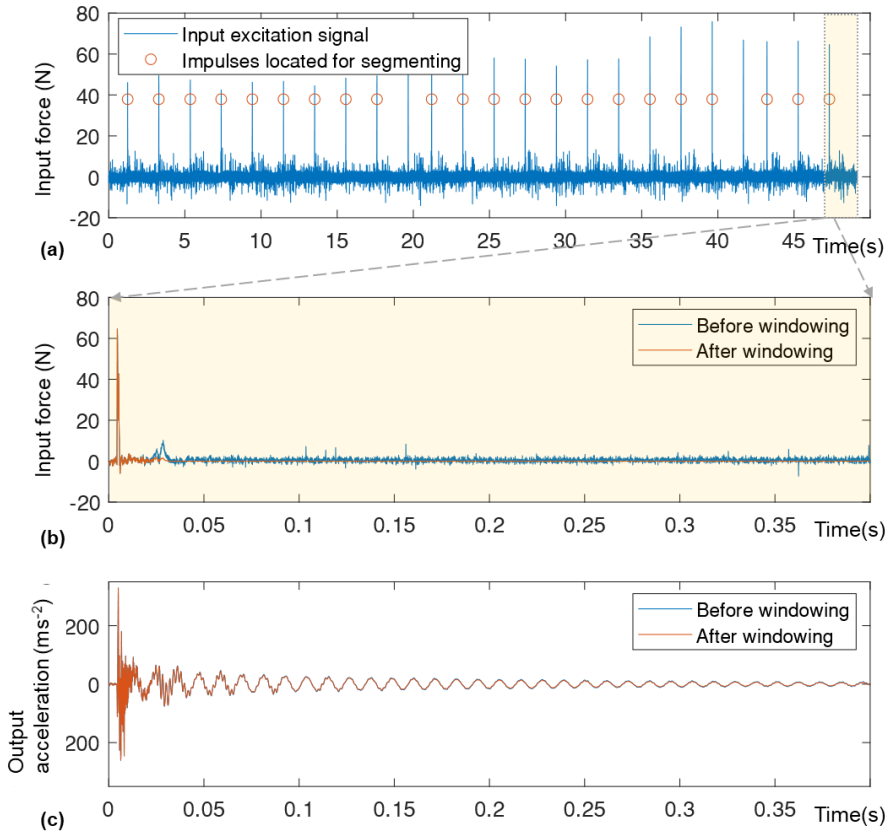


Figure 4.13 Time histories of Model 3 – scour step M3S5 (a) input force, (b) part of a segmented input force and (c) corresponding output acceleration of M3P1

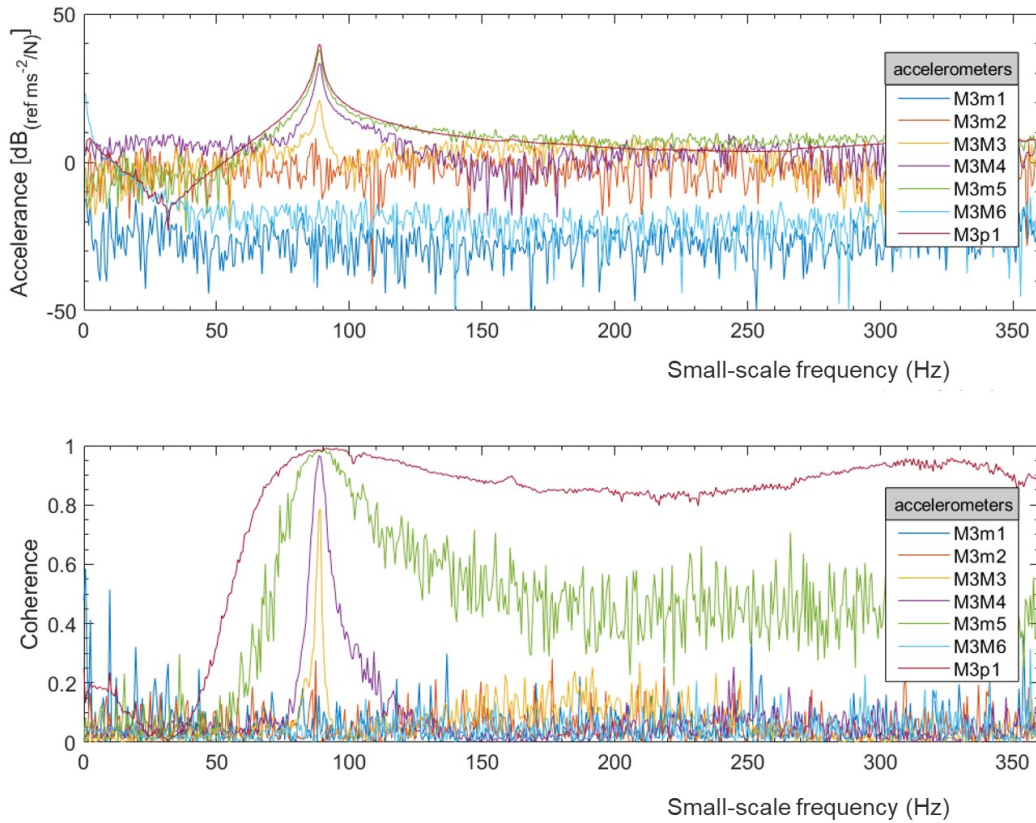


Figure 4.14 Accelerance FRF and coherence spectra of Model 3 during the scour step of M3S5.

4.7.2 Models excited by the piezoelectric actuator

An example input excitation and the corresponding response measured in Model 1 are shown in Figure 4.15. It is clear that the transient (free vibration) response to the APA was short and of insufficient duration to determine the frequency content with acceptable resolution. However, there was sufficient ambient excitation between the APA impulses to perform modal analysis.

Modal analysis for Models 1 and 4 was therefore carried out in MATLAB using the output-only system identification method, frequency domain decomposition (FDD), explained in Section 3.2.5. Figure 4.16 shows the first singular value of the PSD matrix (SVPSD) spectra obtained from FDD of Model 1 acceleration measurements during two centrifuge flights, both having a global scour depth of 60 mm (equivalent to 3.6 m at the full-scale). One centrifuge flight had Model 1 excited by the piezoelectric actuator, while the other had purely the ambient vibration (and the mass of the piezoelectric actuator replaced by a standard mass). As explained in Section 4.5.5, there was an unintended error in these ambient vibration tests since the mass of the piezoelectric actuator (0.44 kg) was somewhat different from the mass of the replaced mass (0.50 kg). Nevertheless, both these tests indicated a sway mode shape of the bridge (See Figure 4.29(c)) at the same frequency (65.9 Hz – 1.1 Hz at full-scale), which indicates

that the error in the replaced mass can be ignored and the ambient vibration alone enables repeatable detection of natural frequency.

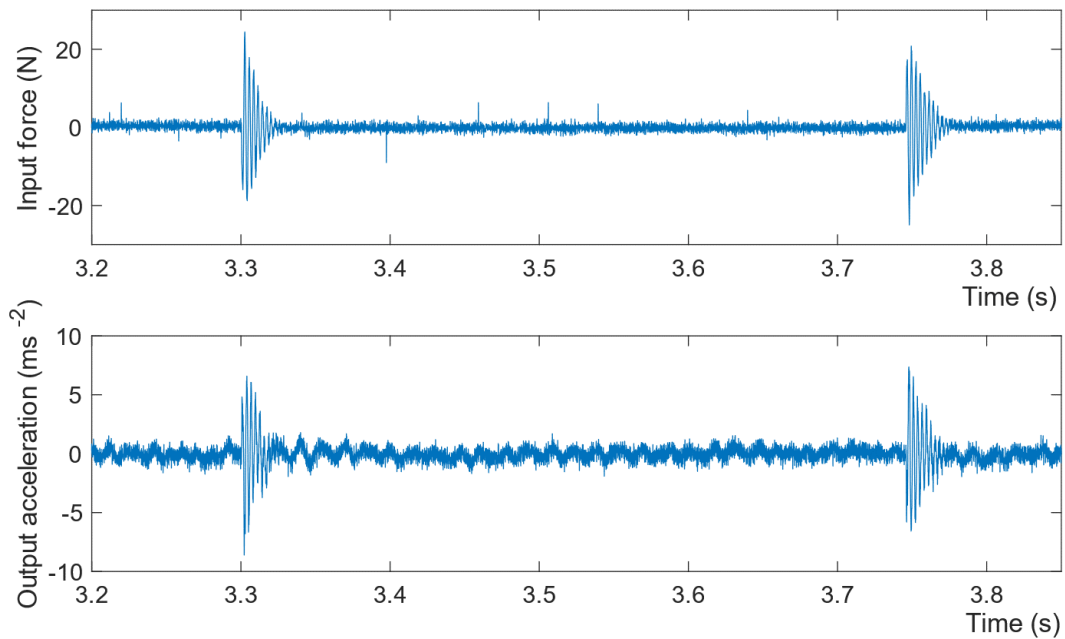


Figure 4.15 Measured input excitation and the response acceleration of one sensor in Model 1 (scour step M1S7b)

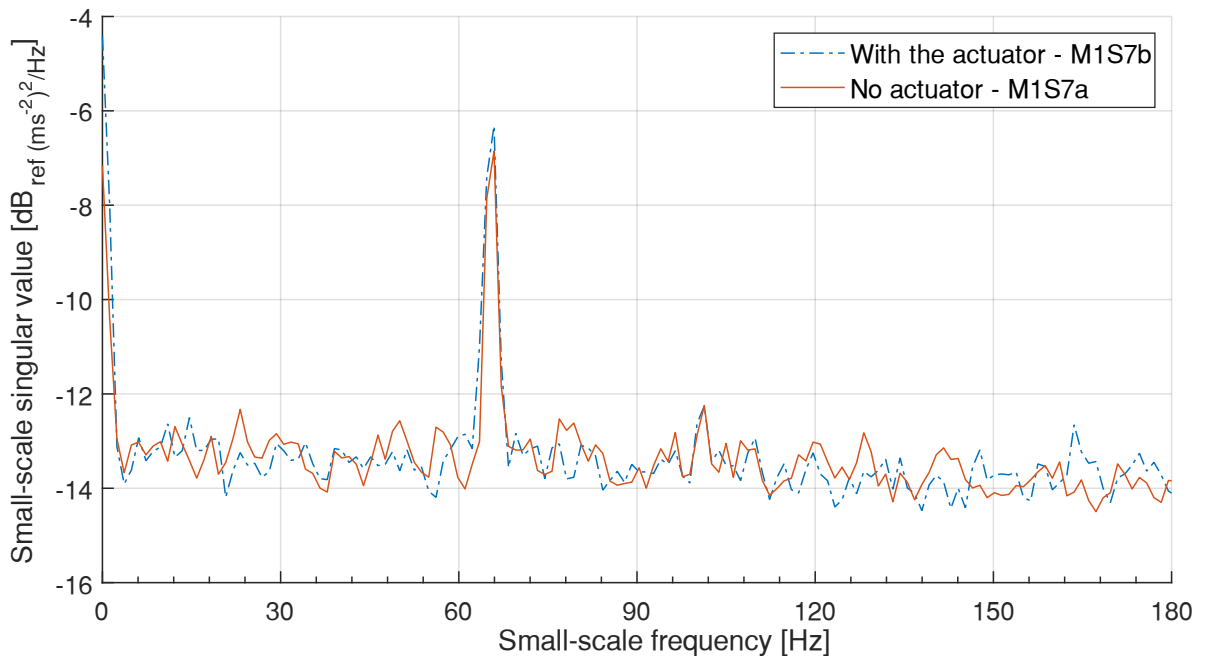


Figure 4.16 First SVPSD of Model 1 response for the same scour depth but with two excitation sources: no actuator (step M1S7a) and with the actuator (step M1S7b)

4.7.3 Abnormal behaviours observed

The modal analysis showed certain abnormal behaviours in some tests. In Model 1, certain vibration measurements in the centrifuge showed a spectral peak exactly at 100 Hz while no

peak was seen at the expected 50 Hz electrical noise. To study whether it was a noise peak or not, ambient vibration measurements were taken at different levels of centrifuge acceleration for the same scour step of M1S6. Figure 4.17 shows the first SVPSD spectra for the tests performed at different centrifuge acceleration levels, given as multiples of the normal gravity ("g"). SVPSD estimates here were estimated for only M1P1 and M1P5, the two accelerometers with the highest signal to noise ratio, to reduce the effect of measurement noise. According to Figure 4.17, the expected mains electrical noise of around 50 Hz was seen when tests were performed below 10g, but it has disappeared in the tests at higher g levels. There were two other groups of peaks. One at around 75 – 80 Hz shows a gradual increase with higher g levels. The other group of peaks only appears when the tests were performed above 40g and lies precisely at 100 Hz. The natural frequency peak of the sway mode should gradually increase with higher g levels due to the stiffening of soil. Therefore, it was confirmed that the 75 – 80 Hz range, in this case, was the natural frequency peak. The peak at 100 Hz was assumed to be due to noise, caused by either electrical noise moving from 50 Hz to 100 Hz during the centrifuge or mechanical noise in the centrifuge.

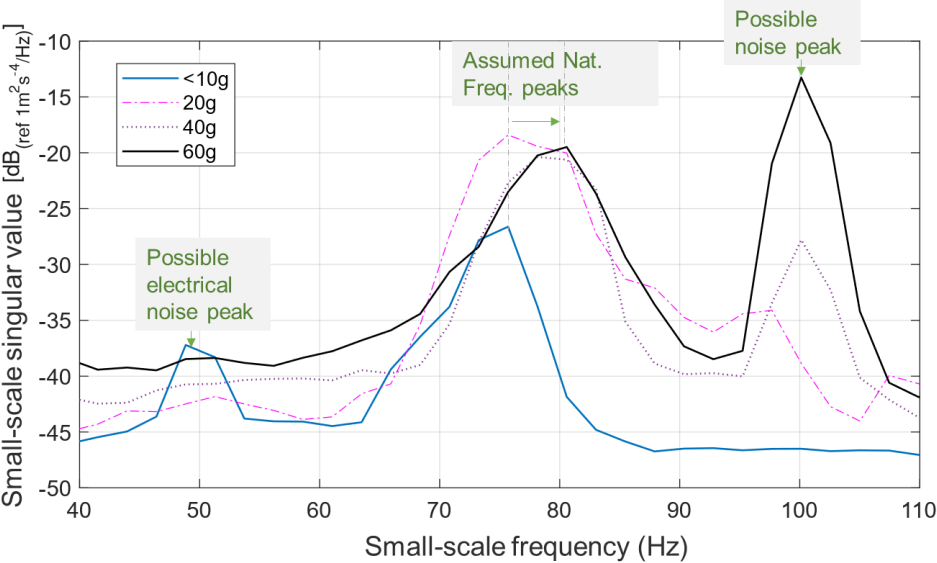


Figure 4.17 Variation of first SVPSD spectrum for tests performed at different centrifuge acceleration levels for the same scour step (M1S6)

In Model 2, the load cell on the automatic modal hammer had not functioned during the test conducted for the scour step of M2S3. Therefore, the natural frequency and mode shapes were estimated for this test using the output-only-FDD method, rather than the FRF method. By way of comparing the frequencies estimated by FDD and FRF for other tests of the model, it was confirmed that both analysis methods gave the same natural frequency estimates.

In the test conducted with the scour step of M2S1, the automatic modal hammer had jammed with the Model 2, as shown in Figure 4.18. The load cell was touching a pile wall even after the impact by the hammer, and hence the free vibration of the model was partially restricted.

Therefore, the vibration behaviour of the model in this test may have been affected. The jamming of the load cell was identified and corrected in all the following tests, in which free vibration can be expected.

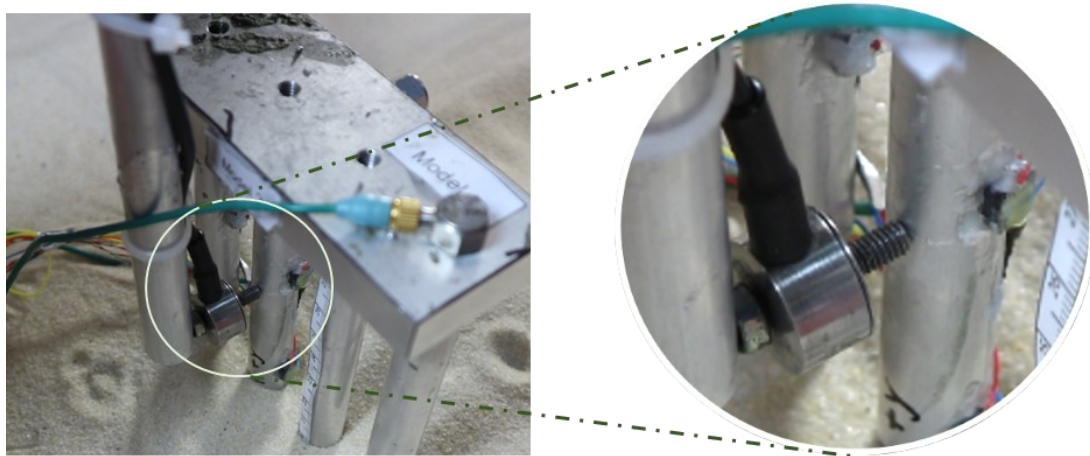


Figure 4.18 *The jammed automatic modal hammer during no scour case*

In Model 3, the vibration measurements taken at normal gravity (1g) did not show clear FRF peaks, nevertheless, during centrifuge testing (40g) and with fixed based tests, clear natural frequency peaks were observed. It was assumed that the soil around the pad foundation at normal gravity might not have provided sufficient fixity to the pad foundation. Another minor issue was that the M1P5 accelerometer might have either malfunctioned or gone above range in tests conducted for the scour steps of M3S1 and M3S2. For these tests, the correct modal properties were estimated using other accelerometers.

In Model 4, no special vibration abnormalities were observed. In all models, Model 1 – 4, higher-order modes did not show sufficient accuracy, only the fundamental sway mode showed high accuracy with clear modal peaks. Therefore, only the fundamental mode is studied in the following sections.

4.8 Natural frequency sensitivity to scour

As the environmental parameters were controlled, any change in natural frequency can be attributed to the scour itself. Therefore, high sensitivity of natural frequency indicates a high potential for it to be used as an indicator of bridge scour while a low sensitivity indicates otherwise.

The natural frequencies found in the modal analysis were plotted against scour depth to illustrate the natural frequency sensitivity to scour. The fundamental sway mode shapes at these natural frequencies are given later in section 4.10. All frequency measurements discussed in the following sections have been scaled to the full-scale using the corresponding scale factors (40 for Model 3 and 60 for all other models).

For comparison, the frequencies measured at “1g” in the centrifuge container with soil, and in the “fixed base” condition, are also plotted. At “1g”, the soil was less stiff than the soil during the centrifuge test, and therefore the “1g” frequency measurements give a lower bound for the frequencies measured during the centrifuge test. The fixed condition represented the maximum stiffness that the soil can provide, and therefore provides an upper bound.

4.8.1 Model 1: Integral bridge

The full-scale natural frequency variation found using the integral bridge model is shown in Figure 4.19. As expected, the natural frequency measurements at 60g remained between the fixed base upper bound and 1g lower bound at all scour levels. A centrifuge noise peak was present at 1.67 Hz (full-scale 100 Hz), as discussed in Section 4.7.3. The natural frequency of the second scour step at 60g had been overshadowed by this noise peak. It is noteworthy that there may have been some partial effect of this strong noise peak to the accuracy of the close-by natural frequency peaks, 1.83 Hz and 1.59 Hz, however such effect was ignored as these were within the expected range, i.e. between 1g and fixed based tests.

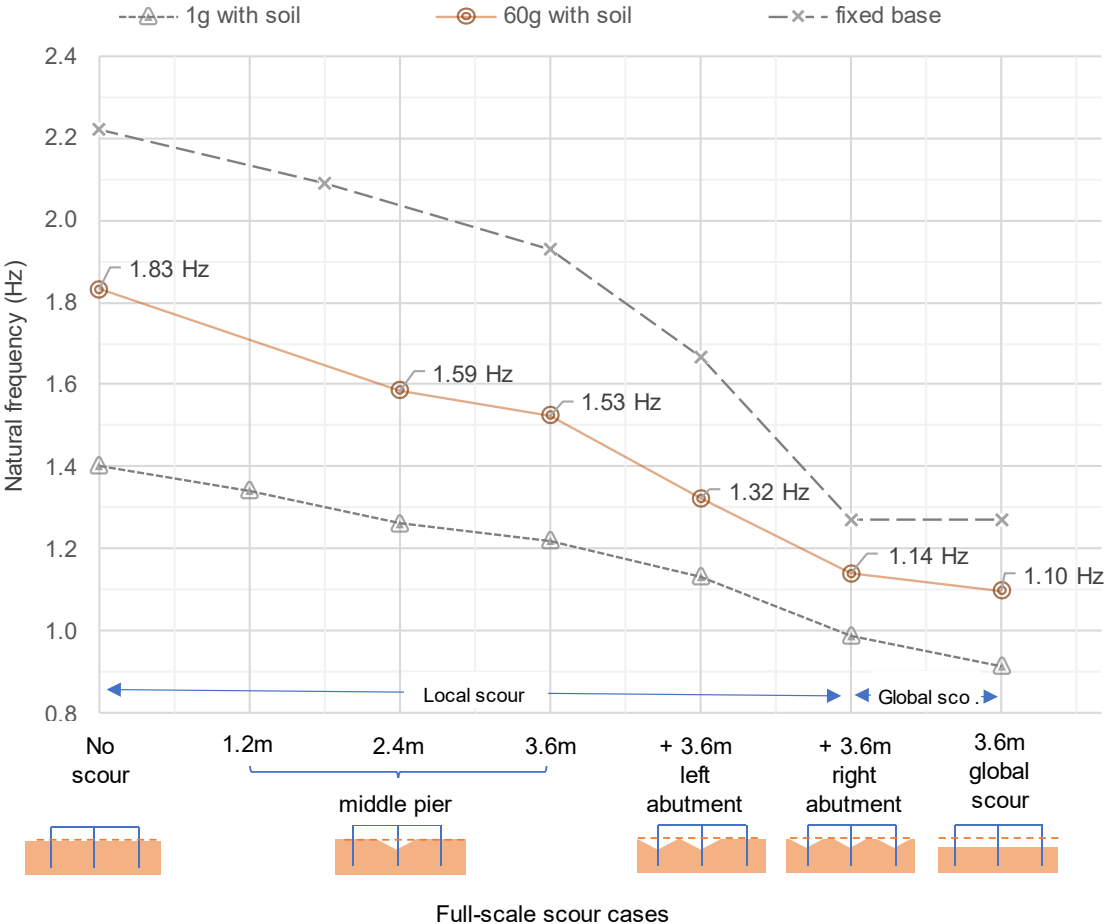


Figure 4.19 Estimated full-scale natural frequency variation of the integral bridge (Model 1) for different cases of scour

4.8.1.1 Local scour

As shown in Figure 4.19, 3.6 m of local scouring at the middle bridge pier foundation resulted in a 16.4% overall reduction in the natural frequency. This corresponds to an average frequency sensitivity of approximately 4.6% per metre of full-scale scour.

An additional 3.6 m of local scouring at the left abutment caused a frequency reduction of 0.21 Hz (-14%) from 1.53 Hz. Furthermore, 3.6 m of local scouring at the right abutment resulted in a 0.18 Hz (-14%) reduction from 1.32 Hz. Both of these local scour cases at the abutments represent approximately 4% of natural frequency shift for every metre of full-scale local scour at one of the abutments.

4.8.1.2 Global scour

As shown in Figure 4.19, 3.6 m of full-scale global scour represents a 40% change in natural frequency, which corresponds to a frequency sensitivity of approximately 11% per metre of global scour. There was only a small difference between the frequency sensitivities to global and local scour at all foundations. The overall change in natural frequency due to local scour at all foundations was 38%, whereas global scour of the same depth represents a 40% change. Therefore, some effect due to the additional confining pressure remained during local scour, but this only caused a 0.5% difference in frequency sensitivity per metre of full-scale scour depth.

4.8.2 Model 2: Pile bent foundation

The full-scale natural frequency variation of the pile bent foundation is shown in Figure 4.20. As expected, all of the natural frequency measurements at 60g fall between the fixed base upper bound and 1g lower bound for all scour levels. As explained in Section 4.7.3, the natural frequency estimate at no scour, 2.95 Hz, may have been affected by jamming of the modal hammer during the experiment, as shown in Figure 4.18.

4.8.2.1 Local scour

The initial 1.8 m of local scour caused the natural frequency at 60g to fall from 2.95 Hz to 2.22 Hz, which represents a 25% reduction in natural frequency. A further 1.8 m of scour resulted in a 22% change, which indicates that the frequency sensitivity to local scour has reduced slightly as the scour deepened.

The total 3.6 m of local scour gave a 41.4% frequency reduction. This reduction corresponds to an average frequency sensitivity of 11.5% per metre of full-scale local scour.

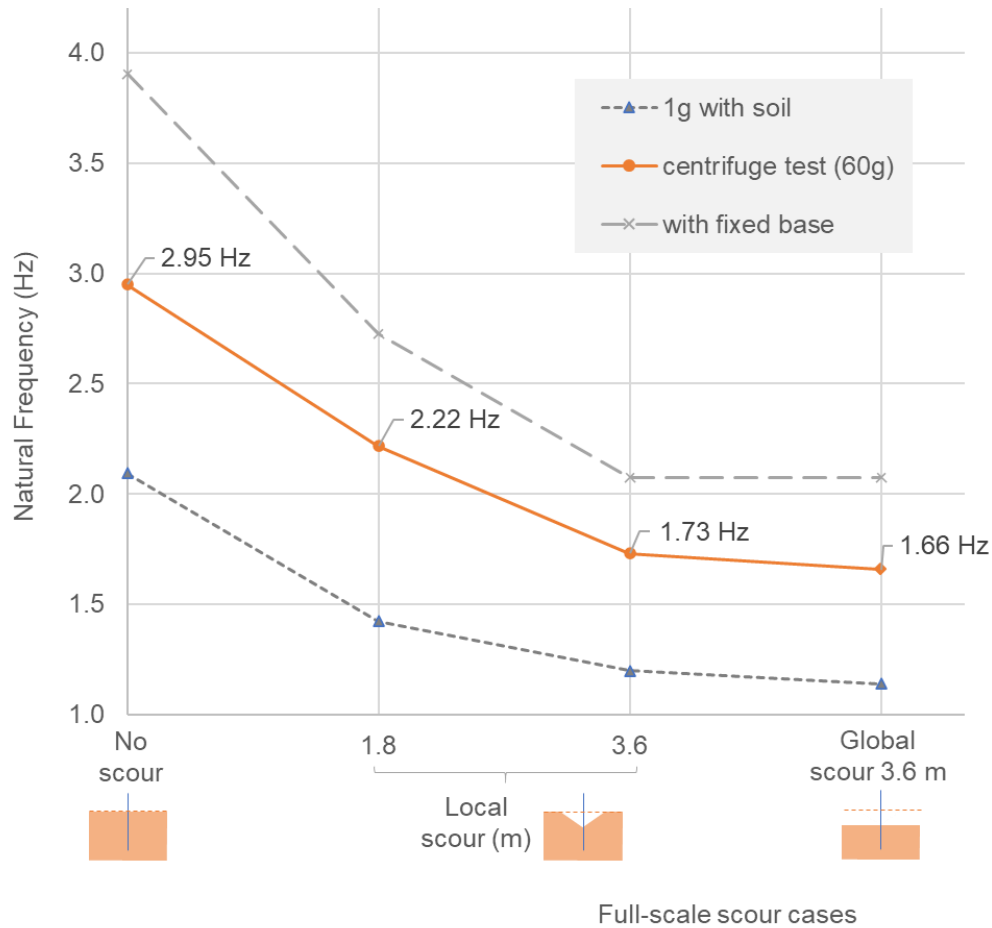


Figure 4.20 Estimated full-scale natural frequency variation of the pile bent foundation (Model 2) for different cases of scour

4.8.2.2 Global scour

The global scour of 3.6 m caused the natural frequency of the model to fall to 1.66 Hz, slightly lower than the representative local scour value of 1.73 Hz. However, the overall natural frequency sensitivities due to the local and global scour were not significantly different. The overall natural frequency sensitivity to global scour of 3.6 m was 43.7%, and due to local scour of 3.6 m was 41.4% – only a 0.6% sensitivity difference due to 1 m of scour.

4.8.3 Model 3: Shallow foundation

The variation of the natural frequency with scour depth of the shallow foundation is shown in Figure 4.21. These frequencies are in representative full-scale and were derived from the small-scale centrifuge (40g) and fixed based experiments. All of the natural frequency measurements from the centrifuge test (40g) lie below the fixed base upper bound line, as expected. The lower bound frequencies of the 1g tests were unable to derive from the observed spectra, as explained in Section 4.7.3.

4.8.3.1 Local scour

Centrifuge Model 3 was studied for an equivalent full-scale scour depth of 2 m in three equal steps. The overall 2 m of local scour depth caused the original natural frequency (2.44 Hz) to fall to 2.27 Hz – on average, a 3.5% frequency shift for every metre of full-scale scour depth. Similar to Model 2, the natural frequency sensitivity of Model 3 showed reduced sensitivity with deeper local scour depths. For example, the frequency changed by 4.7% and 2.3%, respectively, for the first and second metre of local scour depths. In the context of scour monitoring, this implies that the shallower scour depths are easier to capture with the natural frequency.

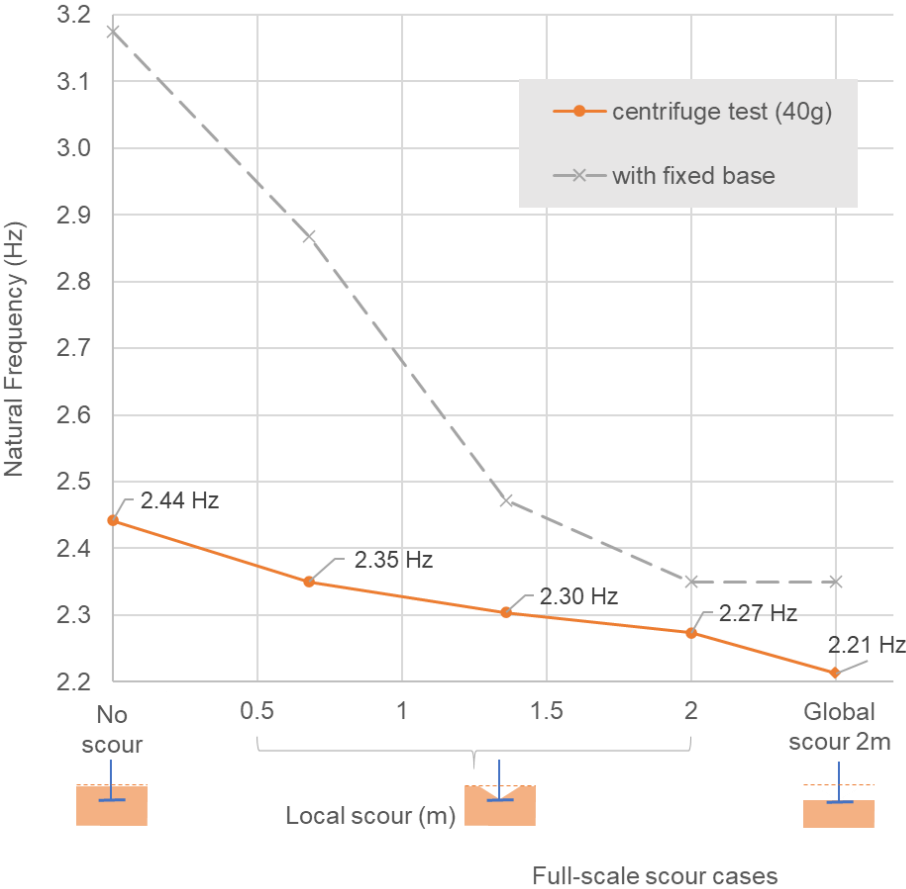


Figure 4.21 Estimated full-scale natural frequency variation of the shallow pad foundation (Model 3) for different cases of scour

4.8.3.2 Global scour

The natural frequency of Model 3 measured with equivalent full-scale global scour depth of 2 m (2.21 Hz) was slightly lower than the natural frequency measured with 2 m of local scour (2.27 Hz). The global scour generated an overall frequency shift of 9.4%, which equates to 4.7% per metre of equivalent full-scale scour depth. Therefore, global scour shows 1.2% higher frequency sensitivity than local scour for every 1 m of full-scale scour. This higher frequency sensitivity is to be expected, as unscoured soil, slightly distant from the foundation, still

provides a degree of increased pad foundation fixity, leading to higher stiffness and hence natural frequency for local scour relative to global scour.

4.8.4 Model 4: single pile foundation

Figure 4.22 shows the full-scale natural frequency variation of the single pile. As expected, all of the natural frequency measurements at 60g fall between the fixed-base upper bound and 1g lower bound for all scour levels.

4.8.4.1 Local scour

The full-scale local scour of 3.6 m around the single pile has caused the fundamental natural frequency to fall from 4.15 to 3.24 Hz. This represents a 22% change in natural frequency, equivalent to approximately 6.1% per metre of full-scale scour.

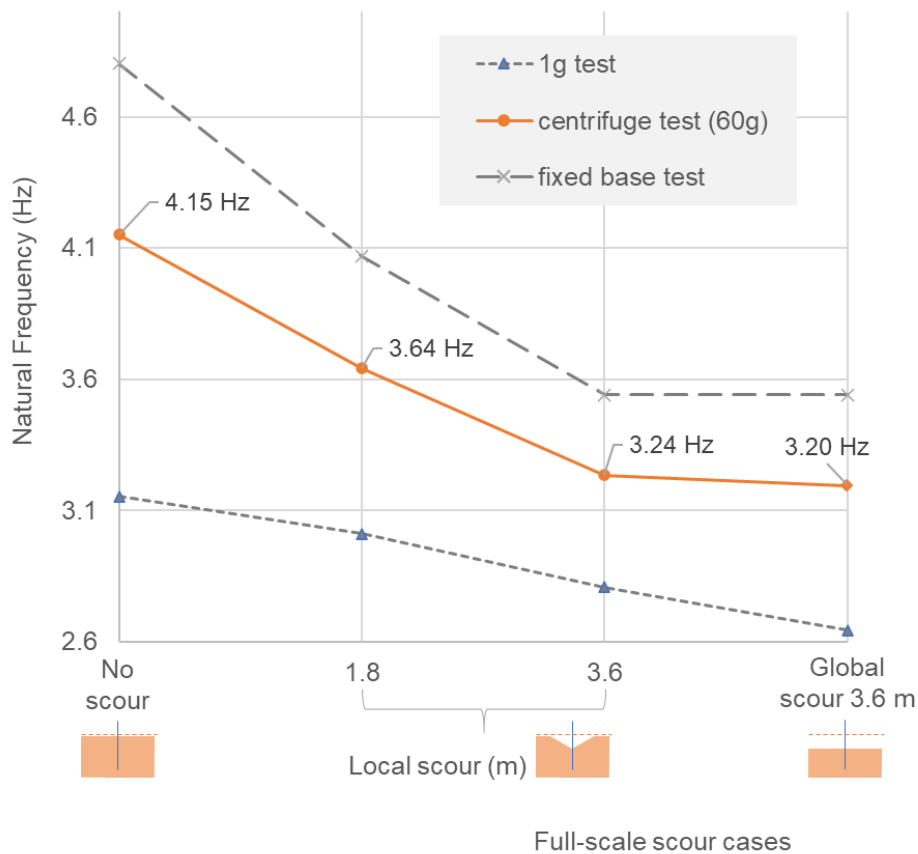


Figure 4.22 Estimated full-scale natural frequency variation of the single pile foundation (Model 4) for different cases of scour

4.8.4.2 Global scour

Global scour of 3.6 m at full-scale represents a natural frequency change of 23%, equivalent to approximately 6.4% per metre of scour. Global scour of 3.6 m caused the natural frequency to reduce slightly more (0.04 Hz) than the local scour of 3.6 m. However, the difference

between the global- and local-scour-induced frequency shifts was only 0.3% per metre of scour.

In all four centrifuge models, the fundamental natural frequencies always reduced with increasing scour. This is an essential behaviour for a reliable scour monitoring parameter. Average frequency sensitivities ranged from 3.5 – 11.5% per metre of local scour and 4.1-12.1% per metre of global scour depth. Therefore, natural frequency reduction was found to be a reliable and sensitive indicator of scour. See Section 4.11 for further interpretation of these results.

4.9 Spectral density sensitivity to scour

Another vibration parameter studied for possible sensitivity to scour is the spectral density at the modal peaks. As explained in Section 4.7, the modal analysis was carried out for the Models 1 and 4 with the output-only method, Fourier Domain Decomposition. Therefore, the spectral density considered for Models 1 and 4 was Singular Value of the power spectral density matrix of multiple accelerometers (SVPSD). The Power Spectral Density (PSD) was also considered in certain instances to study the spectral density of individual accelerometers.

The modal analysis was carried out for Models 2 and 3 with Frequency response function (FRF) method, and therefore the spectral density considered was the accelerance FRF. The SVPSD estimate was also compared with the FRF estimate.

All spectral densities presented in this section are equivalent full-scale values, estimated by dividing the experimental observations by the respective scaling factors. PSD and SVPSD have the units of (acceleration)²/frequency while accelerance FRF has units of acceleration/force. Therefore, based on Table 4.2, both PSD and SVPSD have a scaling factor of N, and accelerance FRF has a scaling factor of N³, reciprocals of which were applied to obtain the full-scale estimates from observed small-scale results.

4.9.1 Model 1: Integral bridge

The progression of first SVPSD value at modal peak with scour depth in the integral bridge is shown in Figure 4.23 in equivalent full-scale. All tests where the piezoelectric actuator was present showed a gradual increase of the SVPSD with scour depth. The global scour of 3.6 m caused the spectral density to change by a significant percentage of 254%, which equates to 70% per metre of scour. The local scour of the middle pier caused, on average, a 40% increase of the first SVPSD per 1 m of scour.

Similarly, all tests with only ambient vibration present also showed a gradual increase in the SVPSD with scour. The right abutment 3.6 m scour case alone caused the SVPSD to increase by 75%, which was a change of about 21% for every metre of abutment scour. The difference

in natural frequency between the local scour at all foundations, and global scour at all foundations was about 17% for every metre of scour depth.

Despite such high sensitivity to scour depth, the SVPSD also showed high sensitivity to the source of vibrations. For example, see the global scour case of 3.6 m in Figure 4.23. Here, the SVPSD observed from “ambient vibrations alone” and vibrations generated “with piezoelectric actuator” were different. This difference can be attributed to the additional excitation provided by the piezoelectric actuator or the additional 60g mass mistakenly added when replacing the mass during the ambient vibration tests (Section 4.5.5). The first two scour steps may also have been affected by the strong noise peak that was present at 100 Hz in small-scale (Section 4.7.3). If part of the noise peak has already been superpositioned to these values of the first two scour steps, the real spectral densities for these initial scour steps might be lower than what is estimated here; thus, the overall SVPSD sensitivities measured could increase even more than what is reported here.

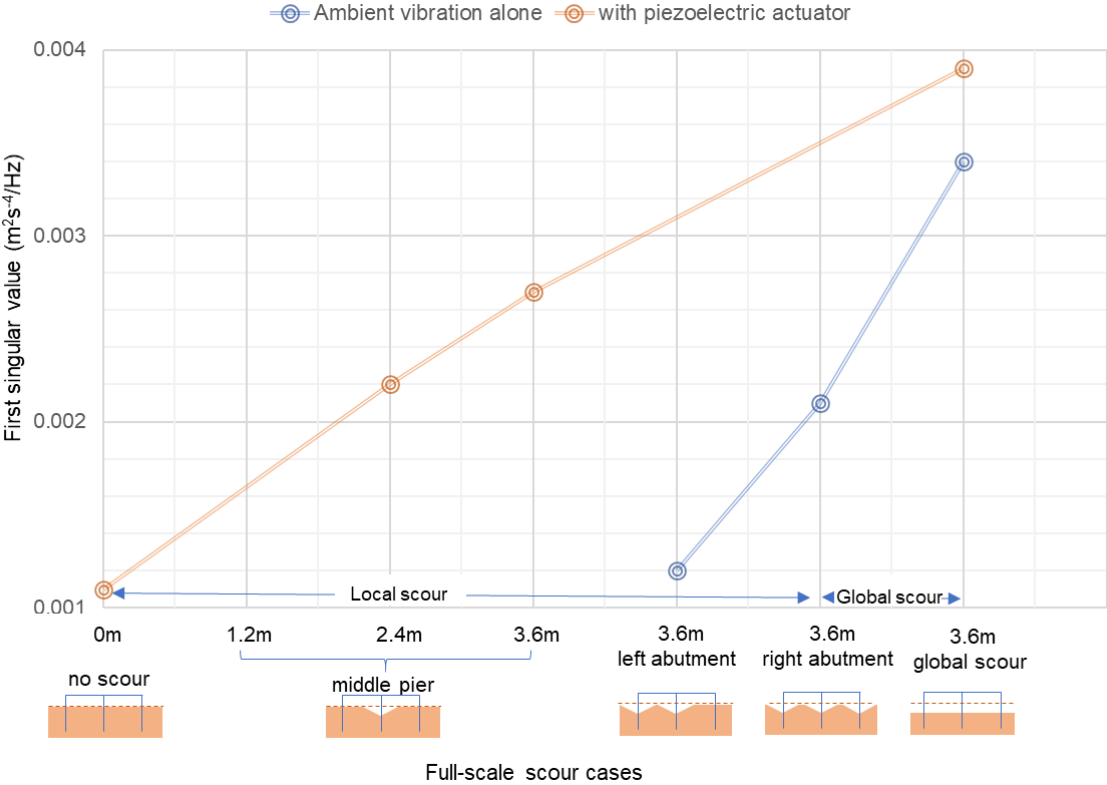


Figure 4.23 First singular values (SVPSD) at the modal peak vs different scour cases of Model 1 (integral bridge) in equivalent full-scale

4.9.2 Model 2: Pile bent foundation

The accelerance FRF magnitude variation with scour depth of Model 2 is shown in Figure 4.24. The FRF magnitudes here have been normalised by the maximum magnitude for each accelerometer channel. The scour step M2S3 (local scour of 3.6 m) was excluded since the input excitation required to compute FRF was unavailable, as discussed in Section 4.7.3.

There were also concerns about the no scour case (M2S1) since the FRF magnitudes may have been affected by jamming of the modal hammer, shown in Figure 4.18. As seen in Figure 4.24, this jamming may have been the reason that the M2S1 case has highly variable scattered FRF magnitudes as opposed to similar magnitudes shown in other cases.

Therefore, reliable FRF magnitudes were offered only at only two scour steps, i.e., 1.8 m local scour and 3.6 m global scour. Between these two scour cases, there was an overall increase of FRF amplitudes by about 90% per 1 m of scour for all accelerometers.

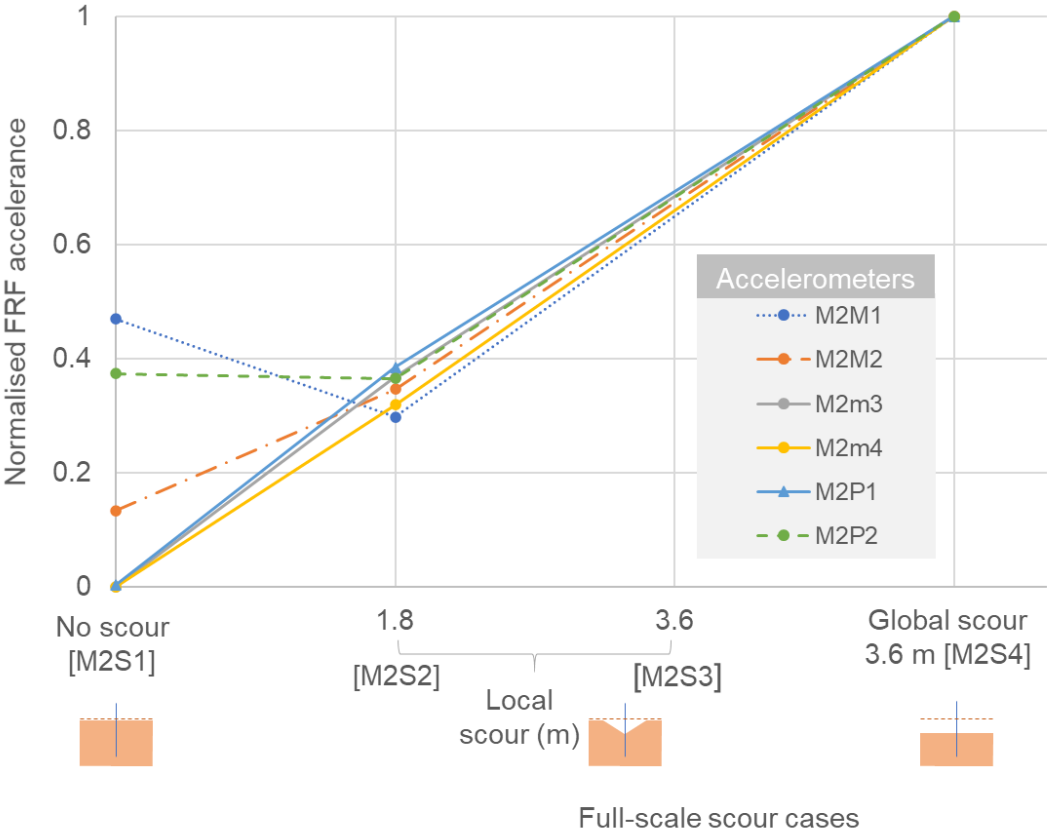


Figure 4.24 The variation of normalised acceleration FRF of Model 2 with scour at its foundation

As the load cell input was measured in one scour case, and some ambient vibration was noticed in the vibration response, output-only FDD was considered for all data cases, though the impulsive input was not entirely random as required for the FDD method. Figure 4.25 shows the spectra of the first SVPSD derived after performing FDD for Model 2 accelerometer data. A peak in the first SVPSD corresponds to a specific mode (fundamental mode in this case). The first peak SVPSD (y-axis value) at the fundamental mode increased with every advancing scour step, unlike the FRF estimate which did not provide reliable results and was limited by the measurement of the input excitation. The change in the first SVPSD was 9.4 dB for 3.6 m of local scour and 14.6 dB for global scour of 3.6 m. Corresponding extremely high sensitivities for scour were 214% for local, and 773% for global scour of 1 m (e.g. 14.6 dB equates to $10^{1.46}$).

= 28840% in SVPSD ratio; thus, the change per 3.6 m was 27840%, and change per 1 m was 773%).

The reduction of the natural frequency (x-axis value of the peaks) can also be seen in Figure 4.25 (frequency reduction already discussed in 4.8.2). Additionally, the peak width also reduced, suggesting a potential reduction in damping ratio with increased amounts of scour. Damping ratio can be estimated by using the half-power bandwidth of the FRF peaks. Damping ratio (ζ) is related to the natural frequency corresponding to the peak frequency (ω_n), half power width (ω_{width}), i.e. width of the FRF peak at the point there is half the power of the peak FRF power by the equation $\zeta = \omega_{width}/2\omega_n$ (He and Fu, 2001). Based on this relationship, the damping ratio of Model 2 was estimated, and it was found to have reduced from 2.44% in M2S2 scour step to 2.11% in M2S4 scour step.

The displacement amplitudes of vibration can be derived by using the spectral density estimates, similar to the method discussed in detail in Section 3.2.5. For example, M2S3 scour case has a full-scale singular value spectral density estimate of 0.65 dB (i.e. $10^{0.065} = 1.16 \text{ m}^2\text{s}^{-4}/\text{Hz}$). Hence the small-scale singular value spectral density is $69.7 \text{ m}^2\text{s}^{-4}/\text{Hz}$ based on the appropriate scale factor of 60 (i.e. 1.16×60 and scale factors for all spectral densities are introduced at the beginning of Section 4.9). The full-scale frequency at the modal peak is 1.73 Hz and hence the small-scale frequency the modal peak is 103.8 Hz (i.e. 1.73×60). The behaviour at the modal peak is governed by a single mode and hence the area surrounding the modal peak is equal to mean square acceleration of corresponding to the mode. As the same singular value estimate is present over the 1Hz band surrounding 103.8Hz, the mean square acceleration is equal to $69.7 \text{ m}^2\text{s}^{-4}/\text{Hz} \times 1\text{Hz} = 69.7 \text{ m}^2\text{s}^{-4}$. Hence the root mean square acceleration is 8.1 ms^{-2} (i.e. $69.7^{0.5}$) and the acceleration amplitude for the mode represented by a sine wave is 11.4 ms^{-2} (i.e. $8.1/0.71$, where 0.71 is the ratio between RMS acceleration and peak acceleration (OpenLearn, 2020)). The corresponding amplitude is $11.4/(2\pi \times 103.8)^2 = 27\mu\text{m}$. Hence the average amplitudes of vibration are minute and the amplitudes of vibration near the ground level could be even lower. Therefore, the soil-structure interaction can be assumed to have provided the small strain stiffnesses conditions as previously assumed.

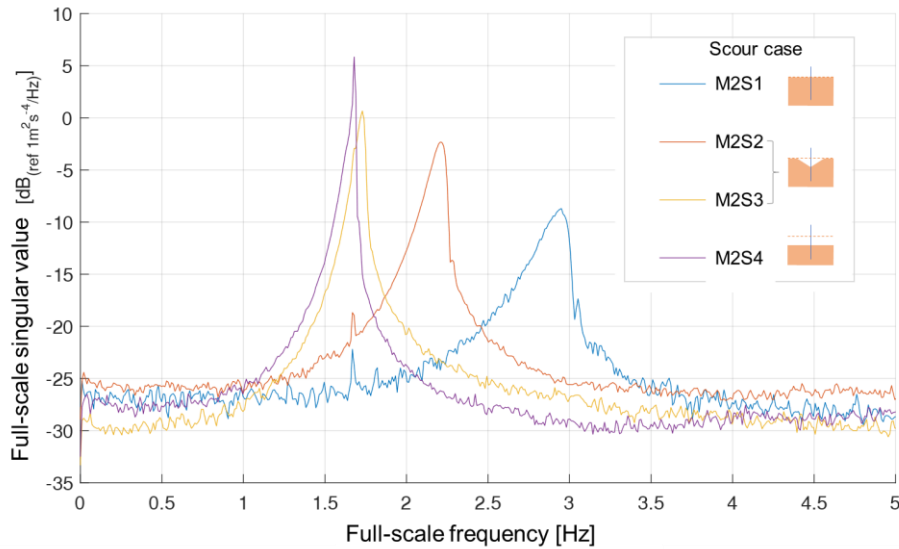


Figure 4.25 Model 2 first singular value (SVP) spectra for different scour cases.

4.9.3 Model 3: Shallow foundation

For Model 3, the magnitude of acceleration FRF at the modal peaks varied with scour, as shown in Figure 4.26. For comparison purposes, these acceleration magnitudes have been normalised by the maximum magnitude for each accelerometer. Figure 4.26 does not show channels where a peak in FRF magnitude was not noticed at the modal peak, i.e., M3m1, M3m2, and last two scour cases of M3M6. As shown in Figure 4.4, these three accelerometers were either on the pad footing or the oriented to measure vertical acceleration on the centrifuge structural models. Therefore, these accelerometers measured low signal to noise ratio since the input excitations were horizontal and near the top of the structural models. As previously explained in Section 4.7.3, the piezoelectric accelerometer (M3P1) had malfunctioned in the first two scour cases.

All other accelerometers in Figure 4.26 show a similar pattern of increasing sensitivity to scour with the first two local scour steps. The average change was between 21 – 44% per 1 m of local scour. However, the FRF magnitude reduced for both local and global scour cases having 2 m depth. It is not known what has caused this change of pattern after the second local scour step, but the loss of overlying soil on the pad foundation and resulting rocking or low signal to noise ratio of input excitation measurement may be suspected. The fact that the acceleration FRF did not change in a single direction but changed both in an increasing and decreasing pattern with increasing depths of scour, imply that FRF, in this case, was not a reliable indicator of scour.

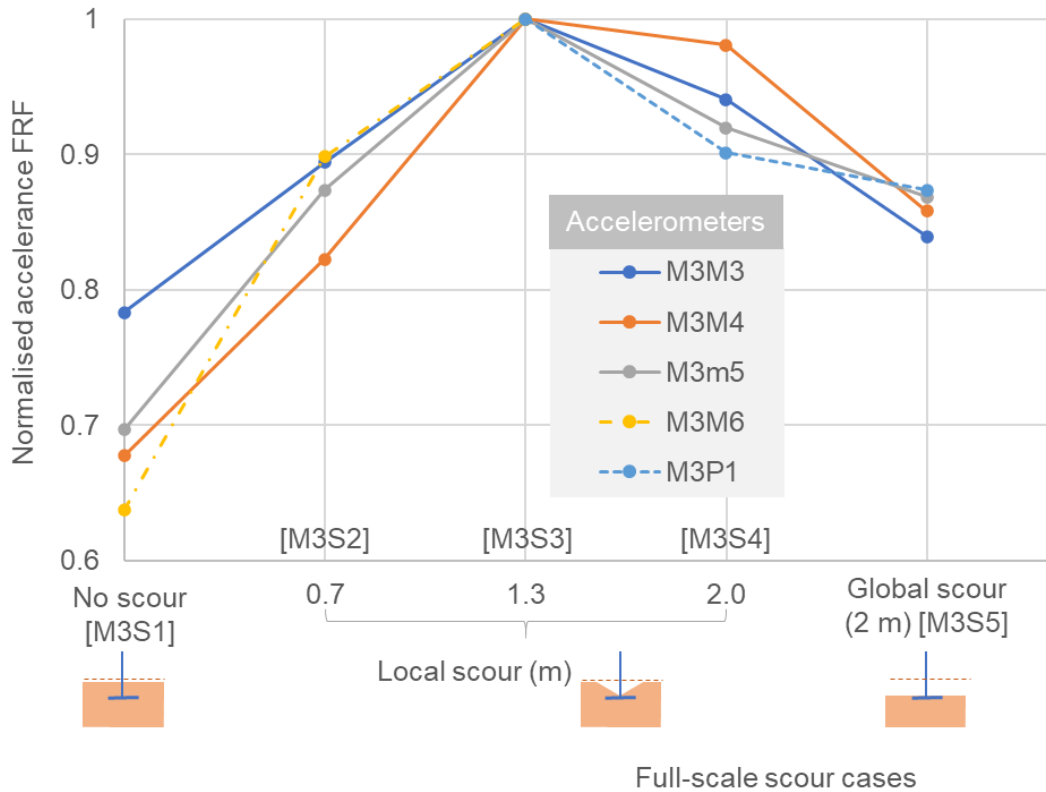


Figure 4.26 Model 3: Variation of FRF acceleration magnitude with scour depth (FRF normalised on maximum resulting from local scour at 1.3 m depth)

As Model 2 showed the SVPSD to be a reliable indicator of scour, although FRF did not, SVPSD was also studied for Model 3. The first SVPSD spectra for different depths of scour is shown in Figure 4.27. The SVPSD at the peaks increased significantly with each advancing scour step. With an overall scour depth of 2 m, there was a 9.7dB increase in the local scour case, and a 14dB increase in the global scour case. Corresponding average changes per 1 m of scour were 417% for local, and 1205% for global scour (e.g. 9.7dB equates to $10^{0.97} = 933\%$ in SVPSD ratios; thus, the change per 2 m was 833%, and change per 1 m was 417%). As was the case with the results for the pile bent (Model 2), the results for this shallow pad foundation gave extremely high scour sensitivities and a large difference in sensitivities between the global and local scour cases, and more importantly an increase of modal SVPSD with every advancing scour step. Therefore, SVPSD seems to be a more reliable indicator than FRF for both Model 2 and 3.

The reduction of the natural frequency (x-axis value of the peaks) can also be seen in Figure 4.27 (frequency reduction already discussed in Section 4.8.3). Based on the half-power bandwidth of the FRF peaks, the damping ratio during the scour steps M3S1, M3S2, M3S3, M3S4 and M3S5 at small-scale were 1.05%, 0.98%, 0.94%, 0.89% and 0.96%, respectively. Thus, the damping ratio has not consistently reduced in every advancing scour step.

The displacement amplitudes of vibration can be derived by using the spectral density estimates as discussed in detail in Section 3.2.5. For example, M3S5 scour case has a full-scale singular value estimate of -1.98 dB (i.e. $10^{-0.198} = 0.63 \text{ m}^2\text{s}^{-4}/\text{Hz}$). Hence the small-scale singular value is $0.63 \times 40 = 25.2 \text{ m}^2\text{s}^{-4}/\text{Hz}$, as the scale factor for Model 3 is 40. The full-scale frequency at the modal peak is 2.21 Hz and the corresponding small-scale frequency is 88.4 Hz (i.e. 2.21×40). The behaviour at the modal peak is governed by a single mode and hence the area surrounding the modal peak is equal to mean square acceleration of corresponding to the mode. As the same singular value estimate is present over the 1Hz band surrounding 88.4 Hz, the mean square acceleration is equal to $25.2 \text{ m}^2\text{s}^{-4}/\text{Hz} \times 1\text{Hz} = 25.2 \text{ m}^2\text{s}^{-4}$. Hence the root mean square acceleration is 5.01 ms^{-2} and the representative peak acceleration amplitude is 7.1 ms^{-2} (i.e. $5.01/0.71$, where 0.71 is the ratio between RMS acceleration and peak acceleration (OpenLearn, 2020)). The corresponding displacement amplitude is $7.1/(2\pi \times 88.4)^2 = 23 \text{ }\mu\text{m}$. Hence the average amplitudes of vibration measured on Model 3 were minute (similar to Model 2) and the amplitudes of vibration near the ground level could be even lower. Therefore, the soil-structure interaction can be assumed to have provided the small strain stiffnesses conditions as previously assumed.

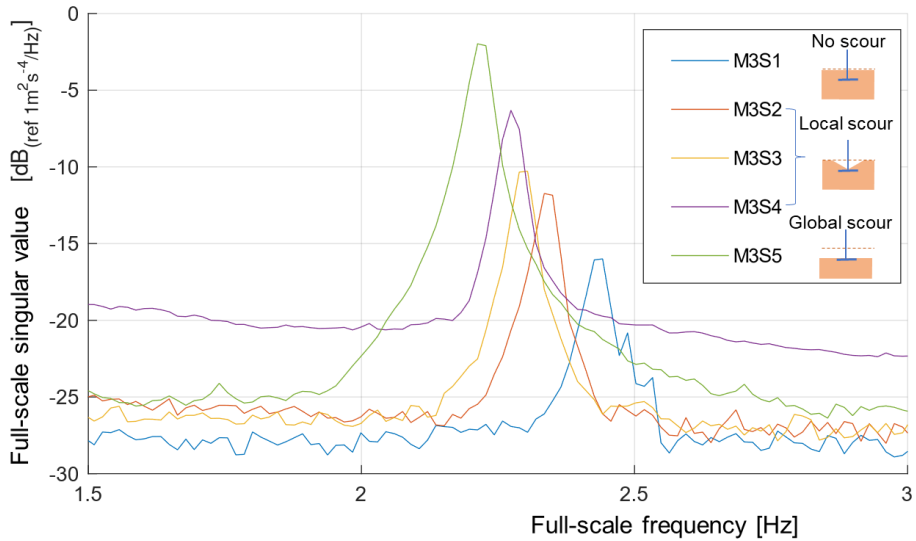


Figure 4.27 Model 3: the first SVPSD of representative full-scale shallow foundation

4.9.4 Model 4: Single pile foundation

Figure 4.28 shows the variation of the modal spectral density when the single pile foundation was subjected to local and global scour. Two spectral density types were considered: Power Spectral Density (PSD) to show the behaviour of individual locations and first SVPSD to show the overall behaviour. These spectral density values were normalised such that the highest spectral density measured for each spectral density estimate has unity.

The normalised PSD level of all the accelerometers increased significantly with increasing depths of local scour. Additionally, the PSD sensitivity to scour shows a gradual increase from the top to the bottom level of accelerometers, i.e., average sensitivity per 1 m of scour was 18% for M4P1, 20% for M4m3, 56% for M4M2 and 120% for M4M1, in the descending order of their heights. The difference in PSD between local and global scour accounts was small (1 – 3% per 1 m) than the significant change observed (18 – 120%) for local scour.

The normalised SVPSD at the modal peaks was also plotted in Figure 4.28. The normalised SVPSD shows a local scour sensitivity of 44% per 1 m, which was equal to the average of all the normalised PSD magnitudes of the accelerometers. The SVPSD sensitivity to 1 m global scour was 46%, i.e. only 2% higher than the SVPSD sensitivity to local scour.

The input force of the piezoelectric actuator was also studied to examine whether the observed increase in output (accelerometer) modal spectral densities was related to an increase of input modal content. As shown in Figure 4.28, the PSD of the load cell input force at the modal peaks show an initial increase from scour step M4S1 to M4S2, and then a gradual decrease from scour step M4S2 to M4S4. Despite this decrease of PSD, the accelerometer spectral densities have increased significantly after the second scour step, M4S2. Therefore, the spectral density increase of the output accelerometer was not related to a change in input force given by the piezoelectric actuator, and hence this change can be fully attributed to scour. Note that the input force imposed by the ambient vibration of the wind in the centrifuge was also present however this can be assumed to be the same strength during testing since all tests were conducted at the same rotational speed of the centrifuge beam.

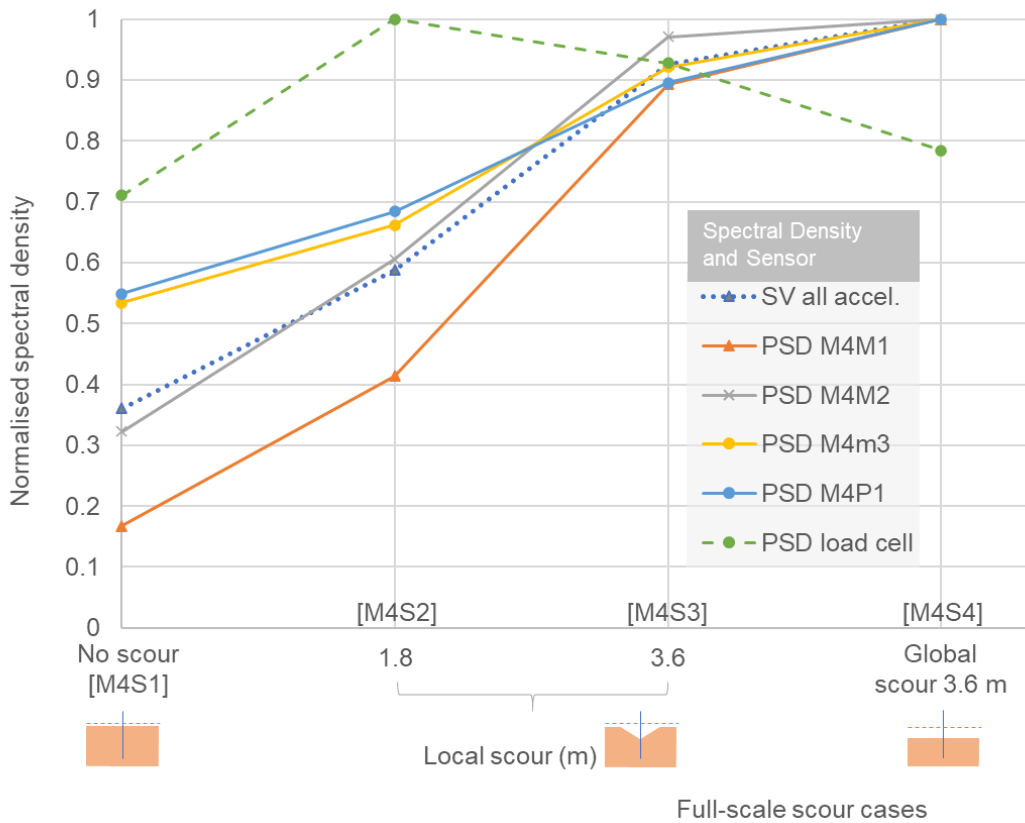


Figure 4.28 Model 4: Relationship between normalised spectral density at first modal peak and full-scale scour

4.10 Mode shape sensitivity to scour

The mode shapes were studied since Baildon Bridge showed potential for mode shapes to indicate the presence of scour and locate where the scour has occurred due to the spatial information that can be observed from a mode shape. Therefore, the changes of mode shape observed in this centrifuge experiment for four models were studied to explore its relation to scour. All mode shapes were normalised with respect to the modal amplitude derived at the top accelerometer, except in Model 3 in which the top accelerometer did not function and thus a lower level accelerometer had to be used for the normalisation. Note that all the mode shapes (e.g. Figure 4.29), in the followings sections are shown in solid lines with lighter colours indicating deeper/more extensive scour cases and the corresponding stationary position of the bridge shown dashed. These mode shapes show the longitudinal elevation view.

4.10.1 Model 1: integral bridge

The change of mode shape of Model 1 for progressively increasing amounts of scour is shown in Figure 4.29(a – c). The MEMS ADXL78 accelerometers (shown as “m” previously in Figure 4.4) were omitted when calculating these mode shapes due to their low signal to noise ratio.

A key hypothesis that needs investigation was whether local scour at a bridge foundation causes mode shape amplitude to increase only at that foundation, thus able to allow scour

localisation, as was observed during the field trial at Baildon Bridge. As there were three foundations in Centrifuge Model 1, any local scour case would have one foundation undergoing scour while the two other foundations not undergoing any scour. Thus, if this hypothesis were to be true for Model 1, the following three requirements have to be true: locally scouring foundation should increase in amplitude, while the other first and the second foundations not undergoing any scour should not change in mode shape. Table 4.6 shows the analysis of these three requirements of the hypothesis for the four different local scour cases, illustrated in Figure 4.29(a – b). The hypothesis was accurate in eight out of the twelve different combinations of local scour cases and requirements (“Yes” in Table 4.6), which shows that it has some accuracy. The four outliers (“No” in Table 4.6) may be partly due to measurement inaccuracies.

Table 4.6 Analysis of the hypothesis: a foundation undergoing local scour can be located using changes of mode shape (Model 1)

Local scour case	The requirement for the hypothesis		
	Increase in mode shape amplitudes at the foundation undergoing scour	No change in mode shape at the first foundation not undergoing scour	No change in mode shape at the second foundation not undergoing scour
M1S1 – M1S3	Yes	Yes	No
M1M3 – M1S4	Yes	Yes	No
M1S4 – M1S5	No	Yes	Yes
M1S5 – M1S6	Yes	Yes	No

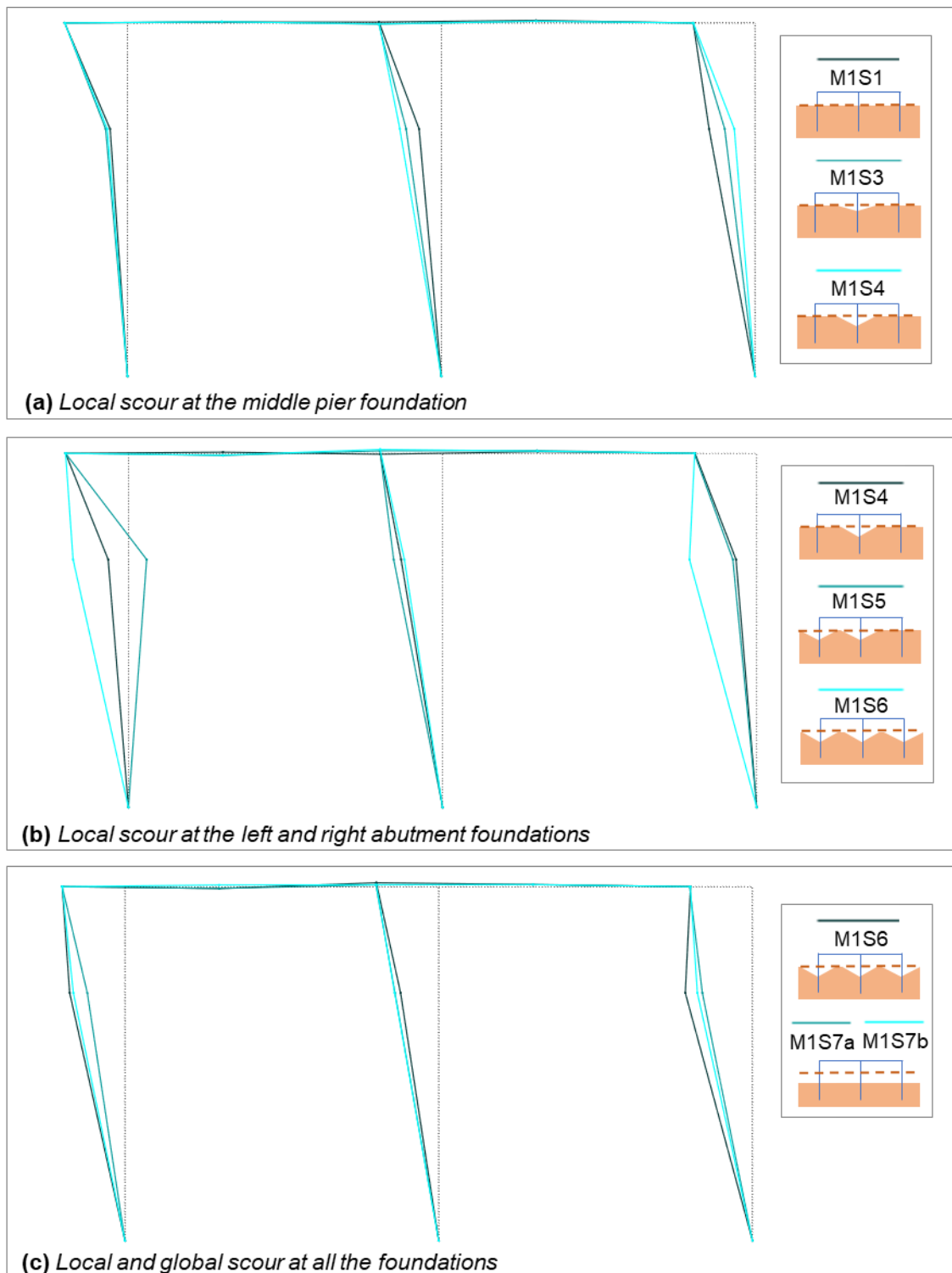


Figure 4.29 Model 1: integral bridge normalised mode shapes.

Mode shape variation for local scour at all foundations and global scour with different excitation sources (scour cases M1S6, M1S7a and M1S7b) is shown in Figure 4.29(c). Moving from local scour at all foundations (M1S6) to global scour case (M1S7a) has slightly reduced the modal amplitudes at the bridge abutments, in contrast to the expectation that global scour causes more flexibility of the bridge substructure. Moving from the case where excitation was due to ambient vibration (M1S7a) to the case where a piezoelectric actuator (M1S7b) excited the bridge model, even with no change of scour, there was a small increase of the modal

amplitudes at all foundations. Therefore, the modal amplitudes have shown some sensitivity to the source of excitation.

Such a high degree of variation in mode shape and the detection of several outliers may be attributable to the low signal to noise ratio observed in the MEMS accelerometers. For example, Figure 4.30 shows how PSD spectra of a piezoelectric accelerometer (M1P1), a MEMS ADXL1002 accelerometer (M1M2) and a MEMS ADSX78 accelerometer (M1m3) vary in three different scour steps. In all the PSD spectra, there was a strong noise peak at 1.67 Hz (100 Hz in small-scale), as previously discussed in Section 4.7.3. The other strong set of peaks, highlighted in a green band in Figure 4.30, represents the fundamental natural frequency. The PSD value at these fundamental natural frequency peaks represent the power of the signal measuring the fundamental mode, and the surrounding plateau represents the sensor noise level that hides that signal. The signal to noise ratios of this fundamental mode was high in piezoelectric accelerometer (M1P1), but low in MEMS accelerometers (M1M2 and M1m3). MEMS accelerometers were present at the mid-height of the foundations, where outliers were observed. Therefore, the cause of these outliers and a high degree of error could be the low signal to noise measured at these locations.

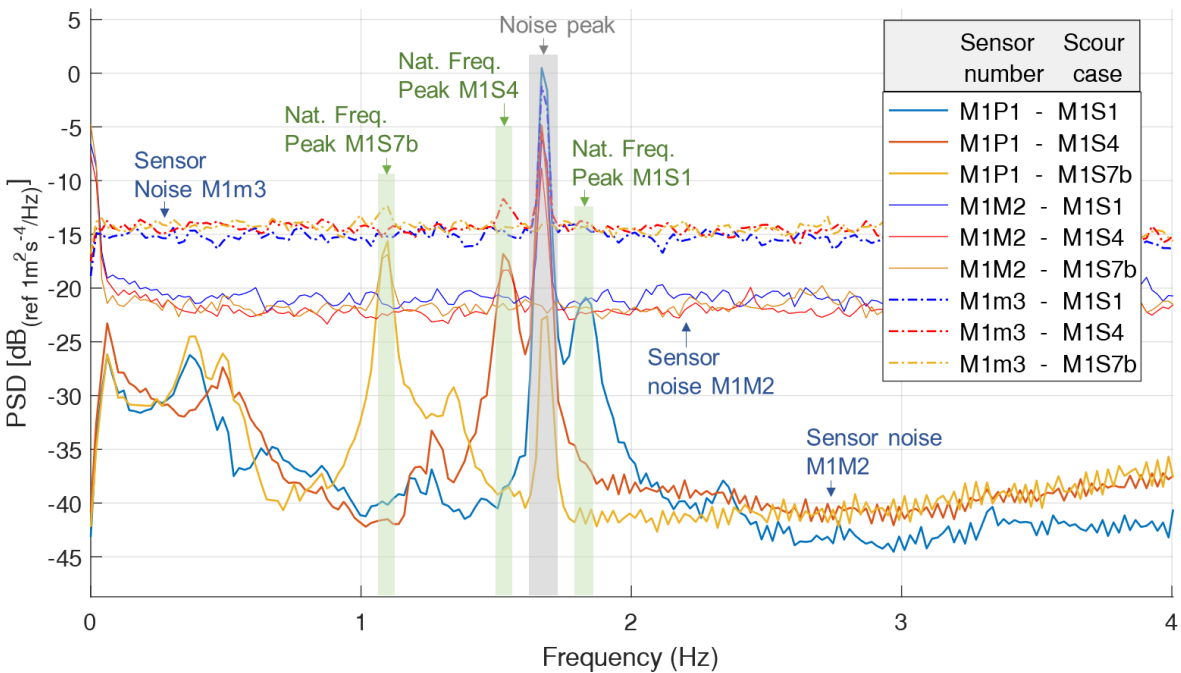


Figure 4.30 Model 1: integral bridge: Power Spectral Density (PSD) of three different sensor types with three different scour cases

4.10.2 Model 2: pile bent foundation

The modes shapes identified for different scour cases of the pile bent are shown in Figure 4.31. Mode shapes along one out of the four piles are shown in solid lines, and another adjacent pile is shown with an “x” mark. As explained in 4.9.2, the scour cases 1 and 3 do not

represent reliable FRF. Their mode shapes, which are shown in Figure 4.31(a), also did not show the expected fundamental sway mode shape.

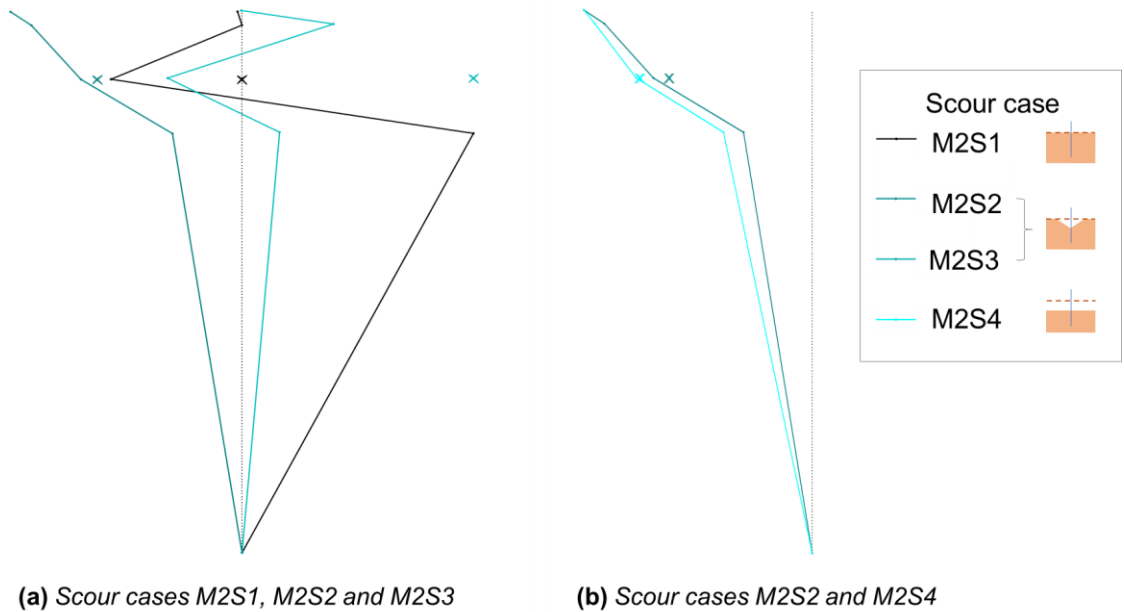


Figure 4.31 Model 2: pile bent mode shape variation with different scour cases.

Figure 4.31(b) shows the mode shapes of two reliable tests. Both these modes show a sway mode shape with increasing modal amplitude with height and similar modal amplitude (“x” mark) at the adjacent piles. Additionally, with increased scour, all normalised modal amplitudes below the top level have increased. This is expected since the removal of soil around the pile allows free lateral movement for the pile section (near the bottom sensors) that was previously partially restrained by soil.

4.10.3 Model 3: shallow foundation

The mode shape variation of the shallow foundation model for local and global scour cases is shown in Figure 4.32. The first two scour cases resulted in almost zero modal amplitude at the top accelerometer, which malfunctioned during these tests, as explained in Section 4.7.3. All mode shapes in Figure 4.32 were, therefore normalised by the modal amplitude of the mid-height accelerometer (M3M4).

The fundamental sway mode shape remained the same throughout all scour processes with little change when the malfunctioned accelerometer at the top was ignored. The normalised modal amplitudes near the top-mid height of the column have shown an overall pattern of initial reduction with the local scour, and an increase of modal amplitudes with the global scour. This suggests a change in modal amplitudes was not a reliable indicator of scour for this shallow foundation.

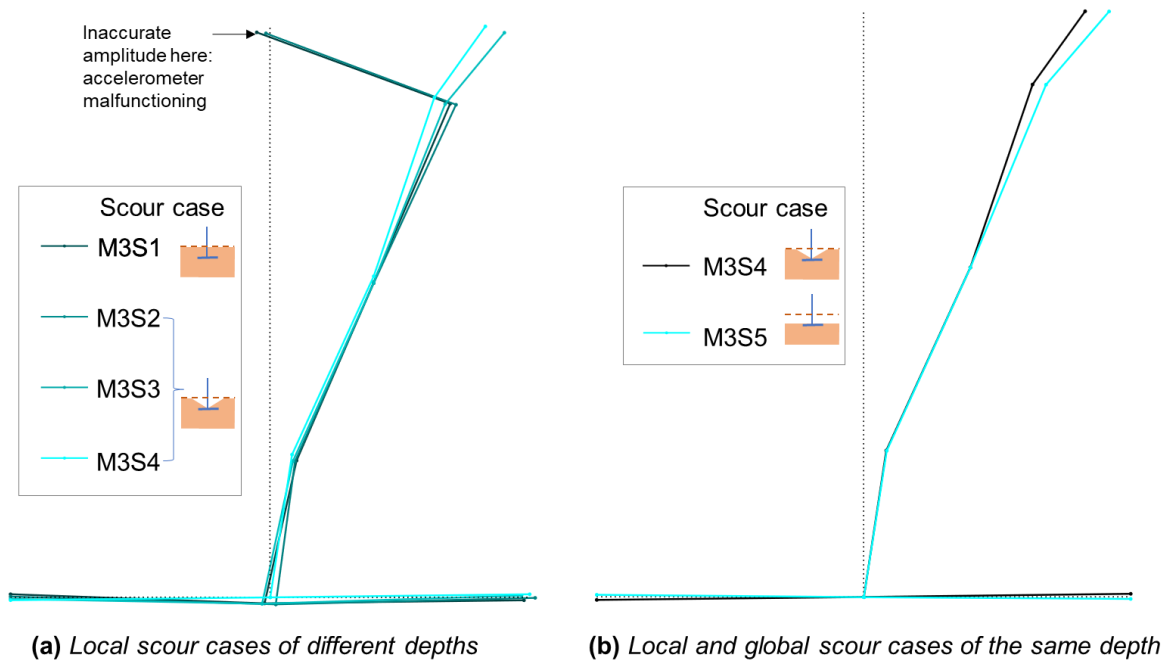


Figure 4.32 Model 3: shallow foundation, the variation of mode shape with local and global scour cases

4.10.4 Model 4: Single pile foundation

The mode shape variation for different scour cases of Model 4 is shown in Figure 4.33. Local scour resulted in a clear increase of modal amplitudes of the pile, especially near the original ground level. However, the modal amplitudes at that level did not differ between the local and the global scour cases of the same depth (M4S3 and M4S4). Therefore, the increase of modal amplitude may primarily be due to the removing (freeing) of the soil stiffness near-ground as the case with local scour, rather than due to a reduction of the stiffness of soil directly underneath that occurs as a result of global scour.

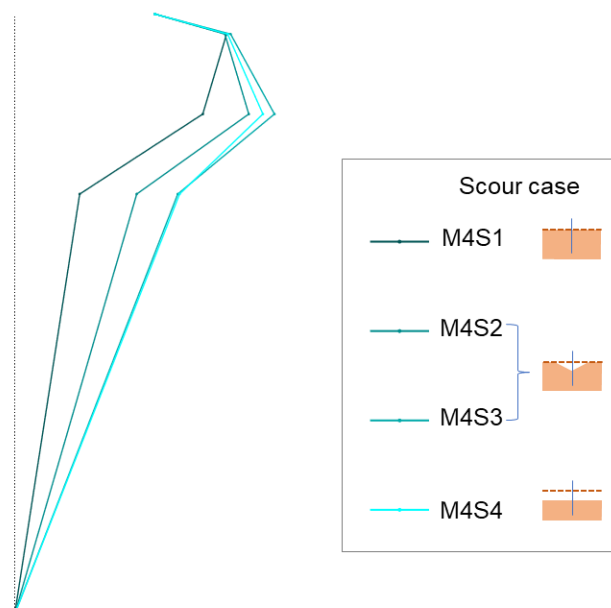


Figure 4.33 Model 4: single pile foundation, the normalised mode shapes under different scour cases

4.11 Overall scour monitoring potential of natural frequencies, modal spectral densities and mode shapes

If a vibration-based parameter were to be a reliable and simple scour indicator, scour should cause it to either increase or decrease in only one direction with sufficient sensitivity. When a potential monitoring parameter shows both increasing and decreasing behaviour with increasing depths of scour, it will be difficult to relate a measured change of the parameter to a change in scour depth. Further, when the sensitivity of the monitoring parameter is low, a change in the parameter due to scour could become insignificant in comparison to the change of the parameter due to the environmental and operational variabilities.

On this basis, the results of this experiment identified the most reliable indicators of scour as natural frequency and modal spectral density (only output-only estimates such as PSD and SVPSD). The FRF estimate showed an oscillating pattern with increasing scour in certain instances and therefore was not reliable. The mode shape showed some potential, especially to locate a locally scouring foundation, but several outliers were also detected.

All foundation types exhibited a measurable change in natural frequency due to scour. A summary of the measured natural frequency sensitivities is shown in Figure 4.34. The natural frequency reduction for global scour was greater than that for local scour. This finding indicates that some additional confining pressure may be provided to the underlying soil by the overlying unscoured soil surrounding a local scour hole.

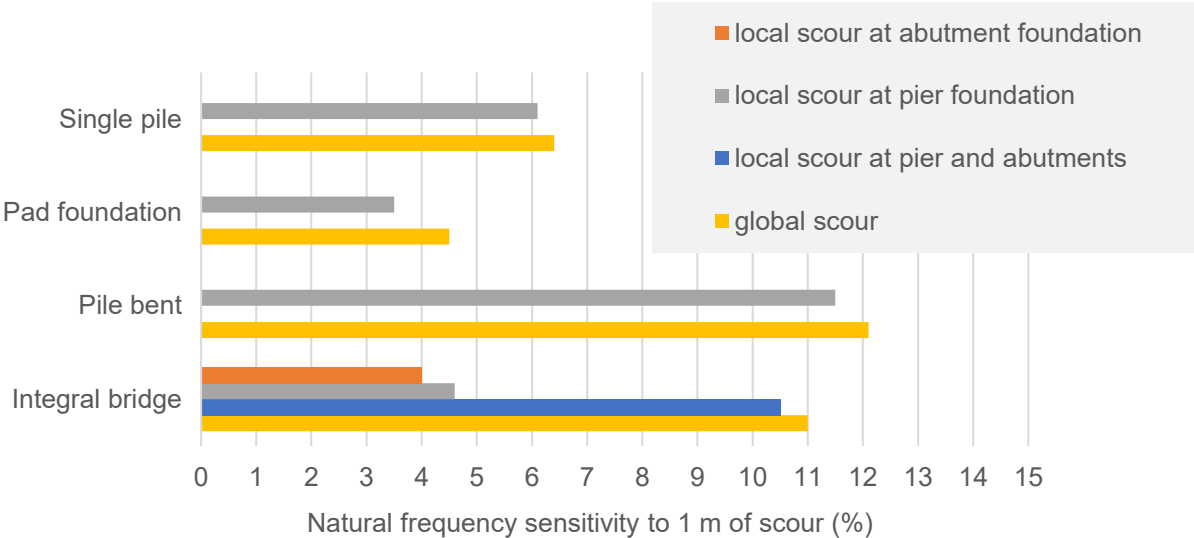


Figure 4.34 Summary of frequency sensitivities at the full-scale

As shown in Figure 4.34, local scour at either the bridge pier or the abutment of the integral bridge model showed a 4 – 5% frequency shift per metre of scour, while the pile bent model showed a 12% frequency shift. The single pile showed a 6% frequency shift, and the shallow

pad foundation showed only a 3.5% frequency shift per metre of local scour. Additionally, the results suggest that the frequency sensitivity to local scour reduces slightly with scour depth.

The depth of embedment of the deep piled foundations of Models 1, 2 and 4 was 12 m in equivalent full-scale, but the depth of embedment was only 3 m for the Model 3 shallow foundation. Therefore, the maximum scour depth for deep foundations (3.6 m) in the Models 1, 2 and 4 was nearly a one-third loss of embedment, for which natural frequency reduced by 14 – 44%. In comparison, the maximum scour depth tested for the shallow foundation (2 m) was a two-third loss of embedment, but the overall change was only 7 – 9%. Despite having a larger fraction of embedment lost, the shallow foundation scour showed some of the lowest natural frequency sensitivities. Therefore, a natural frequency-based scour monitoring technique may be most feasible for deep piled foundations, rather than for a shallow pad foundation.

The natural frequency errors expected due to environmental and operational variabilities found in the literature vary in the order of 3.5%, as explained in Chapter 2 and it can be as high as 14% as found during the field trial at Baildon Bridge. Therefore, the minimum scour depth measurement resolution possible are in metre scale. This reinforces the view that using the natural frequency as a measure of scour depth is mostly suitable for deep piled foundations where countermeasures may only be required when the scour depth is several metres.

A summary of modal peak SVPSD variation with scour is illustrated in Figure 4.35. The sensitivities of SVPSD for local scour of 1 m were near 40% for both the integral bridge and the single pile and significantly higher for others, i.e. 214% for pile bent and 417% for the shallow pad foundation. The SVPSD showed 2% higher sensitivity in global scour than in local scour for single pile, but 30% higher sensitivity in global scour than in local scour for the integral bridge. For the pile bent and pad foundation, global scour of 1 m caused the SVPSD to increase by 773% and 1205% respectively. The pad foundation showed the highest SVPSD sensitivity, though it was the structure with the lowest natural frequency sensitivity.

All the sensitivities observed for these spectral density estimates were much higher than the sensitivities of natural frequency. However, the environmental variabilities of spectral density estimates can also be high compared to the variabilities expected for natural frequency. For example, when the actuator (0.44 kg) in Model 1 was replaced with the actuator mass of 0.5 kg and ambient excitations in the centrifuge, the natural frequency did not change but the SVPSD changed by 13% due to its sensitivity to either the change in mass or the input excitation. Furthermore, Baildon Bridge instrumentation found 25% error of measurement of the PSD value measured within a one-hour period, when insignificant changes in environmental parameters can be expected. With such an error of measurement, SVPSD could potentially allow measurement of sub-metre scale scour depth changes.

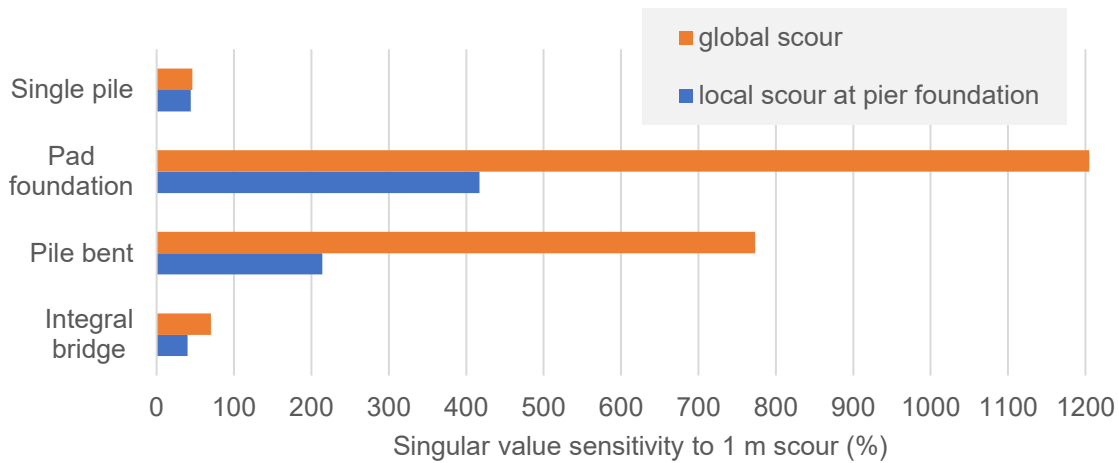


Figure 4.35 Sensitivity of SVPSD at the modal peak to scour

The errors related to the load cell led to limited FRF available in Model 2, for which the FRF magnitude increased for all sensor channels. The FRF magnitudes of Model 3 showed an initial increase and a later decrease, suggesting little potential to be a reliable indicator of scour. The reason for the unreliable nature of FRF may be the low signal to noise ratio of the measured input excitation. In a real bridge, similar low signal to noise ratio could be expected unless forced vibration is used with a large excitation source. Due to the multiple types of ambient excitation sources present in a real bridge, it would be difficult to capture ambient excitations with enough accuracy. Therefore, an output-only method where only the output acceleration measurements are considered is more practical. In addition to the practicality of output-only spectral density, the findings of this experiment suggest that it is a reliable and highly sensitive vibration-based approach to detect scour.

The normalised mode shape variation due to local scour primarily affected the closest part of the bridge element to the scouring soil. There was no significant change in mode shape between local and global scour of the same depth. In the single pile and pile bent models, the part of the piles closest to the ground level had the greatest change due to scour. In the integral bridge model, local scour near one foundation showed the primary increase of modal amplitude in that foundation, though several outliers were detected in this model. This local increase of modal amplitude may primarily be due to the freeing of the near-ground-level pile section, which was partially restrained by the soil surrounding the pile before local scour was introduced into the model.

It is noteworthy that the experimental results observed for the Models 2 – 4, all of which have standalone foundations, were not directly representative of the full-scale bridges with added stiffness and mass from bridge decks, bearings in addition to the foundation. This aspect will be investigated numerically in the next chapter.

4.12 Small-strain shear modulus of soil

The small-strain shear modulus of soil is an essential parameter for numerical modelling of the full-scale structures. It was estimated using the shear wave velocities captured during the experiment. A comparison of these shear modulus profiles against empirical estimates is presented in this section in representative full-scale. The numerical models in the next chapter will be developed based on these shear modulus profiles.

4.12.1 Derivation of small-strain shear modulus from the observed shear waves

As explained in Section 4.5.2.3 and illustrated in Figure 4.4, the shear waves generated by the two air hammers travel vertically through the soil passing the accelerometers C01 – C15 adjacent to the structural model foundations. Figure 4.36 shows such a shear wave captured by a column of accelerometers C11 – C15 (Figure 4.4(b)), which were embedded in the soil adjacent to the Model 2. The air hammer and the accelerometer arrangement are shown on the left side of Figure 4.36 for comparison with the measured acceleration time-history of each accelerometer shown on the right side. A shear wave causes oscillations of soil transverse to the direction of propagation. Therefore, the accelerometers pointing in the horizontal direction capture these shear waves travelling vertically as a short-term oscillation in the observed acceleration when the shear wave passes the accelerometers. In Figure 4.36, such an oscillation was first seen in C11 (lowest accelerometer) and last seen in C15 (topmost accelerometer).

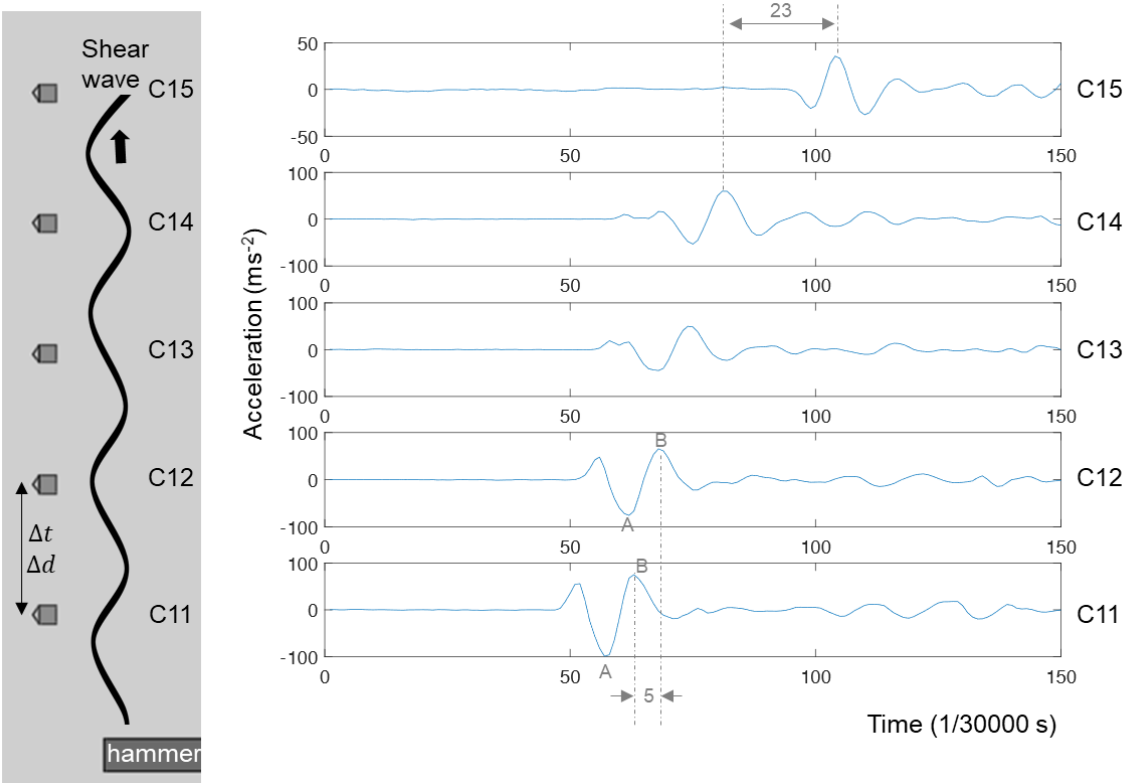


Figure 4.36 A shear wave captured by a column of accelerometers, C11 – C15.

The shear wave velocity (v_s) between two adjacent accelerometers is given as follows

$$v_s = \frac{\Delta d}{\Delta t} \quad \text{Equation 4.4}$$

where Δd and Δt are the vertical spacing of accelerometers and time lag in shear wave arrival.

The small-strain shear modulus (G_0) is related to the bulk density (ρ) and the shear wave velocity (v_s) as given in Cha et al. (2014):

$$G_0 = \rho v_s^2 \quad \text{Equation 4.5}$$

The example in Figure 4.36 has a time lag of 5/30000 s for the bottommost accelerometers and 23/30000 s for the topmost accelerometers. This suggests v_s , and hence G_0 , increases with depth, which is the behaviour expected for a typical soil profile.

It is worth noting that there was a significant error of the v_s and G_0 values estimated from the experimental data due to insufficient sampling frequency. The sampling frequency was 30,000 Hz for the accelerometers. Therefore, the time measurements had a resolution of 1/30000 s. In the above example, the time lag (Δt) was estimated with only five such time resolution points between the two bottommost accelerometers (e.g. between the peaks “B – B” or valleys “A – A” in Figure 4.36). Another method, the cross-correlation method used in Dong (2016), also provided the same Δt estimates for these accelerometers. As there can be a maximum error equal to the measurement resolution, the maximum error in both Δt and v_s was about $\pm 20\%$ (1/5) and thus the maximum error in G_0 becomes $\pm 44\%$, according to Equations 4.4 and 4.5. In comparison, the topmost accelerometers had 23 data points for the time lag suggesting a $\pm 4\%$ error for Δt and $\pm 9\%$ error for G_0 estimates. Therefore, there was a significant error in the G_0 estimates, especially at the bottom levels. For future experiments, it is recommended to use sampling rates higher than 30kHz to reduce this measurement error.

Both the velocity and density have a scaling factor of 1 and hence, the G_0 estimates in the full-scale is the same as the G_0 estimates in the small-scale (Dong, 2016). The shear modulus estimate between two accelerometers was represented at their mid-depth.

These derived full-scale G_0 values from the centrifuge test were compared against two published empirical estimates to verify their reliability. Firstly, Hardin and Drnevich (1972) estimate G_0 (in kPa) for sands as the following:

$$G_0 = 3230 \frac{(2.973 - e)^2}{(1 + e)} \sigma_0'^{0.5} \quad \text{Equation 4.6}$$

where e is the void ratio (0.71 for this experiment) and σ_0' (in kPa) is the mean principle effective stress σ_0' is related to the vertical effective stress (σ_v') by the following equation (Dong (2016)).

$$\sigma'_0 = \frac{(1+2K_0)\sigma'_v}{3} \quad \text{Equation 4.7}$$

The coefficient of lateral earth pressure at rest (K_0) was taken as 0.5. Therefore, Equations 4.6 and 4.7 simplify to the following equation for this experiment,

$$G_0 = 7918 \sigma'_v{}^{0.5} \quad \text{Equation 4.8}$$

The second empirical equation used is given by Seed and Idriss (1970), which estimates G_0 (in kPa) for sands as the following,

$$G_0 = 1000 K_2 \sigma'_0{}^{0.5} \quad \text{Equation 4.9}$$

K_2 is a constant that depends on the strain level and relative density. For small-strain behaviour and 66% relative density (D_r) applicable to this K_2 experiment, K_2 is approximately 11.5 according to Seed and Idriss (1970). Note that this K_2 value of 11.5 is derived for σ'_0 in units of kPa (for units of psf, K_2 is 53). This value was also confirmed by the equation of $K_2=0.586+16.5D_r$ given in Futai et al. (2018) for $30\% \leq D_r \leq 90\%$.

Both these estimates show G_0 is proportional to $\sigma'_0{}^{0.5}$ and hence to $\sigma'_v{}^{0.5}$. The vertical effective stress σ'_v is directly proportional to the depth from the ground level (d), given the ground level is flat. Therefore, G_0 is taken as directly proportional to $d^{0.5}$, in order to fit an appropriate curve to the experimental data. As flat ground level is only available for the no scour and global scour cases, the curve fitting was carried out only for those two cases.

4.12.2 Estimated small-strain shear modulus profiles

Figure 4.37(a – c) shows the estimated full-scale G_0 profiles derived from both the experimental shear wave measurements (near Models 1, 3 and 4) and the empirical equations described in Section 4.12.1.

The experimental observations showed a reduction in G_0 primarily at the shallow depths near Models 3 and 4, as shown in Figure 4.37(b and c). A reduction in G_0 is to be expected as a result of the loss of overburden soil due to scour of overlying soil. The G_0 at deeper levels has not shown a change, and this could be due to the low measurement resolution of G_0 (i.e. a G_0 change above $\pm 44\%$ would be required to change one measurement resolution) (see Section 4.12.1).

Some G_0 measurements, for example G_0 at the shallow depths near Model 1 (Figure 4.37(a)), were not available due to either accelerometer malfunctioning or interference of multiple shear waves; interference occurred when shear waves from the two air hammers reached certain accelerometers at the same time.

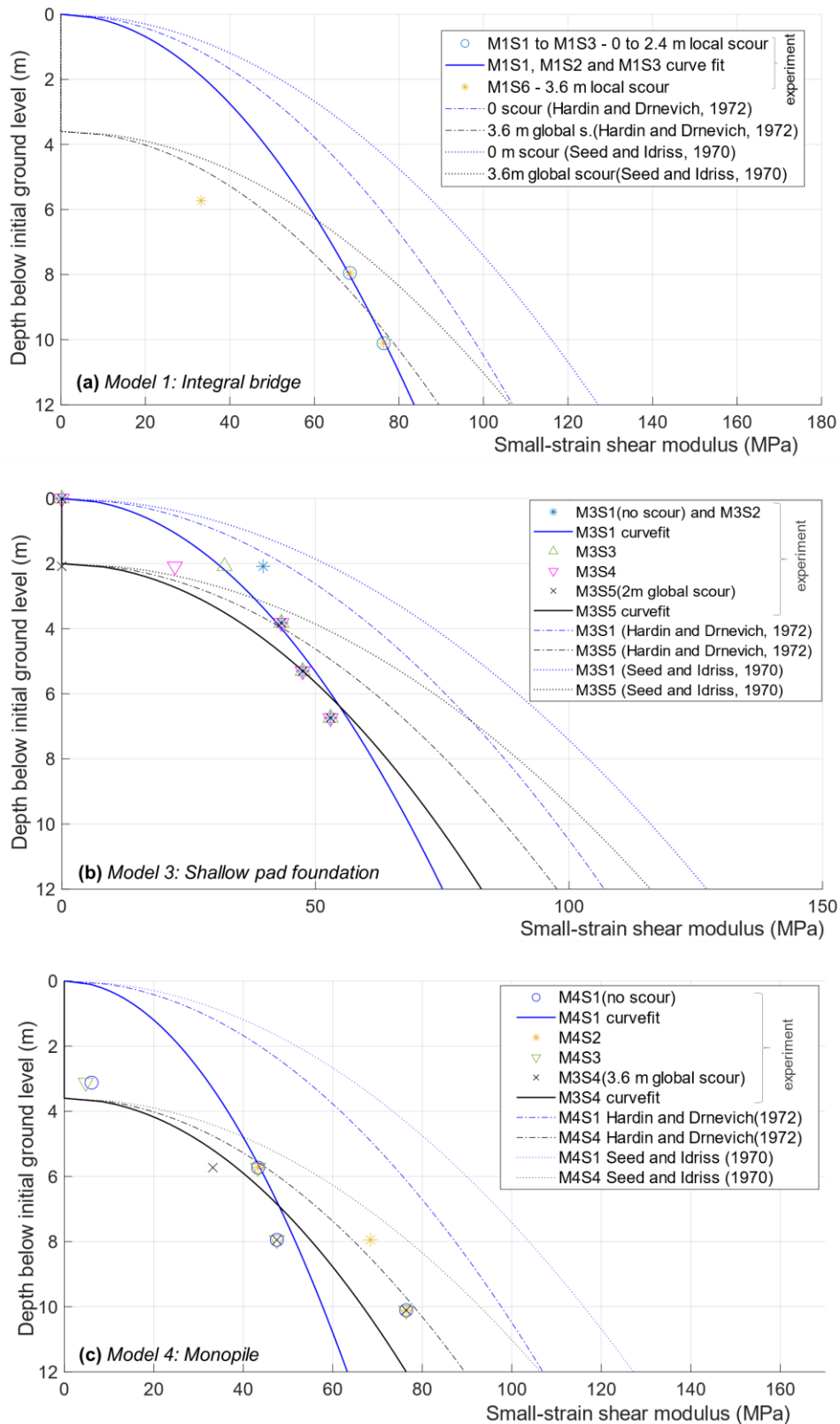


Figure 4.37 Variation of G_0 profiles with scour near the Model 1 integral bridge in equivalent full-scale

As shown in Figure 4.37 (a – c), curves were fitted to the available experimental G_0 estimates at no scour and global cases, assuming G_0 to be directly proportional to the depth raised to the power of 0.5 (Section 4.12.1). Empirical estimates were also obtained for these two scour cases using empirical Equations 4.9 and 4.10 given by Hardin and Drnevich (1972), and Seed and Idriss (1970). The G_0 estimated by these two empirical equations were higher than the

curves fitted to the experimental G_0 observations. For these empirical estimates, global scour (for example M3S5) graphs could be obtained by shifting the no scour (M3S1) curve down by the depth of global scour; this was expected as global scour represent a case where the ground level lowers everywhere, thus lowering the stiffness profile as well. However, for experimental observations, this expected behaviour was not shown with the curves fitted for “no scour” and “global scour” cases, which indicates there were significant measurement inaccuracies.

4.13 Summary

This chapter described the development of a centrifuge testing methodology to measure natural frequency sensitivity to scour at the foundations of different bridge types. A scaled-down two-span integral bridge model and three discrete bridge foundation models were constructed in the sand with 66% relative density to simulate field-scale soil-structure interactions. These structural models were excited with a piezoelectric actuator and an automatic modal hammer developed for this test. The modal hammer provided better input excitation than the piezoelectric actuator. The tests were conducted at the required centrifuge acceleration to simulate the dynamic behaviour of the full-scale structures. With all four models, the fundamental mode of vibration was measured successfully. It was found that the natural frequency measurements during centrifuge testing, for all scour cases of all models, lay between the upper-bound frequency limit of fixed base tests and the lower-bound frequency limit of 1g tests, which helped to confirm the frequency measurements during the centrifuge tests. The most reliable indicators of scour were natural frequency and output-only spectral density at modal peaks (SVPSD or PSD).

Local scour of 1 m at either the pier or the abutments of the integral bridge model produced a 4 – 5% frequency shift at full-scale. One metre of local scour at the standalone foundation models produced the highest frequency sensitivity for the pile bent (12%), the second highest for a single pile (6%) and the lowest for a shallow foundation (3.5%). The natural frequency reduction for global scour was slightly (0.5-1%) greater than that for local scour in all bridge types. The frequency sensitivity to local scour tended to reduce as the scour hole deepened. The sensitivities of SVPSD for scour of 1 m near the models ranged from 40 – 417% for local scour and 46 – 1205% for global scour. The shallow foundation, which was least in natural frequency sensitivity, had the highest sensitivity to SVPSD. The normalised mode shape variation due to local scour primarily affected the part of the bridge element closest to the scouring soil. The experimental measurements of small-strain stiffness (G_0) of soil did not show an acceptable level of accuracy due to low measurement resolution of G_0 at deeper depths and accelerometer malfunctioning and shear wave interference at shallower depths.

In summary, this experimental study demonstrated that natural frequency, mode shapes and modal spectral density have significant potential as indicators of scour.

Chapter 5

Numerical simulation of sensitivities in bridge natural frequencies and mode shapes to scour

Highlights

- A numerical scour simulation technique was developed based on the observed centrifuge test results.
- The developed numerical scour simulation technique was extrapolated to full-scale bridge structures the centrifuge tests represent.
- Fundamental natural frequency sensitivity of the integral bridge with the numerical model was 11% for 1 m of scour, similar to the centrifuge test, validating its feasibility to be used as a scour indicator.
- For simply supported bridges, the fundamental mode was found not to be a sensitive indicator of scour, but higher order modes showed potential.
- Mode shape change was limited to the foundations undergoing scour, suggesting that this has the potential to be used to locate the foundations undergoing scour.

This chapter presents numerical modelling and scour simulations carried out to achieve two key objectives. The first objective was to develop numerical scour simulation techniques to simulate the effects observed in centrifuge experiments (Chapter 4). It is anticipated that such a scour simulation technique would help bridge engineers estimate the expected change in the dynamic behaviour of a bridge subjected to scour. The second objective was to extrapolate the results of simple standalone foundation models tested in the centrifuge to the corresponding bridges, which have a bridge deck and bearings in addition to the foundations.

The initial sections of this chapter introduce the methodology used in this chapter to perform numerical modelling, the proposed numerical scour simulation techniques and detailed information on the soil-structure interaction models used for the numerical models. The later part of the chapter presents the results of the numerical modelling of the small-scale centrifuge models and their corresponding full-scale bridge structures.

5.1 Introduction

All the numerical, Finite Element (FE), models presented here represent bridge structures using various FE elements, and they incorporate a set of linear elastic springs representing soil-structure interaction. The numerical model for piles and its scour simulation technique extends from the previous work of Prendergast, Hester and Gavin (2016), where scour of a single pile foundation was simulated by deleting the springs down to the depth of scour while maintaining the stiffness of all the other springs. As shown in Figure 5.1, such a simulation technique is more representative of a local scour case, where the stiffness of underlying soil is remaining the same due to the overburden pressure given by the soil surrounding the scour hole. However, a global scour case does not have such overlying soil to maintain the stiffness of the underlying soil. Therefore, this research proposes another scour simulation technique based on the lowering of all spring stiffnesses due to ground level lowering, as shown in Figure 5.1. These two techniques will be referred to with the following naming:

1. Top stiffness/springs lowering (proposed to be more representative of global scour case)
2. Top stiffness/springs deleting (proposed to be more representative of local scour case)

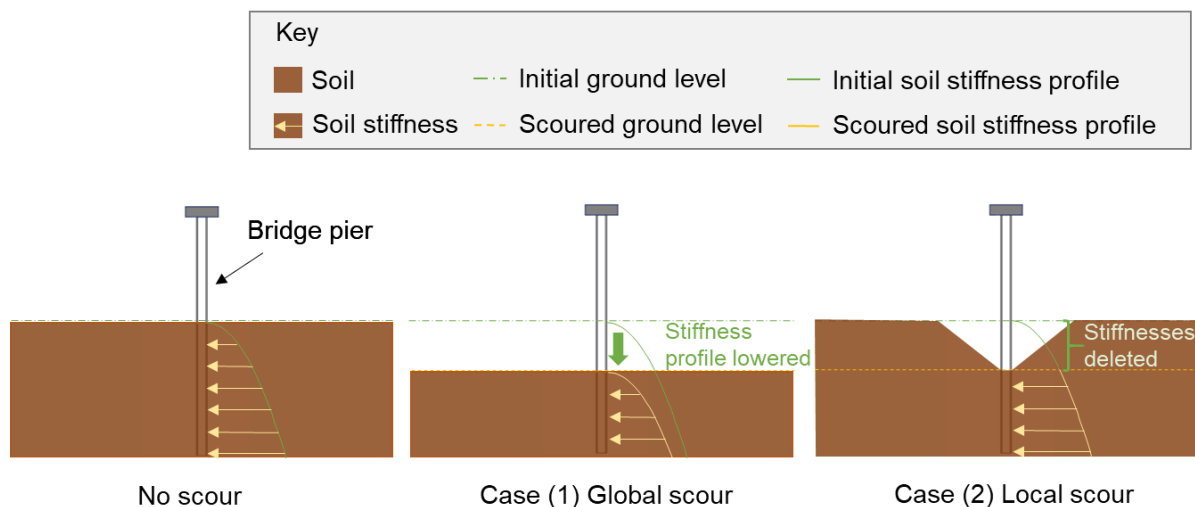


Figure 5.1 Change in stiffness profile around a bridge due to local and global scour cases

In addition to the spring-based model for pile foundation, a shallow foundation spring-based model was also developed and tested for scour simulation. All FE models were created with the CSiBridge2017 structural analysis software.

The centrifuge experiment discussed in Chapter 4 studied three parameters that were sensitive to scour: natural frequency, mode shape and spectral density. The numerical modelling in this chapter will only focus on simulating natural frequency and mode shape variation due to scour, as they can be simulated by only considering the soil-bridge interaction. Spectral density simulation of a full-scale bridge would require bridge-soil-vehicle interaction models, which are

out of the scope of this research. However, the validity of all these three parameters was studied in the field trial at Baildon Bridge, described in Chapter 3.

As explained in Chapter 4, the small-scale centrifuge tests were aimed at modelling the behaviour of three full-scale bridges (named as Bridge 1, 2 and 3). All three of these full-scale bridges were simplified to full-scale simplified bridges (or standalone foundations), which were easier and small-enough to construct accurately at small-scale (Figure 4.3). Bridge 1 with composite bridge deck was simplified to a bridge model with a rectangular slab deck with the same flexural rigidity and mass. The Bridges 2 and 3 with both the deck and foundations were simplified to standalone foundations without bridge decks. These simplified versions of full-scale Bridges 1, 2, 3 were scaled down to create small-scale Models 1, 2 and 3, respectively. An additional small-scale single pile model, called Model 4, was also created by scaling down a pile of Bridge 2 since a single pile provides a simple configuration to study numerically. An issue with studying simplified models in the experiments is that the experimental results may not be representative of the more complex bridge behaviour that these models attempt to simulate. For example, the natural frequencies estimated by the experiments of standalone foundations may differ from the natural frequencies expected in a realistic bridge with both foundations and a bridge deck due to the additional mass and stiffness provided by the bridge deck. Thus, the results of small-scale simplified models were more representative for a full-scale simplified bridge/model than for more complex arrangements expected in Bridges 1 – 3. Therefore, numerical models were used to extrapolate the experimental results (obtained for the simplified models) to more complex and more realistic full-scale bridges.

Figure 5.2 summarises the numerical modelling methodology. For each centrifuge model, initially, the fixed based numerical models were developed for both small-scale and full-scale simplified bridges to verify the accuracy of scaling. These two numerical models could be verified using the fixed base experimental results available for different levels of modelled scour (i.e. lowering of the ground level, which was modelled as fixed). Verification of scaling is important as the change of material properties from small-scale (aluminium) to full-scale (concrete) resulted in only a selected number of scaling laws being met (Section 4.4.2). Once the scaling was verified, the numerical model of the full-scale simplified bridge was extended to include springs representing soil-structure interaction. This soil-structure model of the simplified bridge could be calibrated by using the centrifuge test results converted to full-scale using appropriate scaling factors. For calibration, multiple soil-structure interaction models were compared to find the one that best estimates the experimentally observed dynamic behaviour for different levels of scour. The calibrated full-scale simplified bridge with soil-structure interaction was finally extended to a full-scale bridge with a realistic bridge deck arrangement to estimate the expected natural frequency and mode shape variations.

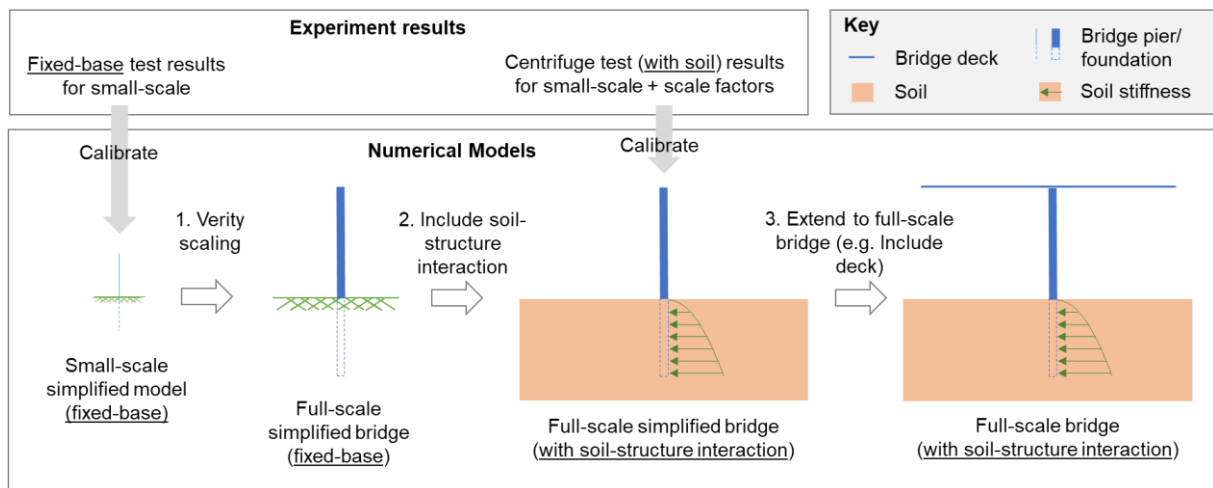


Figure 5.2 Methodology followed to create a numerical model for the full-scale bridge using experiment results

The soil-structure interaction was idealised in the FE model by using springs to represent the soil-structure interaction. Two types of spring-based methods were adopted. A “Winkler spring model” was used to represent the pile-soil interaction in all the bridges with pile/stub column foundations. A “macro element model” represented the pad footing of the bridges with shallow pad foundations.

5.2 Winkler spring model for piles of Bridges 1 and 2

The Winkler model idealises the soil-structure interaction of a foundation element by a system of discrete, mutually independent, closely spaced springs (Winkler, 1867; Dutta and Roy, 2002; Prendergast, Hester and Gavin, 2016a). The Winkler model has been extensively used to model pile foundations (Ashford and Juirnarongrit, 2003; Prendergast and Gavin, 2016). Figure 5.3 shows a Winkler spring representation of a pile. It is assumed that the springs along the length of the pile represent both the vertical shear stiffness (K_V) and the lateral stiffness (K_H) provided by the soil. The high stiffness at the toe (tip) of a pile is represented by a spring (K_T) as well.

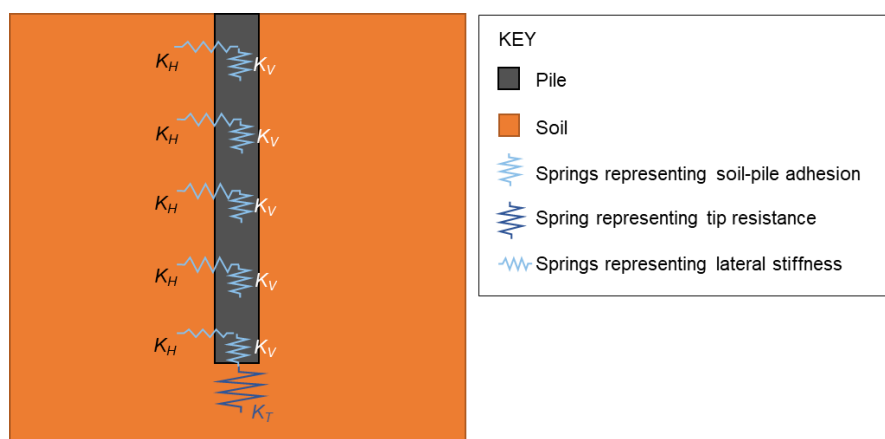


Figure 5.3 Winkler spring representation of soil-pile interaction

The following sections present the API method for calculating all K_V , K_H and K_T springs and other empirical methods to convert the derived small-strain stiffness values in Chapter 5 to K_H springs.

5.2.1 Lateral spring stiffness from the American Petroleum Institute (API) method

The API design code estimates the relationship between the lateral soil resistance per unit length, P (kNm^{-1}), and deflection, y (m), at any depth below the ground level, d (m), along a pile embedded in sand, as given in Equation 5.1. In this equation, k_i (kNm^{-3}) is the initial modulus of subgrade reaction, P_u (kNm^{-1}) is the ultimate bearing capacity of soil at depth d and A is an empirically derived factor of 0.9 for cyclic loading.

$$P = A \times P_u \times \tanh \left[\frac{k_i \times d}{A \times P_u} \times y \right] \quad \text{Equation 5.1}$$

Differentiating both sides of the equation and taking the small strain behaviour ($y = 0$) gives:

$$\left(\frac{dP}{dy} \right)_{y=0} = A \times P_u \times \frac{k_i \times d}{A \times P_u} \left\{ 1 - \tanh^2 \left[\frac{k_i \times d}{A \times P_u} \times y \right] \right\}_{y=0}$$

$$\left(\frac{dP}{dy} \right)_{y=0} = k_i d$$

If lateral springs are at a spacing of s along the pile, a deflection of ΔL induces a force of sP . Therefore, the stiffness (K_H) of each spring linearised for small strain behaviour is:

$$K_H = \left(s \frac{dP}{dy} \right)_{y=0} = s k_i d \quad \text{Equation 5.2}$$

Equation 5.2 shows that the stiffnesses of the lateral springs increase linearly with depth. For dry sand of 66% relative density, as was the case with this centrifuge test, k_i is given as $6 \times 10^4 \text{ kNm}^{-3}$ (API, 2002).

5.2.2 Lateral spring stiffness from small strain shear modulus

The small strain shear modulus, G_0 (Pa), estimates were found from the experiment and derived using empirical equations, as given in Section 4.12. For isotropic materials, G_0 can be related to the small strain elastic modulus, E_0 (Pa), using the relationship given in Equation 5.3 (Sas et al., 2016). ν_s is the Poisson's ratio, considered as 0.3 for Houston sand (Futai et al., 2018).

$$E_0 = 2G_0(1 + \nu_s) \quad \text{Equation 5.3}$$

There are a number of methods given in the literature relating an E_0 profile of soil to a Winkler spring model idealising soil-structure interaction. Ashford and Juirnarongrit (2003) give an empirical estimate for the coefficient of subgrade reaction k_s (Nm^{-3}) of small-strain lateral vibration of a pile in soil as the following equation.

$$k_s = \frac{1.0E_0}{D(1 - \nu_s^2)} \left[\frac{E_0 D^4}{E_s I_s} \right]^{1/12}$$

Another relationship between E_0 and k_s is given by Kloeppe and Glock (1970) as

$$k_s = \frac{2E_0}{D(1 + \nu_s)}$$

where $E_s I_s$ (Nm²) and D (m) are the flexural rigidity and the width (diameter of a pile) of the foundation structural element, respectively. When the horizontal Winkler springs are at a spacing of s (m) along a pile of diameter D (m), each spring stiffness K_H (kNm⁻¹) is given by Equation 5.4.

$$K_H = k_s \times s \times D \times 10^3 \quad \text{Equation 5.4}$$

5.2.3 Soil-pile adhesion spring stiffness from API method

The API design code assumes the maximum soil-pile adhesion in sandy soils is reached after 0.1 inch (2.54 mm) of axial local pile displacement. The soil-pile adhesion, t (kPa), and local pile deflection, z (m), relationship is considered linear before reaching the 2.54 mm of local displacement. Therefore, the $t - z$ relationship can be represented as

$$\left(\frac{t}{z} \right)_{z \leq 0.00254} = \frac{t_{max}}{2.54 \times 10^{-3}} \quad \text{Equation 5.5}$$

$$\left(\frac{t}{z} \right)_{z > 0.00254} = \frac{t_{max}}{z} \quad \text{Equation 5.6}$$

where t_{max} (kPa) is the maximum soil-pile adhesion given by Equation 5.7, where s is the spacing of the springs along the pile of diameter, D is the pile diameter. The coefficient of lateral earth pressure (K_0) was assumed to be 1.0 for full displacement piles (a closed-end pile or an open-ended driven pile having soil plugging at the open end). The centrifuge test was conducted on thin open-ended piles. Therefore, the thin piles were assumed to have sufficient soil plugged at the open end when driven into the soil. The full-scale reinforced concrete piles were closed-ended. Therefore, both the centrifuge model piles and the full-scale piles that they represent have a K_0 value of 1.0. σ'_v (kPa) is the effective overburden pressure, which increases with depth. The friction angle between the soil and the pile wall (δ) is 30° for dense sand. The API code limits soil-pile adhesion to 95.7 kPa for dense sand (API, 2002).

$$t_{max} = \pi D s \times K_0 \sigma'_v \tan \delta, \quad t_{max} \leq 95.7 \text{ kPa} \quad \text{Equation 5.7}$$

Equations 5.5 – 5.7 can be combined to obtain the stiffness (K_V) of each spring for small strain behaviour as given below.

$$(K_V)_{z < 0.00254} = \pi D s \left(\frac{t}{z} \right)_{z < 0.00254} = \pi D s \times \frac{t_{max}}{2.54 \times 10^{-3}}$$

$$(K_V)_{z>0.00254} = \pi D s \left(\frac{t}{z} \right)_{z>0.00254} = \pi D s \times \frac{t_{max}}{z}$$

$$(K_V)_{t_{max}>95.7} = \pi D s \left(\frac{t}{z} \right)_{z>0.00254} = \pi D s \times \frac{95.7}{z}$$

5.2.4 Tip resistance spring stiffness from API method

The API design code assumes that the maximum tip resistance of a pile is mobilised at an axial tip deflection, z (m), of 0.1 of the pile diameter, D . There is a non-linear behaviour between the mobilised tip resistance, Q (kPa), and axial tip deflection, z (m). Therefore, a spring with non-linear stiffness of K_T can be used to represent the tip resistance (end bearing), as shown in Equation 5.8 given below.

$$K_T = \frac{\pi D^2}{4} \left(\frac{Q}{z} \right) \quad \text{Equation 5.8}$$

The Q - z relationship is shown in Table 5.1 and it is estimated as secant modulus. Q_{max} (kPa) is the maximum tip resistance calculated by Equation 5.9. N_q is a dimensionless bearing capacity factor, which equates to 40 for dense sand. σ'_v (kPa) is the effective overburden pressure at the pile tip. The tip resistance is limited to 9.6 MPa for dense sand.

$$Q_{max} = \sigma'_v N_q, Q_{max} \leq 9.6 \text{ MPa} \quad \text{Equation 5.9}$$

Table 5.1 The relationship between tip resistance and axial tip deflection of a pile (API, 2002)

$\Delta z/D$	Q/Q_{max}	Q/z
0	0	-
0.002	0.25	$125.0 \times \frac{Q_{max}}{D}$
0.013	0.5	$38.5 \times \frac{Q_{max}}{D}$
0.042	0.75	$17.9 \times \frac{Q_{max}}{D}$
0.073	0.9	$12.3 \times \frac{Q_{max}}{D}$
0.1	1	$10.0 \times \frac{Q_{max}}{D}$
∞	1	$1.0 \times \frac{Q_{max}}{D}$

5.3 Numerical modelling of a single pile of full-scale Bridge 2 using experimental results for small-scale Model 4: single pile

The extra model tested in the centrifuge (single pile: Model 4) was considered first since it has the simplest form (one pile) out of the four centrifuge models, though it does not represent the full foundation of a bridge (Bridge 2 in this case) as the other centrifuge models do. A numerical model was first created to simulate the fixed based single pile structural model, without any soil-structure interaction, with the aim of calibrating this numerical model for the fixed based experimental results. The following sections will discuss some of the challenges faced when attempting to calibrate the FE model and why Model 4 was not further studied. However, it did not affect the planned methodology of developing numerical models for the three bridges since Model 4 was only an extra model but not a key model required to develop numerical models of Bridges 1 – 3.

5.3.1 Numerical modelling of the single pile foundation with a fixed base

The setup of the fixed base experiment representing the no scour case of Model 4 is shown in Figure 5.4(a). Fixed based condition is a simple setup that can be used to validate the FE model of the structure alone without involving any soil-structure interactions. The Model 4 was modelled using FE as a cantilever beam with lumped mass at the top, as shown in Figure 5.4(b). In this FE model, the pile was modelled using “frame” elements each 5 mm in length. Frame elements allow beam-column formations in CSiBridge software (Computers & Structures Inc., 2016a). The top slab and the actuator were idealised as a lumped mass of 0.5 kg at the top of the pile. This FE model estimated a fundamental natural frequency of 78.2 Hz (sway mode), which was far below the corresponding experimental observation of 288.1 Hz for the same mode.

To find the cause for the lower estimate of natural frequency of the FE model, a sensitivity study was carried out on the effect of three of the key input properties, namely, lumped mass, tube wall thickness and the length of each finite element. These were three properties which could have small errors due to potential inaccuracies of measurements or the selection of FE. As shown in Figure 5.5, the natural frequency of the FE model did not show significant sensitivity to any small errors of these input properties. Therefore, the reason for the significantly high estimate of 288.1 Hz by this FE model was not the input properties used, but potentially its idealisation as a lumped mass system.

The lumped mass was completely removed to make the FE model a fixed cantilever column with a uniformly distributed mass. This change surged the natural frequency estimate to 1166 Hz. The analytical solution to the natural frequency of a fixed cantilever Euler-Bernoulli beam is shown in Equation 5.10 (Amrita, 2011), where f is the principle natural frequency, L is the beam length, EI is the flexural rigidity, ρ is the density and A is the cross-sectional area.

Equation 5.10 estimated the analytical natural frequency as 1192 Hz, which was slightly different from what was estimated by the FE model (1166 Hz). This difference in natural frequency could be attributable to the more flexible Timoshenko beam that was used in CSiBridge; Timoshenko beam is more flexible than Euler-Bernoulli beam due to provision of shear deformations between cross-sectional planes and the neutral axis of the beam elements. When the shear deformations were restricted, the CSiBridge FE model estimated a natural frequency of 1191 Hz, which is almost equal to the analytical estimate (1192 Hz). Therefore, the FE model in the CSiBridge has provided a theoretically accurate estimate when the lumped mass was completely removed.

$$f = \frac{1.875^2}{2\pi L^2} \sqrt{\frac{EI}{\rho A}} \tag{Equation 5.10}$$

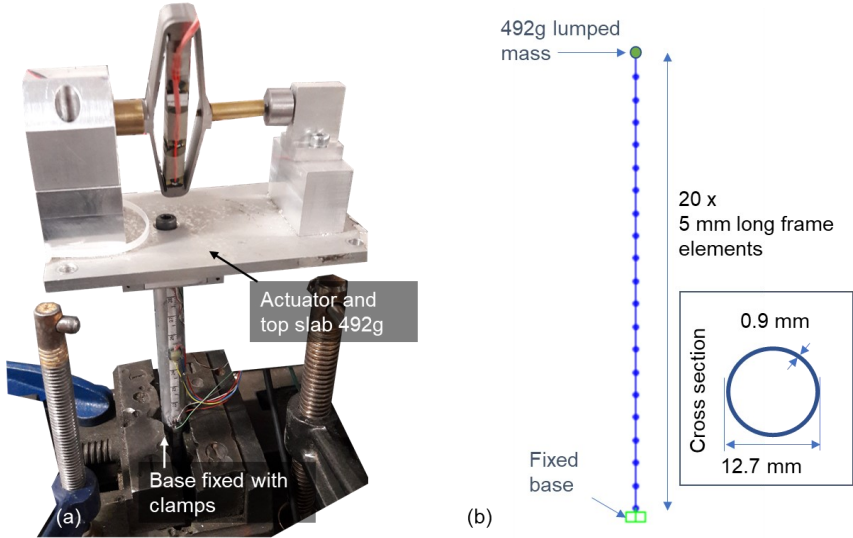


Figure 5.4 Model 4 fixed base (a) experimental setup and (b) FE model

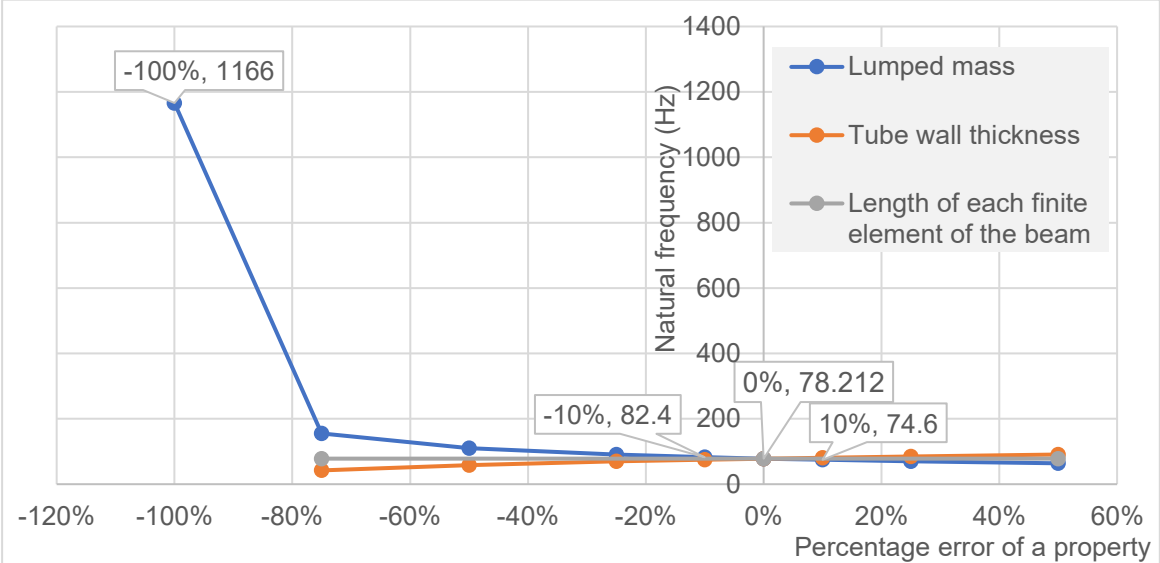


Figure 5.5 Sensitivity of natural frequency of the FE model to its input properties

As highlighted above, the FE model with no lumped mass accurately estimated the same natural frequency as the analytical estimate, and the three main input properties of the FE model did not show any significant natural frequency sensitivity. Thus, the lumped mass idealisation was the most probable cause for the difference in natural frequencies estimates of the FE model (78.1 Hz) and the experiment (288.1 Hz). The lumped mass idealisation in the FE model assumes the actuator at the top of the model does not provide any stiffness. However, as the single pile has low stiffness, the relative stiffness of the actuator may be high compared to the total system stiffness, leading to the stiffness of the actuator making largest contribution to the system stiffness. Modelling the actuator is complicated as it depends on the fixity provided by the screws, and it does not represent a bridge deck. Further to that, centrifuge Model 4 was only an extra centrifuge model studied for its simplicity with a single pile and centrifuge Model 2 (pile bent) models the foundation of the full-scale Bridge 2. Therefore, the pile bent model, which does not have the actuator, will be studied to develop the numerical model of Bridge 2.

5.4 Numerical modelling of full-scale Bridge 2 (simply supported bridge with a pile bent foundation) using the experimental results for small-scale Model 2 (pile bent foundation)

This section attempts to develop a calibrated numerical model for full-scale Bridge 2 by following the method illustrated in Figure 5.2. Bridge 2 was studied before Bridge 1 since the small-scale model corresponding to Bridge 2 (Model 2) was only a standalone foundation, not an entire bridge as in the case of the small-scale model of Bridge 1 (Model 1), and hence Bridge 2 was simpler to study numerically.

First, numerical models were created for the standalone pile bent foundation (Model 2) in both small-scale and full-scale, and these numerical models were calibrated against the corresponding fixed-base experimental results, with the aim of verifying the accuracy of scaling. Second, the fixed base support condition of this verified full-scale numerical model was replaced with a Winkler spring model representing soil-structure interaction, and this numerical model was calibrated against the results of the centrifuge experiment. Scour simulation techniques were also identified to simulate the experimentally observed effects of local and global scour at these standalone foundations. Finally, this calibrated numerical model of the full-scale standalone foundation was included with a simply supported bridge deck to create the numerical model of full-scale Bridge 2, and its vibration parameters were assessed for the potential to indicate scour.

5.4.1 Numerical modelling of the pile bent foundation with a fixed base in small- and full-scales

In order to validate the property scaling from small-scale to full-scale, numerical models were created in both full- and small-scales representing a fixed base support condition (without soil) and compared with the corresponding experimental results as described in the following sections.

5.4.1.1 Small-scale behaviour of the aluminium Model 2 (pile bent foundation)

The experimental setup of Model 2 with a fixed base is shown in Figure 5.6(a). The four piles in this model were firmly clamped at the base to simulate a fully fixed end restraint for the piles. The scour was simulated by reclamping the model at a base level lowered by an amount representative of the scour depth.

This experimental setup was modelled with FE, as shown in Figure 5.6(b). The slab at the top of the Model 2 has a second moment of area of $I_s = 6830 \text{ mm}^4$ and a mass of $M_s = 137 \text{ g}$, and it was idealised using 2.5 mm long frame elements. Each of the four piles with second moment of area of $I_p = 584 \text{ mm}^4$ and mass of $m_p = 9 \text{ g}$ was represented by 5-mm-long frame elements. The two piezoelectric accelerometers of mass $M_a = 20 \text{ g}$ was assigned as a concentrated mass at the middle of the top slab. All translational and rotational degrees of freedom were fixed at the base level. The scour depth was simulated by extending the pile heights by the representative scour depth.

In order to further support the numerical modelling predictions, a simplified analytical model was created representing the same fixed base experimental setup (Figure 5.6(c)). This analytical model represented the piles of Model 2 as one massless column with all the mass lumped at the top. The equivalent lumped mass for a uniformly distributed mass of a fixed cantilever beam is 0.24 (33/140) to obtain similar dynamic behaviour (Lasithan, 2014). Therefore, the lumped mass of the analytical model is the sum of the masses of the top slab, sensors and the 0.24 component of the distributed mass of the piles ($M = M_s + M_a + 0.24M_p = 166 \text{ g}$). Since all four piles are connected to the same base and the top slab, they act as parallel stiffness elements when simplified to a single column. Therefore, the massless column has four times the second moment of area ($I = 4I_p$) of one pile. The frequency (f) of this fixed cantilever beam with lumped mass is given by Equation 2.6, where L is the column height above the level of the fixed base and E is Young's modulus (Section 4.5.1).

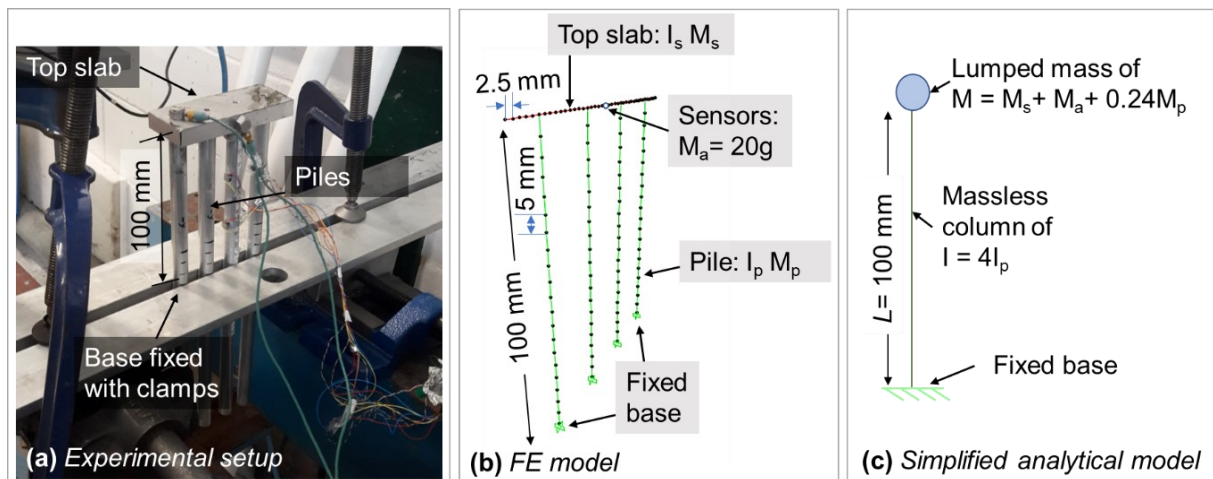


Figure 5.6 The fixed base small-scale Model 2 for the case of no scour

The natural frequency variation observed with the simulated scour depth is shown in Figure 5.7. All three simulations show a similar pattern of decreasing natural frequencies and decreasing gradient of the natural frequency curve with increased scour depth. The experimentally observed natural frequencies were lower than both the analytical solution and FE model results. This is expected as the perfect fixed base condition, idealised in the analytical solution and the FE model, would not be achieved in real life. The damping present in the experimental model may also have contributed to the lower natural frequencies observed in the experiment when compared to the results from the FE models. The difference between the numerical results and the experimental observations reduced with increased scour depth. This behaviour is assumed to be due to the reduction of the model stiffness as the pile height increases and hence the increase of the relative stiffness provided by the clamp fixity (closer to perfect fixity than before).

The predictions obtained using the simplified analytical model and the FE model showed close agreement with less than 2% difference in natural frequencies. This small difference in frequency is attributed to the additional shear flexibility introduced with the Timoshenko beam used in the frame elements of the FE model. For example, when shear flexibility was ignored for the no scour case, the FE model gave a frequency of 273.8 Hz, which is almost equal to the representative analytical model frequency of 273.9 Hz.

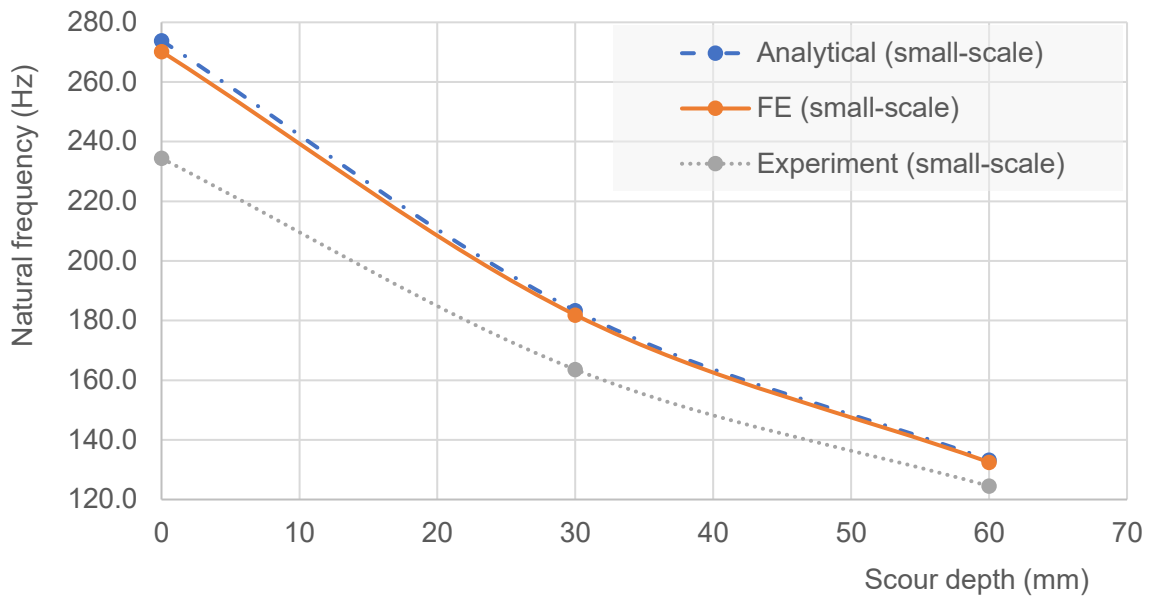


Figure 5.7 Variation of the fundamental natural frequency with scour depth of Model 2 with fixed base

5.4.1.2 Full-scale behaviour of the reinforced concrete pile bent foundation corresponding to Model 2

An FE model was created for the fixed base full-scale pile bent foundation using the properties defined in Table 4.3 in Chapter 4. Figure 5.8(a) shows the full-scale pile bent structural foundation. The top capping beam of this pile bent has a second moment of area of $I_b = 0.179 \text{ m}^4$ and a mass of $M_b = 29,700 \text{ kg}$. Each pile has a diameter of 0.74 m and an exposed height of L , which increases with increasing depths of scour. Therefore, the mass of the exposed pile section also increases with increasing depths of scour. Each of these piles has a second moment of area of $I_p = 0.0147 \text{ m}^4$. The stage where there was no scour, each pile has a mass of $M_p = 6580 \text{ kg}$. As shown in Figure 5.8(b), the FE model was created with a top capping beam and four identical piles. The top capping beam of the FE model was created with frame elements of 0.15 m in length, and the piles were also created with frame elements of 0.3 m in length.

To further support the numerical estimates, a simple analytical model was also created, as previously explained. This analytical model idealised a lumped mass at the top of a massless cantilever column, as shown in Figure 5.8(c). The magnitude of the lumped mass of the analytical model (M) was obtained from the addition of the effective mass of the column ($0.24M_p$) and the mass of the top beam (M_b) as discussed previously in Section 5.4.1.2. The second moment of area of the massless column is equal to the sum of the four individual piles ($I=4I_p$). The natural frequency of the analytical model is given by Equation 2.6.

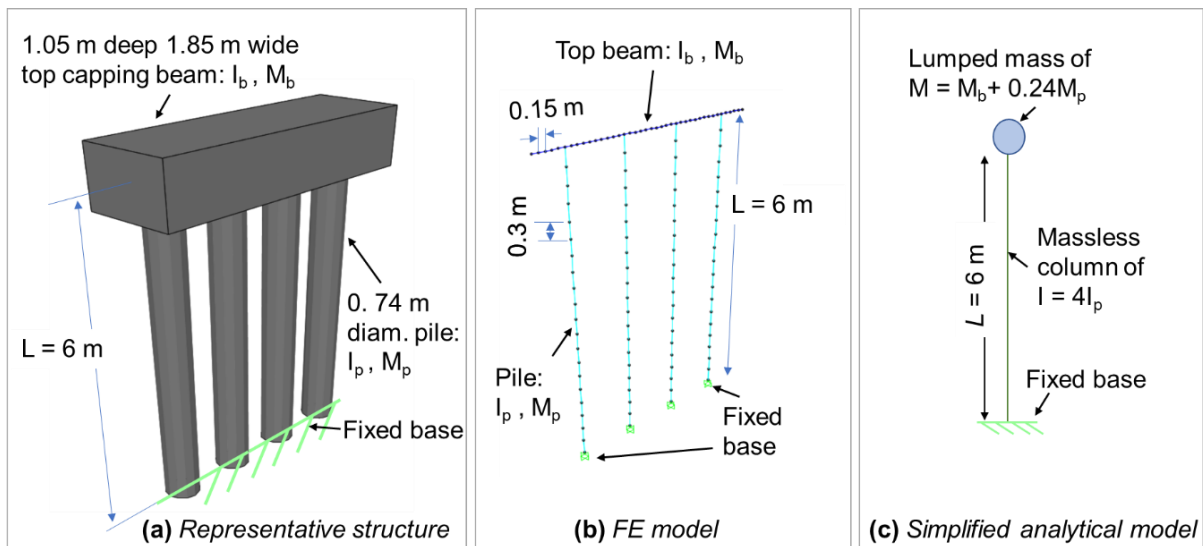


Figure 5.8 The fixed base small-scale Model 2 for the case of no scour

The effect of removing soil around the base of the piles was simulated for the fixed base models (shown in Figure 5.8) by lowering their fixed base support level by the respective scour depth. These numerical and analytical models estimated natural frequency variation at different scour depths, as shown in Figure 5.9. There was a close relationship with the analytical and FE results of the full-scale model. The natural frequency variations estimated using the experimental, analytical and FE results for small-scale aluminium pile bent are also plotted in Figure 5.9. The small-scale natural frequencies were converted to full-scale by using the scaling factor of $1/N$ (Table 4.2). There was a good match between the FE and analytical estimates of natural frequency for both small-scale aluminium model and full-scale reinforced concrete pile (1 – 5% difference). Therefore, the scaling was accurate between the small-scale aluminium pile bent, and the full-scale reinforced concrete pile bent. There was a slight (up to 5%) deviation of the full-scale FE model frequencies from the small-scale FE model/ N results with increased scour depth. This deviation can be attributed to the fact that all properties of the full-scale pile could not be scaled down at the same time, and thus for the piles, the critical properties such as flexural rigidity and pile diameter were scaled down while the mass could not be scaled to the expected value, as explained in Section 4.4.2.

The natural frequencies of the full-scale FE model and analytical model have higher frequencies than the representative experimental estimates. This behaviour is expected as the perfect fixity idealised in the FE models would not be present in real life. The lower than perfect fixity and thus, the lower stiffness provided to the model at the base, results in a lower natural frequency in the experiment. The difference between experimental and FE estimates reduces with increasing depths of scour. As explained before, this behaviour was assumed to be due to the relatively higher fixity provided by the base in the model with increased flexibility resulting when the simulated scour depth increases.

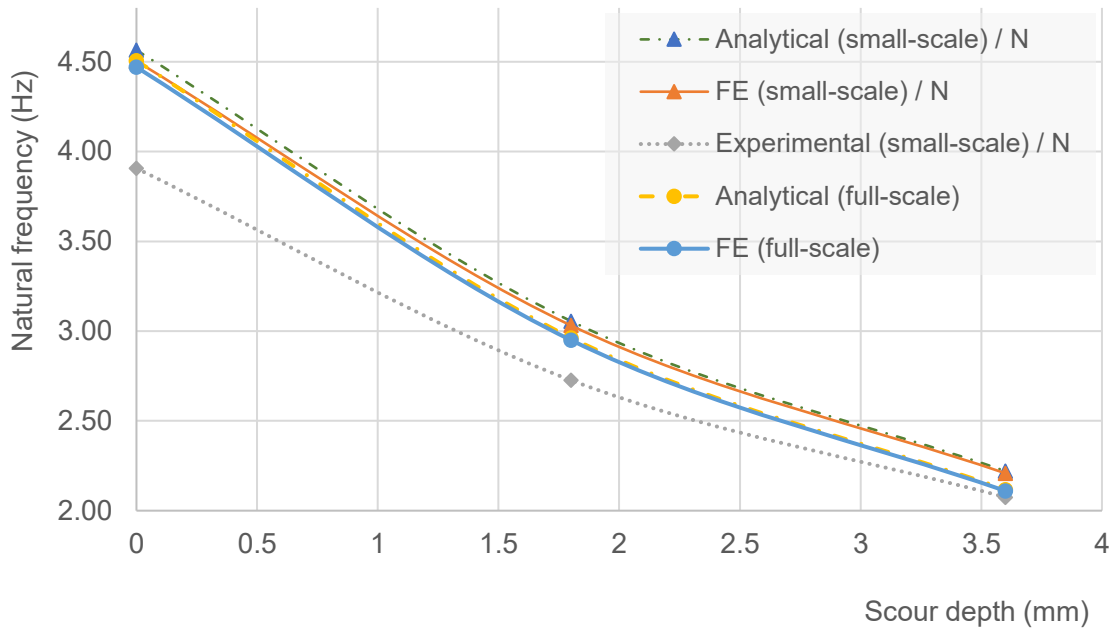


Figure 5.9 Comparison of natural frequency vs scour depth at full-scale and small-scale (converted to full-scale) for fixed base pile bent foundation

5.4.2 Inclusion of soil-structure interaction to the full-scale pile bent numerical model

Previously, the numerical model developed for the full-scale pile bent foundation successfully simulated the fixed based behaviour while confirming the scaling. Now, the soil-structure interaction is added to the previously created numerical model of full-scale pile bent, and it is calibrated against the centrifuge modelling results. The centrifuge model tested is shown in Figure 5.10(a). The centrifuge Model 2 has 200 mm of the depth of the piles embedded in the soil. This centrifuge model represents a full-scale pile bent, which has 12 m depth of piles in the soil, as shown in Figure 5.10(b).

Figure 5.10(c) illustrates the soil-structure FE model developed. The above-ground properties of the FE model were the same as the fixed base FE model. The piles were extended below-ground level by adding 24 frame elements each having 0.5 m in length. The soil-structure interaction was simulated by the Winkler spring model, which was described in Section 5.2. The Winkler spring stiffnesses were provided in the FE model using link elements, which provides stiffness.

The link elements were introduced at 1 m spacings from -0.5 m below ground level to -11.5 m below ground level. Each link element was assigned with three springs orthogonal to each other. Two linear springs were provided in the longitudinal and transverse direction of the model representing the lateral stiffness of soil. One non-linear spring was provided in the vertical direction representing the soil-pile adhesion. An additional four non-linear springs were

provided at the toe of the piles in the vertical direction to represent pile-tip resistances. The stiffnesses of these springs were found using the API method, as described in Section 5.2.

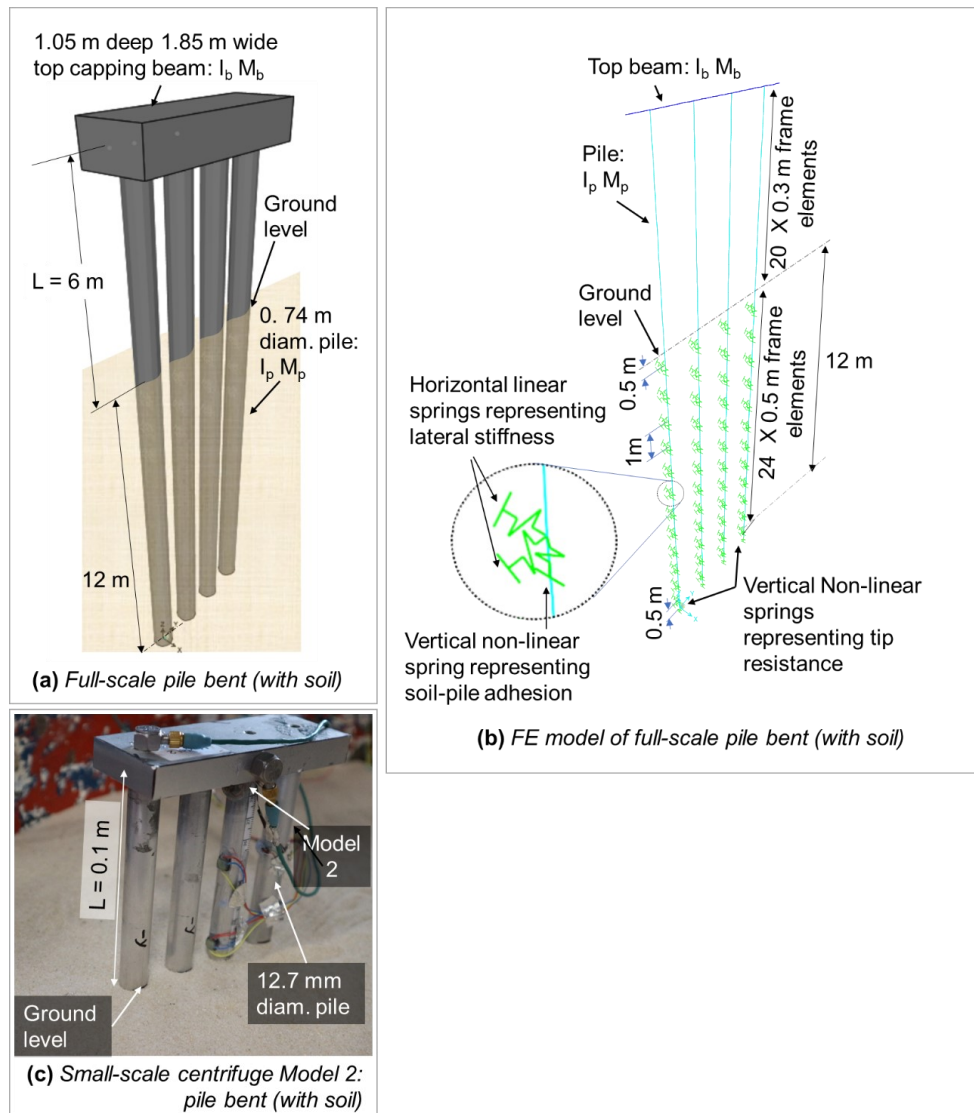


Figure 5.10 Pile bent (with soil) for the case of no scour numerical modelling and experiment setup

Small-strain behaviour can be assumed for horizontal stiffness but not for the vertical stiffnesses due to the weight of the bridge pier acting vertically. Therefore, vertical stiffnesses should be considered after the weight of the bridge is introduced. The modal analysis with CSiBridge with non-linear springs involves an initial non-linear analysis by adding a load case. Therefore, the dead load due to the self-weight of the top beam and the piles was introduced to find the effective stiffness of the non-linear springs. These effective stiffnesses of the springs at the end of the non-linear analysis were used to carry out the eigenvalue analysis required to obtain the natural frequencies.

According to Winkler spring model, the springs should be closely spaced, and therefore there was an uncertainty as to whether the springs should be closer than 1 m initially chosen. In order to estimate how close the springs should be placed, “deflection bowl” concept was

considered. Deflection bowl is concept typically considered in railway engineering to estimate sleeper spacing under a rail track. The deflection bowl length (L_d) refers to the length of the deflection region of a foundation element subjected to a point load, as shown in Figure 5.11. According to Powrie and Pen (2016), deflection bowl length is given by

$$L_d = \left(\frac{E_s I_s}{K/s} \right)^{0.25} \quad \text{Equation 5.11}$$

where $E_s I_s$ (Nm^2) is the flexural rigidity of the foundation structural element (pile), K (Nm^{-1}) is the stiffness of springs, s (m) is the spacings of springs. This model assumes all the springs to have the same stiffness, which can be assumed to be true over a small depth range of a pile. Each 740 mm diameter pile of the Bridge 2 pier has a flexural rigidity of $5.2 \times 10^8 \text{ Nm}^2$ (from Table 4.3). The springs should be close enough such that there should be at least one spring within the deflection bowl such that any point load along the foundation element is supported by at least one spring. The minimum deflection bowl length is reached when the spring stiffness is the highest (Equation 5.11), which occurs at the tip of the pile. The spring spacing was first considered to be 1 m, and for that spacing, the lateral spring stiffness near the pile tip was found to be 690 MNm^{-1} . This gives, L_d as 0.93 m from Equation 5.11 and hence the deflection bowl length is slightly below the considered 1m spring spacing. Therefore, a new set of spring spacings ranging from 0.3 m - 0.5 m were also considered in addition to the initially considered spring spacing of 1 m.

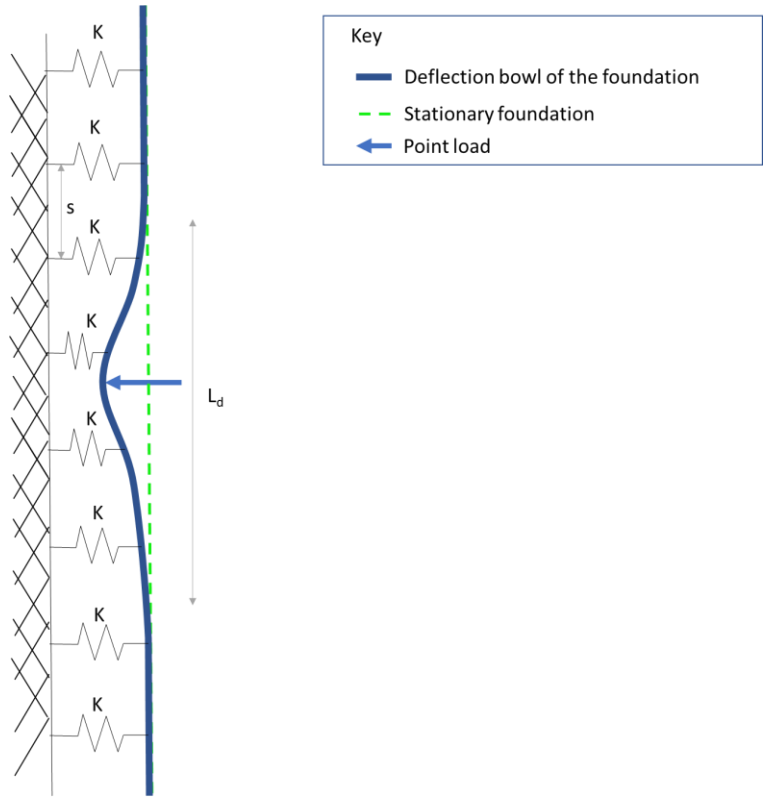


Figure 5.11 Deflection bowl of a foundation element on springs

In addition to the spring spacing, there were several other uncertainties behind the modelling assumptions. The first uncertainty was regarding the use of non-linear springs. As the experimental first mode of vibrations involves only horizontal vibration, the vertical non-linear springs may not be necessary. Therefore, the non-linear vertical springs may be ignored by restraining the vertical translation at the bottom tip of the piles. Second uncertainty was whether the shear flexibility introduced by Timoshenko beams change the results of the FE model. Third uncertainty was regarding which of the spring stiffness estimates discussed in Sections 5.2.1 – 5.2.4 were most suitable.

To address the uncertainties behind these modelling assumptions, a sensitivity study was performed by creating eight different FE models (referred to as analysis Case 1 – 8) with the assumptions shown in Table 5.2. Case 1 was the default case, and its spring arrangement is illustrated in Figure 5.10(b). This case has non-linear springs vertically, shear flexibility of the FE models was allowed, there was a 1 m spacing between springs and the spring stiffnesses were obtained from the API method. Cases 1 – 4 maintained the same spring stiffnesses given by the API method, but other assumptions were changed one at a time. Cases 5 – 8 checked different spring estimation methods other than the API method, the lateral spring stiffnesses values of which are given in Figure 5.12.

Table 5.2 Eight numerical analysis cases with different modelling assumptions

Case / Assumption	1	2	3	4	5	6	7	8
Spring stiffness estimation method	API (2002)				G_o profile from centrifuge experiment + k_s profile from Ashford and Juirnarongrit (2003)	G_o profile from Seed and Idriss (1970) + k_s profile from Ashford and Juirnarongrit (2003)	G_o profile from Seed and Idriss (1970) + k_s profile from Kloeppel and Glock (1970)	
Spacing between springs	1		0.5	1	0.5			0.3
The vertical translation was fixed at the pile tip	No	Yes	No		Yes			
Shear flexibility allowed for the piles	Yes			No	Yes			

These spring stiffnesses were estimated from the equations presented in Section 5.2. The API method has a uniform variation of lateral spring stiffness (K_H) with depth, whereas the other

methods provide a parabolic variation of K_H with depth. The spring locations are shown with a circular or triangular marker in Figure 5.12. When the spring locations are closer to each other, the estimated spring stiffnesses increases based on the equations in Section 5.2. For example, for API method, the springs were located at 1 m spacing in Cases 1,2 and 4, but the springs were located only at 0.5 m spacing in Case 3, and hence a larger K_H value was estimated for the Cases 1,2 and 4 in comparison to the Case 3. This is expected since the same spring stiffness estimation method should provide the same overall stiffness, although the spring spacings were different.

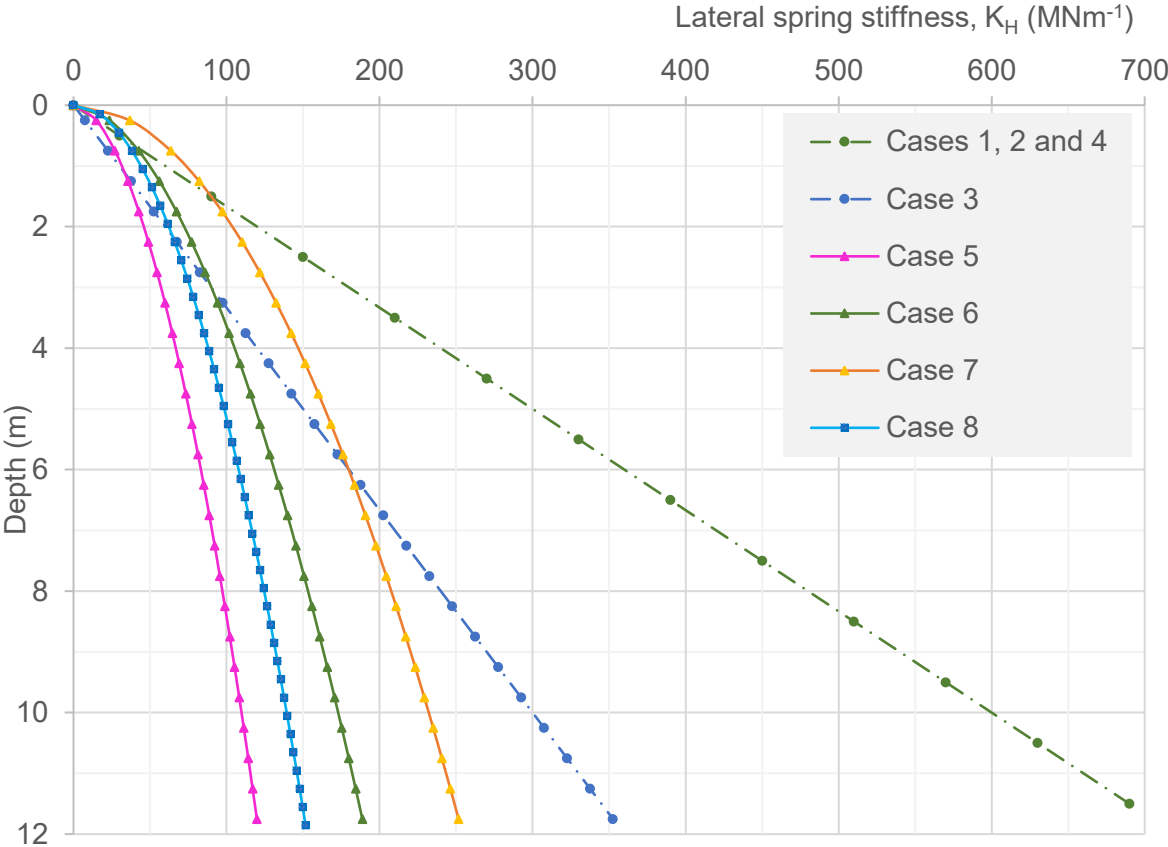


Figure 5.12 Lateral spring stiffness (K_H) profiles used in different FE numerical analysis cases

5.4.2.1 Natural frequency variation due to local and global scour

Local scour was simulated in the FE models by deleting the springs which lie above the new level of the soil surface after the loss of soil due to scour (i.e. the “spring deleting” technique previously discussed in Section 5.1). With this technique of simulation, the stiffnesses of the remaining springs below the scour level were unchanged, assuming there is a significant overburden pressure provided by the remaining soil around the local scour hole. Figure 5.13 shows the natural frequency sensitivity to scour simulated by the eight different modelling cases. Cases 1 and 2 provided the same frequencies at all different scour levels. Therefore, the lateral stiffness of soil is the only parameter which would have affected the fundamental natural frequencies of this pile bent FE model. The Cases 3 and 4 with the same spring

stiffness profiles also have frequencies close to Cases 1 and 2. Hence, the spring spacing and the shear flexibility of the piles provided in the FE model have shown little sensitivity to the frequency estimates.

The API based FE models (Cases 1 – 4) showed a much lower frequency sensitivity to scour at shallow scour depths, especially at shallow depths, in comparison to the experimental observations (see Figure 5.13). This suggests that the stiffness provided by the lateral springs at shallow depths should have been higher than what was recommended by the API design code. The small strain spring stiffness (K_H) derived from the API design code increases linearly with depth, as shown in Figure 5.12. At shallower depths, the K_H estimate by the parabolic stiffness variation (Cases 5 – 8), estimates were higher than the API estimates (Cases 1 – 4). Therefore, the natural frequency sensitivities at shallower depths of Cases 5 – 8 were also higher and closer to the experimental observations. Therefore, these parabolic variations were better suited to simulate the observed experimental conditions.

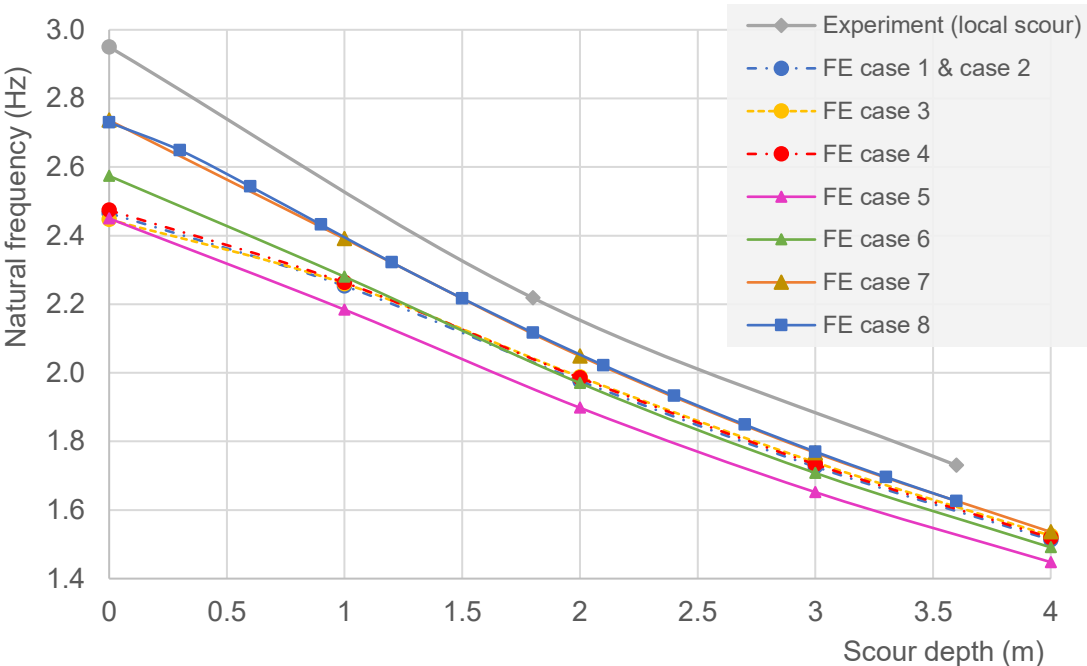


Figure 5.13 Natural frequency variation with scour depth: Experimental observations and FE estimation for local scour simulated by using spring deleting method

The natural frequencies estimated experimentally were higher than the estimates from all the eight numerical analysis cases (by about 7 – 17%). This can be attributed to the inability to scale down the mass of the piles when the other properties such as the diameter and the flexural rigidity were scaled down (see Section 4.4.2); as the small-scale aluminium tubes used in the experiment had lower mass than they should have according to the scaling laws, their natural frequencies in the experiment should be slightly higher than what was expected with perfectly accurate scaling. The natural frequency estimates for Cases 7 and 8 were almost the same (difference less than 0.5%), suggesting that changing the spring spacing in a parabolic

variation of soil stiffness also do not affect the estimated natural frequencies. The natural frequency estimations in the FE models were highest in the order of Case 5, 6, 7(= 8), which was the same order of K_H variation in these cases (Figure 5.12). Although K_H differs significantly among these cases (55 – 150% at 11.75 m depth), the natural frequencies do not differ as significantly (5 – 12%). With no scour, the difference between experimental observations and FE model Cases 5, 6, 7(or 8) were only 17%, 13% and 7% respectively.

The overall sensitivity of natural frequency per 1 m of scour was 9.5% for Cases 1 – 4 which used the API model for spring stiffness, and 10.2%, 10.5% and 11% respectively for Cases 5, 6 and 7(or 8) which used a parabolic spring stiffness profile. The overall experimental sensitivity was 11.5% per 1 m of local scour. Cases 7 and 8 provided the closest overall sensitivity and closest natural frequencies to the experimental observations. Case 8, in particular, has a smaller spring spacing as well. Therefore, Cases 8 was selected as the FE model calibrated to best describe the centrifuge experimental observations.

The sensitivity study described above only studied the “spring deleting method” assuming local scour behaviour. As explained in Section 5.1, the global scour could potentially be simulated better by the “spring lowering method”, which lowers all the springs of the model.

Figure 5.14 shows the variation of natural frequency estimated on spring deleting method and spring lowering method to estimate local and global scour, respectively. The limited natural frequency data points observed experimentally were fitted to an exponential curve. Similar to the natural frequency being higher sensitive to global scour than to local scour, spring lowering method gave lower natural frequencies and thus higher frequency sensitivity estimates than spring deleting method. The difference between experimental observations and FE Case 8 at no scour was 7%. The difference between spring deleting method FE estimate and local scour of 3.6 m experimental observation was 6%, whereas it was 9% for FE spring lowering method and global scour of 3.6 m. Further, the average sensitivity of experimental local and global scour per 1 m were 11.5% and 12.1%, respectively. The average sensitivities of the FE model with scour simulated by spring deleting method and the spring lowering method were 11.0% and 11.9%, respectively. Therefore, it was assumed that the spring lowering method has simulated global scour like behaviour, while the spring deleting method has simulated local scour like behaviour.

Note the difference between natural frequency values of the experimental observation and the FE model was assumed to be due to the inability to scale down the mass of the piles according to the scaling laws when other critical parameters were scaled down as previously explained. This was verified by correcting the mass scaling inaccuracy in the full-scale structure, i.e. adding a hollow aluminium pile above ground gave the full-scale frequency at no scour as 2.93 Hz, which was closer to the experimental observation (2.95 Hz). However, the previous full-

scale model, with the concrete piles, which give 7% difference to the experimental observations, was still used as it represents a typical full-scale field structure.

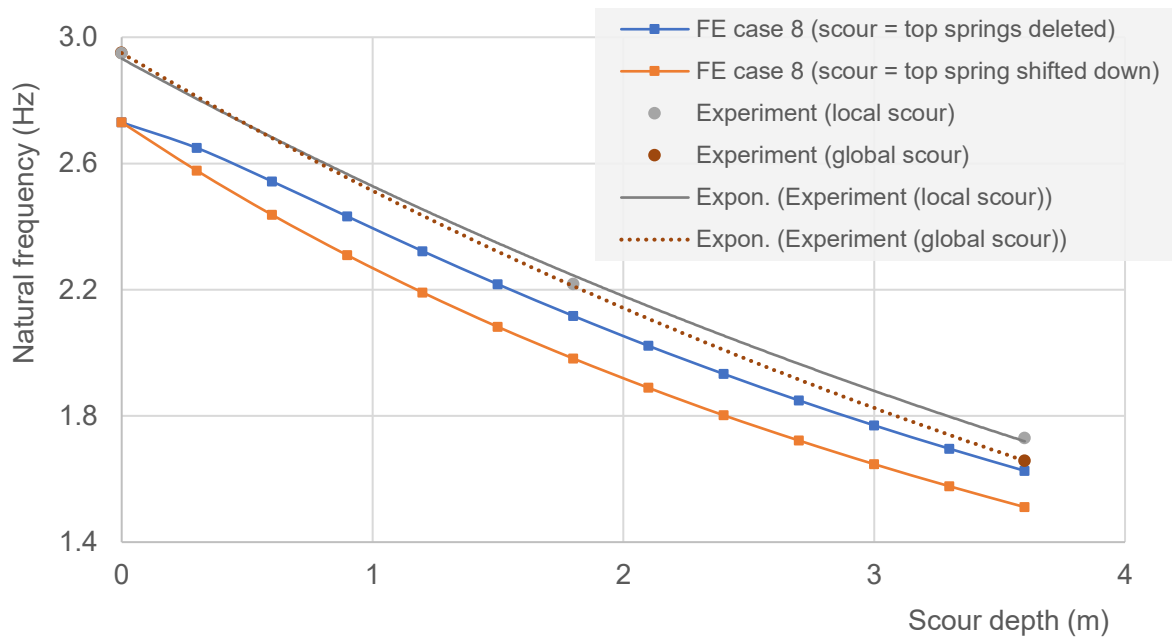


Figure 5.14 Comparison of natural frequency variation estimated by two simulation techniques and experimentally observed for local and global scour

5.4.2.2 Mode shapes variation due to local and global scour

The fundamental sway mode shape corresponding to the natural frequencies discussed above was also studied for different levels of simulated scour. Figure 5.15 shows the variation of mode shape with simulated cases of scour in the FE model and the experiment. All these mode shapes were normalised by the modal amplitude at the top of the pile bent. At +3 m above ground level, pairs of experimental modal amplitudes can be seen (i.e. two “*” or two “o” in Figure 5.15), which corresponds to amplitudes at two identical adjacent piles out of the four piles, and hence they should have the same amplitude for the fundamental sway mode shape. Any difference between the pair of amplitudes is, therefore, an error of the measurement. There was a difference of 2% between the pair of measurements in 1.8 m local scour case and a difference of 12% between the pair of measurements in a 3.6 m global scour case. Therefore, measurement errors of the modal amplitudes ranged 2 – 12% according to the experiment.

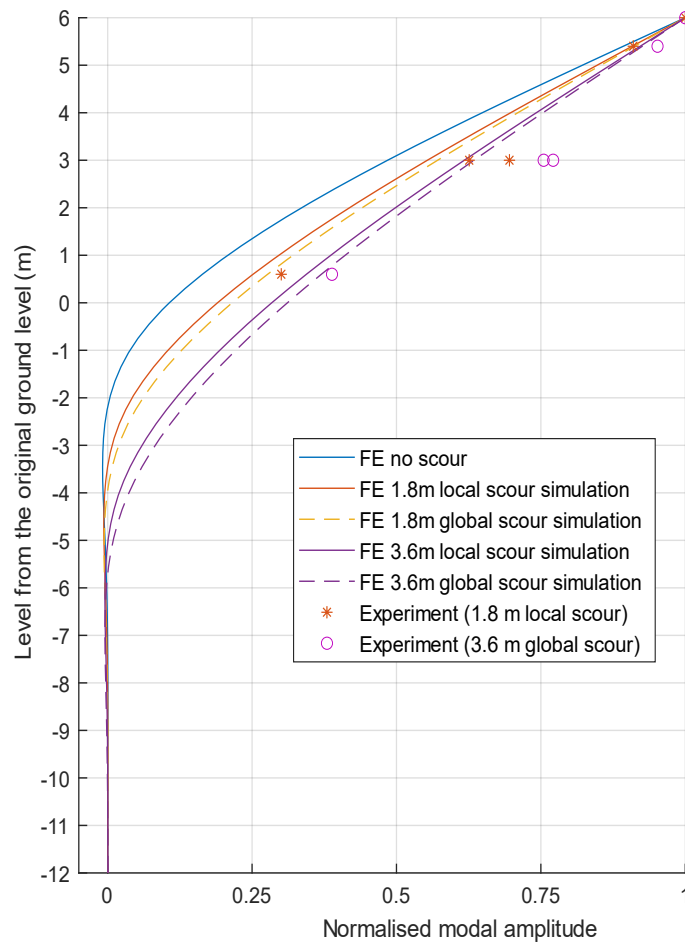


Figure 5.15 Change of mode shape with scour – FE simulation and experimental observations

Both the experiment and FE simulation results show the scour causes the normalised amplitudes to increase, with the highest increase (27% per 1 m) being near the original ground level. The global scour case shows higher normalised modal amplitudes than the local scour case (higher by 12% – 0% between 0 – 6 m above the original ground level). The experiment had only two scour cases providing reliable mode shapes, as discussed in Section 4.10.2. The normalised modal amplitudes estimated by FE for both these, 1.8 m and 3.6 m of scour, were similar in shape and reasonably similar (20% difference) in modal amplitudes to the corresponding experimental observations. The maximum difference between experimental and FE models lie at +3 m above the original ground level; it was thought that the low accuracy accelerometer (M2m4) used at this level have contributed to this error.

Based on these observations, the FE model and the two scour simulation techniques used have estimated the experimentally observed mode shape variation. Similar to the experimental observations, the FE model estimated the mode shape amplitudes to increase with scour depth. The increase in modal amplitudes due to increase of scour depth was sufficiently large (27% per 1 m scour depth) in comparison to the measurement errors observed (2 – 12%). However, the change in modal amplitudes between the local scour and global scour of the

same depth would have been difficult to capture (less than 12%), as it was in the same order of magnitude as the expected measurement errors (2 – 12%).

5.4.3 Extension of the calibrated pile bent FE model to represent Bridge 2

Although variations of the natural frequency and mode shape were observed with the FE model and the experiment for a pile bent foundation (Model 2), it does not entirely represent Bridge 2, which has the pile bent, bridge bearings and a simply supported deck. The bearings and the deck mass and stiffness may change the overall natural frequencies and mode shapes. Therefore, the FE model of the pile bent foundation, which was already calibrated for soil-structure interaction, was extended to represent Bridge 2, a simply supported bridge with deck and bearings, as shown in Figure 5.16.

The properties of Bridge 2 were previously described in Section 4.4.1. The Bridge 2 had a simply supported bridge deck. Each simply supported span has 8 Y1 precast beams, which were modelled using frame sections in CSiBridge software program. The deck slab of 0.2 m depth was modelled with area elements. Two simply supported deck spans connect to an abutment at one end and the middle at the other end. Each of these spans had a diaphragm beam at the top of the abutments and at the top of the pier. At the top of the abutments, a 1.85 m wide 1.05 m deep, transverse diaphragm beam was added to the deck using frame sections. A similar diaphragm beam with half the width was placed at the top of the pier such that the deck arrangement remains the same in Bridge 1, 2 and 3, as initially proposed in Section 4.4.1. The mass of the diaphragm beam was partially reduced to account for the mass of the overlapping composite beam slab sections of the deck, which would otherwise have contributed to double counting of mass at the overlapping locations.

The bridge abutment was assumed to be rigid. Each precast beam rests on an elastomeric bearing, which was modelled with link elements on top of abutments and the pier. The bearing stiffnesses were obtained from the literature; the bearing stiffnesses against horizontal translation, vertical translation and horizontal rotation were respectively 1.76 MNm^{-1} , 1.14 GNm^{-1} and 16.3 MNmrad^{-1} (Akogul and Celik, 2008). The bearings were assumed to be fixed against torsion. Eight link elements with these bearing properties were placed at each end of the spans, as shown in Figure 5.16.

Local scour was simulated by “spring deleting” method and global scour was simulated by “spring lowering” method, both of which were previously explained in Section 5.1 and verified against experimental results in Section 5.4.2.

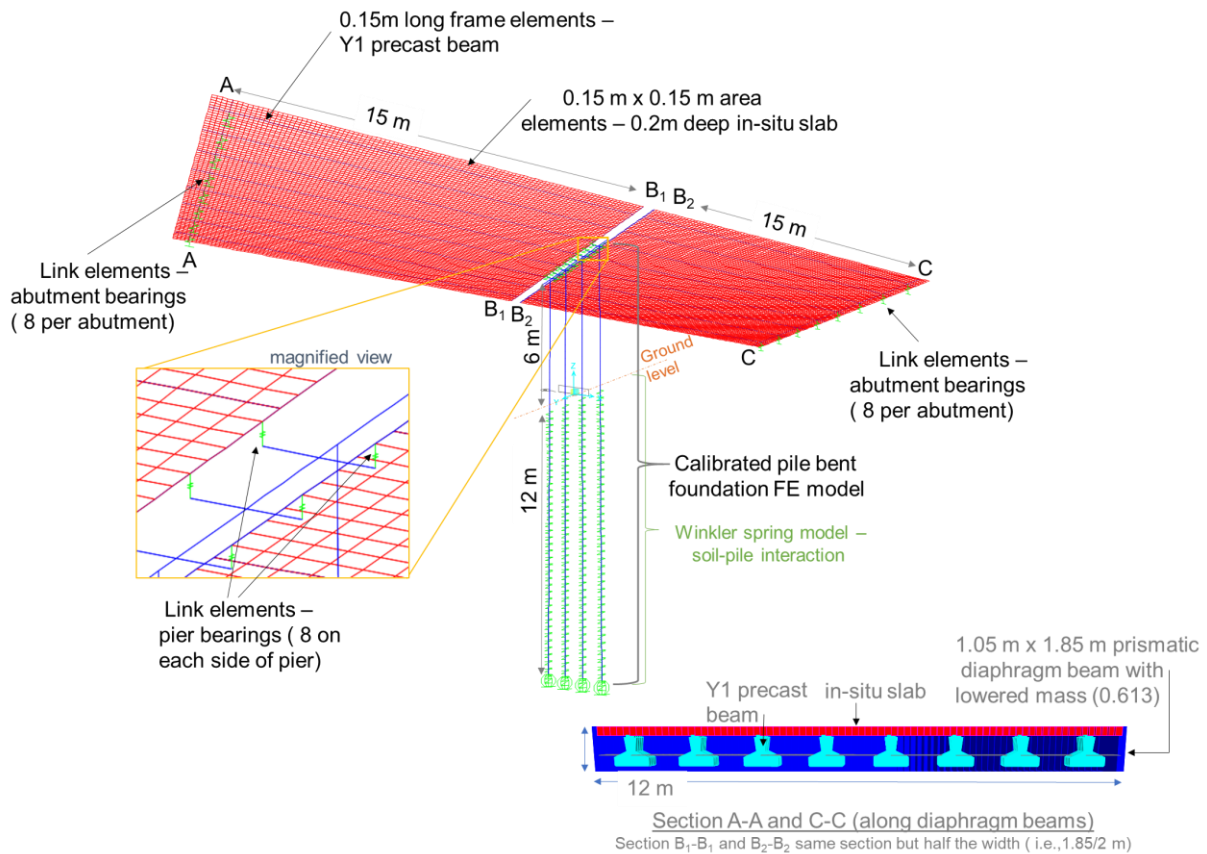


Figure 5.16 FE model developed to simulate simply supported bridge with deep pile bent in full-scale (Bridge 2)

5.4.3.1 Natural frequency variation of Bridge 2

Figure 5.17 shows the change in natural frequency due to local and global scour simulated by the FE model. For Mode 1 (longitudinal sway mode shape) the natural frequency sensitivity in the FE model of Bridge 2 was lower than what was previously estimated for the standalone pile bent FE modelling and the centrifuge experiment (Section 5.4.2). The local and global scour of 1 m of the simply supported bridge showed the first mode frequency sensitivities of 2% and 2.3%, respectively. The same scour cases in the previous standalone pile bent FE model showed 11% and 11.9% sensitivities, which were similar to the experimental observations. This suggests that the bearing translational stiffness and the mass of the deck that are involved in the simply supported bridge have caused a significant reduction in natural frequency sensitivity to scour. This is an undesirable condition for vibration-based scour monitoring since the fundamental (first) mode shape usually is easiest to capture with a high signal to noise ratio, especially using ambient vibrations (Wenzel and Pichler, 2005).

Nevertheless, several other higher-order modes have shown significant natural frequency sensitivities to scour. Highest overall sensitivity was shown by Mode 19 (pier and deck bending), which showed sensitivities of 8.1% and 9.7% for local and global scour of 1m. This mode showed a gradually rising sensitivity until 1.5 m of scour depth that was followed by a significantly higher and uniform sensitivity. The transverse modes generally showed slightly

higher natural frequency sensitivities than their longitudinal counterparts. Mode 2, transverse sway mode, has 4.2% and 4.7% natural frequency sensitivity for local and global scour. Mode 6, pier only transverse sway mode, has 6.4% and 7.1% frequency sensitivities. The pier only longitudinal modes showed 4.2%, and 4.7% sensitivities for local and global scour. These higher-order modes could potentially aid as scour monitoring indicators.

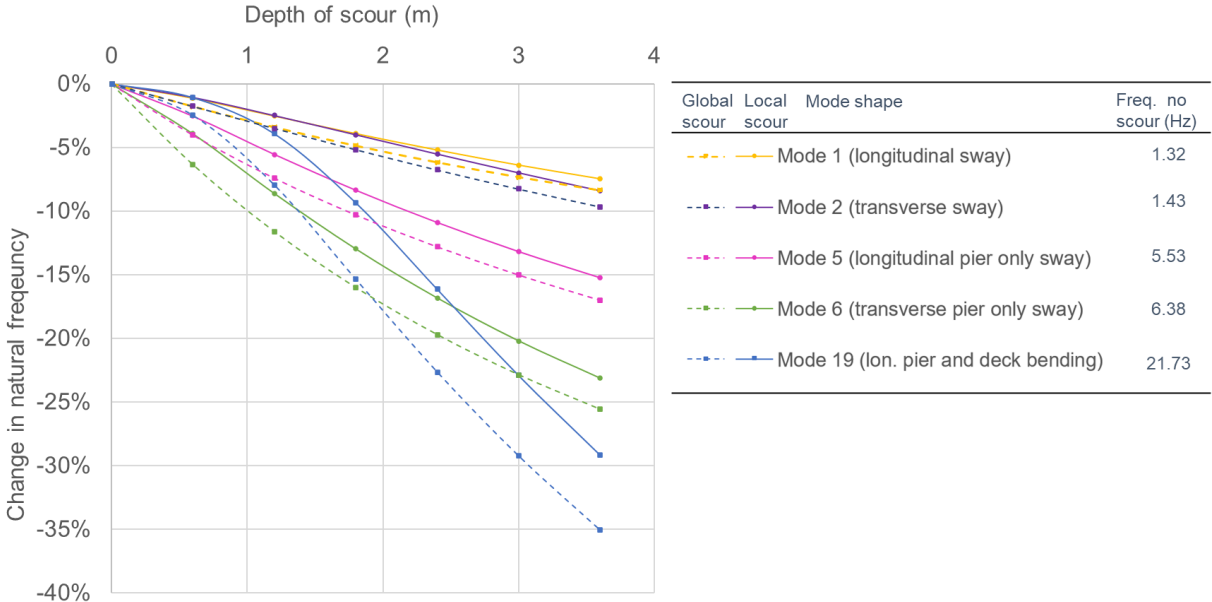


Figure 5.17 Change in frequency with scour depth for the simply supported bridge with deep pile bent foundation (Bridge 2) estimated by the FE model

5.4.3.2 Mode shape variation of Bridge 2

Figure 5.18 shows the variation of three longitudinal direction mode shapes due to simulated local and global scour. All mode shapes have been normalised by the maximum modal amplitudes. Mode 1 (Figure 5.18(a)) shows the highest modal amplitude on the bridge deck and some deformation of the pier bearings. As scour depth increased, the modal amplitudes of the bridge pier have significantly increased (8% amplitude increase near the top of the pier per 1 m of local scour). This behaviour may be due to the fact that increased scour depths result in a smaller relative stiffness of the soil-pier system with respect to the stiffness provided by the deck and bearings; thus, increased scour depths result in relatively higher modal amplitudes in the pier and lower modal amplitudes in the deck and bearings. There was a difference of 3% in modal amplitudes between local and global scour of the same depth, but this difference was too small compared to the measurement uncertainties (2 – 12% Section 5.4.2.2).

The Bridge 2 pier vibration in the Mode 5 (Figure 5.18(b)) was similar to that estimated for the standalone pile bent foundation (Section 5.4.2.2), though the boundary conditions in Bridge 2 and the standalone foundation were not similar and thus some differences were expected. The FE simulation shows an increase in the modal amplitude with increased local scour depth,

especially near the mid-height level of the bridge pier (9% modal amplitude increase per 1 m of scour depth at +3 m above the ground level). Global scour has caused only a slight (about 1% per 1 m scour at +3 m above the ground level) increase in modal amplitude than the local scour of the same depth.

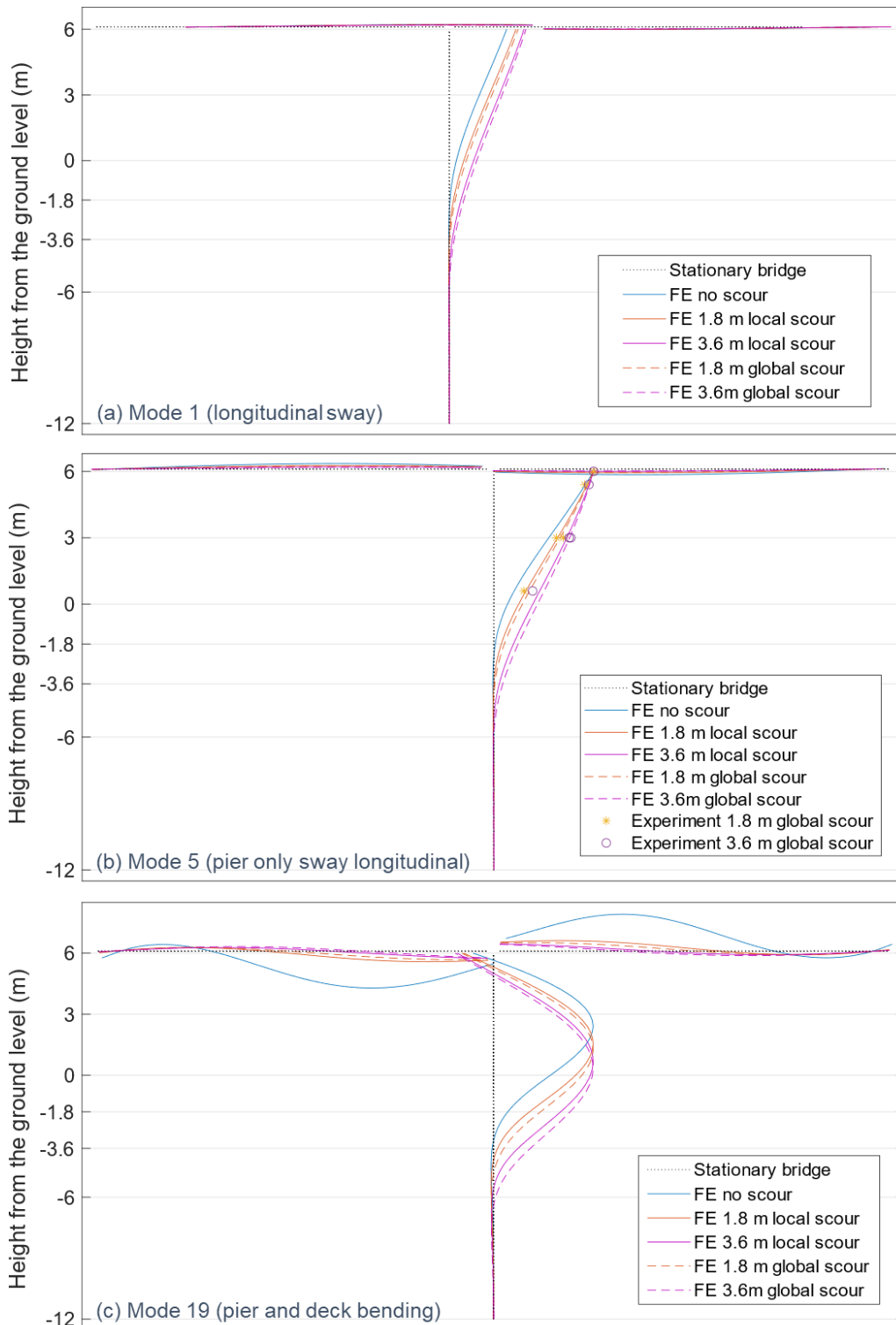


Figure 5.18 Change in mode shape with scour depth for Bridge 2 (two-span simply supported bridge with piled foundation)

Mode 19 (Figure 5.18(c)) is a bending mode with significant vibration of the deck when no scour was present. However, the deck vibration diminished with increased scour. This phenomenon may also be explained by the relative stiffness effect, as explained for Mode 1. The relative stiffness of the pier with respect to the deck reduces with increased scour, and therefore the pier has higher modal amplitudes than the deck with increased scour.

In three of these modes of vibration, the change in mode shape of the pier showed potential to indicate the change of scour depth. Mode 1 and Mode 5, in particular, have the changes in modal amplitudes due to scour limited to the pier, thus, in a multi-span bridge, these two modes may potentially help localise scour depth to the piers that are undergoing scour.

5.5 Numerical modelling of full-scale Bridge 1 (integral bridge with pile bent foundations) using the experimental results for small-scale Model 1 (integral bridge with pile bent foundations)

This section attempts to develop a calibrated numerical model for full-scale Bridge 1 by following the method illustrated in Figure 5.2. First, a numerical model was created for the small- and full- scale bridge models (Model 1 and Bridge 1: integral bridge), and it was compared with the fixed base experimental results to verify the accuracy of the scaling. Second, the scaling-verified full-scale numerical model of Bridge 1 was included with soil-structure interaction and it was calibrated against the observed centrifuge test results. The soil-structure model previously calibrated for pile bent foundation of Bridge 2 was adopted here in Bridge 1 since both these bridges have similar foundations. Finally, this numerical model of Bridge 1 was analysed to identify numerical scour simulation techniques for local and global scour cases and to assess the potential of vibration-based scour monitoring.

5.5.1 Numerical modelling of the Integral bridge with a fixed base in small- and full-scales

As explained in Section 4.4, the small-scale aluminium Model 1 in the centrifuge container aimed to simulate the behaviour of a full-scale reinforced concrete integral bridge. Due to the change of material properties in the two scales, only certain selected properties could be scaled, and it may have influenced the vibration behaviour. Therefore, it was essential to verify the accuracy of the scaling, and this was done using FE models at both small- and full-scales. As a fixed base experiment involves only the structural properties (i.e. no soil-structure interaction), it was an ideal experiment to simulate in both scales and compare the natural frequency estimates to verify scaling.

The numerical FE model for the small-scale fixed base Model 1 experiment is shown in Figure 5.19 and its experimental setup is shown in Figure 4.12. The properties of Model 1 were

previously given in Section 4.4.2. The 12.7-mm-deep rectangular slab (aluminium plate) deck of Model 1 was modelled in FE by 2.5 mm x 2.5 mm shell area elements having the same depth (12.7 mm). The deck spans of 250 mm and width of 100 mm were also maintained to be the same as the real Model 1. All piles were modelled using 5 mm long frame elements. The pier piles were 12.7 mm outer diameter circular hollow piles with 0.9 mm; the abutment piles were 9.0 mm outer diameter with 0.9 mm wall thickness. The original ground level before scour was set to give 100 mm of exposed height for the piles when no scour was present. Young's Modulus of 70 GPa and a density of 2700 kgm⁻³ were used for all sections (deck and piles). The mass of the piezoelectric actuator and the accelerometers together weighing 0.5 kg were added as a concentrated mass at the middle of the plate deck.

The full-scale Bridge 1 was also modelled with FE, as shown in Figure 5.20. The piles were modelled with 0.3 m long frame elements. The pier and abutment piles were 0.74 m and 0.56 m in diameters, respectively. Each pier and abutment has four piles at 3 m spacing and a 12 m long diaphragm capping beam at the top. The diaphragm beam was modelled with 0.15 m frame elements with cross-section properties of 1.05 m depth and 1.85 m width. The composite deck was modelled using two different elements for the Y1 beams and top slab. The Y1 beams were modelled using 0.15 m long frame elements over the full length of the bridge deck. Eight such precast beams were placed at their respective locations (i.e. at 1.5 m spacing). The top slab was modelled with area elements each 0.15 m x 0.15 m in plan and 0.2 m in depth. Such area elements were provided over the full deck of 12 m width and 31.2 m length. The required offsets were provided to the deck elements in the software to obtain the composite element properties. Where the composite beam crosses the diaphragm beams (sections A – A, B – B, C – C) in Figure 5.20, there could be double counting of mass and, therefore, to account for the mass of the composite beam, the diaphragm beam mass was reduced to 0.613 times its original value. This FE model was initially assigned with fixities for the bottom 12 m of all piles, to simulate the fixed based test with the aim of replacing these later with a Winkler spring model. The reinforced/prestressed-concrete (C40 concrete) modulus of elasticity of 35 GPa and a bulk density of 2550 kgm⁻³ were used for the numerical FE model.

Scour in these FE models was simulated by releasing the fixities down to the level of scour depth in any selected bridge pier or abutment, similar to how scour was simulated in the fixed based experiments. The natural frequencies of the models for different scour cases are shown in Figure 5.20. The small-scale natural frequencies have been converted to the full-scale equivalent values by applying the scale factor (1/N Table 4.2). The FE models of the small-scale and full-scale bridges show similar frequency estimates and variations, with differences below 3%. This suggests the assumptions related to scaling were reasonable. Further, it suggests the aluminium integral bridge model of 250 mm spans was able to simulate the dynamic behaviour of the concrete integral bridge with 15 m spans.

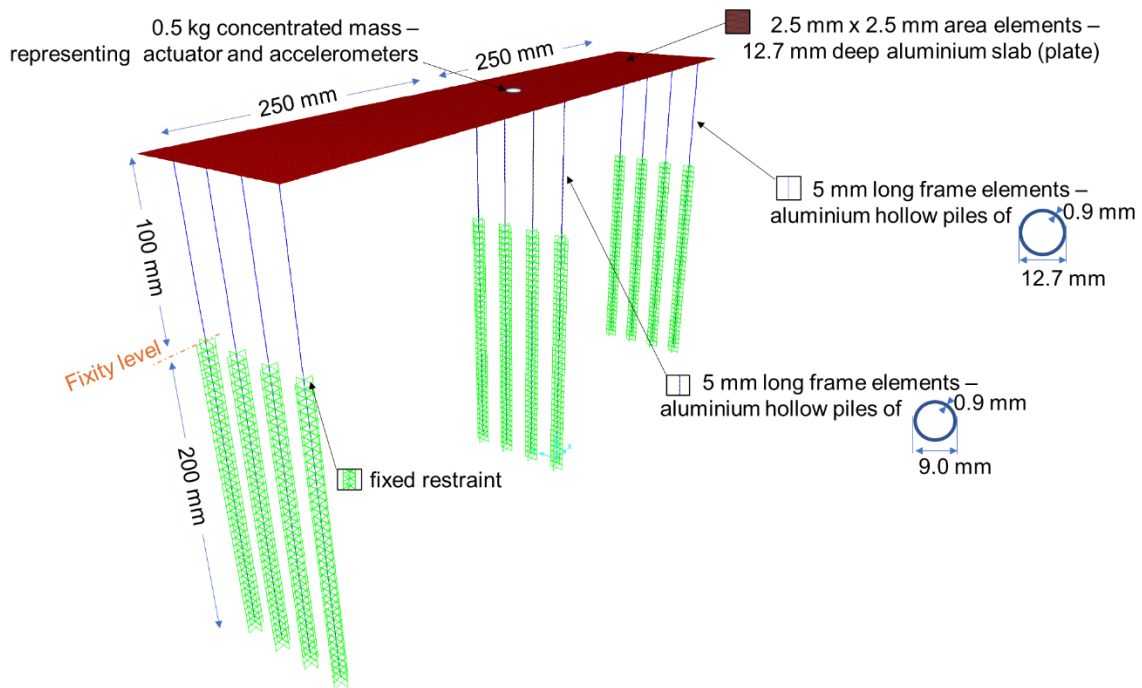


Figure 5.19 FE model developed to represent small-scale Model 1 (two-span integral bridge with piled foundations) with a fixed base

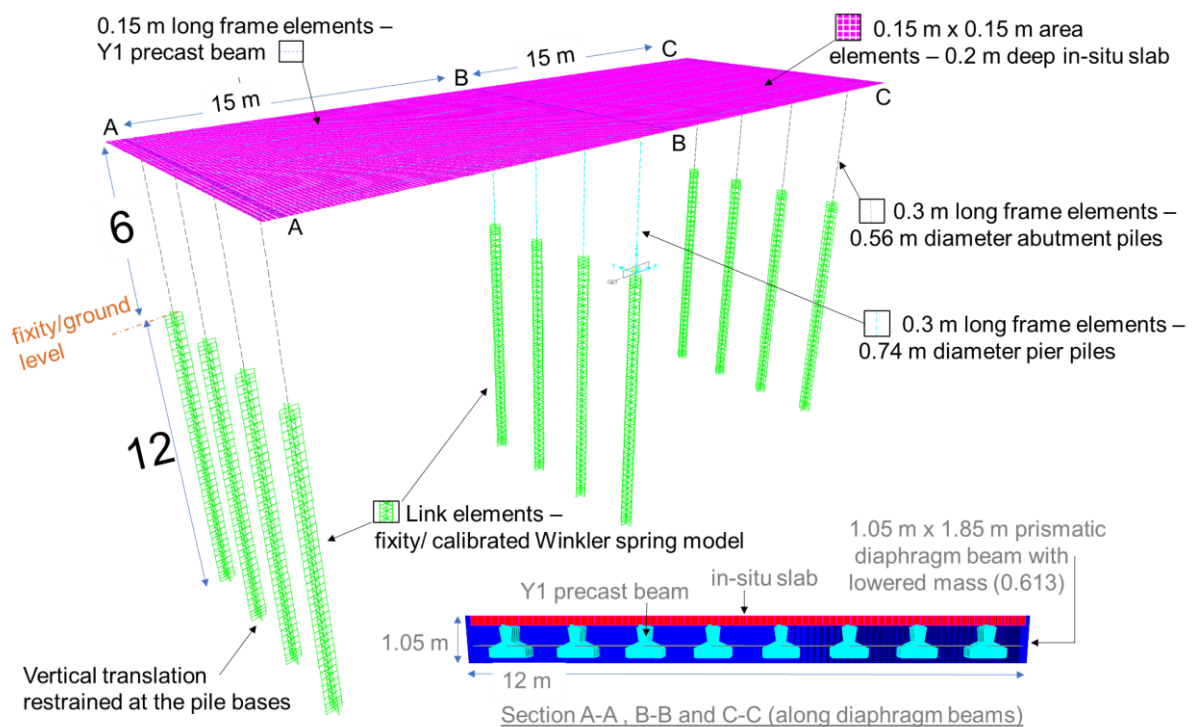


Figure 5.20 FE model developed to represent full-scale Bridge 1 (two-span integral bridge with piled foundations) with either fixed base or soil-structure interaction

As shown in Figure 5.21, the FE model estimates of natural frequency for the fixed base were higher than the corresponding experimental observations, which is similar a behaviour observed for Model 2 (Section 5.4.1). This behaviour was expected since the ideal fixity

assumed in the numerical FE model would not be present in real life. A real-life experiment with clamps provides a lower stiffness than the ideal fixity (i.e. infinite stiffness) and therefore results in lower natural frequency. The magnitude of the difference between experimental and FE estimates reduces with increased scour, as was also observed for Model 2. This behaviour could be assumed to be due to the fact that clamps provided a finite amount of fixity, and its relative stiffness magnitude became higher with increased scour as the bridge model becomes more flexible for longer pile heights.

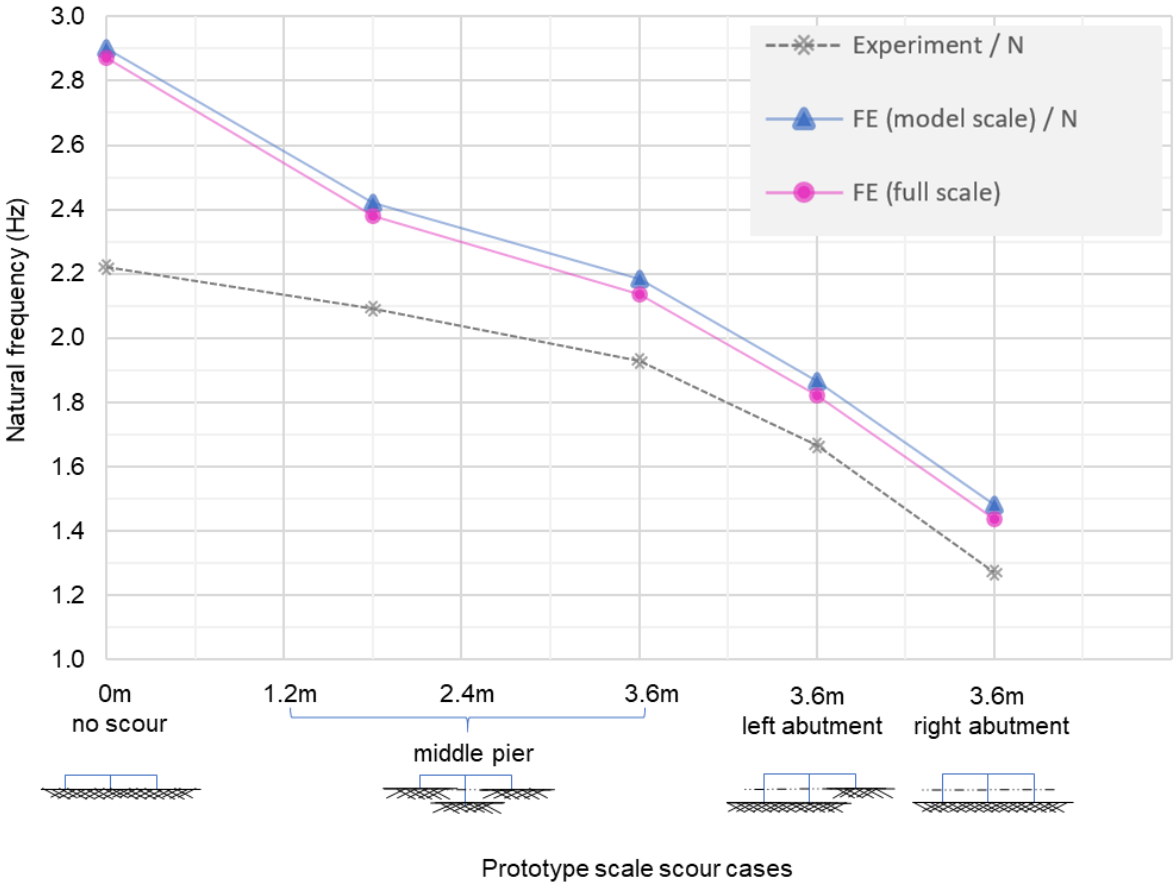


Figure 5.21 FE models with fixed base simulating scour at all different scales

5.5.2 Inclusion of soil-structure interaction to the full-scale Bridge 1 numerical model

This FE model of the full-scale bridge verified for accurate scaling was combined with the Winkler spring arrangement calibrated for the standalone pile bent of Bridge 2 in Section 5.4.2. The pier piles of the integral bridge (Bridge 1) are of the same arrangement and size as this standalone pile bent foundation of Bridge 2. The abutment piles of Bridge 1 also have the same pile arrangement but with smaller diameter piles than the pile bent of Bridge 2. As explained in Section 5.2.1, the lateral spring stiffness used here is independent of the pile diameter according to Kloeppe and Glock, (1970) equation. Therefore, the same spring stiffness profile was considered applicable to both pier piles and abutment piles. This calibrated lateral spring

arrangement of the pile bent is shown in Figure 5.12 as case 8, and it was obtained using (Seed and Idriss, 1970) and (Kloeppe and Glock, 1970). The Bridge 2 FE model with Winkler spring model simulated the effects of local scour by using the “spring deleting” method and global scour by “spring lowering” method, explained previously in Section 5.1.

5.5.2.1 Natural frequency variation of Bridge 1

The natural frequency variations estimated by the numerical scour simulation is shown in Figure 5.22. When there was no scour, the FE model estimated the natural frequency to be remarkably close (3% difference) to the experimental observations. Both FE model scour simulation techniques for local and global scour have shown similar sensitivities to that observed in the experiment. Average frequency sensitivity for 1 m of local scour at the middle bridge pier was 4.6% in the experiment, while it was 5.1% and 5.6% for FE with the spring deleting method and the spring lowering method, respectively. For 1 m of local scour at the abutments, the average frequency sensitivity was 3.7 – 3.8% for the experiment and the spring deleting method gave 3.2 – 4.1%, and the spring lowering method gave 3.5 – 4.7%. The overall frequency sensitivity experimentally observed for 3.6 m of local scour and 3.6 m of global scour was 37.8% and 40.0%, respectively. The FE models showed changes of 38.5% for 3.6 m scour simulated by spring deleting method, 42.4% for 3.6 m of scour simulated by spring lowering method. Therefore, the spring deleting method has closely simulated the effects of local scour, and the spring lowering method has closely simulated the effects of global scour, as expected.

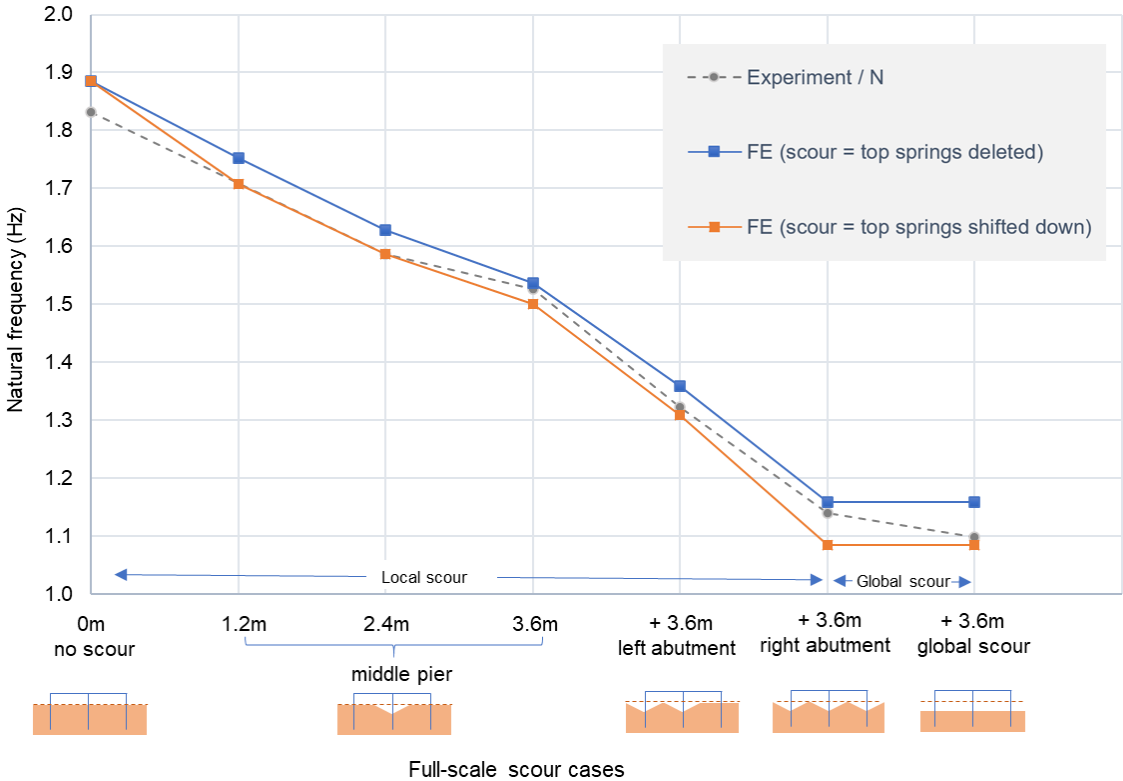


Figure 5.22 Scour simulation with the FE model and the centrifuge experiment

5.5.2.2 Mode shape variation of Bridge 1

Figure 5.23 shows the mode shapes of Bridge 1 (with no scour) estimated by the FE model and the experiment. The FE model provided a fine spatial resolution for the mode shape, whereas the experimental mode shape was measured at only ten locations by seven horizontal accelerometers and three vertical accelerometers. Although the experimental mode shapes drawn using straight lines between the measured points, the real mode shape in the experiment would be curved (similar to FE estimate) rather than straight between the measurement points, as expected for a typical continuous element.

The mode shape amplitudes at all foundations (pier/abutments) differ significantly between the experimental observations and the corresponding FE estimates. This means there is some inaccuracy in either the FE model or the experimental measurements. The properties of the FE model were rechecked and was confirmed to be accurate. Further, the FE model accurately predicted the natural frequencies. The mode shape estimated by FE model showed no significant difference between the amplitudes at the same point, as expected, but the experimental mode shape showed a sudden change of amplitudes at the top of the middle pier, where the amplitudes at the bridge deck and the amplitude at the top of the pier were significantly different, although they should be the same. The modal amplitudes at the top of the bridge deck were measured by piezoelectric accelerometers, while the modal amplitudes at all pier and abutment foundations were measured by MEMS accelerometers. Therefore, it was assumed that the calibration factors applicable to the MEMS accelerometers were overestimated. Therefore, all amplitudes found by MEMS accelerometers were reduced (by 0.56 times) such that the two modal amplitudes at the same level at the top of the pier were equal. After this correction, there was a better match between the experimental and FE derived mode shapes, as shown in Figure 5.23.

The experimental mode shape at +3 m level of the middle pier was measured by a pair of accelerometers (“x” and “x” or “∇” and “∇” symbols in Figure 5.23), which were on two out of the four adjacent piles of the pier foundation. Though these amplitudes of adjacent piles should be the same for the sway mode shape observed here, they were found to be different, perhaps due to low signal to noise ratio of the type of accelerometers used at that level (M1m3 and M1m6). This implies that there was significant uncertainty (49%) involved when attempting to derive mode shapes experimentally using M1m3 and M1m6 accelerometers, although the lower-noise accelerometers used at the other locations may provide a lower uncertainty. Any change of mode shape due to scour should be more than these uncertainties to reliably detect the scour case.

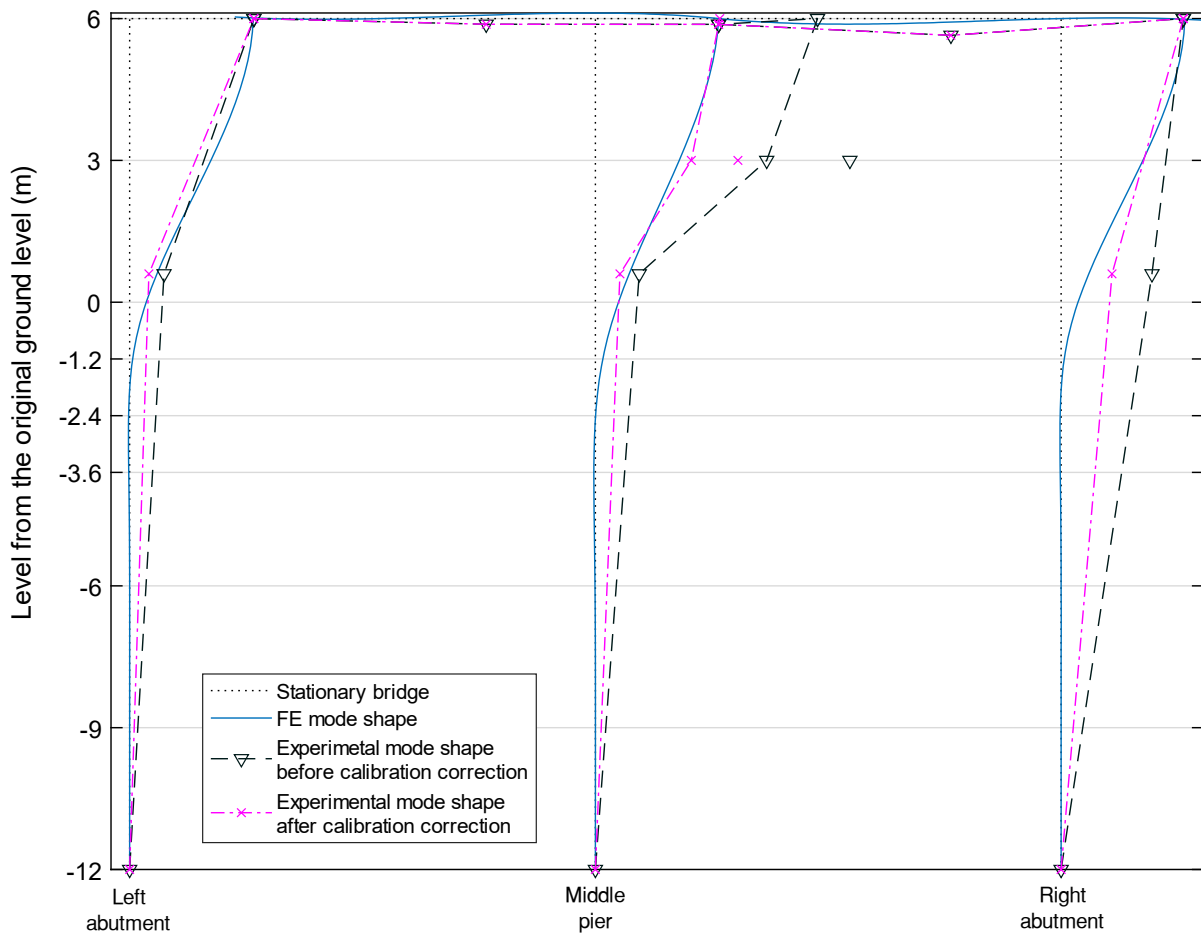


Figure 5.23 Comparison of the mode shapes estimated by the FE and the experiment for the case where there was no scour present

The experimental mode shapes corrected for MEMS accelerometer outputs were compared with the FE estimates of different scour cases. At each scour level, the two scour simulation techniques were compared (i.e., the spring deleting method simulating local scour and the spring lowering method simulating global scour).

Figure 5.24 shows the change of modal amplitudes for local scour at the middle bridge pier. The mode shapes given by FE match closely with the corrected experimental observations, though the FE model estimates a greater change of mode shape than the experimental observations. The amplitudes at +3 m level of the pier show high variability. As discussed previously, this is potentially due to low signal to noise ratio of the type of accelerometers used at that level.

Similar to the experimental observations (Section 4.10.1), the FE model also shows that local scour at a foundation causes mode shape changes only near that foundation. During the course of three steps of scour simulation used at the pier using the spring deleting method (local scour) and the spring lowering method (global scour), only the modal amplitudes at that pier has changed while almost no change occurred at the other foundations or at the deck. Further, the largest change of amplitude was seen near the ground level (39% per 1 m of local

scour), where the effect of the loss of soil due to scour may have been directly affected the local stiffness. According to the FE model, the change of modal amplitude at mid-height of the pier (+3 m above the original ground level) was 6% per 1 m of local scour depth. The mode shapes show a sway mode shape with almost zero amplitude -1.2 to -6 m below ground. This level of zero modal amplitude seems to lower as scour depth increases at a foundation. The FE models show that the spring lowering method causes a higher increase in modal amplitude (by 2.5% at + 3 m above the original ground level per 1 m of scour) than the spring deleting method.

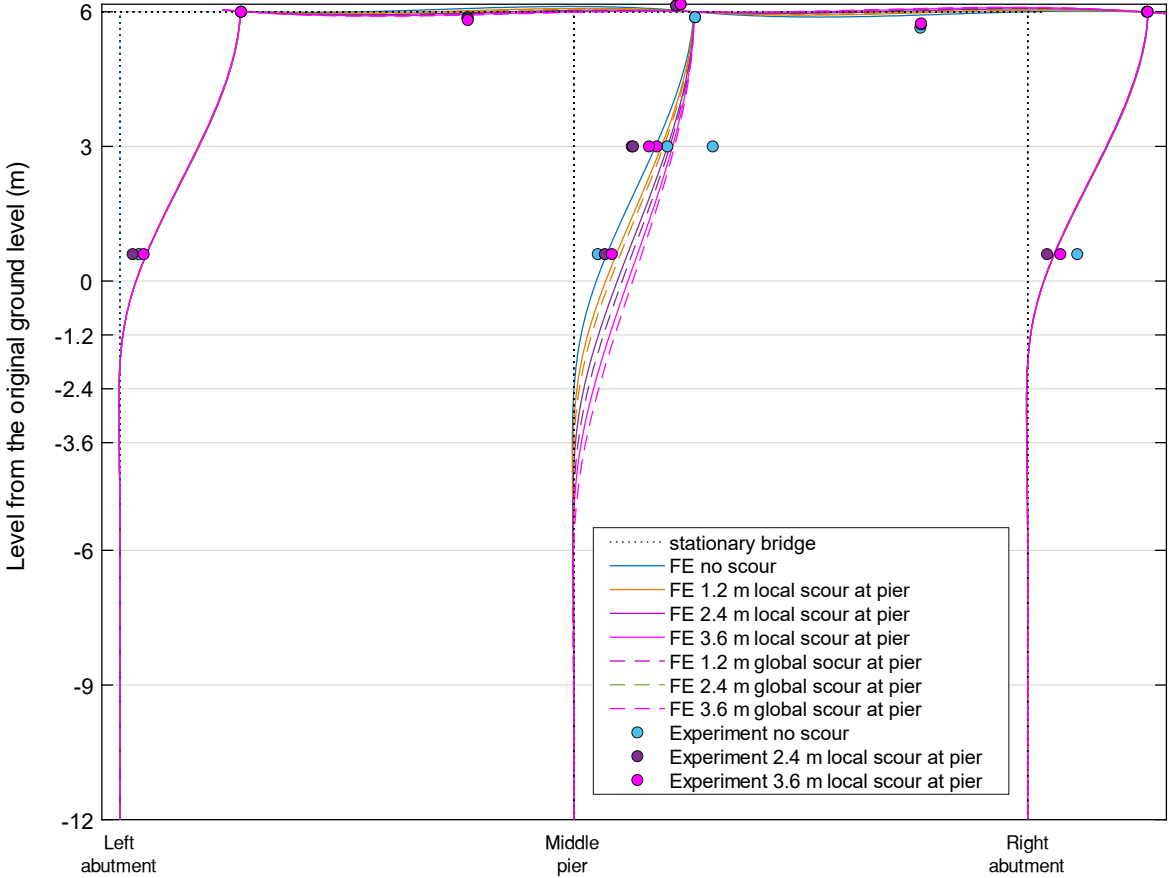


Figure 5.24 Mode shape variation with pier scour (FE estimates vs experiment observations).

The mode shape variation for scour cases involving abutments are shown in Figure 5.25. The experimentally observed modal amplitudes match closely with the FE estimates, except for several outliers previously discussed in Section 4.10.1. All FE simulations and the experimental mode shapes without the outliers support the previous finding that local scour at a foundation causes modal amplitude to change mainly near the foundation. When scour was simulated at the left abutment in the FE model using the two simulation techniques for local and global scour, only the left abutment changed in mode shape while the other foundations showed almost no change of mode shape. Similar behaviour was seen when local scour was

simulated in the right abutment. This important finding indicates that any foundation undergoing local scour can be identified by studying the local changes in mode shapes.

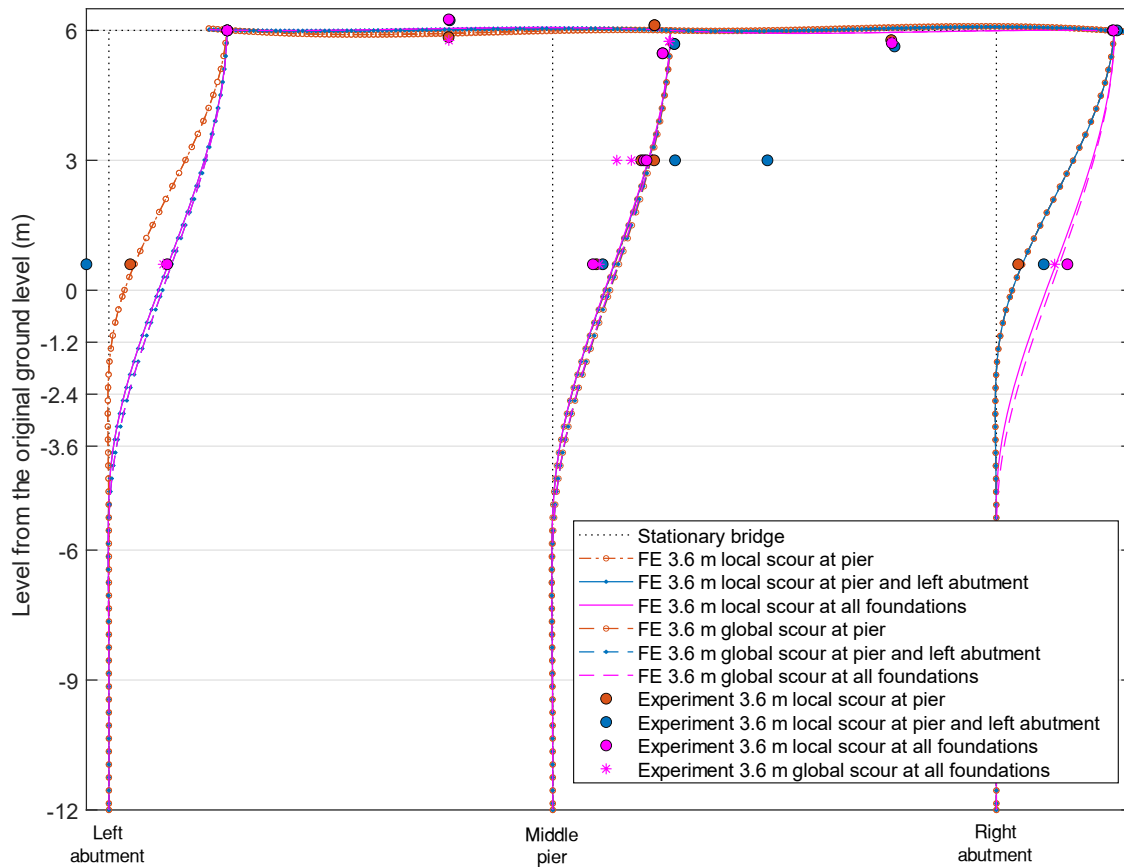


Figure 5.25 Mode shape variation for abutment scour cases (FE estimates vs experiment observations).

As shown in Figure 5.25, scour simulation in with “spring lowering” method (global scour) has resulted in higher modal amplitudes than the amplitudes estimated by the “spring deleting” method (local scour). This higher modal amplitude was expected as the global scour results in a lower soil stiffness in the bridge soil system compared to a local scour case of the same depth. However, the difference in mode shape between local and global scour cases was not significant (less than 0.6% at mid-height of the pier per 1 m of scour) compared to the change in amplitude due to increase of the scour depth (7% of modal amplitude change at +3 m at the mid-height of the left abutment per 1 m depth of scour). Similar to the FE estimates, the experiment has not shown much variation between local and global scour cases.

Both the local scour at the pier and the abutment show the modal amplitude increase was highest near the ground level. Therefore, sensor placement to capture this variation should be as close to the ground level as possible on the pier. However, the accelerometers should ideally be above the water level in order to maintain the advantages of this technique, such as easy installation and durability.

Overall, the Bridge 1, the integral bridge with pile foundations, showed significant changes in both fundamental natural frequency and mode shape due to the effects of local and global scour.

5.6 Macro and Winkler spring element soil-structure interaction representation for shallow pad foundation of Bridge 3

The Bridge 3 has a shallow pad foundation, and thus this section will create a spring element representation to simulate the effects of soil-shallow pad foundation interaction. A shallow pad foundation of a bridge has a stub column and a pad footing at the base, both of which are in contact with soil. Therefore, soil-structure interaction of both these elements has to be incorporated into the FE model. However, many spring-based shallow foundation-soil interaction models available in the literature tend to ignore the embedment of the pad footing (API, 2002; Harden et al., 2005; Chatzigogos, Pecker and Salencon, 2008). These consider a pad on the surface of the soil, and thus only the soil-structure interaction of the base of the pad with soil is considered. The models that consider the embedment consider the soil structure interaction of a pad footing element without a stub column. Therefore, two separate spring-based models were used to model soil-stub column interaction and soil-pad footing interaction. As shown in Figure 5.26, the soil-stub column interaction was idealised by the Winkler spring model, as explained in Section 5.2, while the soil-pad footing interaction was idealised by using a macro element spring model.

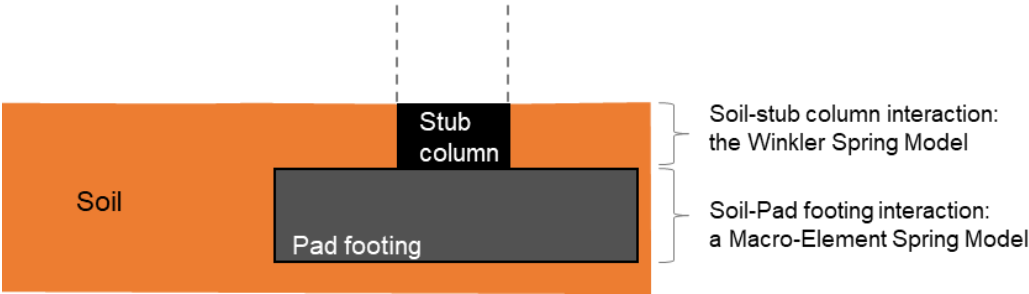


Figure 5.26 Types of soil-structure interaction models used to represent a pad foundation

A macro element spring model idealises the whole pad footing-soil interaction by a single element (Chatzigogos, Pecker and Salencon, 2008). For the scope of this research, only the linear undamped soil-structure interaction was considered. In such a setting, the microelement model element has six mutually independent springs. As shown in Figure 5.27, three translational springs provide the overall translational stiffness of the pad in longitudinal (x), transverse (y) and vertical directions (z). Three rotational springs provide stiffnesses against bending about both x and y axes and torsion about the z-axis. Two empirical spring stiffness estimates, Gazetas Method and API method will be discussed in the following section.

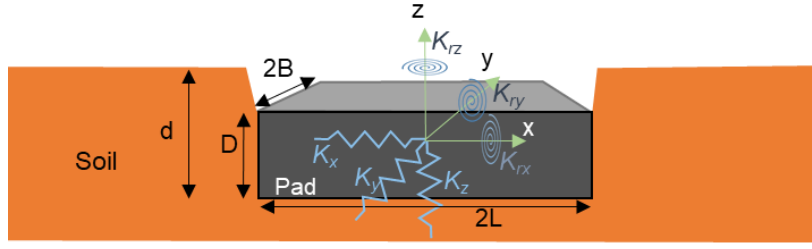


Figure 5.27 Micro-element model representation of a soil-pad footing interaction

5.6.1 Gazetas Method for determining the stiffnesses of the macro element model for modelling soil-pad footing interaction

Gazetas (1991) provides empirical equations for stiffnesses for microelement representation of an embedded shallow foundation that is rigid but massless. As shown in Figure 5.27, consider a pad foundation of $2L$ in length, $2B$ in width, D in sidewall depth, and d in the embedment. Its translational stiffnesses K_x, K_y and K_z and the rotational stiffness K_{rx}, K_{ry} and K_{rz} , are given as follows.

$$K_z = \frac{2GL}{1-\nu_p} (0.73 + 1.54X_a^{0.75}) \left[1 + \frac{1}{21} \left(\frac{d}{B} \right) (1 + 1.3X_a) \right] \left[1 + 0.2 \left(\frac{A_w}{A_b} \right)^{2/3} \right]$$

$$K_y = \frac{2GL}{2-\nu_p} (2 + 2.5X_a^{0.85}) \left[1 + 0.15 \left(\frac{d}{B} \right)^{0.5} \right] \left\{ 1 + 0.52 \left[\left(\frac{h}{B} \right) \left(\frac{A_w}{L^2} \right)^{0.4} \right] \right\}$$

$$K_x = \left[K_y - \frac{0.2GL}{0.75-\nu_p} (1 - B/L) \right] \left[\frac{K_y}{\frac{2GL}{2-\nu_p} (2 + 2.5X_a^{0.85})} \right]$$

$$K_{rx} = \frac{GI_{bx}^{0.75}}{1-\nu_p} \left(\frac{L}{B} \right)^{0.25} \left[2.4 + 0.5 \left(\frac{B}{L} \right) \right] \left\{ 1 + 1.26 \left(\frac{D}{B} \right) \left[1 + \left(\frac{D}{B} \right) \left(\frac{D}{d} \right)^{-0.2} \left(\frac{B}{L} \right)^{0.5} \right] \right\}$$

$$K_{ry} = \frac{3GI_{by}^{0.75}}{1-\nu_p} \left(\frac{L}{B} \right)^{0.15} \left\{ 1 + 0.92 \left(\frac{D}{L} \right)^{0.6} \left[1.5 + \left(\frac{D}{L} \right)^{1.9} \left(\frac{D}{L} \right)^{-0.6} \right] \right\}$$

$$K_{rz} = 3.5GI_{bz}^{0.75} \left(\frac{B}{L} \right)^{0.4} \left(\frac{I_{bz}}{B^4} \right)^{0.15} \left\{ 1 + 0.4 \left(\frac{d}{D} \right)^{0.5} \left(\frac{B}{d} \right)^{0.6} \left[\frac{D(B^3+L^3)+3BLD(L+B)}{BL(B^2+L^2)} \right] \right\} \times T_{tre}$$

$$T_{tre} = 1 + 0.5 \left(\frac{d}{B} \right)^{0.1} \left(\frac{B^4}{I_{bz}} \right)^{0.13}$$

where G is the shear modulus of soil, A_b is the area of the bottom of the pad, ν_p is the Poisson's ratio of the soil, A_w is the sidewall contact area and $X_a = A_b/4L^2$. Additionally, I_{bx} , I_{by} and I_{bz} are second moment of areas of the bottom of the pad about x, y and z axes, respectively.

While these equations have considered the embedment of the foundation, note that the soil contact with the top of the pad has been ignored. Additionally, the static stiffness has to be multiplied by a dynamic stiffness coefficient to obtain the stiffness under dynamic input excitations. This dynamic stiffness coefficient is dependent on input excitation frequency but is unity for low-frequency input excitations. Assuming low-frequency input excitation, the stiffnesses under dynamic conditions were taken as equal to the static stiffness give here. This

assumption may be valid for low-frequency modes of vibrations, which are the focus of this research.

5.6.2 API method for determining the stiffnesses of the macro element model for modelling soil-pad footing interaction

The American Petroleum Institute (API) provides deformation-force relationships for translation and rotation of a shallow foundation in all degrees of freedom (API, 2002). These equations were rearranged as translational stiffness = force/deformation and rotational stiffness = moment/rotation to obtain macro element stiffnesses. As shown in Figure 5.27, consider a pad foundation of $2L$ in length and $2B$ in width. The translational stiffnesses K_x , K_y and K_z and the rotational stiffness K_{rx} , K_{ry} and K_{rz} , are given as follows.

$$K_z = \frac{4GR}{1 - \nu_p}$$

$$K_x = K_y = \frac{32(1 - \nu_p)GR}{7 - 8\nu_p}$$

$$K_{rx} = K_{ry} = \frac{8GR^3}{3(1 - \nu_p)}$$

$$K_{rz} = \frac{16GR^3}{3}$$

where R is the radius of the pad, G is the shear modulus of soil, ν_p is the Poisson's ratio of the soil. These equations do not consider the embedment effect and are for a circular footing. API (2002) states that the equations are approximately valid for a square base of equal area. Further, these equations are for short term static deformations but were considered for dynamic behaviour, assuming that static and dynamic stiffnesses are similar for low-frequency input excitations, as explained in Gazetas Method.

5.7 Numerical modelling of full-scale Bridge 3 (simply supported bridge with a shallow pad foundation) using the experimental results for small-scale Model 3 (shallow pad foundation)

This section attempts to develop a calibrated numerical model for the full-scale Bridge 3 (simply supported bridge with shallow pad foundation) by following the method illustrated in Figure 5.2. First, numerical models were created for the standalone shallow pad foundation (Model 3) in both small-scale and full-scale, and these numerical models were calibrated against the corresponding fixed-base experimental results, with the aim of verifying the accuracy of scaling. Second, the fixed base support condition of this verified full-scale numerical model was replaced with a macro element and Winkler spring model representing soil-structure

interaction as discussed in Section 5.6, and this numerical model was calibrated against the results of the centrifuge experiment. Scour simulation techniques were also identified to simulate the experimentally observed effects of local and global scour at these standalone foundations. Finally, this calibrated numerical model of the full-scale standalone foundation was included with a simply supported bridge deck to create the numerical model of full-scale Bridge 3, and its vibration parameters were assessed for the potential to indicate scour.

5.7.1 Numerical modelling of the shallow pad foundation with a fixed base in small- and full-scales

Initially, a fixed based experiment was modelled numerically, without the presence of soil-structure interaction, to confirm the accuracy of scaling. Figure 5.28 shows the fixed based experiment and the corresponding FE models of the shallow pad foundations that simulate the small- and full-scale behaviour. The pier column was fixed at the base during the experiment, and therefore, only the pier column was modelled with FE. Frame elements, having the properties of small-scale (12.7 mm x 32.5 mm cross-section) and full-scale (0.7 m x 1 m), were adopted for the respective models. The fixity in the experiment was provided by clamps, which provided fixity everywhere below ground level. Scour was simulated in the experiments by lowering the top location of fixity. Similarly, scour in the FE models was simulated by releasing the fixities where scour was introduced such that exposed length of the pier increases. The FE model in the small-scale was introduced with 25 g of the mass of the accelerometer and its holder, which was found to cause a change in frequency. Its equivalent full-scale mass of 1.6 kg was added at the top of the full-scale FE model.

The natural frequencies estimated by these FE models and the experiment are shown in Figure 5.29. Here, the natural frequencies estimated by the small-scale experiment and the FE model have been brought to the equivalent full-scale by applying scale factors ($1/N$). The FE models at small-scale with scale factors gave almost the same natural frequencies to the full-scale FE model estimates. This confirms the accuracy of scaling of the column. Both these FE frequency estimates were higher than the experimental estimates, as was seen in Models 1 and 2 (Sections 5.3.1 and 5.4.1). The difference between experimental observations and FE estimates range from 3.5 – 8%. The higher natural frequencies found in the FE models of Model 3 (similar behaviour to Models 1 and 2) were expected since the ideal fixities provided in these FE models would not be attainable during the experiment. Since the range of difference observed was considered not significant (less than 8%), the full-scale FE model was extended to include soil-structure interaction.

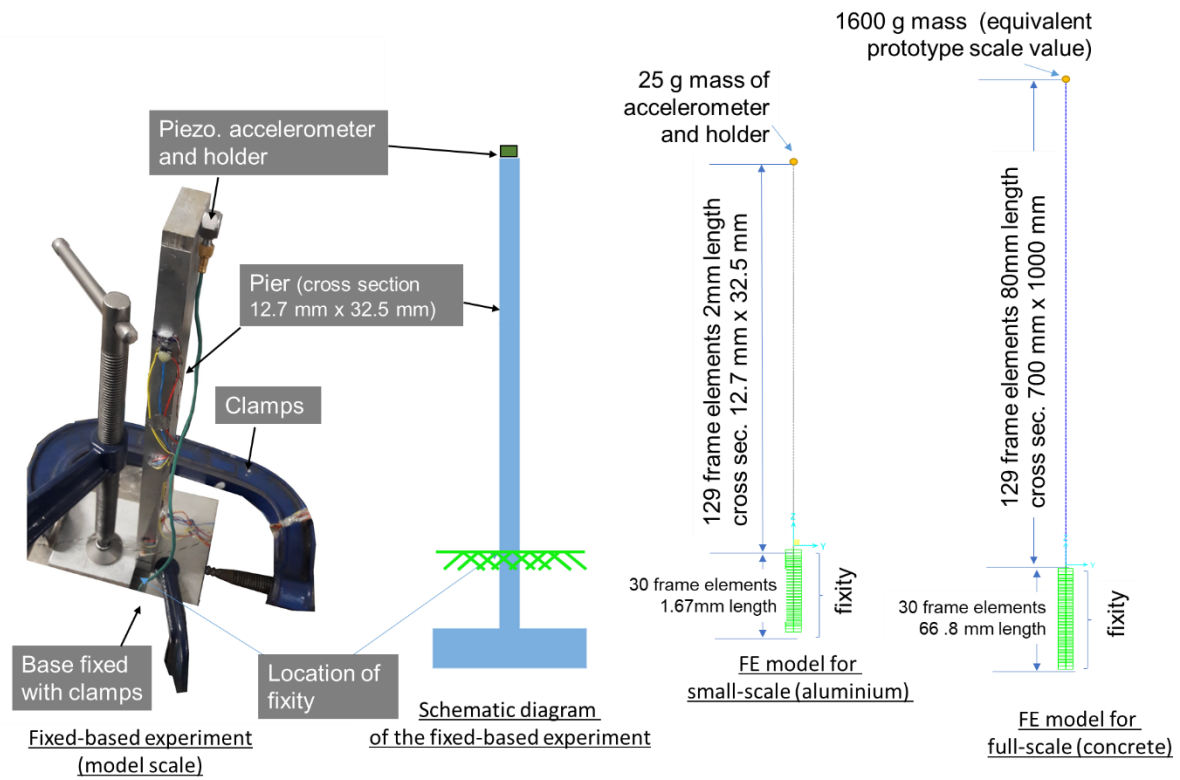


Figure 5.28 The fixed based experiment and the FE models simulating it at small-scale and full-scale

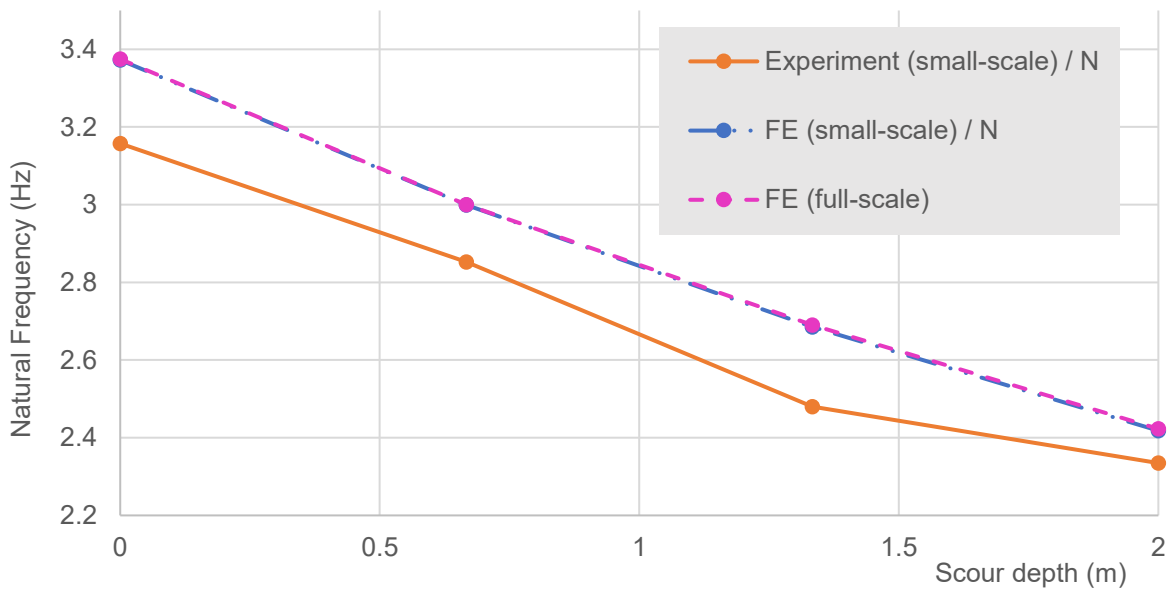


Figure 5.29 Natural frequency variation simulated by the fixed based experiment and the FE models at small-scale and full-scale

5.7.2 Inclusion of soil-structure interaction to the full-scale shallow pad foundation

A numerical spring-based model was previously developed in Section 5.6 to represent the soil-structure interaction of a shallow pad foundation. This model uses different soil-structure interaction representations for two key elements of the shallow foundation (i.e. the stub column and the pad footing). The stub column can be assumed to behave as a pile in the region where

it is below ground level. Therefore, the soil-stub column interaction was represented by a Winkler spring model as was used for piles. The soil-pad foundation interaction was given by a macro element at the centroid of the pad, having translational and rotational stiffnesses in all three directions (vertical, longitudinal, and transverse). Figure 5.30(b) shows the FE model of the shallow foundation combining the pad foundation macro element model and the stub column Winkler spring model. The structural FE model was the same as the fixed base FE model for the shallow pad foundation (Figure 5.28).

The soil-stub column interaction was represented by the validated elastic modulus distribution for the piles in Model 2 (the spring stiffnesses were however different due to the smaller spring spacing here). Since this elastic modulus distribution is based on Seed and Idriss (1970) and Kloeppe and Glock (1970), both of which are independent of the pile diameter, the change of cross-section from pile bent piles (0.74 m diameters circular) to the column of the shallow foundation (0.7 m x 1.2 m rectangular) was ignored.

The soil stiffness properties of the shallow pad foundation were modelled using two techniques, the API method and the Gazetas method, which were explained in Section 5.6. The API method assumes the pad is on the ground surface while the Gazetas method considers the embedment of the pad footing in the soil as well. Therefore, Gazetas method gave significantly higher stiffness estimates than the API method. The shear modulus of soil at the level of embedment (bottom of the pad) was considered for both methods when calculating the stiffnesses.

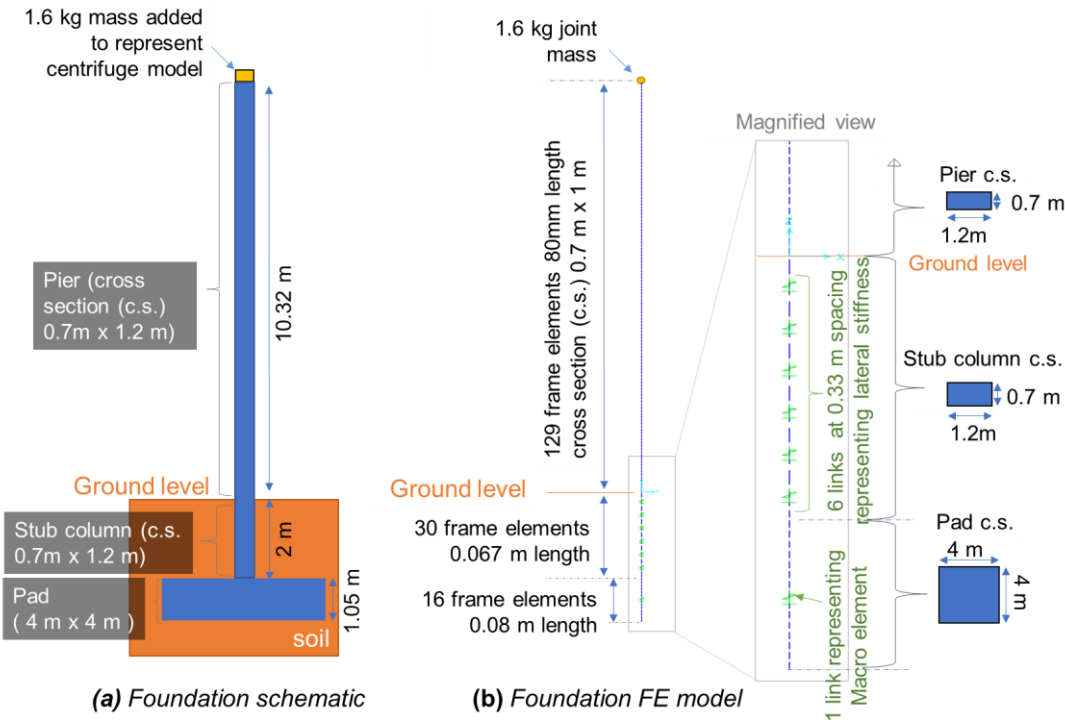


Figure 5.30 FE model for the structure of the shallow foundation combined with a Winkler model and a macro element model representing soil.

The numerical FE model developed incorporating soil-structure interaction was simulated for scour using the two methods explained in Section 5.1. The “spring deleting” method was used to simulate local scour, and this method deletes the top springs down to the depth of scour, while maintaining the lower springs at the same stiffness. The global scour was simulated by “stiffness lowering method”, which considers the lowering of the entire ground level due to the global scour case. It is noteworthy that the phrase “stiffness lowering” is more appropriate than “spring lowering” for this shallow foundation FE model as the location of the macro element does not lower but only its stiffness value reduce due to the lowered ground level, unlike the case of pile foundations. In the context of deep foundations, “stiffness lowering” due to scour also results in the “springs lowering” down.

Though the experimental global scour data points were only available at 2 m and when there was no scour, the FE model considered local and global scour depths of 0.67 m, in order to understand the progression of modal parameters with the increase of the scour depth.

5.7.2.1 Natural frequency variation of shallow pad foundation

The scour simulation with the FE model and the experimental scour simulation results are shown in Figure 5.31. With no scour, the frequency estimate using the API approach has a difference of 7%, whereas with Gazetas method the frequency estimate has a difference of 4% to the experimental observations, both of which were acceptably low. With 2 m of local and global scour the experimental natural frequency reduced by 7.3% and 9.9% respectively. The numerical FE model with API method estimated 4.2% and 10% frequency sensitivity for simulating 2 m of scour using the “spring deleting” method and the “stiffness lowering” method. The numerical FE model with Gazetas method simulated with the “spring deleting” method and the “stiffness lowering” method showed natural frequency sensitivities of 2.3% and 5.7%, respectively. Therefore, the numerical FE model with API method gave closer prediction to the experimental estimates than the Gazetas method, although it does not consider the embedment effect. As the API method gave close enough (difference of 3.1% for local and 0.1% for global scour) sensitivities to experimental natural frequency estimates as well, it was selected as the most suitable macro element representation for this shallow foundation.

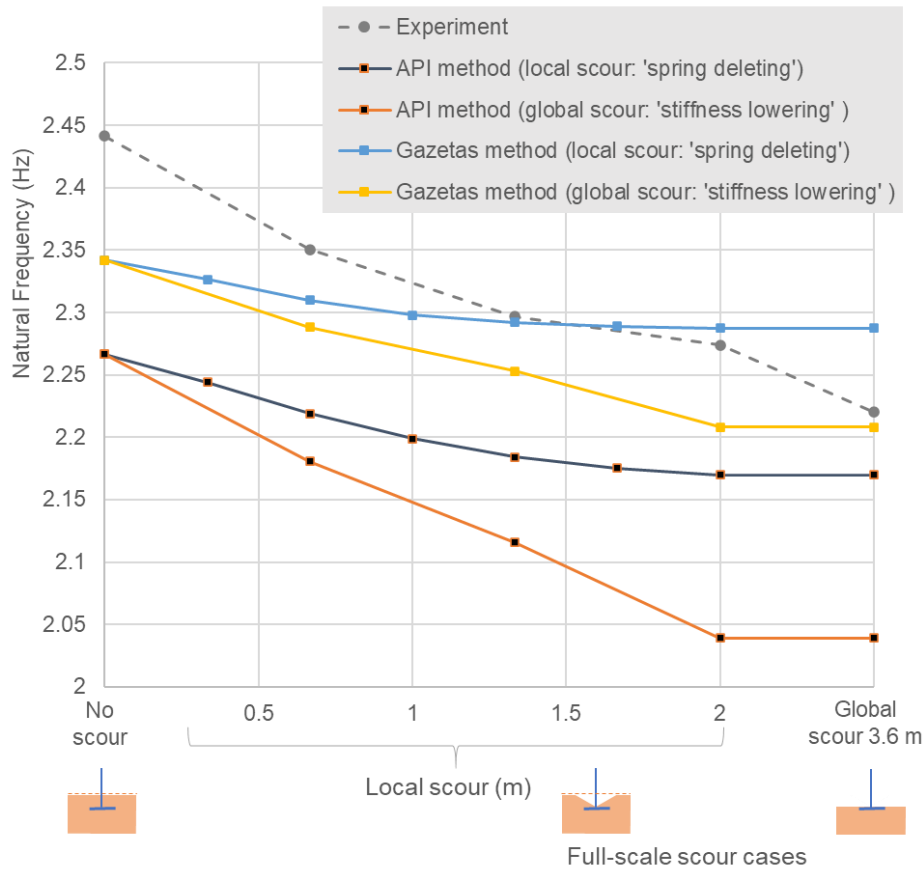


Figure 5.31 Natural frequency estimated by the FE model and the experiment

5.7.2.2 Mode shape variation of shallow pad foundation

The mode shapes estimated by these FE models and the experiment are compared in Figure 5.32. All these mode shapes have been normalised by the modal amplitude at the top of the pier. The experimental mode shapes of the first two scour cases (no scour and 0.33 m local scour) are not shown here since their modal amplitude at the top was inaccurate due to accelerometer malfunctioning, as discussed in Section 4.10.3.

In the previous chapter, Chapter 5, the mode shapes were normalised by a top mid-level accelerometer and found the experimental mode shapes of the shallow foundation does not show much variation due to scour. The same behaviour of mode shapes is confirmed by the results of the FE models, which showed that scour cause only small changes in modal amplitudes of this shallow foundation (e.g. 1.5% modal amplitude change at mid-height of the column per 1 m of local scour).

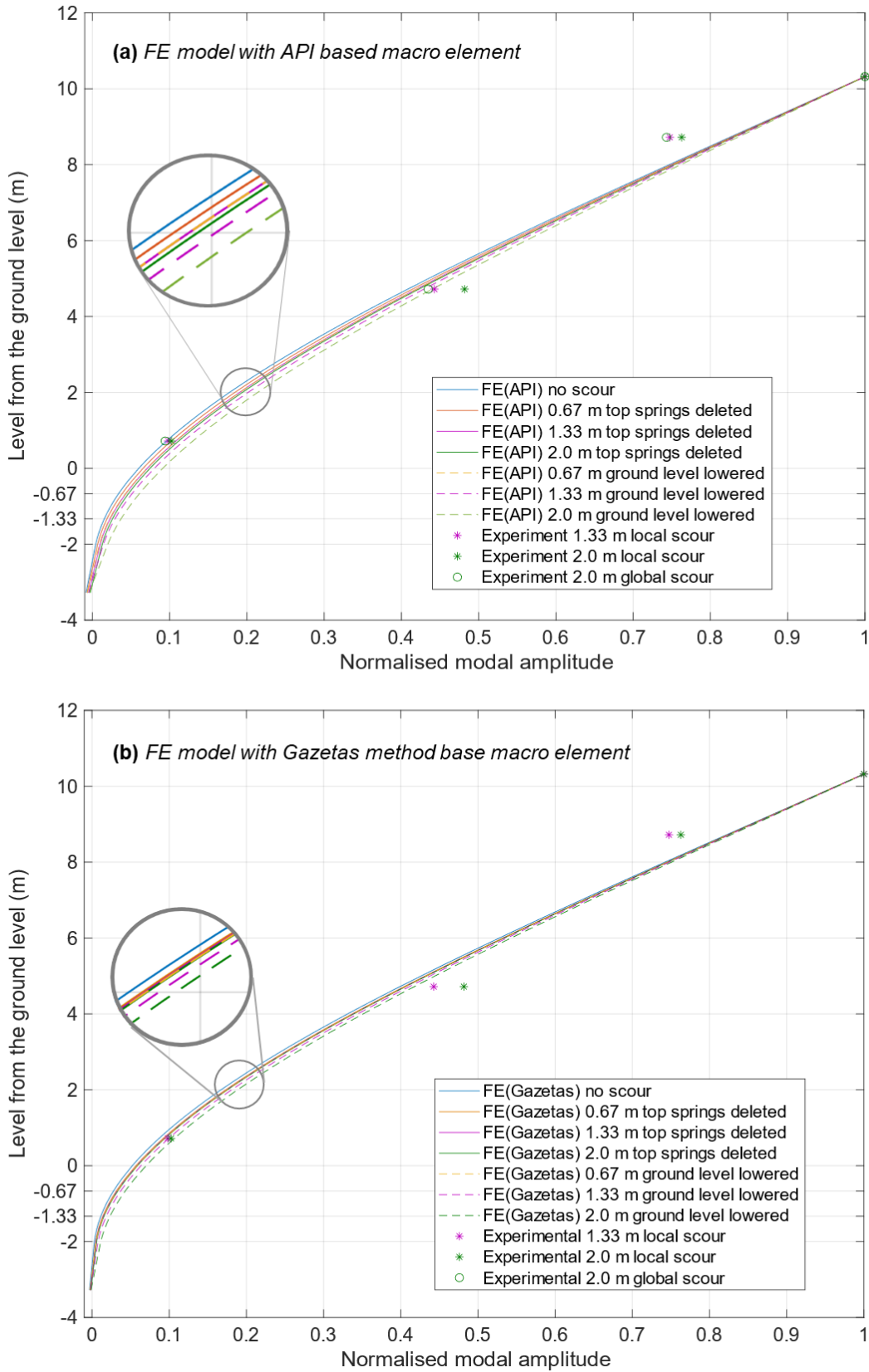


Figure 5.32 Experiment and FE estimate of the fundamental mode shape (shallow foundation)

The experimental modal amplitudes at the four levels shown were similar to the FE estimates. The higher experimental amplitude near +5 m level above ground (15% difference) and lower

amplitude near +9 m level (11% difference) were thought to be due to the low signal to noise ratio of the accelerometers or due to the limitations of the idealisations used in the FE model. Both FE models showed the normalised amplitudes increase with scour, the highest increase (around 12% per 1 m of local scour) being near the ground level, similar to the Models 1 and 2. However, this increase was small at higher levels of the column (e.g. mid-height has only 1.5% change per 1 m local scour). The FE model with the macro element stiffnesses from the API method showed higher amplitude increase than the FE model with Gazetas method macro element (e.g. 1.5% vs 0.45% per 1 m of local scour). The global scour showed a greater change of mode shapes than local scour (e.g. 3.1% vs 1.5% change at the mid-height per 1 m of scour). As the API method gave similar mode shapes to the experiment and better natural frequency sensitivities than Gazetas method, the API method was adopted for the Bridge 3 as well.

5.7.3 Extension of the calibrated shallow foundation FE model to represent Bridge 3

Although a natural frequency variation was observed with the FE model and the centrifuge experiment Model 3, they represented a standalone shallow pad foundation but not the Bridge 3 with bridge bearings and deck as well. The mass and stiffness of the bearings and the deck may significantly change the overall natural frequencies and mode shapes that were estimated for the standalone pad foundation. The FE model of the shallow foundation, which was validated for soil-structure interaction, was therefore extended to a simply supported bridge with deck and bearings to obtain an FE model for Bridge 3.

The FE model of the Bridge 3 is shown in Figure 5.33. Bridge 3 has the same simply supported bridge deck used for Bridge 2 (in Section 5.4.3). The numerical model of the bridge pier foundation was the same as the calibrated shallow pad foundation model with springs estimated by API method (Section 5.7.2).

As previously verified in Section 5.7.2, local scour was simulated by “spring deleting” method and global scour was simulated by “stiffness lowering” method.

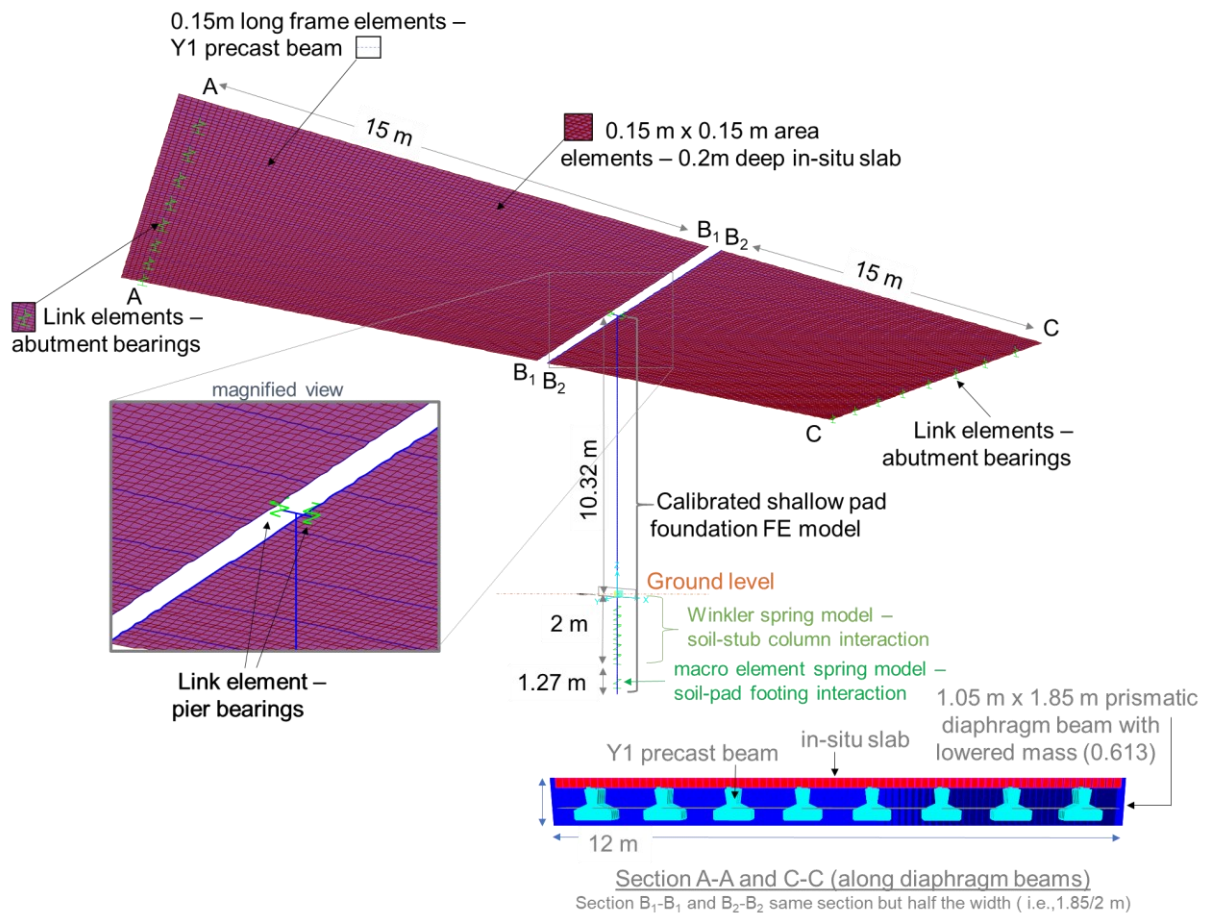


Figure 5.33 FE model of the Bridge 3 (a two-span simply supported bridge with the shallow foundation: view from the bottom of the bridge)

5.7.3.1 Natural frequency variation of Bridge 3

Figure 5.34 shows the natural frequency sensitivities for increasing depths of scour simulated using the FE model of Bridge 3. The local deck bending modes and other scour insensitive modes have not been plotted. The natural frequency variation indicates a significantly higher sensitivity to global scour than to local scour.

The Mode 1 (longitudinal sway) gave 0.08% and 0.15% variation of natural frequency for 1 m of local and global scour. The centrifuge experiment, which also captured the fundamental longitudinal sway mode of the pier, showed that the standalone shallow foundation of Bridge 3 has low sensitivities in natural frequency to scour (3.5 – 4.5% per 1 m); however, the FE model of the entire Bridge 3 has estimated even lower frequency sensitivities.

Nevertheless, the natural frequencies of the higher-order modes show high sensitivities to the depth of scour. Mode 7 (pier vertical translation) shows 7% frequency sensitivity to 1 m of global scour. Mode 16 (pier only bottom and top sway longitudinal) shows 6% and 15% frequency sensitivities to local and global scour depth of 1 m. Although these higher-order modes show higher frequency sensitivities than typical environmental variations, they may be difficult to capture in a real bridge using ambient vibration (Wenzel and Pichler, 2005).

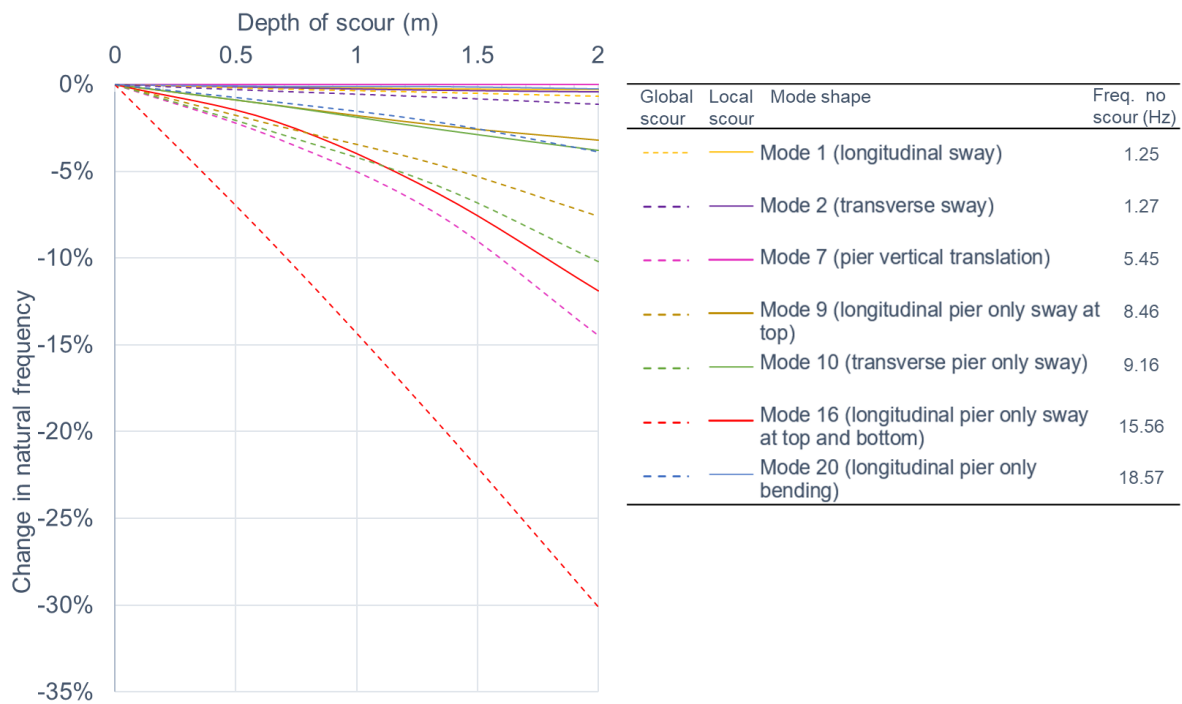


Figure 5.34 Natural frequency sensitivity to scour of the Bridge 3 (a two-span simply supported bridge with the shallow pad foundation)

In this FE model, both the bridge bearings and the effect of the soil were modelled with spring-based elements (Figure 5.33). There was a question as to whether the natural frequency sensitivities significantly change if the bearing stiffness differs from what was assumed (referred to as “normal bearing stiffness”). In order to study the effect of the bearing stiffness, most extreme cases of bearing stiffness were studied as a sensitivity study. The most extremely high stiffness of the bearings is infinite stiffness (“fully stiff condition”), which would result in the bridge deck to be connected to both pier and abutments with full fixity. The most extremely low bearing stiffness possible is zero stiffness (“fully free”), and it would mean the bridge deck movement is completely independent (free) from the pier and abutment foundations movement. These two extreme cases of bearing stiffness, “fully stiff” and the “fully free” conditions, and the “normal bearing stiffness” were used in three different FE models, and all these models were simulated for local and global scour of 2 m depth. The results are shown in Figure 5.35.

The “fully stiff” bearing condition does not allow any translational or rotational stiffness; thus, it results in an integral connection at the bridge piers and fully fixed at abutments. Therefore, the sway modes (Mode 1 and 2), where the bridge sways over the abutment bearings, were not present in a fully fixed bearing condition, as shown in Figure 5.35. The “fully free” bearing stiffness allows independent vibration between the pier foundation and the deck. Therefore this condition should be equivalent to the behaviour of the standalone foundation studied previously (Section 5.7.2). The sensitivity of natural frequency of Mode 1 for the fully free condition in Figure 5.35 is 10%, the same as the previous FE estimate for the standalone

foundation (Section 5.7.2). The changes in natural frequency of sway modes (Mode 1 and 2) were highly sensitive to the stiffness of the bearings; the frequency change has fallen significantly as the bearing stiffness increases (from around 10% to almost 0%). Therefore, sway modes of this shallow foundation are only suitable as scour indicators if the bearings are not stiff. Mode 20 showed that the normal bearing condition provides a lower change in natural frequency than the two extreme bearing condition cases. The natural frequencies of Mode 7 and Mode 16 were significant (more than 10%) across all bearing conditions. Therefore, the natural frequency change as an indicator of scour has shown the most potential in Mode 7 and 16.

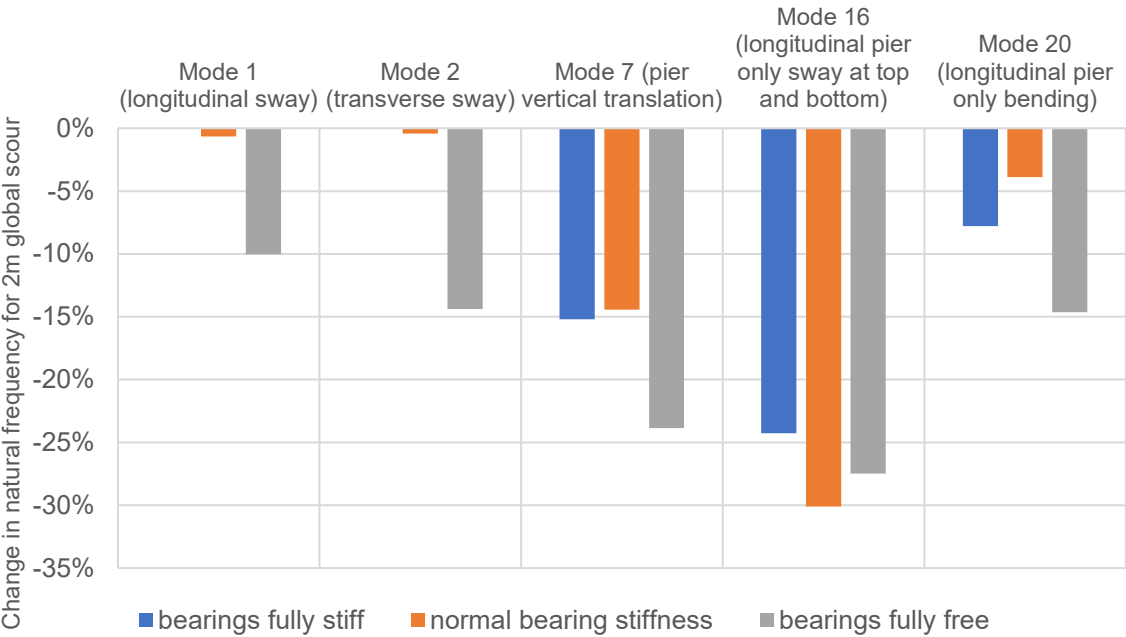


Figure 5.35 Sensitivity study on the effect of change in bearing stiffness on the natural frequency change resulting from scour.

5.7.3.2 Mode shape variation of Bridge 3

The potential to capture scour using mode shapes was also studied using the FE model of Bridge 3. Mode shapes 1, 7 and 16 were studied to examine the variation of mode shapes due to scour and are shown in Figure 5.36. It shows an elevation view of the bridge modes.

As shown in Figure 5.36(a), Mode 1 (longitudinal sway) did not show much variation of mode shape due to local scour; the simply supported spans have not shown any mode shape variation due to scour, whereas the pier has about 2% modal amplitude change at the mid-height for 1 m of local scour. Global scour has caused higher modal amplitude increases than local scour (5% modal amplitude change at the mid-height of the pier for 1 m of global scour). The experimental modal shape corresponding to the standalone foundation model (centrifuge Model 3) is similar to the Mode 1 numerically predicated for Bridge 3. The experiment modal amplitudes did not show a progressive increase of modal amplitudes with increasing scour

depth (as estimated numerically). This could be since the modal amplitude increases were too small to capture using the types of accelerometers used.

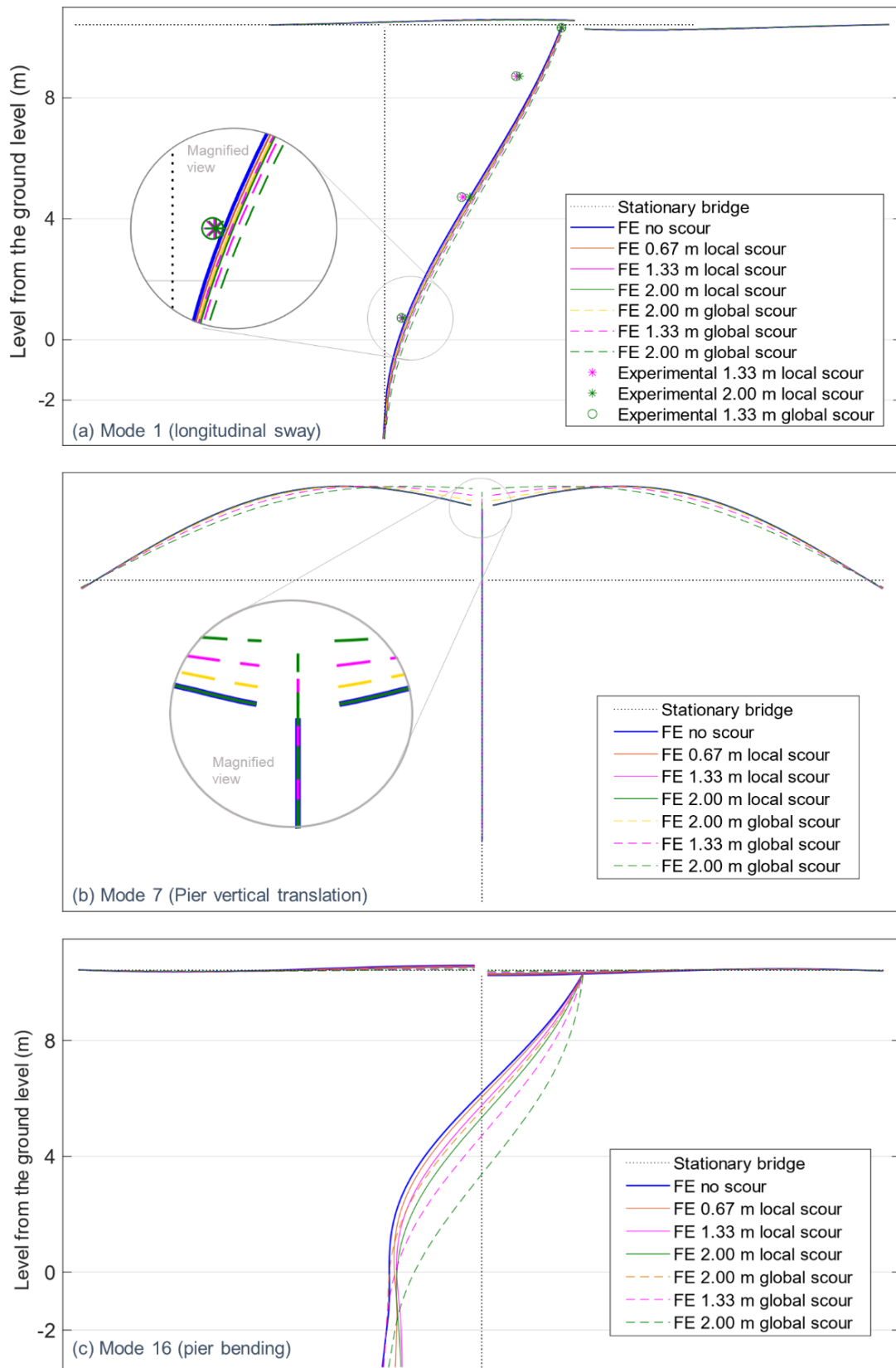


Figure 5.36 Variation of mode shapes for local and global scour, as simulated by the FE model of the simply supported bridge with shallow foundation (Bridge 3).

Figure 5.36(b) shows the variation of Mode 7 (vertical pier translation) with scour depth. Local scour did not show any modal amplitude increase. Global scour showed the vertical pier translation amplitude has increased with higher global scour depth (the deck just above the pier has increased modal amplitude by 10% per 1 m). The bridge deck amplitude also varied in conjunction. Therefore, this mode shape can be captured with sensors only on the bridge deck.

Figure 5.36(c) shows the variation of Mode 16 (pier bending) with scour depth. This is a local mode shape of the bridge pier with the soil and the bearings excitations as well but without any vibration of the deck. With increasing scour depths, the modal magnitude of pier reduced near the ground level and increased near the top of the pier. At +8 m above the original ground level, the local scour of 1 m depth has increased the modal amplitudes by 13%, and global scour of the same depth has increased the modal amplitudes by 35% mid-height of the pier. Therefore, Mode 16 of Bridge 3 has significant change due to scour.

5.8 Summary

This chapter developed numerical FE models to examine vibration-based scour monitoring potential of three full-scale bridges (Bridges 1, 2 and 3), which were represented by the small-scale models tested in the centrifuge (Models 1, 2 and 3, respectively).

The previous chapter, Chapter 4, discussed how all three of these full-scale bridges were simplified to full-scale simplified bridges (or standalone foundations) and then to small-scale simplified bridges. The methodology followed in this chapter went back in the same path by developing small-scale FE models first and then gradually build these numerical models up to the full-scale bridges, as illustrated in Figure 5.2. The scaling between Models 1,2 and 3 in small-scale and their full-scale simplified bridges (standalone foundations) was found have been accurately scaled, based on the results of numerical and experimental study with fixed bases. All these scaling-verified full-scale bridges were included with soil-structure interaction models; a Winkler spring model was used to represent soil-pile/column interaction, and a macro element model was used to represent the soil-pad footing interaction. All these FE models representative of simplified bridges were successfully calibrated against the centrifuge test results for Models 1, 2, 3 with appropriate scaling factors. Then these calibrated FE models were extended to the Bridges 1,2 and 3 with composite bridge deck and bearings in addition to the foundations.

Two scour simulation techniques were studied to represent local and global scour cases when soil-structure interaction was represented by Winkler and macro element spring models (Figure 5.1). Numerical modelling and comparison with experimental results found that global scour can be simulated by “spring/stiffness lowering” method, which lowers the stiffness profile

by the same depth as the depth of scour; local scour can be simulated by “spring deleting” method, which deletes the springs down to the depth of scour without changing the stiffness of the springs below the scoured ground level.

The final FE model of the Bridge 2, simply supported bridge with piled foundations, estimated the fundamental natural frequency sensitivity of 2 – 2.3% per 1 m of scour, which was undesirably lower than the corresponding experimental estimate for standalone pile bent foundation, Model 2 (11.5 – 12.1% per 1m of scour). Nevertheless, the higher-order modes provided high scour sensitivities in the ranges of 4.2 – 9.7% per 1 m of global scour. The mode shape of the fundamental mode and several higher-order modes were also found to show high sensitivity to scour (8 – 10% change in modal amplitudes at the mid-height of the pier per 1 m of scour depth).

The final FE model of Bridge 1, the integral bridge with piled foundations, showed a remarkable similarity of natural frequency sensitivities between the experimental local (10.5% per 1 m) / global scour (11.1% per 1 m) cases and numerical local (10.7% per 1 m) / global scour (11.8% per 1 m) cases. These significant sensitivities of the fundamental mode to scour demonstrates that the natural frequency could become a reliable scour indicator. The mode shape amplitudes at the mid-height of the pier/abutments changed by 6-7% because of local scour. The global scour cases were found to result in only slightly higher modal amplitudes than local scour (0.6-2.5 % at mid-height of the column per 1 m of scour). A key finding was that local scour of a single foundation causes amplitude increase primarily on that foundation. This finding was in line with the experimental observations when minor outliers were ignored. Therefore, there is potential for scour localisation to a specific pier that is undergoing scour.

The final FE model of Bridge 3, simply supported bridge with shallow pad foundation, estimated drastically lower sensitivities of natural frequency, 0.15 – 0.3% per 1 m of scour, than the already lower estimate in the experiments of standalone shallow pad foundation. Nevertheless, higher-order modes showed sensitivities in the order of 7 – 15% per 1 m of global scour. Similar to the natural frequency, the fundamental sway mode shape showed insufficient sensitivity to scour, but higher-order modes did show high sensitivity (up to 35% modal amplitude change at the mid-height of the column per 1 m of scour).

In conclusion, the fundamental natural frequency of the integral bridge was sensitive to scour. The fundamental frequency sensitivities were significantly lower for the simply supported bridges, for which high natural frequency sensitivities were observed for higher-order modes, though there is a practical challenge of capturing these in real life as only high energy input forces excite these higher-order modes. The mode shape variation of all three bridges showed potential for indicating the location of a foundation that is undergoing local scour.

Chapter 6

Discussion

This research was initiated with the primary objective of examining the potential of a vibration-based technique for monitoring bridge scour. Such a technique has the benefit of helping bridge owners safeguard their bridges from scour, the leading cause of historical bridge failure (Melville and Coleman, 2000; Hunt, 2009; Dikanski et al., 2016). In order to develop this monitoring technique, five sub-objectives were initially identified. The first sub-objective was to evaluate the comparative feasibility of vibration-based, and other scour monitoring techniques. Based on a detailed literature review of current scour monitoring approaches (Chapter 2), the vibration-based scour monitoring technique was found to have significant potential, and the research gaps were identified. The second sub-objective, evaluating the field viability of vibration-based scour monitoring, was achieved with a feasibility study on Nine Wells Bridge and a field deployment trial at Baildon Bridge (Chapter 3). The third sub-objective, discovering vibration-based parameters other than natural frequency, was successfully realised with the demonstration of scour-sensitive behaviour of mode shapes and modal spectral density (Chapters 3 to 5). The fourth sub-objective, developing a small-scale centrifuge experimental regime, was also successfully achieved with the geotechnical centrifuge modelling of different bridge and scour types (Chapter 4). Based on the results of the centrifuge test, the fifth and last objective, developing a numerical technique for simulating the effects of local and global scour, was also achieved (Chapter 5). Therefore, all the research objectives were successfully attained, as discussed below.

6.1 Comparative feasibility of vibration-based scour monitoring

A key question at the start of this research project was how vibration-based scour monitoring compares with other techniques. The literature review in Chapter 2 found that most scour monitoring techniques have limitations related to: (1) non-durability; (2) measurement of scour depth at only a single point; (3) not being able to carry out remote and real-time monitoring; (4) measurement inaccuracies; and/or (5) costly installation and operation. The field trial at Baildon Bridge (Section 3.2) found that vibration-based scour monitoring does not have the first three limitations but does have the last two listed above, as discussed below, with reference to each limitation.

(1) The monitoring instrumentation at Baildon Bridge could be considered durable, as the accelerometers and the data-acquisition system functioned continuously during the six-month monitoring period. A key advantage of this monitoring technique is that the required parameters could be derived without having any instrumentation underwater. (2) The scour depth indication with vibration-based techniques is not a point measurement of scour depth

since there should be sufficient scour around the whole bridge pier to cause a measurable change in vibration parameters, unlike magnetic sliding collar and other monitoring devices that measure scour depth at a single point (Section 2.3.7). (3) The vibration measurements could also be acquired remotely and analysed in real time when required. The real-time modal analysis at Baildon Bridge was performed by manual download and processing of data; nevertheless, fully automated real-time monitoring is also possible, as explained in Caetano and Magalha (2009). (4) High measurement inaccuracies were, however, observed with vibration-based scour monitoring; and (5) the instrumentation at Baildon Bridge was costly since extremely low noise accelerometers had to be used (EPSON M-A550, each £1,430 in May 2018), and this short span bridge had low levels of ambient vibrations. The accelerometers used in the centrifuge tests were cheaper (Analog Devices ADXL1002, each £40 in March 2019) but had higher noise density.

Another limitation is that vibration-based scour monitoring could only indicate the *changes* in scour depth, but not the *absolute* scour depth immediately after sensor deployment, as is possible with sonar-based scour monitoring. One could argue that FE models could be used to estimate the absolute depths of scour. Although modal parameters can be estimated before the sensor deployment by using an FE model, such estimates often have errors that are of the same order of magnitude as the expected changes due to significant depths of scour. Therefore, it is challenging to estimate the absolute depth of scour by comparing FE and initial experimental results. Nevertheless, such FE models could be used to predict the *changes* in modal parameters due to scour after performing model updating based on the initial experimental results (Section 3.2.6).

Therefore, vibration-based scour monitoring overcomes some key limitations present in the other monitoring techniques, while it still has several limitations, which needs to be taken into consideration when a bridge engineer plans to use this technique in practice.

6.2 Scour sensitivity of the three scour indicators

Let us now revisit the scour monitoring potential of the three parameters considered in this research. The first parameter, the natural frequency, based on all experiments and numerical modelling, showed the potential to indicate extensive scour depths. The natural frequency reduction due to scour can be attributed to the loss of stiffness provided by the soil, and perhaps to the loss of mass participation and damping of soil. The soil stiffness effect was verified by the numerical simulations using Winkler and macro element spring models, which modelled soil as springs representing stiffness. Even though these models did not consider the damping and mass participation of soil, the reduction of natural frequency estimated by them closely matched the experimental results (Chapter 5), demonstrating that the natural frequency reduction caused by scour was primarily due to the loss of the stiffness given by

soil. According to the laboratory experiments and numerical modelling performed in this research and the literature, natural frequency is a reliable indicator of scour, with its *maximum* sensitivity as high as double-digit percentages (Ko et al., 2010; Klinga and Alipour, 2015; Prendergast, Hester and Gavin, 2016a). Therefore, natural-frequency-based scour detection showed significantly higher potential than natural-frequency-based detection of other damage, such as cracking, which have shown sensitivities only as high as single-digit percentages (Farrar et al., 1994; Kim, Yun and Yi, 2003; Döhler et al., 2014).

A natural frequency reduction, however, was not observed in the field trial because its expected change due to scour was in the same order of magnitude as the observed measurement uncertainties. Overcoming measurement uncertainties is, therefore, likely to be a key challenge in using natural frequency as an indicator of scour in practice. The same challenge was faced in previous field trials in two bridges studied by Yao et al. (2010b), but not in Ko et al. (2010). The success of Ko et al. (2010) could be attributed to the significant global scour depth of 3 m, whereas Baildon Bridge had local scour with a maximum depth of 1.8 m, limited to a narrow section of one bridge pier. Numerical modelling simulations of more extensive scour cases at Baildon Bridge found that the measurement uncertainties observed would limit local and global scour depth resolutions at this bridge to 1.7 m and 0.5 m, respectively. In comparison to the pile embedment depths of 6 m, these local and global scour depth resolutions would still provide sufficiently early indications of scour damage. However, these metre-scale depths are significantly coarser than the centimetre-scale scour depth resolutions of sonar, as claimed by manufacturers such as AIRMAR (2017) and observed in the sonar scan images of the riverbed below Baildon Bridge. Therefore, the natural frequency is more of a severe scour damage indicator, unless its measurement uncertainty is lower than what was observed at Baildon Bridge. There is a potential that typical bridges that are less bulky and stiff than Baildon Bridge may have lower natural frequency uncertainties. For example, several weeks of monitoring natural frequency of a long span bridge by Caetano and Magalha (2009) produced maximum measurement uncertainties and operational variabilities of 0.3%, which would have provided significantly finer scour depth resolutions with the natural frequencies.

The second parameter, mode shapes, showed significant potential as an indicator of the presence and location of scour. When scour occurred at a bridge pier, the mode shape amplitudes increased only at that pier, while little change was seen elsewhere. The largest increase was seen near the part of the pier that lost the soil support/restraint as a result of scour. Therefore, such a mode shape change can be attributed to the loss of the partial restraint previously provided by the scoured soil. With this loss of partial restraint, the mode shape of the part of the pier near the scoured location increases in amplitude. However, as the stiffness of the elements elsewhere in the bridge remains the same, this amplitude increase remains local to the bridge elements near the scoured region, paving the way for scour

localisation. While such an amplitude increase was seen in the majority of scour cases in the centrifuge experiments, there were several outliers, which were not observed in the associated numerical modelling. These outliers were assumed to be due to measurement inaccuracies resulting from the low signal to noise ratio of the vibration signal measured by the accelerometers. Despite such outliers, the fact that the performance of the mode shapes was better than the natural frequency in the field trial demonstrates that mode shapes have significant scour monitoring potential.

Third, the output-only spectral density at the modal peaks also showed significant scour monitoring potential, both in the field trial and in the centrifuge modelling experiment. One issue with the output-only spectral density is its dependence on the input excitation. Therefore, the frequency response function (FRF), which removes the effects of input excitation, was considered. However, FRF did not produce a reliable correlation to scour in the experiments. The output-only spectral density showed a good correlation to scour, either as the power spectral density (PSD) of an individual accelerometer or as the first singular value of PSD matrix (SVPSD) of all accelerometers. The scour-induced change of PSD at the modal peaks was greatest for the accelerometers near to the scour location, while the first SVPSD provided an average change to all the individual accelerometer PSD changes due to scour. The spectral-density-based methods have an added benefit over mode-shape-based methods since the spectral-density-based methods can work even with only one accelerometer on a pier. For example, accelerometer 2 alone in Baildon Bridge indicated the gradual reduction in the scour level as a gradual reduction of the mean modal PSD value (Figure 3.20). In comparison, mode-shape-based methods require at least two, and preferably several, accelerometers to derive the mode shapes. The modal peak displacement PSD ($S_y(\omega_N)$) estimate of a single degree of freedom system is inversely proportional to the second power of natural angular frequency (ω_N) and the second power of damping factor (c), given that the input is constant broad-band excitation (Newland, 1993, p.75). The acceleration PSD discussed in this thesis can be obtained by multiplying the displacement PSD by the fourth power of ω_N (Equation 2.3). And the damping coefficient (c) is equal to $(2\zeta\sqrt{km})$, where k is the stiffness, m is the mass and ζ is the damping ratio (Pathak and Pathak, 2018). As $\omega_N^2 = k/m$, all the above equations give acceleration PSD to be inversely proportional to the second power of mass and second power of damping ratio. There may have been some reduction in mass participation of soil due to scour and hence the mass of the system would be lost, however mass participation of soil was not considered in the numerical models. A reduction in damping ratio is also a potential cause; however, experimental results did not show a consistent and clear reduction in damping ratio. For example, based on the narrowing of the half-band-width of FRF modal peaks, a reduction in damping ratio was seen in Centrifuge Model 2 but not in Centrifuge Model 3, although both models showed significant increases in spectral densities (Sections 4.9.2 and 4.9.3). Therefore, an increase in spectral density could

be attributed to either reduction in the mass participation or reduction in damping ratio; however, this aspect needs further investigation in the future. Nevertheless, significant changes in spectral density were observed in both the field trial and the centrifuge tests. Despite the spectral density being more uncertain than the natural frequency in Baildon Bridge, the uncertainty had been compensated for by the significant sensitivity of the spectral density to scour. Therefore, spectral density was found to be a reliable indicator of scour.

6.3 Assumptions

A key assumption made by the output-only system identification techniques such as frequency domain decomposition was that the input ambient excitation is broad-band. The ambient excitations were present at Baildon Bridge, mainly as a result of traffic excitations. Traffic excitations often have the vibration properties of the vehicles, which differ from one vehicle to another. Therefore, broad-band input excitation could be assumed only during peak hour traffic or when there are a large number of different vehicles passing over the bridge. This would limit the time window when scour monitoring could be carried out. However, when there is a flooding event, the ambient vibrations will also be generated as a result of the impact of the turbulent water on the surface of bridge piers and abutments (Masui and Suzuki, 2009). Additionally, other bridges with longer spans would also experience significant amounts of wind-induced ambient vibrations, which would increase the potential to identify the scour-sensitive modal parameters of a bridge in real-time.

Centrifuge modelling was assumed to correct the inaccurate scaling of stiffness and other properties of small-scale soil-structure models. Since natural frequency is highly sensitive to the stiffness of soil (Prendergast, Hester and Gavin, 2016a), an inaccuracy in soil stiffness scaling can have a significant effect, resulting in natural-frequency estimates that are not representative of full-scale bridges. The accuracy of the natural frequency estimates during the centrifuge tests was confirmed by comparing with the natural frequencies observed at normal gravity and with fixed base instead of soil. Although the centrifuge modelling corrects the scaling inaccuracies, it involves complicated designs of impacting techniques to excite the structure, a technique to remove soil to simulate scour, and vibration measurement techniques that are functional under high centrifuge acceleration of up to a hundred times the normal gravity on the earth's surface. This research outlined techniques and tools that can be used for centrifuge modelling of vibration-based bridge models. For example, the automatic modal hammer device that uses air pressure successfully excited the models during the centrifuge testing. Furthermore, the assumptions that were made during the scaling process to choose only the critical parameters required were found to be valid in the numerical model simulations in Chapter 5. The successful centrifuge experimental programme carried out in this research

demonstrated the potential of centrifuge modelling to assess the feasibility and applicability of this monitoring technique in the future, using only small-scale models.

The full bridge model tested in the centrifuge, Model 1, showed a strong noise peak at 100 Hz in small-scale (Section 4.7.3). This noise peak was examined at different centrifuge accelerations and was found not to be different in different centrifuge accelerations, in contrast to a typical vibration mode, and was only present when 50 Hz electrical noise was not present, and centrifuge acceleration was high. Therefore, it was assumed to be either electrical or mechanical noise in the centrifuge. Although this was investigated further, the exact source of the noise could not be found. The presence of this strong noise peak may have affected the accuracy of the modal characteristics determined from the modes with natural frequencies close to 100 Hz in small scale.

Much of the modal analysis in this thesis was based on peak picking of SVPSD and PSD plots. Peak picking method assumes a single vibration mode dominates the structural response over a peak. However, this assumption may not be valid if closely spaced modes are present. The modes were therefore examined by comparing mode shapes derived at different times, and they were found to be similar for the peaks suggesting a single mode dominated the behaviour near the modal peaks. If closely spaced modes are present, modal discrimination methods such as that described for singular values in Brincker, Anderson and Jacobsen (2007) and for stochastic subspace in Wu *et al.* (2018) can be used.

Several assumptions were made during initial numerical modelling of Baildon Bridge. For example, simple properties were assumed for the joint connectivity, material properties and boundary conditions, and these could be verified and updated where necessary after obtaining the modal characteristics of the bridge from the experimental vibration signals. In a typical bridge with some uncertain properties, this is a likely process for implementing this monitoring technique – an initial numerical model would have to be developed with a number of assumptions, and it can be updated based on the experimental observations. Once updated, this model can aid in estimating the scour depths corresponding to the experimentally observed changes in modal characteristics.

The numerical models developed in Chapter 5 also examined the validity of assumed global and local scour simulation techniques. Global scour involves ground-level lowering everywhere; thus, the soil stiffnesses of springs below the ground level should, in theory, be reduced to account for the new ground level. Therefore, Chapter 5 studied two simulation techniques: “spring deletion”, a method similar to the previous research (Section 2.4.1.3); and “spring lowering”, a new method that calculates the soil springs for the changed ground level, which represents the global scour better in theory. The comparison of these two scour simulation techniques with the experimental results found that global scour is indeed better represented by the “spring lowering” method. The “spring deleting” method was more

representative of the local scour type of behaviour, as expected, although it estimated a slightly lower natural frequency sensitivity estimate than the experimental local scour. Therefore, future scour simulations using spring-based models could adopt these two techniques based on the type of scour considered.

Various other assumptions were made for the stiffness variation with depth, small-strain condition of soil and effect of water-soil interaction and these assumptions are discussed in detail next in Section 6.4.

6.4 Nonlinearities

This thesis either observed or assumed several types of nonlinear and linear behaviour of material and vibration properties. For example, based on the levels of stress/strain expected, linear and nonlinear elastic springs were considered to represent the soil-pile interaction. Shear modulus of soil was considered to vary with depth linearly in some cases and nonlinearly in the other cases. Certain nonlinear behaviour was however ignored such as that due to pore water pressure effects, damping, gapping effects of soil, temperature variations and cracking on the structure. These nonlinear behaviours of material and vibration properties will be discussed in the following section.

The soil-structure interaction of piles was represented by Winkler spring model, which provided closely spaced elastic springs along the length of bridge piles springs (Winkler, 1867; Dutta and Roy, 2002; Prendergast, Hester and Gavin, 2016a). Initially, the springs were provided in both horizontal (to model lateral soil-pile interaction) and vertical directions (to model soil-pile adhesion and tip resistance). The horizontal spring stiffness was determined, assuming small-strain linear elastic behaviour. The experimental observations showcased this assumption to be accurate, as the horizontal vibration amplitudes measured were minute. The amplitudes of vibration observed at Baildon Bridge was in the range of 40nm (Section 3.2.5), and the amplitudes of vibrations of the centrifuge models were in the range of 23-27 μm (Sections 4.9.2 and 4.9.3). While these are significantly low amplitudes, capturing of the corresponding accelerations was verified by the fact that the sensor noise claimed by the manufacturer was lower than the accelerations measured, as elaborated in Section 3.2.5. These minute amplitudes of vibration were measured on the pier above the ground level. Hence for a typical fundamental sway mode, which involves lower amplitudes of vibration with lower height, the amplitudes of vibration on the pier foundation underground could be even lower than the 40nm for Baildon Bridge and 23-27 μm for centrifuge models. Therefore, small-strain linear elastic behaviour can be considered accurate for horizontal soil-structure interactions.

While small-strain linear behaviour was considered for horizontal springs of the piles, the vertical springs representing the soil-pile adhesion and tip resistance were considered to be nonlinear in the initial set of analysis in Section 3.2.3 and Section 5.4. The small-strain

assumption is not applicable for the vertical spring stiffnesses as a significant dead load of the bridge is imposed vertically. Therefore, the numerical models considered the secant modulus of elasticity of soil that is applicable when the dead load was applied. And this secant stiffness was used for calculating the eigenvalues using the numerical models. It was however found that there is little effect of this non-linear assumption since the vertical stiffness of the bridge was significant. Hence, the non-linear assumption had little effect on the lower order horizontal modes of vibration.

If the strains were large, the stiffnesses provided by soil would show nonlinear behaviour. This is perhaps a behaviour that can be expected when a significant amount of scour occurs, especially under a shallow foundation. The shallow foundation soil-structure interaction estimates used for numerical models in Section 5.6 are based on empirical equations developed for massless foundations. Hence, the small-strain stiffness should have been assumed in these empirical estimates. However, the removal of soil, especially under a shallow pad foundation could lead to significantly higher stresses and strains exerted on the unscoured region of soil. Higher stress and strain levels exerted on soil lead to lower secant modulus of elasticity (Figure 6.1(a)) and lower shear modulus of soil (Figure 6.1(b)). The highest stiffness is provided in the small-strain range, and beyond this range, the stiffness shows a nonlinear degrading pattern with higher strain. Thus, significant scour depths may lead to lower stiffness and thus lower natural frequency estimates after scour. This implies that the sensitivities in natural frequencies due to scour could be even higher than the numerical estimates in this thesis if the soil goes into large strains after scour occurs. This is desirable for vibration-based scour monitoring as a larger natural frequency (or any other modal parameter) change is easier to detect.

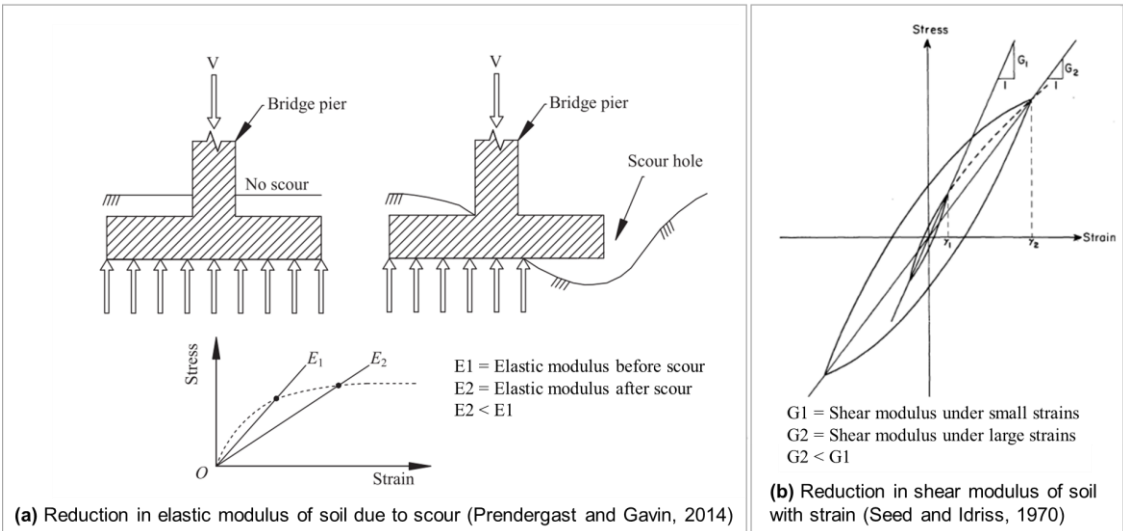


Figure 6.1 Reduction in stiffness properties due to increased strain caused by scour

This research considered two different small-strain soil stiffness representations. API (2002) method estimates the stiffness to increase linearly with depth. Seed and Idriss (1970) estimates stiffness to increase nonlinearly (hyperbolically) with depth, as shown in Figure 5.12. The nonlinear stiffness profile estimated in Seed and Idriss (1970) provided a better prediction of the natural frequency variations observed in the experiment. This non-linear behaviour arises due to the fact that Seed and Idriss (1970) assumes the small-strain shear modulus of sands to be proportional to the 0.5 power of the effective stress, given the relative density remain the same, and the strains are small.

Saturated conditions can also provide some nonlinearity. At the same depth, self-weight effective stress under saturated conditions (typical for a bridge crossing a water body) is lower than the self-weight effective stress under dry condition (considered for the centrifuge model). As discussed above, the small-strain shear modulus of soil is directly dependent on the effective stress. Therefore, lower effective stress of saturated soil leads to a lower shear modulus of soil and thus lower natural frequency of the bridge. Additionally, the presence of water around bridge pier in the field could further reduce the natural frequency of bridges due to the added mass of water the bridge piers submerged in water have to displace when vibrating. However previous research has found that the natural frequency sensitivity to scour does not depend significantly on the level of saturation of the soil and the water level, given the bridge piers are stiff (Ju, 2013; Prendergast *et al.*, 2013) (further discussed in Section 2.4.1.4).

Vibration behaviour observed in the models also showed some nonlinearity. For example, the natural frequency reduction due to scour was nonlinear. For the simple lumped mass fixed cantilever in Section 2.4.1, the natural frequency sensitivity was found to have a negative power relationship with the exposed height of the pier (scour depth + initial pier height). Similar nonlinear behaviour was observed for the four centrifuge models, where the natural frequency sensitivity to scour reduced slightly with the depth of scour. Another nonlinear vibration behaviour was observed in the PDS estimates. The shape of the PSD values over the peaks in Figure 4.25 showed some asymmetry – peaks leaned more towards higher frequency - suggesting there may have been nonlinear “stiffening spring” effect (Gui *et al.*, 1998; Benedettini, Zulli and Vasta, 2006). Stiffening spring effect refers to the increase of the effective stiffnesses provides by the spring of a system represented as a spring-mass system. This may be a behaviour that happens in soil-structure interaction, where the soil may have become stiffer due to ratcheting, i.e. accumulation of strain (Houlsby *et al.*, 2017), however, it is difficult to pinpoint this stiffening behaviour to the soil since the amplitudes of vibration of soil-structure interaction were found to be minute (lower than 23-27 μm).

Other nonlinearities could be present in a bridge under special circumstances. When the amount of cracking on the superstructure is significant, the overall stiffness of the bridge

elements would be lower than the uncracked state, and thus the natural frequencies would reduce and mode shape amplitudes would increase. However, previous research has found that natural frequencies of a bridge are not significantly sensitive to cracking, as discussed in Section 6.2. Additional nonlinearities could arise when the temperature and other environmental effects on the modal parameters change significantly. However, these changes have also not been found to be significant (Section 6.2), although they could add some nonlinearities to the observed changes in the modal parameters. Gapping effects could also add some nonlinearity since the gaps around a pile add some discontinuity up to the depth of the gaps, however gapping is mainly a concern only for high amplitudes of vibration in cohesive soils (Pranjoto and Pender, 2003).

As discussed above, nonlinear behaviour of soil, structure, soil-structure interaction and vibration behaviour could be expected, and these should be carefully considered when attempting to use vibration-based scour monitoring techniques in practice.

6.5 Potential behaviour in cohesive soils

The primary scope of this research has been on non-cohesive soils such as sand and gravel. Cohesive soils (clay and silt) would differ to a certain extent in their scour mechanisms and the stiffnesses provided.

Non-cohesive soil most commonly forms the bed of a channel whilst finer and cohesive sediments generally form the floodplain (Arneson *et al.*, 2012). In the case of non-cohesive sediments, individual particles are prone to scour when the fluid forces are higher than the combined force of gravity and contact friction of the bed particles. In the case of cohesive sediments, most fine-grained sediments possess some cohesion, the clay content being of great importance. Also, submerged fine-grained soil can become cohesive due to biological action like the growth of algae. While granular soil erodes particle by particle, cohesive soil erodes in clumps. Cohesive sediments typically require relatively large forces to initiate movement, but relatively small forces to transport the particles away. The maximum scour depth is comparable to that of non-cohesive soils, and therefore, there may be little effect of the scour mechanism to the potential to implement vibration-based scour monitoring. The difference in scour mechanism is in the rate of erosion and location of where the maximum scour occurs (around cylindrical bridge piers, cohesive soils develop the deepest scour at the sides of piers whereas non-cohesive soils develop the deepest scour in front of the piers) (CIRIA, 2015). This research considered only two shapes of scour, local scour along the full width of the bridge piers with all sides with a 30° inclination and global scour where the full ground level reduces by the depth of scour. However, there was little effect of the shapes of scour on the sensitivities of natural frequency and mode shapes. Therefore, natural frequency

and mode shapes are unlikely to be affected by the differences in the scour mechanisms of cohesive and cohesionless soil.

In both sands and clays, the small-strain shear modulus (G_0) can be related to the effective stress (σ'_0) by the following power law: $G_0 \propto \sigma'^m_0$. For a given void ratio, the exponent m has been found to be 0.5 for sands and 0.7-1.0 for clays (Benz, 2007). This means the small-strain stiffness variation with depth is more linear in clay than in sand. And this exponent m for clay increases with higher liquid limit or plasticity index. Sands show the same G_0 for a given effective stress (σ'_0), irrespective of the level of saturation, that is, whether it is dry or fully saturated sand (Benz, 2007). However, saturation has a major impact on G_0 of clays. If the water content in clay is close to the liquid limit, G_0 reduces significantly. On the other hand, the large strain shear modulus is highly dependent on the plasticity index, the higher the plasticity index, the closer the large strain stiffness of clays to the small-strain value (Vucetic and Dobry, 1991). Therefore, the changes in water content could vary the modal parameters of the bridge significantly.

With cohesive soils, large strain vibrations could result in gapping as a result of plastic deformations (Pranjoto and Pender, 2003). For horizontal vibrations of a pile, the gaps may form in both vibrating sides of the piles. However, these types of gaps form primarily during large strain vibrations that result from, for example, earthquakes, but not during traffic and other ambient vibrations that are of interest to vibration-based scour monitoring.

Another aspect that affects the properties of clay is the level of overconsolidation. G_0 increases with higher overconsolidation ratio (OCR) according to the relationship $G_0 \propto OCR^k$ (Hardin and Black, 1969). k exponent is near 0 for sands (G_0 is independent of OCR) but it is near 0.5 for high plasticity clays. Therefore the effect of OCR (ratio between maximum past vertical effective stress and current vertical effective stress) on G_0 is mostly seen in clays as opposed to sands. This implies that the “spring shifting” assumption made for the global scour (Section 2.4.1.3) may be valid for sands, but it would have to be improved for clays as the new ground after scour is overconsolidated due to the released confining pressure of the overlying layer of soil that was scoured away. However, G_0 for clays depend on the effective stress as discussed above and hence the new ground level after scour should, in theory, have zero stiffness. Therefore, the global scour case for clay riverbeds is also unlikely to be close to the existing “spring deleting” since that method assumes the new ground level has some residual stiffness at the new ground level after scour. Therefore, numerical simulation of global scour of cohesive soil requires a case in between “spring deleting” and spring shifting” assumptions.

Therefore, vibration-based scour monitoring of bridges on cohesive beds, rather than on cohesionless beds, require additional considerations of the effects of soil-structure interaction due to gapping, saturation and overconsolidation.

6.6 Scour monitoring potential in different types of bridges and forms of scour

Comparisons of the two foundation types (deep and shallow) studied with centrifuge modelling and associated numerical modelling (Chapter 4 and 5), found that bridges with deep foundations have scour monitoring potential with any of the three vibration parameters considered. In contrast, spectral density was the only parameter that exhibited a significant change in shallow foundations undergoing scour. For example, for a metre of local scour, the fundamental natural frequencies showed greater changes in the deep foundation (12.1%) than in the shallow pad foundation (3.5%). The mode shapes showed almost no change in the shallow foundation model but exhibited some changes in the deep pile bent. The spectral density for the same scour case showed a greater change in the shallow foundations (417%) than the deep foundations (214%). Therefore, spectral density seems to be the best, and perhaps only, feasible parameter for evaluating the effects of scour for bridges with shallow foundations. This means that vibration-based scour monitoring can be used in bridges with both deep and shallow foundations; however, it has the most potential in bridges with deep foundations.

Comparison of the two different scour types found a greater change in all modal parameters for global than for local scour, although the difference was only significant for spectral density. For example, the integral bridge model showed 40% and 70% spectral density changes for local and global scour, respectively, a significant difference between the two scour types. However, natural frequency and mode shapes in the same bridge model did not show a significant difference between global scour and local scour in all foundations. One can argue that local scour of the pier causes a much smaller frequency change (4.6% per 1 m) than global scour (12.1% per 1 m) in the integral bridge (Section 4.8.1). However, this significant difference is due to the global scour case involving scour in all foundations, including the abutments, while the local pier scour case does not include abutment scour. Once abutment local scour is also considered, which is a more reasonable comparison to global scour, local and global scour show only a 0.5% difference in frequency change for each 1 m of scour. For the shallow foundation considered, there was a slightly higher, but still not significant, natural frequency difference between local and global scour (about 1% for 1 m of scour). Such a different behaviour between the two scour cases is to be expected, as unscoured soil, slightly distant from the stub column, still provides a degree of increased pad foundation fixity, leading to higher stiffness and hence higher natural frequency for local scour relative to global scour. Therefore, the scour type considered for the same bridge foundations has a significant effect on the spectral density only out of the three vibration-based parameters considered.

Comparison of the deck type found more vibration-based scour monitoring potential in the integral than in the simply supported bridge. A full-scale integral bridge and a simply supported

bridge were studied, with all bridge deck and pier elements having similar properties (Chapter 5). The integral bridge showed an approximately 5% change in fundamental natural frequency for 1 m of local scour, while the simply supported bridge showed only a 2% change for the same scour case. It is noteworthy that the simply supported bridge showed a high natural frequency change in the higher-order modes. For example, Mode 2 and Mode 19 of the simply supported bridge showed changes of approximately 4% and 8%, respectively, in natural frequency for local scour of 1 m. There would be, however, practical limitations to capturing significantly higher-order modes such as Mode 19 in the field, as they would not be sufficiently excited by ambient vibrations (Wenzel and Pichler, 2005). The mode shapes, however, showed potential in both simply supported and integral bridges.

In summary, vibration-based techniques have significant scour monitoring potential, especially when all three vibration-based parameters highlighted in this research are integrated. The first parameter, natural frequency, is a reliable indicator of scour; however, the measurement uncertainties in the field would limit the measurement resolution to extensive, metre-scale scour depths. The other two parameters, mode shapes and spectral densities, showed the potential to indicate scour earlier than natural frequency. Mode shapes also showed the potential for scour localisation, which is certainly beneficial for bridge engineers in understanding where the scour repair is needed. These parameters can be derived with ambient vibration data measured by accelerometers on the bridge above water level. Therefore, this monitoring technique is safe from damage due to debris and rapid water flow and is easily implementable as a real-time monitoring solution, unlike most other scour monitoring techniques. Therefore, when the parameters of natural frequency, mode shape and spectral density are combined, vibration-based methods provide a powerful approach to detect extensive scour at bridges, irrespective of the type of bridge or scour present.

Chapter 7

Limitations of this research and suggestions for future research and practice

Several aspects that were not addressed in this research and were limitations of this research require attention in the future for further development of vibration-based bridge scour monitoring techniques.

7.1 Recommended further research areas

The findings of this research are based on a limited number of beam-slab type bridges. Other types of bridges, such as masonry arch bridges and suspension bridges, were not considered in this research. Additionally, other bridges with similar bridge types, but different dimensions and material properties, may not behave exactly the same as those considered in this research. Therefore, more experimental and numerical research is needed as sensitivity studies on different bridge types and configurations.

One main assumption in the centrifuge experiments and numerical models was that the water-bridge interaction is negligible. Based on this assumption, the centrifuge test was conducted in dry soil, but this assumption may not hold entirely true in a typical field-scale bridge. Boujia et al. (2019) and Prendergast et al. (2013) found that natural frequency change is not sensitive to water level or soil saturation. However, it is unknown whether the mode shapes and spectral density are sensitive to the water-structure interaction, and therefore this assumption needs to be investigated in the future. It is likely that the water-bridge interaction would not prevent the vibration-based scour monitoring, as the field trial was successful at capturing the effects of scour even when water-soil interaction was present.

The field trial and centrifuge experiments were on bridges that are situated on sand and gravel beds. Further experimental research is required to study the natural frequency sensitivity of bridges with foundations in clay and saturated sand layers. Additionally, the soil model in the centrifuge experiment was of uniform density, whereas, in practice, density and material properties may vary with depth in different layers of soil. It is not clear to what extent this may be significant, especially in the case of piles where the pile-soil stiffness is dominated by the soil restraint around the pile head (top interface at the surface of the soil), rather than the restraint offered at depth. A gradual reduction in frequency sensitivity with scour depth may not be noticed with a real bridge on layered or non-uniform soil. This aspect needs further investigation, with enhanced models to represent layered soils.

The spectral density parameter was studied with field and laboratory experiments but not with numerical models. It is recommended that future research could study this parameter, with vehicle-soil-bridge interaction models that consider damping for different bridge configurations.

The mode shape variation of a bridge pier undergoing scour was found to be highest near the ground level. If the greatest changes in mode shape amplitude were to be measured, the accelerometers would need to be on the part of the pier underwater, although instrumentation durability issues might arise when they are underwater. Such an accelerometer may also measure noise due to the turbulence of water around the accelerometer, in addition to the structural vibration that it intends to capture. This aspect requires further research.

Future centrifuge modelling experiments attempting to derive the changes in the small-strain shear modulus of soil underlying a scoured region should use significant sampling rates (above 100 kHz) for the accelerometers embedded in soil to capture shear waves. This research used a sampling rate of 30 kHz, which provided insufficient measurement resolutions. Furthermore, if multiple air hammers were to be used, it is recommended to use multiple relay switches rather than one switch to control the pressure to the air hammers, in order to avoid interference of multiple shear waves reaching an accelerometer at the same time from different air hammers.

Future research on scour monitoring techniques could potentially benefit from the location-based categorisation and the new scour monitoring solutions suggested in Table 2.13.

In summary, while this research demonstrates the significant potential of a vibration-based scour monitoring method, further research involving multiple full-scale bridges in the field, centrifuge experimental research considering water-bridge interaction, and numerical sensitivity studies on spectral density could provide valuable additional insights into the applicability of this approach to monitoring scour.

7.2 A recommended approach for using this vibration-based scour monitoring method in practice

As a result of the field trial carried out in this research, the author has identified a set of recommendations for how this approach can be used in practice to monitor bridge scour. The recommended first step is collecting information on the bridge properties and the history of underwater scour. Scour monitoring can be planned if the bridge is found to be scour-susceptible based on the collected information and risk analysis using standard guidance such as Highways Agency (2012). The second step is studying whether the three vibration-based parameters proposed are feasible for the specific bridge. For such a feasibility study, an initial numerical model should be developed, as was done for Baildon Bridge (Chapter 3). If the numerical model indicates sufficient modal parameter changes due to scour, field deployment

can then be planned. The third step is developing a method statement for the instrumentation. To develop this method statement, the initial numerical model can aid by establishing the scour-sensitive mode shapes. For example, the natural frequencies of the scour-sensitive modes indicate the bandwidth of the required accelerometers. Furthermore, the mode shapes of the scour-sensitive modes can help in determining the sensor arrangement; in other words, sensor locations with high modal amplitudes are preferable. The fourth step is preparing all parts of the instrumentation system that can be pre-built and pre-tested before being taken to the site. For example, the data-acquisition system was pre-built and pre-tested before visiting Baildon Bridge.

The fifth step is instrumenting the planned system at the bridge, which would take between one and several days, depending on the complexity of the instrumentation and the size of the bridge. In Baildon Bridge instrumentation, the use of special techniques minimised drilling and reduced the time spent on a boat over the water, while also improving safety. Once the ambient vibration measurement system is up and running, the sixth step is using the initial vibration measurements to update the initial numerical model. In the initial numerical model of Baildon Bridge, several errors in boundary condition estimates could be identified and corrected based on the first experimental observation of natural frequencies. Such model updating allows self-calibration of the numerical model, similar to the self-calibration explained in vibration-based rod devices (Zarafshan, Iranmanesh and Ansari, 2012). This updated numerical model would help in estimating the relationship between scour depth and scour-sensitive parameter, similar to the graph of natural frequency versus scour in Figure 3.18 and mode shape versus scour in Figure 3.19. The last, but most crucial, step is continuous ambient vibration monitoring, ideally with real-time modal identification, until a change in the scour-sensitive modal parameter is observed. Bridge engineers or technicians can interpret the changes in natural frequency, mode shape and spectral density using the pre-prepared graphs, or the trends suggested in this research, to determine the corresponding scour depth. These steps would help future deployments of vibration-based scour monitoring techniques, as they helped in the deployment at Baildon Bridge.

Chapter 8

Conclusions and recommendations

This research describes an experimental and numerical study developed to investigate the potential for using vibration-based scour monitoring techniques to monitor scour at bridge foundations. The experiments involved small-scale bridge models tested in a centrifuge and a full-scale road bridge (Baildon Bridge) monitored during a scour backfilling repair programme. The small-scale centrifuge models attempted to simulate the dynamic behaviour of three full-scale bridges with different bridge deck and foundation configurations (i.e. integral/ simply supported decks and shallow/deep foundations) and two forms of scour (i.e. local/global). Numerical modelling examined these bridges using various finite elements representing the bridge structure and Winkler and macro element spring models representing the soil-structure interaction. Based on these experiments and the associated numerical modelling, the following main conclusions are drawn:

1. A vibration-based scour monitoring technique examining the combined effect of three vibration parameters (modal spectral density, mode shape and natural frequency) has the potential to identify and locate changes in scour depth at bridge foundations to a resolution of approximately 0.5 m for global scour and 0.6 m for local scour. Such a vibration-based technique has several advantages over existing methods for monitoring scour. These include the ability to remotely monitor bridges in real-time using ambient vibration, including during flood events; the durability and robustness of the sensor system as it is located above the water level on the bridge piers and superstructure; and it is not restricted to giving a scour depth measure at a single point location.
2. A novel vibration-based scour monitoring parameter – modal spectral density – showed significant sensitivity to scour depth. The field trial at Baildon Bridge demonstrated the potential of this parameter to capture the progressive scour backfilling of a 1.8 m local scour hole, with a change of 75% (measurement uncertainty $\pm 25\%$); thus it provided a scour depth measurement resolution of approximately 0.6 m. The centrifuge experiments with different bridge and scour types estimated significant modal spectral density changes, ranging from 40% to 1200% per 1 m of scour. Furthermore, this parameter showed significantly more sensitivity to global scour than to local scour. This parameter was the only reliable indicator of scour (out of the three parameters considered) for the shallow pad foundation model studied in the centrifuge.

3. A vibration-based parameter that has received little attention as a scour monitoring parameter – mode shape – showed significant scour monitoring potential, according to both the field trial at Baildon Bridge and the centrifuge experiment. Mode shapes showed a localised increase in modal amplitudes, primarily on the pier near the location of scour, allowing scour localisation to the specific bridge pier undergoing scour. The study on different bridge configurations found that mode-shape-based scour monitoring techniques are best suited to bridges with deep foundations, and not to bridges with shallow foundations, unless higher-order (difficult to measure in practice) modes are considered. Mode-shape-based scour monitoring showed potential for both integral and simply supported bridges. The mode shape sensitivity to global scour was only negligibly higher than it was to local scour.
4. The commonly used vibration-based scour monitoring parameter – natural frequency – also has the potential to indicate metre-scale scour depths. The natural frequency change in the field trial was not captured because of its high measurement uncertainty. Numerical modelling of more extensive scour cases found that this uncertainty limits the scour depth resolutions to 0.5 m of global scour and 1.7 m of local pier scour. The centrifuge experiment and numerical modelling found natural frequency reductions in the range of 4 – 8% per 1 m of scour for the most scour-sensitive mode. The natural-frequency-based methods using the fundamental mode were found to be most suitable for bridges with the integral deck and deep piled foundations, rather than for bridges with a simply supported deck and/or shallow foundations. The fundamental natural frequency reduction due to global scour was only slightly (less than 1% per 1 m) higher than that caused by local scour.
5. The centrifuge modelling experiment programme and the methodology developed in this research successfully simulated full-scale bridge scour and the resulting vibration behaviour using small-scale models. The tools and techniques developed would be beneficial for future experimental research on vibration-based scour monitoring.
6. Winkler spring models and macro element model representations closely simulated the global and local scour using the “stiffness/springs lowering” method and “stiffness/springs deleting” method, respectively (see Section 5.1).

References

- Aalco (2019a) *Aluminium Alloy - Commercial Alloy - 6061 - T6 Extrusions*. Available at: http://www.aalco.co.uk/datasheets/Aluminium-Alloy-6061-T6-Extrusions_145.ashx (Accessed: 10 January 2020).
- Aalco (2019b) *Aluminium Alloy - Commercial Alloy - 6082 - T6~T651 Plate*. Available at: http://www.aalco.co.uk/datasheets/Aluminium-Alloy_6082-T6~T651_148.ashx (Accessed: 10 January 2020).
- AIRMAR (2017) *EchoRange™ Smart™ Sensor & Dual Frequency EchoRange™ Smart™ Sensor Low-Cost and Portable Depth Sensors for Hydrographic Survey*. NH, USA: Airmar Technology Corporation.
- Akogul, C. and Celik, O. C. (2008) 'Effect of elastomeric bearing modeling parameters on the Seismic design of RC highway bridges with precast concrete girders', in *The 14 World Conference on Earthquake Engineering*. Beijing, China.
- Amrita (2011) *Free Vibration of a Cantilever Beam (Continuous System)*. Available at: <http://vlab.amrita.edu/?sub=3&brch=175&sim=1080&cnt=1> (Accessed: 8 September 2020).
- Analog Devices (2010) *Single-Axis, High-g, iMEMS® Accelerometers ADXL78*. Available at: <https://www.analog.com/media/en/technical-documentation/data-sheets/ADXL78.pdf>.
- Analog Devices (2017) *Low Noise, High Frequency MEMS Accelerometers ADXL 1001/ADXL 1002*. Available at: <https://www.analog.com/media/en/technical-documentation/data-sheets/ADXL1001-1002.pdf>.
- Anderson, N. L., Ismael, A. M. and Thitimakorn, T. (2007) 'Ground-penetrating radar: A tool for monitoring bridge scour', *Environmental and Engineering Geoscience*, 13(1), pp. 1–10. doi: 10.2113/gseegeosci.13.1.1.
- API (2002) *Recommended Practice for Planning, Designing and Constructing Fixed Offshore Platforms — Working Stress Design*. 2nd edn. Washington DC, United States: American Petroleum Institute.
- Arneson, L. A., Zevenbergen, L. W., Lagasse, P. F. and Clopper, P. E. (2012) *Evaluating Scour at Bridges*. 5th edn. Colorado, USA: U.S. Department of Transportation Federal Highway Administration. Available at: <http://www.fhwa.dot.gov/engineering/hydraulics/pubs/hif12003.pdf>.
- Ashford, S. A. and Juirnarongrit, T. (2003) 'Evaluation of Pile Diameter Effect on Initial Modulus of Subgrade Reaction', *Journal of Geotechnical and Geoenvironmental Engineering*, 129(3), pp. 234–242. doi: 10.1061/(ASCE)1090-0241(2003)129:3(234).
- Bao, T. and Liu, Z. (2016) 'Vibration-based bridge scour detection: A review', *Structural Control and Health Monitoring*, 24(e1937). doi: 10.1002/stc.1937.
- Benedettini, F., Zulli, D. and Vasta, M. (2006) 'Nonlinear response of SDOF systems under combined deterministic and random excitations', *Nonlinear Dyn*, 46(January 2017), pp. 375–385. doi:

10.1007/s11071-006-9029-9.

Benz, T. (2007) *Small-Strain Stiffness of Soils and its Numerical Consequences*. Doctoral dissertation. University of Stuttgart.

Boujja, N., Schmidt, F., Siegert, D., Bang, D. P. Van and Chevalier, C. (2017) 'Modelling of a bridge pier subjected to scour', *Procedia Engineering*, 199, pp. 2925–2930. doi: 10.1016/j.proeng.2017.09.343.

Boujja, N., Schmidt, F., Chevalier, C., Siegert, D. and Bang, D. P. Van (2019) 'Effect of Scour on the Natural Frequency Responses of Bridge Piers : Development of a Scour Depth Sensor', *infrastructures*, 4(21). doi: 10.3390/infrastructures4020021.

Bovio, E. (2005) 'Autonomous Underwater Vehicles for Port Protection', in *New Concepts for Harbour Protection, Littoral Security and Shallow- Water Acoustic Communication*. Istanbul, Turkey.

Brandt, A. and Brincker, R. (2010) 'Impact Excitation Processing for Improved Frequency Response Quality', in *Proceedings of the IMAC-XXVIII*. Florida, USA: Society for Experimental Mechanics.

Briaud, J., Hurlebaus, S., Chang, K., Yao, C., Sharma, H., Yu, O., Darby, C., Hunt, B. E. and Price, G. R. (2011) *Realtime monitoring of bridge scour using remote monitoring technology*. Austin, Texas. Available at: <http://tti.tamu.edu/documents/0-6060-1.pdf>.

Briaud, J., Yao, C., Darby, C., Sharma, H., Hurlebaus, S., Price, G. R., Hunt, B. E. and Yu, O. Y. (2010) 'Motion Sensors for Scour Monitoring: Laboratory Experiments and Numerical Simulations', in *Transportation Research Board 89th Annual Meeting*. Washington DC, United States: Transportation Research Board, pp. 1–22.

Brincker, R., Anderson, P. and Jacobsen, N.-J. (2007) 'Automated Frequency Domain Decomposition for Operational Modal Analysis', in *IMAC-XXV: Conference & Exposition on Structural Dynamics*. Florida, USA: Society for Experimental Mechanics.

Brincker, R., Zhang, L. and Andersen, P. (2001) 'Modal identification of output-only systems using frequency domain decomposition', *Smart Mater. Struct.*, 10(3), pp. 441–445.

Caetano, E. and Magalha, F. (2009) 'Online automatic identification of the modal parameters of a long span arch bridge', *Mechanical Systems and Signal Processing*, 23(2), pp. 316–329. doi: 10.1016/j.ymssp.2008.05.003.

Cantero, D., Ülker-Kaustell, M. and Karoumi, R. (2016) 'Time-frequency analysis of railway bridge response in forced vibration', *Mechanical Systems and Signal Processing*, 76–77, pp. 518–530. doi: 10.1016/j.ymssp.2016.01.016.

Cedrat Technologies (2014) *APA400MML datasheet*. Maylan, France. Available at: <https://www.cedrat-technologies.com/fileadmin/datasheets/APA400MML.pdf>.

Cha, M., Santamarina, J. C., Kim, H. and Cho, G. (2014) 'Small-Strain Stiffness, Shear-Wave Velocity, and Soil Compressibility', *J. Geotech. Geoenviron. Eng.*, 140(10), pp. 1–4. doi: 10.1061/(ASCE)GT.1943-5606.0001157.

Chatzigogos, C., Pecker, A. and Salencon, J. (2008) 'Macroelement modeling of shallow foundations',

- Soil Dynamics and Earthquake Engineering*, 29(5), pp. 1–30. doi: 10.1016/j.soildyn.2008.08.009.
- Chen, Y., Tang, F., Li, Z. and Chen, G. (2018) 'Bridge scour monitoring using smart rocks based on magnetic field interference', *Smart Mater. Struct.*, 27(8). doi: 10.1088/1361-665X/aacbf9.
- CIRIA (2015) *Manual on Scour at Bridges and Other Hydraulic Structures*. 2nd edn. Edited by A. Kirby et al. London, UK: Department for Transport.
- Clark, L. A. and Cope, R. J. (1984) *Concrete Slabs: Analysis and design*. Essex, England: CRC Press.
- CNTV (2010) *Train cars fall into Sichuan river*. Available at: <http://english.cntv.cn/program/china24/20100820/101641.shtml> (Accessed: 1 May 2017).
- Computers & Structures Inc. (2016a) *CSI Analysis Reference Manual CSiBridge 2017*. California, USA: Computers & Structures, Inc.
- Computers & Structures Inc. (2016b) *CSI Analysis Reference Manual SAP2000*. California, USA.
- Concast Precast Ltd (2009) *Precast Concrete Beam Technical Manual*. Dublin, Ireland. Available at: https://www.concast.ie/wp-content/uploads/2020/03/Concast_Civil.pdf.
- Deng, L. and Cai, C. S. (2010) 'Bridge Scour: Prediction, Modeling, Monitoring, and Countermeasures — Review', *Pract. Period. Struct. Des. Constr.*, 15(2), pp. 125–134.
- Department for Transport UK (2016) *Rail Accident Report-Structural failure caused by scour at Lamington viaduct, South Lanarkshire 31 December 2015*. Available at: https://www.railwaysarchive.co.uk/documents/RAIB_LamingtonViaduct2015.pdf.
- Dikanski, H., Hagen-Zanker, A., Imam, B. and Avery, K. (2016) 'Climate change impacts on railway structures : bridge scour', *Proceedings of the Institution of Civil Engineers Engineering Sustainability*, 170(5). doi: 10.1680/jensu.15.00021.
- Diving Services Inc. (2017) *Underwater bridge inspections*. Available at: [http://www.divingservicesinc.com/Bridge Inspections.html](http://www.divingservicesinc.com/Bridge%20Inspections.html) (Accessed: 10 May 2017).
- DJB Instruments (2018) *A / 23 / TS Piezoelectric Accelerometer*. Available at: <http://www.djbinstruments.com/app/djb/files-module/local/datasheets/A-23-TS.pdf>.
- Döhler, M., Hille, F., Mevel, L. and Rucker, W. (2014) 'Structural health monitoring with statistical methods during progressive damage test of S101 Bridge', *Engineering Structures*, 69, pp. 183–193. doi: 10.1016/j.engstruct.2014.03.010.
- Dong, J. (2016) *THE NATURAL FREQUENCY OF MONOPILE FOUNDATION FOR OFFSHORE WIND TURBINES*. M.Phil. dissertation, University of Cambridge.
- Dutta, S. C. and Roy, R. (2002) 'A critical review on idealization and modeling for interaction among soil – foundation – structure system', *Computers and Structures*, 80(20–21), pp. 1579–1594.
- Elsaid, A. H. and Seracino, R. (2012) 'Vibration Based Damage Detections of Scour in Coastal Bridges', *Homeland Security Affairs*, 4(2).

Elsaid, A. and Seracino, R. (2014) 'Rapid assessment of foundation scour using the dynamic features of bridge superstructure', *Construction and Building Materials*, 50, pp. 42–49. doi: 10.1016/j.conbuildmat.2013.08.079.

EPSON (2018) *M-A550AR2x Data Sheet (P/N: E91E60814x)*. Fujimi, Japan: Seiko Epson Corporation. Available at: https://global.epson.com/products_and_drivers/sensing_system/download_hidden/pdf/m-a550ar2x_datasheet_e_20180315.pdf.

European Standard (2002) *Eurocode 1: Actions on structures – Part 1-1: General actions – Densities, self-weight, imposed loads for buildings*. Brussels.

European Standard (2004) *Eurocode 2: Design of concrete structures – Part 1-1: General rules and rules for buildings*. Brussels.

Fadool, J. C., Francis, G., Clark, J. E., Liu, G. F. and DeBrunner, V. (2012) 'Robotic Device for 3D Imaging of Scour around Bridge Piles', in *Proceedings of the ASME International Design Engineering Technical Conferences and Computers and Information in Engineering Conference 2012, Vol 4, Pts A and B*, pp. 1125–1131. doi: 10.1115/DETC2012-71335.

Falco, F. De and Mele, R. (2002) 'The monitoring of bridges for scour by sonar and sediment', *NDT&E International*, 35, pp. 117–123.

Farrar, C. R., Baker, W. E., Bell, T. M., Cone, K. M., Darling, T. W., Duffey, T. A., Eklund, A. and Migliori, A. (1994) *Dynamic characterization and damage detection in the I-40 bridge over the Rio Grande (Technical report)*. California, USA: Los Alamos National Lab.

Fisher, M., Chowdhury, M. N., Khan, A. A. and Atamturktur, S. (2013) 'An evaluation of scour measurement devices', *Flow Measurement and Instrumentation*, 33, pp. 55–67. doi: 10.1016/j.flowmeasinst.2013.05.001.

Fitzgerald, P. C., Malekjafarian, A., Cantero, D., O'Brien, E. J. and Prendergast, L. J. (2019) 'Drive-by scour monitoring of railway bridges using a wavelet-based approach', *Engineering Structures*, 191, pp. 1–11. doi: 10.1016/j.engstruct.2019.04.046.

Fondriest Environmental Inc. (2017) *Scour Monitoring Equipment*. Available at: <http://www.fondriest.com/environmental-measurements/equipment/monitoring-equipment/scour-monitoring-equipment/> (Accessed: 6 March 2017).

Futai, M. M., Dong, J., Haigh, S. K. and Madabhushi, S. P. G. (2018) 'Dynamic response of monopiles in sand using centrifuge modelling', *Soil Dynamics and Earthquake Engineering*, 115, pp. 90–103. doi: 10.1016/j.soildyn.2018.08.007.

Gazetas, G. (1991) 'Formulas and charts for impedances of surface and embedded foundations', *Journal of Geotechnical Engineering*, 117(9), pp. 1363–1381. doi: 10.1061/%28ASCE%290733-9410%281991%29117%3A9%281363%29.

Gui, C., Legtenberg, R., Tilmans, H. A. C., Fluitman, J. H. J. and Elwenspoek, M. (1998) 'Nonlinearity and Hysteresis of Resonant Strain Gauges', *Journal of microelectromechanical systems*, 7(1), pp. 122–127.

- Hafez, Y. I. (2016) 'Mathematical Modeling of Local Scour at Slender and Wide Bridge Piers', *Journal of Fluids*, 2016. doi: 10.1155/2016/4835253.
- Harden, C., Hutchinson, T., Martin, G. R. and Kutter, B. L. (2005) *Numerical Modeling of the Nonlinear Cyclic Response of Shallow Foundations*. California, USA: Pacific Earthquake Engineering Research Centre, University of California, Berkeley.
- Hardin, B. O. and Black, W. L. (1969) 'Closure to : Vibration Modulus of Normally Consolidated Clay', *Journal of the soil mechanics and foundation division*, 95(SM6), pp. 1531–1537.
- Hardin, B. O. and Drnevich, V. P. (1972) 'Shear modulus and damping in soils: design equations and curves', *Journal of Soil Mechanics & Foundations Division*, 98(sm7), pp. 667–691.
- Hayes, D. C. and Drummond, F. E. (1995) *Use of Fathometers and Electrical-Conductivity Probes to Monitor Riverbed Scour at Bridge Piers: Investigations Report 94-4164*. Richmond, Virginia: U.S. GEOLOGICAL SURVEY Water-Resources.
- He, J. and Fu, Z.-F. (2001) *Modal analysis*. Oxford, UK: Butterworth Heinemann.
- Highways Agency (2001) 'The assessment of highway bridges and structures', in *Design Manual for Roads and Bridges, Volume 3, Section 4, Part 3 BD 21/01*.
- Highways Agency (2012) 'The Assessment of Scour and Other Hydraulic Actions at Highway Structures (BD97/12)', in *Design Manual for Roads and Bridges, Volume 3, Section 4, Part 21 BD 97/12*.
- Hill, D. (2016) 'Unmanned Vessels Could Be Used to Inspect Bridges', *Civ. Eng.*, 86(1), pp. 36–36.
- Holnbeck, S. R. and McCarthy, P. M. (2010) 'Monitoring Hydraulic Conditions and Scour at I-90 Bridges on Blackfoot River Following Removal of Milltown Dam near Bonner, Montana, 2009', in *International Conference on Scour and Erosion 2010*, pp. 968–977.
- Houlsby, G. T., Abadie, C. N., Beuckelaers, W. J. A. P. and Byrne, B. W. (2017) 'A model for nonlinear hysteretic and ratcheting behaviour', *International Journal of Solids and Structures*, 120, pp. 67–80. doi: 10.1016/j.ijsolstr.2017.04.031.
- Hunt, B. E. (2005) 'Scour Monitoring Programs for Bridge Health', *Transportation Research Record: Journal of the Transportation Research Board*, pp. 531–536.
- Hunt, B. E. (2009) *Monitoring Scour Critical Bridges, NCHRP Synthesis 396*. DC, USA: The National Academies Press. doi: 10.17226/22979.
- Imhof, D. (2004) *Risk Assessment of Existing Bridge Structures*. Doctoral dissertation, University of Cambridge.
- Jacobsen, N., Andersen, P. and Brincker, R. (2007) 'Eliminating the Influence of Harmonic Components in Operational Modal Analysis', in *IMAC-XXIV: A Conference & Exposition on Structural Dynamics*. MO, USA: Society for Experimental Mechanics.
- Ju, S. H. (2013) 'Determination of scoured bridge natural frequencies with soil-structure interaction', *Soil Dynamics and Earthquake Engineering*, 55, pp. 247–254. doi: 10.1016/j.soildyn.2013.09.015.

- Kariyawasam, K., Fidler, P., Talbot, J. and Middleton, C. (2019a) *Data supporting field deployment of an ambient vibration-based scour monitoring system at Baildon Bridge UK*. doi: 10.17863/CAM.38041.
- Kariyawasam, K., Fidler, P., Talbot, J. and Middleton, C. (2019b) 'Field assessment of ambient vibration-based bridge scour detection', in *Structural Health Monitoring*. Stanford, CA, USA, pp. 374–381. doi: 10.12783/shm2019/32137.
- Kariyawasam, K., Fidler, P., Talbot, J. and Middleton, C. (2019c) 'Field deployment of an ambient vibration-based scour monitoring system at Baildon Bridge, UK', in *Proceedings of the International Conference on Smart Infrastructure and Construction*. Cambridge, UK: ICE UK, pp. 711–719. doi: 10.1680/icsic.64669.711.
- Kariyawasam, K., Middleton, C., Madabhushi, G., Haigh, S. and Talbot, J. P. (2020a) 'Assessment of bridge natural frequency as an indicator of scour using centrifuge modelling', *Journal of Civil Structural Health Monitoring*, (Accepted for publication). doi: 10.1007/s13349-020-00420-5.
- Kariyawasam, K., Middleton, C., Madabhushi, G., Haigh, S. and Talbot, J. P. (2020b) *Data supporting assessment of bridge natural frequency as an indicator of scour using centrifuge modelling*. doi: 10.17863/CAM.54904.
- Kariyawasam, K., Middleton, C., Talbot, J., Fidler, P., Haigh, S. and Madabhushi, G. (2021) 'On the potential for using bridge natural frequencies to detect scour: an experimental study with a field sensor deployment and geotechnical centrifuge modelling', in *IABSE Congress – Resilient technologies for sustainable infrastructure*. Christchurch, New Zealand: IABSE.
- Kaundinya, I. and Heimbecher, F. (2011) 'Identification and Classification of European Bridge and Tunnel Types', in *IABSE–IASS Symposium*. London, UK. Available at: http://www.seron-project.eu/download/Full-paper_IABSE_IASS_2011_Kaundinya.pdf.
- Kim, J. T., Yun, C.-B. and Yi, J.-H. (2003) 'Temperature Effects on Modal Properties and Damage Detection in Plate-Girder Bridges', *KSCE Journal of Civil Engineering*, 7(6), pp. 725–733. doi: 10.1007/BF02829141.
- Klinga, J. V. and Alipour, A. (2015) 'Assessment of structural integrity of bridges under extreme scour conditions', *Engineering Structures*, 82, pp. 55–71. doi: 10.1016/j.engstruct.2014.07.021.
- Kloppel, K. and Glock, D. (1970) 'Theoretische und experimentelle untersuchungen zu den traglastproblemen biegeweicher', in *die Evde eigenbetten Rohre*. Germany: Institut fuer Statik and Stahlbau.
- Ko, Y. Y., Lee, W. F., Chang, W. K., Mei, H. T. and Chen, C. H. (2010) 'Scour Evaluation of Bridge Foundations Using Vibration Measurement', in *5th International Conference on Scour and Erosion (ICSE-5)*. California, USA: ASCE, pp. 884–293.
- Koo, K. Y., Brownjohn, D. I. and Cole, R. (2010) 'Structural health monitoring of the Tamar Suspension', *Structural Control and Health Monitoring*, 20(4), pp. 609–625. doi: 10.1002/stc.1481.
- Lade, P. V., Liggio, C. D. and Yamamuro, J. A. (1998) 'Effects of Non-Plastic Fines on Minimum and Maximum Void Ratios of Sand', *Geotechnical testing journal*, 21(4), pp. 336–347. doi:

10.1520/GTJ11373J.

Lagasse, P. F., Clopper, P. E., Pagan-Ortiz, J. E., Zevenbergen, L. W., Arneson, L. a., Schall, J. D. and Girard, L. G. (2009) *Bridge Scour and Stream Instability Countermeasures: Experience, Selection, and Design Guidance-Third Edition, Hydraulic Engineering Circular No. 23*. United States.

Lasithan, L. G. (2014) *Mechanical Vibrations and Industrial Noise Control*. Delhi, India: PHI Learning Private Limited.

Lee, G. C., Mohan, S. B., Huang, C. and Fard, B. N. (2013) *A Study of U.S. Bridge Failures (1980-2012)*. New York, USA: University at Buffalo.

Liao, K. W., Cheng, M. Y., Chiu, Y. F. and Lee, J. H. (2016) 'Preliminary bridge health evaluation using the pier vibration frequency', *Construction and Building Materials*, 102, pp. 552–563. doi: 10.1016/j.conbuildmat.2015.11.011.

Lin, C., Han, J., Bennett, C. and Parsons, R. L. (2013) 'Case History Analysis of Bridge Failures due to Scour', in *International Symposium of Climatic Effects on Pavement and Geotechnical Infrastructure*. Alaska, USA, pp. 204–216.

Liu, K., Liu, J. L. and Yu, W. C. (2017) '2007~2015 年洪水导致垮塌桥梁的统计分析 (Statistical Analysis of Collapsed Bridges by Floods from 2007 to 2015)', *Urban Roads Bridges Flood Control*, 90, pp. 90–92. doi: 10.16799/j.cnki.csdqyfh.2017.01.025.

Livermore, C. (2007) *course materials for 6.777J / 2.372J Design and Fabrication of Microelectromechanical Devices, MIT OpenCourseWare*. Available at: <https://ocw.mit.edu/courses/electrical-engineering-and-computer-science/6-777j-design-and-fabrication-of-microelectromechanical-devices-spring-2007/lecture-notes/07lecture07split.pdf> (Accessed: 7 September 2020).

Madabhushi, G. (2014) *Centrifuge Modelling for Civil Engineers*. Florida, USA: CRC Press. Available at: <https://books.google.com/books?id=PL3LBQAAQBAJ&pgis=1>.

Madabhushi, S., Houghton, N. and Haigh, S. (2006) 'A new automatic sand pourer for model preparation at University of Cambridge', *Physical modelling in geotechnics -- 6th ICPMG '06*, pp. 217–222.

Malekjafarian, A., Prendergast, L. J. and OBrien, E. (2019) 'Use of mode shape ratios for pier scour monitoring in two-span integral bridges under changing environmental conditions', *Canadian Journal of Civil Engineering*, 47(8), pp. 962–973.

Masui, Y. and Suzuki, O. (2009) 'Development of a Soundness Evaluation System for Bridge Substructured', *JR EAST Technical Review*, 14, pp. 65–68.

Melville, B. W. and Coleman, S. E. (2000) *Bridge scour*. CO, USA: Water Resources Publications.

Mohamed, A. (2012) 'Chapter 1: Introduction to Offshore Structures', in *Offshore Structures : design*. Waltham, USA: Elsevier, p. 627. doi: 10.1016/B978-0-12-385475-9.00001-8.

Mory, M., Larroude, P., Carreiras, J. and Seabra Santos, F. (1999) 'Wave Scour Around Piles', in Losada

(ed.) *27th International Conference on Coastal Engineering*. Santander, Spain: Rotterdam, pp. 773–781. doi: 10.1061/40549(276)145.

Murphy, R. R., Steimle, E., Hall, M., Lindemuth, M., Trejo, D., Hurlebaus, S., Medina-Cetina, Z. and Slocum, D. (2011) 'Robot-assisted bridge inspection', *Journal of Intelligent and Robotic Systems: Theory and Applications*, 64, pp. 77–95. doi: 10.1007/s10846-010-9514-8.

Nassif, H., Ertekin, A. and Davis, J. (2002) *Evaluation of Bridge Scour Monitoring Methods*. New Jersey, USA: New Jersey Department of Transportation.

Newland, D. E. (1993) *An introduction to random vibrations and spectral analysis*. 3rd edn. Essex, England: Pearson Education Limited.

NI (2016) *User manual NI cRIO-9063*. Texas, USA: National Instruments. Available at: <http://www.ni.com/pdf/manuals/376507b.pdf>.

O'Brien, E. . and Keogh, D. . (1998) 'Upstand finite element analysis of slab bridges', *Computers & Structures*, 69(6), pp. 671–683. doi: 10.1016/S0045-7949(98)00148-5.

O'Brien, E. J. and Keogh, D. L. (1999) *Bridge Deck Analysis*. 1st edn. London: E & FN Spon.

OpenLearn (2020) *Root-mean-square amplitude*. doi: 10-09-2020.

Pastor, M., Binda, M. and Harcarik, T. (2012) 'Modal Assurance Criterion', *Procedia Engineering*, 48, pp. 543–548. doi: 10.1016/j.proeng.2012.09.551.

Pathak, R. and Pathak, S. (2018) 'A Mathematical Model to Dynamically Evaluate the Validity of Accelerometer Sensors', *SSRN*, pp. 1–7.

Peeters, B. and Roeck, G. De (2001) 'One-year monitoring of the Z24-Bridge : environmental effects versus damage events', *Earthquake Engng Struct. Dyn.*, 30, pp. 149–171.

Powrie, W. and Pen, L. Le (2016) *A guide to track stiffness*. Southampton, UK: University of Southampton.

Pranjoto, S. and Pender, M. J. (2003) 'Gapping effects on the lateral stiffness of piles in cohesive soil', in *7th Pacific Conference on Earthquake Engineering*. Christchurch, New Zealand: New Zealand Society for Earthquake Engineering.

Prendergast, Hester, D. and Gavin, K. (2016a) 'Determining the presence of scour around bridge foundations using vehicle-induced vibrations', *Journal Of Bridge Engineering*, 21(10), pp. 1–14. doi: 10.1061/(ASCE)BE.1943-5592.0000931.

Prendergast, Hester, D. and Gavin, K. (2016b) 'Development of a vehicle-bridge-soil dynamic interaction model for scour damage modelling', *Shock and Vibration*, 2016. doi: 10.1155/2016/7871089.

Prendergast, L. J., Hester, D., Gavin, K. and O'Sullivan, J. J. (2013) 'An investigation of the changes in the natural frequency of a pile affected by scour', *Journal of Sound and Vibration*, 332, pp. 6685–6702. doi: 10.1016/j.jsv.2013.08.020.

Prendergast, L. J. and Gavin, K. (2014) 'A review of bridge scour monitoring techniques', *Journal of*

- Rock Mechanics and Geotechnical Engineering*, 6(2), pp. 138–149. doi: 10.1016/j.jrmge.2014.01.007.
- Prendergast, L. J. and Gavin, K. (2016) 'A comparison of initial stiffness formulations for small-strain soil-pile dynamic Winkler modelling', *Soil Dynamics and Earthquake Engineering*, 81, pp. 27–41. doi: 10.1016/j.soildyn.2015.11.006.
- Prendergast, L. J., Gavin, K. and Hester, D. (2017) 'Isolating the location of scour-induced stiffness loss in bridges using local modal behaviour', *Journal of Civil Structural Health Monitoring*, 7, pp. 483–503. doi: 10.1007/s13349-017-0238-3.
- Roberts, J. (2017) *BridgeCat: Presentation at the 54th UK Bridge Owners Forum*. Available at: [http://www.bridgeforum.org/bof/meetings/bof54/BOF54 - Scour06 - Roberts - Gaist BridgeCat \(no video\).pdf](http://www.bridgeforum.org/bof/meetings/bof54/BOF54 - Scour06 - Roberts - Gaist BridgeCat (no video).pdf) (Accessed: 23 January 2019).
- Rudolph, D., Bos, K. and Luijendijk, A. (2004) 'Scour Around Offshore Structures - Analysis Of Field Measurements', in Chiew, Y.-M., Lim, S.-Y., and Cheng, N.-S. (eds) *2nd International Conference on Scour and Erosion*. Nanyang, Singapore.
- Sas, W., Gabryś, K., Soból, E. and Szymański, A. (2016) 'Dynamic Characterization of Cohesive Material Based on Wave Velocity Measurements', *Applied Sciences*, 6(49), pp. 1–21. doi: 10.3390/app6020049.
- Schofield, A. N. (1980) 'Cambridge Geotechnical Centrifuge Operations', *Geotechnique*, 30(3), pp. 227–268.
- Schwamb, T. (2010) *Optical Strain Sensing for Piled Foundations at Ninewell's Bridge*. MPhil Dissertation, University of Cambridge, UK.
- Seed, H. B. and Idriss, I. M. (1970) *Soil Moduli and damping factors for dynamic response analyses Report EERC 70-10*. California, USA: Earthquake Engineering Research Center, University of California Berkeley.
- SERIES (2011) *Turner Beam Centrifuge*. Available at: <http://www.series.upatras.gr/TBCentr> (Accessed: 27 December 2019).
- Shinoda, M., Haya, H. and Murata, S. (2008) 'Nondestructive Evaluation of Railway Bridge Substructures By PERCUSSION TEST', in *Fourth International Conference on Scour and Erosion*. Tokyo, Japan, pp. 285–290.
- Shirole, A. M. and Holt, R. C. (1991) 'Planning for a comprehensive bridge safety assurance program', *Transportation Research Record No. 1290*, 1, pp. 39–50.
- State of Wisconsin Department of Transport (2018) *WisDOT Bridge Manual Chapter 11 – Foundation Support*. Available at: <https://wisconsindot.gov/dtsdManuals/strct/manuals/bridge/ch11.pdf>.
- Steel Construction Institute (2018) *Integral bridges*. Available at: https://www.steelconstruction.info/Integral_bridges (Accessed: 10 February 2018).
- Sumer, B. M., Bundgaard, K. and Fredsøe, J. (2005) 'Global and Local Scour at Pile Groups', *International Journal of Offshore and Polar Engineering*, 15(3), pp. 204–209.

- Tang, F., Chen, Y., Li, Z., Hu, X., Chen, G. and Tang, Y. (2019) 'Characterization and field validation of smart rocks for bridge scour monitoring', *Structural Health Monitoring*, 18(5–6). doi: 10.1177/1475921718824944.
- Tang, Y. (2017) *Remote sensing and localization of smart rocks with orientation-controlled magnets for real-time monitoring of bridge scour and riprap effectiveness*. Doctoral Dissertation, Missouri University of Science and Technology.
- Teymur, B. and Madabhushi, S. P. G. (2003) 'Experimental study of boundary effects in dynamic centrifuge modelling', *Géotechnique*, 53(7), pp. 655–663. doi: 10.1680/geot.2003.53.7.655.
- Vucetic, M. and Dobry, R. (1991) 'Effect of soil plasticity on cyclic response', *J. Geotech. Engrg.*, 117(1), pp. 89–107.
- Wardhana, K. and Hadipriono, F. C. (2003) 'Analysis of recent bridge failures in the United States', *Journal of Performance of Constructed Facilities*, 17(3), pp. 144–150. doi: Doi 10.1061/(Asce)0887-3828(2003)17:3(144).
- Waterman (2016) *B0104 Baildon River Bridge, Shipley : principle inspection*. City of Bradford MDC.
- Wenzel, H. and Pichler, D. (2005) *Ambient Vibration*. West Sussex, UK: John Wiley & Sons.
- Whelan, M. J., Gangone, M. V, Janoyan, K. D., Hault, N. A., Middleton, C. R. and Soga, K. (2010) 'Wireless operational modal analysis of a multi-span prestressed concrete bridge for structural identification', *Smart Structures and Systems*, 6(5–6), pp. 579–593.
- Winkler, E. (1867) *Theory of elasticity and strength*. Prague, CZK: Dominicus.
- Wu, W., Wang, S., Chen, C. and Lai, G. (2018) 'Modal parameter identification for closely spaced modes of civil structures based on an upgraded stochastic subspace methodology', *Structure and Infrastructure Engineering*, 15(3), pp. 1–18. doi: 10.1080/15732479.2018.1547770.
- Wynn, R. B. *et al.* (2014) 'Autonomous Underwater Vehicles (AUVs): Their past, present and future contributions to the advancement of marine geoscience', *Marine Geology*, 352, pp. 451–468. doi: 10.1016/j.margeo.2014.03.012.
- Yao, C., Darby, C., Hurlebaus, S., Price, G. R., Sharma, H., Hunt, B. E., Yu, O. Y., Chang, K. A. and Briaud, J. L. (2010a) 'Motion Sensors for Scour Monitoring: Laboratory Experiment with a Shallow Foundation', in *GeoFlorida 2010: Advanced in Analysis, Modeling & Design*. Florida, USA: ASCE, pp. 970–979.
- Yao, C., Darby, C., Hurlebaus, S., Price, G. R., Sharma, H., Hunt, B. E., Yu, O. Y., Chang, K. A. and Briaud, J. L. (2010b) 'Scour Monitoring Development for Two Bridges in Texas', in *International Conference on Scour and Erosion 2010 (ICSE-5)*. San Francisco, California: ASCE, pp. 958–967.
- Yu, X. (2009) 'Sensor apparatus and system for time domain reflectometry', *US Patent Application Publication*. United States. Available at: <https://www.google.com/patents/US20090273352>.
- Yu, X., Zhang, B. and Tao, J. (2013) 'A new time-domain reflectometry bridge scour sensor', *Structural Health Monitoring*, 12(2), pp. 99–113. doi: 10.1177/1475921713476331.

Yu, Xiong and Yu, Xinbao (2010) 'Laboratory evaluation of Time-Domain Reflectometry for bridge scour measurement: Comparison with the ultrasonic method', *Advances in Civil Engineering*, 2010, p. 12. doi: 10.1155/2010/508172.

Zampieri, P., Zanini, M. A., Faleschini, F., Hofer, L. and Pellegrino, C. (2017) 'Failure analysis of masonry arch bridges subject to local pier scour', *Engineering Failure Analysis*, 79, pp. 371–384. doi: 10.1016/j.engfailanal.2017.05.028.

Zarafshan, A., Iranmanesh, A. and Ansari, F. (2012) 'Vibration-Based Method and Sensor for Monitoring of Bridge Scour', *Journal of Bridge Engineering*, 17(6), pp. 829–838. doi: 10.1061/(ASCE)BE.1943-5592.0000362.